THE
PHYSICAL REVIEW
A Journal of Experimental and Theoretical Physics Established by E. L. Nichols in 1893
VOL. 59, NO. 3 FEBRUARY 1, 1941 SECOND SERIES

Variation of the Rate of Decay of Mesotrons with Momentum

BRUNO ROSSI* AND DAVID B. HALL
University of Chicago, Chicago, Illinois
(Received December 13, 1940)

In order to determine the dependence of the probability of decay on momentum, mesotrons with range between 196 and 311 g/cm² of lead and mesotrons with range larger than 311 g/cm² of lead were investigated separately. The softer group of mesotrons was found to disintegrate at a rate about three times faster than the more penetrating group, in agreement with the theoretical predictions based on the relativity change in rate of a moving clock. A new value of the proper lifetime of mesotrons of $(2.4\pm0.3)\times10^{-6}$ sec. is determined, based upon measurements with particles with momentum of approximately 5×10^{8} ev/c.

INTRODUCTION

RECENT experiments on the variation of cosmic-ray intensity with altitude have shown that the rate of decrease of the mesotron component with increasing atmospheric depth cannot be accounted for completely by ordinary ionization losses. It has been established, namely, that the number of mesotrons is much more strongly reduced by a layer of air than by a layer of condensed material which is equivalent to the air layer with regard to ionization losses.[1-5]

The anomalous absorption in air is interpreted on the hypothesis that mesotrons disintegrate spontaneously with a proper lifetime of the order of a few microseconds. According to this assumption, a considerable fraction of the mesotron beam will disappear by disintegration while traveling in the atmosphere. No appreciable number of mesotrons, however, will disintegrate within a condensed absorber, even equivalent in mass to the whole thickness of the atmosphere, because the time required for the traversal of such an absorber is very short compared with the lifetime of mesotrons.

A simple relativistic consideration shows that if the absorption anomaly of mesotrons is due to spontaneous decay it must be more pronounced for mesotrons of low energy than for mesotrons of high energy. In fact, let τ_0 be the "proper lifetime" of mesotrons; i.e., the lifetime measured in a frame of reference in which the mesotron is at rest, and τ the lifetime measured in a frame of reference in which the mesotron is moving with a velocity β.[6] Then

$$\tau=\tau_0/(1-\beta^2)^{\frac{1}{2}} \qquad (1)$$

and the "average range before decay" L; i.e., the average distance traveled by the mesotrons before disintegrating, becomes

$$L=\beta\tau=p\tau_0/\mu, \qquad (2)$$

* Now at Cornell University, Ithaca, New York.

[1] B. Rossi, N. Hilberry and J. B. Hoag, (a) Phys. Rev. **56**, 837 (1939); and (b) Phys. Rev. **57**, 461 (1940).

[2] W. M. Nielsen, C. M. Ryerson, L. W. Nordheim and K. Z. Morgan, Phys. Rev. **57**, 158 (1940).

[3] M. Ageno, G. Bernardini, N. B. Cacciapuoti, B. Ferretti and G. C. Wick, Phys. Rev. **57**, 945 (1940).

[4] H. V. Neher and H. G. Stever, Phys. Rev. **58**, 766 (1940).

[5] A. Ehmert, Zeits. f. Physik **115**, 333 (1940).

[6] We shall use throughout the paper the system of units described by B. Rossi, Phys. Rev. **57**, 660 (1940).

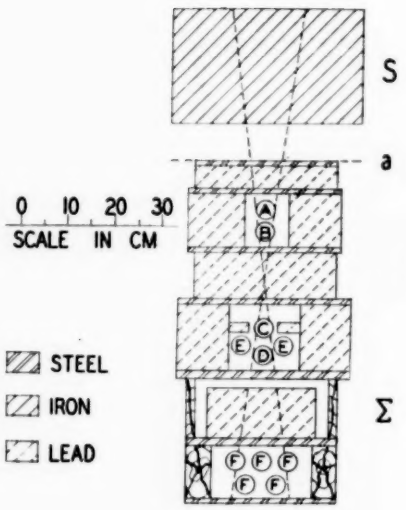

FIG. 1. Experimental arrangement.

where μ is the mass and $p=\mu\beta/(1-\beta^2)^{\frac{1}{2}}$ is the momentum of the mesotrons. The probability of decay per centimeter path is obviously $1/L$. It is seen that the average range is directly proportional, and the probability of decay inversely proportional, to the momentum.

The experiments described in the present paper were primarily designed to test the dependence of disintegration probability on momentum expressed by Eq. (2). The purpose was to provide an additional check of the disintegration hypothesis and simultaneously to verify the relativistic transformation formula for time intervals. Further experimental evidence on the subject of the decay was particularly desirable in view of Fermi's recent theory showing that the energy losses of fast particles in condensed materials are appreciably reduced by the dielectric polarization of the medium.[7] According to this theory even *stable* mesotrons are absorbed by gases more strongly than by solid or liquid materials of the same mass per cm². The difference in absorption due to polarization increases with increasing mesotron momentum; i.e., varies oppositely from the difference due to decay. The polarization effect, as calculated by Fermi, was quantitatively inadequate to account for the experimental results already obtained. Yet it was interesting to investigate whether the observed absorption anomaly was a decreasing function of the mesotron momentum, as the anomaly attributed to the decay, or an increasing function, as the anomaly attributed to the polarization.

An attempt to determine the rates of decay of mesotrons of different momenta has been reported by Nielsen, Ryerson, Nordheim and Morgan.[2] Mesotron groups of different average momentum were selected by taking the difference between the intensities of the mesotron beam after filtration through various thicknesses of lead. By this method, however, it is hardly possible to reach a sufficient accuracy, since the difference is small compared with the quantities directly measured. In our experiments the statistical precision was greatly improved by measuring the difference directly; i.e., by recording only mesotrons which can traverse a given thickness of lead but are stopped by a certain additional absorber.

EXPERIMENTAL METHOD

The experimental arrangement is schematically represented in Fig. 1. The Geiger-Müller counter tubes were of the self-quenching type. Their internal diameter was 4 cm and their effective lengths were as follows: counters A, B, C and E, 27 cm; counter D, 20 cm; counters F, 60 cm. The five counters F and the two counters E were all connected in parallel. The counter battery F covered completely the solid angle subtended by counters A, B, C and D. In order to cut off the soft component, 5 cm of lead was permanently placed above counter A and 10 cm of lead between counters B and C. Including the material of the frame, the permanent absorber above or between counters A, B, C and D was equivalent in absorption power to 186 g/cm² of lead, while that between D and F was equivalent to 10 g/cm² of lead. Counters A, B, C and D were protected on the side by lead walls 11.5 cm thick. An additional lead absorber Σ of 115 g/cm² could be introduced between D and F and an absorber S made of iron plates could be arranged above the apparatus so as to cover the whole solid angle subtended by counters A, B, C and D. The apparatus was set up in a moving van which could be taken to different altitudes on mountain roads. The whole system, except for the absorber S, was enclosed in a thermostatic box.

By means of an appropriate vacuum-tube

[7] E. Fermi, Phys. Rev. 57, 485 (1940).

circuit, the following events were simultaneously recorded: (1) Fivefold coincidences between counters A, B, C, D and one of counters F or E (coincidences $[ABCD(E+F)]$); (2) coincidences between counters A, B, C and D not accompanied by a pulse either of counters F or of counters E (anticoincidences $[ABCD-(E+F)]$). The coincidences $[ABCD(E+F)]$ were mainly caused by mesotrons going through counters A, B, C, D and F. After entering the apparatus; i.e., after crossing the surface indicated by a in Fig. 1, these mesotrons had to traverse 196 g/cm² of lead when there was no absorber in Σ, or 311 g/cm² of lead when 115 g/cm² of lead were placed in Σ. Chance coincidences were negligible and coincidences due to air showers were certainly rare on account of the heavy lead shield at the side of the counters. Coincidences caused by ionization showers generated by mesotrons in the various absorbers could not introduce any error because they were a small and *constant* fraction of the coincidences caused directly by mesotron traversals.[8] Thus, one is justified in taking the counting rate $[ABCD(E+F)]$ as a measure of the number N of mesotrons entering the apparatus with a residual range larger than the total amount of matter present above or between the counters.

Anticoincidences $[ABCD-(E+F)]$ could be accounted for by one of the following events. (a) A mesotron has traversed A, B, C and D and has been stopped between D and F. (b) A mesotron has gone through A, B, C, D and F, but the counter battery F has failed to detect it for lack of efficiency. (c) A chance coincidence between pulses of counters A, B, C and D has occurred. (d) A mesotron has traversed counters A, B, C and D, but has been scattered through a wide angle so as to miss the counter battery F.

The stopping of mesotrons between D and F (case (a)) is certainly the main origin of the anticoincidences recorded with lead in Σ, which are, as we shall see, several times more frequent than those recorded without lead. The events described under (b) and (c) are about equally frequent with and without the absorber Σ. The scattering (case (d)) may contribute a small number of anticoincidences, which is not necessarily the same with and without the absorber. Since, however, only slow mesotrons are appreciably scattered as well as absorbed, the difference in the number of anticoincidences due to scattering is a small and constant fraction of the difference in the number of anticoincidences due to absorption. Thus, the difference between the number of anticoincidences recorded with and without lead in Σ is proportional, if not accurately equal, to the number of mesotrons which traverse 10 g/cm² of lead and are absorbed by 125 g/cm² of lead between D and F. These mesotrons are those which enter the apparatus with a residual range between $R_a = 196$ and $R_b = 311$ g/cm² of lead.

[8] This was not always the case for the experimental arrangements previously used. See the discussion on p. 464, reference 1(b).

The Measurements

Measurements were taken alternately at Denver, Colorado, and at Echo Lake, approximately 30 miles west of Denver. The geomagnetic latitude is practically the same (49° N) for both locations. The difference in altitude is 1624 m. The difference in atmospheric pressure, as measured during the experiments, was 108 mm Hg, equivalent to 147 g/cm².

The measurements at Echo Lake were performed partly with an iron absorber of 200 g/cm² in S and partly without this absorber. No iron absorber was used at Denver. Three complete sets of measurements were carried out at Denver and two at Echo Lake. The deviations of the single readings from the averages were within the statistical fluctuations. The final results are summarized in Table I. The errors given are the standard statistical deviations.

Table I. *Summary of the measurements at Denver and Echo Lake.* $[ABCD(E+F)]$ *and* $[ABCD-(E+F)]$ *are the numbers of coincidences and anticoincidences per minute.* Δ *is the difference between the numbers of anticoincidences per minute recorded with and without 115 g/cm² of lead in* Σ. *The errors are the standard statistical deviations.*

Location	Absorber g/cm² S(Fe)	Absorber g/cm² Σ(Pb)	Time Min.	$[ABCD \times (E+F)]$	$[ABCD -(E+F)]$	Δ
Denver $z=1616$ m $h=856$ g/cm²	0	0	3384	5.16±0.048	0.091±0.0052	0.276 ±0.009
	0	115	6783	4.79±0.027	0.367±0.0074	
Echo Lake $z=3240$ m $h=709$ g/cm²	0	0	308	6.87±0.15	0.15 ±0.02	0.53 ±0.03
	0	115	1469	6.49±0.066	0.68 ±0.021	
	200	0	2846	5.73±0.045	0.119±0.0064	0.394 ±0.012
	200	115	5362	5.43±0.032	0.513±0.0098	

According to the discussion in the foregoing section, the counting rates $[ABCD(E+F)]$ with 115 g/cm² of lead in Σ can be taken as a measure of the number N of mesotrons entering the apparatus with a residual range larger than $R_b=311$ g/cm² of lead, while the figures listed under Δ can be taken as a measure of the number n of mesotrons entering the apparatus with a residual range between $R_a=196$ and $R_b=311$ g/cm² of lead.

Let N_1, N_1' and N_2 be the values of N at Echo Lake under 200 g/cm² of iron, at Echo Lake without the iron absorber and at Denver without the iron absorber, respectively. Let n_1, n_1' and n_2 be the corresponding values of n. Considering first the measurements taken without the iron absorber, we have

$$n_1'/N_1'=0.082\pm0.005, \quad n_2/N_2=0.058\pm0.002.$$

It appears that the fractional number of slow mesotrons increases rapidly with altitude, in agreement with the results of the absorption measurements in carbon by Rossi, Hilberry and Hoag.[1] Because of a possible effect of scattering on the determination of n, the above figures cannot be trusted to represent accurately the absolute values of the ratios n_1'/N_1' and n_2/N_2. However, the ratios between values of $[ABCD(E+F)]$ or Δ at different depths should not be appreciably affected by scattering or by other disturbing effects. Thus we have

$$N_2/N_1=0.883\pm0.007 \quad n_2/n_1=0.698\pm0.031$$
$$N_2/N_1'=0.738\pm0.009 \quad n_2/n_1'=0.520\pm0.035$$

where the actual errors should not exceed the statistical errors indicated.

Discussion

In order to discuss our experimental results, we need a relation between ranges and momenta for mesotrons. The *momentum* loss due to collision is given by the Bethe-Bloch formula

$$-\frac{dp}{dx}=2\pi r_0^2 NZ\mu_e\frac{1}{\beta^3}\left[\log\frac{W_m\mu_e\beta^2}{I^2Z^2(1-\beta^2)}+1-\beta^2\right], \quad (3)$$

where r_0 is the classical radius of the electron, N the number of atoms per cm³, Z the atomic number, μ_e the rest energy of the electron, β the velocity of the mesotron, W_m the maximum transferable energy, and $I=13.5$ ev (this expression differs by a factor $1/\beta$ from the expression for the *energy* loss). A correction has to be applied to account for the polarization effect pointed out by Fermi. The correction, however, is very small for the mesotron momenta in which we are interested. According to some recent calculations of Halpern and Hall, it is of the order of 2 percent for iron and of 3 percent for lead.[9] Numerical integration of the equation for the momentum loss yields the range as a function of the momentum. The ranges $R_a=196$ g/cm² of lead and $R_b=311$ g/cm² of lead, which define the mesotron groups considered in the present experiments, are thus found to correspond to the momenta $p_a=3.1\times10^8$ and $p_b=4.5\times10^8$ ev/c, respectively. Mesotrons reaching Denver with momenta equal to p_a and p_b had momenta equal to 5.9×10^8 and 7.3×10^8, respectively, at the altitude of Echo Lake. For mesotrons with momentum between 3.1×10^8 and 7.3×10^8 ev/c the ratio between momentum losses per g/cm² of air and of iron is very nearly a constant and equal to 1.23. Thus, as far as collision losses are concerned, 200 g/cm² of iron is approximately equivalent to 147 g/cm² of air.[10] Consequently, if the mesotrons were stable, one should observe the same mesotron intensity at Echo Lake under 709 g/cm² of air plus 200 g/cm² of iron as at Denver under 856 g/cm² of air alone. This applies to the mesotron band between 3.1×10^8 and 4.5×10^8 ev/c as well as to the whole mesotron spectrum above 4.5×10^8 ev/c.

Our experimental results show that both N and n are larger at Echo Lake under the iron absorber than at Denver without this absorber. The difference is accounted for by the decay of mesotrons on their way down from 3240 m to 1616 m. Let us define the *probability of survival* w_{12} between two elevations z_1 and z_2 as the

[9] See O. Halpern and H. Hall, Phys. Rev. **57**, 459 (1940). We are greatly indebted to the authors for kindly communicating to us the numerical results of their calculations, which are not yet published.

[10] The thickness of the iron absorber is actually slightly larger than it should be. When the experiments were performed, the results of Halpern and Hall on the polarization effect were not yet available and previous calculations had given a larger correction for this effect (see reference (7)). However, both the coincidences $[ABCD(E+F)]$ and the anticoincidences $[ABCD-(E+F)]$ change so slowly with the thickness of the absorber S, that it is hardly necessary to apply any correction to the experimental results.

TABLE II. *Comparison between various determinations of the average range before decay L from measurements on the absorption anomaly for vertical mesotrons; z_1 is the elevation of the higher station, p_2 the momentum of the recorded mesotrons, p the effective momentum. The data of Rossi and Hall for $p_2 > 3.0 \times 10^8$ ev/c have been obtained from Table I, adding the counting rates [ABCD(E+F)] and [ABCD −(E+F)]. This sum represents the number of mesotrons with range > 186 g/cm² of lead.*

AUTHORS	z_1 METERS	p_2 10^8 EV/C	p 10^8 EV/C	L 10^5 CM	COMPENSATING ABSORBER
Rossi *et al.*[1]	4300	>2.5	>3.3	9.4±0.9	carbon above the counters
	3240	>2.5	>3.3	9.9±1.2	
	1616	>2.5	>3.3	9.5±1.7	
	180	>2.5	>2.5	9.4±1.6	
Nielsen *et al.*[2]	2040	>1.8	>3.5	6.2±0.5	carbon above the counters
	2040	>3.5	>5.3	8.9±1.2	
	2040	>5.9	>7.8	15.1±3.5	
	2040	1.8→3.5	3.5→5.3	2.45	
	2040	3.5→5.9	5.3→7.8	2.26	
Ageno *et al.*[3]	3460	>2.2	>4.5	31±5	lead between the counters
Rossi and Hall	3240	>3.0	>4.3	12.3±0.6	iron above the counters
	3240	>4.5	>5.8	13.3±0.9	
	3240	3.1→4.5	4.4→5.8	4.5±0.6	

probability that a mesotron present at the higher level z_1 does not disintegrate before reaching the lower level z_2. Then $w_{12}=n_2/n_1=0.698$ is the experimental value for the average probability of survival between $z_1=3240$ m and $z_2=1616$ m of the mesotrons which reach z_2 with momenta between p_a and p_b, and $W_{12}=N_2/N_1=0.883$ is the corresponding value for the mesotrons which reach z_2 with momenta larger than p_b. One sees that w_{12} is much smaller than W_{12}, which shows that slow mesotrons disintegrate at a much faster rate than the more energetic ones. This result is in agreement with the predictions based upon the disintegration hypothesis (see Eq. (2)) and affords strong support to the hypothesis itself. For a mono-energetic group of mesotrons, the probability of decay has a very simple theoretical expression, provided the momentum loss in the air layer between z_1 and z_2 can be neglected. In this case, Eq. (2) gives

$$\log w_{12} = -(z_1-z_2)/L. \qquad (4)$$

It is convenient to use Eq. (4) as a definition of L also when the momentum loss cannot be neglected. It can easily be proved that L is still related to the lifetime τ_0 by an expression of the type of Eq. (2)

$$L = p\tau_0/\mu, \qquad (2)$$

where, however, p has now the following meaning:

$$p=(p_2+ah_2)\times\left[1+\log\frac{p_2+a(h_2-h_1)}{p_2}\Big/\log\frac{h_2}{h_1}\right]^{-1}. \qquad (5)$$

Here h_1 and h_2 are the atmospheric depths at the elevations z_1 and z_2, p_2 is the momentum of mesotrons at z_2 and a is the momentum loss per g/cm² of air.[11] The momentum p is intermediate between the initial momentum $p_1=p_2+a(h_2-h_1)$ and the final momentum p_2. We shall refer to it as the *effective momentum*.

Let us first consider the experimental results concerning mesotrons which have residual momenta between 3.1×10^8 and 4.5×10^8 ev/c at the lower elevation. The corresponding effective momenta are 4.4×10^8 and 5.8×10^8 ev/c and we may take 5.0×10^8 ev/c as an average. For this mesotron group the experimental value of the probability of survival between 3240 and 1616 m is $w_{12}=0.698\pm0.031$, and therefore $\boldsymbol{L=(4.5\pm0.6)\times10^5}$ **cm.** It then follows from (2): $\tau_0/\mu=(9.07\pm1.3)\times10^{-4}$ cm c/ev and accordingly, taking $\mu=8\times10^7$ ev/c², $\tau_0=(7.2\pm0.9)\times10^4$ cm/c, or $\boldsymbol{\tau_0=(2.4\pm0.3)\times10^{-6}}$ **sec.** We shall next consider the continuous mesotron spectrum which reaches 1616 m with a residual momentum larger than 4.5×10^8 ev/c. The probability of survival for this mesotron group is $W_{12}=0.883$, and if we take Eq. (4) as an experimental definition of L we get $\boldsymbol{L=(13.3\pm0.9)\times10^5}$ **cm.** Assuming $\tau_0=2.4\times10^{-6}$ sec., we then calculate formally, from Eq. (2), $p=1.5\times10^9$ ev/c. This momentum should represent a sort of average effective momentum for the mesotron group considered. The value $p=1.5\times10^9$ ev/c is quite compatible with our present knowledge of the momentum spectrum of mesotrons.[12] Thus, while a quantitative proof of Eq. (2) is still wanting, its approximative validity may be considered as established.

In evaluating the experimental results we have only considered mesotrons coming in the vertical direction. As a matter of fact, our experimental arrangement was strongly selective for vertical

[11] This follows immediately, for instance, from Eq. (14) of the paper "The disintegration of mesotrons" by B. Rossi, Rev. Mod. Phys. **11**, 296 (1939).

[12] Cf., e.g., P. M. S. Blackett, Proc. Roy. Soc. **A159**, 1 (1937); D. J. Hughes, Phys. Rev. **57**, 592 (1940).

mesotrons, but detected also mesotrons coming in directions inclined up to an angle of almost 45°. The inclined mesotrons travel a longer distance and have on that account a smaller probability of survival than the vertical ones. The increase in the path length, however, is partially compensated by an increase in the effective momentum. Thus the correction is not large and can be disregarded at the present state of the experimental accuracy.

Comparison with Previous Results

Table II summarizes the data on the mesotron decay which can be deduced from the measurements so far reported on the absorption anomaly for vertical mesotrons. L is calculated, according to Eq. (4), from the experimental values of the probability of survival. The results of Nielsen, Ryerson, Nordheim and Morgan on the mesotron groups with p_2 from 1.8×10^8 to 3.5×10^8 ev/c and from 3.5×10^8 to 5.9×10^8 ev/c are not accurate enough for a quantitative comparison with our data on the mesotron group with p_2 from 3.1 ± 10^8 to 4.5×10^8 ev/c. No other measurements on selected groups of mesotrons are available. All the remaining data in Table II refer to mesotrons for which only the lower limit of the momentum is defined. A comparison between these data is not straightforward because L depends not only on the minimum effective momentum $p_{\min}$ of the mesotrons recorded, but also on the shape of the momentum spectrum, which is probably different at different altitudes. One may expect, however, an approximate correlation to exist between the values of $p_{\min}$ and L in the various experiments. Table II shows that this is actually the case if we exclude the measurements of Ageno, Bernardini, Cacciapuoti, Ferretti and Wick, who found a value of L much larger than that determined by other authors for nearly the same value of $p_{\min}$. The reason for the disagreement is not completely clear. It may be noted that Ageno and collaborators used a lead absorber placed *between* the counters to compensate for the difference in atmospheric depth between the higher and the lower station. With this arrangement an appreciable number of mesotrons may have been removed from the beam by scattering, and this may have reduced the magnitude of the absorption anomaly due to decay. We may add that the results recently obtained by Neher and Stever[4] with an ionization chamber, concerning mesotrons coming in all directions, agree better with our present results and with those of Rossi, Hilberry and Hoag and of Nielsen, Ryerson, Nordheim and Morgan than with the results of Ageno, Bernardini, Cacciapuoti, Ferretti and Wick.

Conclusion

The experiments described have shown, in agreement with previous results, that the number of cosmic-ray mesotrons is more strongly reduced by a layer of air than by a dense absorber equivalent to the air layer with regard to ionization losses. The indication from earlier experiments[13] that the difference in stopping power between air and condensed materials increases when the mesotron momentum is decreased has been definitely established. This result verifies a theoretical prediction based upon the disintegration hypothesis, thus confirming the view that the absorption anomaly is caused by spontaneous decay of mesotrons in the atmosphere. A value of the proper lifetime $\tau_0=2.4\times10^{-6}$ sec. is deduced from measurements on a fairly monokinetic group of mesotrons.

We are greatly indebted to Professor A. H. Compton for discussions of the problem and for the encouragement given to this work. We also express our appreciation to Professor J. C. Stearns of Denver University for his friendly collaboration, and to Professor N. Hilberry and Mrs. Jane E. Hamilton for their valuable assistance throughout the experiments. To the Willet Company for making available for two months a suitable truck, to the Denver City Parks for their helpful cooperation and to the Carnegie Institution of Washington for financial support, we wish to express our sincere gratitude. One of us (B. R.) acknowledges with thanks the financial support granted to him by the Committee in aid of Displaced Foreign Scholars.

[13] See reference 2. Also M. A. Pomerantz, Phys. Rev. 57, 3 (1940).

The Scattering of Mesotrons in Tungsten

F. LESLIE CODE
Ryerson Physical Laboratory, University of Chicago, Chicago, Illinois
(Received September 5, 1940)

Measurements of the scattering of mesotrons have been made with a 30-cm counter-controlled cloud chamber in a 12,900-oersted magnetic field. The scattering block consisted of 3.8 cm of tungsten, and the lowest Geiger-Mueller counter was mounted directly over the center of the tungsten. Scattering angle and curvature measurements were made on 359 tracks. In addition, there were 92 high energy tracks with a deflection too small to be measurable. The scattering angles varied from 0 to 18.7°, and the mean energies $\bar{E}$ were nearly all less than 2×10^9 ev. The values of the product $\bar{E}\theta$ varied from zero to a maximum of 13.7×10^9 ev degrees. These results confirm Williams' prediction of a Gaussian distribution of multiple scattering. A number of cases of anomalous large-angle scattering were obtained, as contrasted with the single case of large-angle scattering observed by Wilson, establishing a departure at these angles from the Gaussian law. This further substantiates Williams' theory with reference to large-angle scattering caused by nuclear forces. The mean value of the multiple electrical scattering calculated from Wilson's equation is 2.2×10^9 ev degrees for this experimental arrangement, which compares with the experimental value of 2.14×10^9. This very satisfactory agreement supports Williams' assumption that the main force responsible for the Gaussian part of the scattering is that arising from the electric charges of the mesotron and of the nucleus.

INTRODUCTION

THE scattering of cosmic-ray particles was first investigated by Anderson[1] in 1933. More extensive scattering measurements were later made by Blackett and Wilson,[2] who found their results to be in approximate agreement with the simple theory then available. The theory of scattering for very energetic particles was developed in 1939 by Williams,[3] who differentiated between the scattering caused by the Coulomb field of the nucleus and that arising from the short range interaction with the individual protons and neutrons of which the nucleus is composed. According to this theory, when the impact parameter is greater than r_0 (approximately the nuclear radius), the scattering occurs in the Coulomb field of the nucleus. Most of the scattering observed arises from this, and Williams assigned two limits for the extreme collision distances. An upper limit is determined by the shielding of the orbital electrons, and a lower limit r_0 by the modification of the electrostatic field within the nuclear radius.

Williams concluded that these Coulomb collisions result mainly in multiple scattering, and predicted that the distribution of the observed scattering angles should be Gaussian. These Coulomb collisions would normally also lead to a "tail" of large-angle single scattering, corresponding to close collisions which generally do not occur more than once per particle in the scattering plate. However, Williams showed that the effect of the lower limit of the impact parameter is to suppress this "tail" completely.

When the impact parameter is less than r_0, the incoming particle approaches closer to the center of the nucleus than the nuclear radius. Any scattering in this region is caused by the short range interaction between the incoming particle and the individual neutrons and protons in the nucleus. Williams showed that, for these short range collisions, the scattering in the Coulomb field of separate nuclear protons is negligible. Many more large-angle deflections are likely to be produced by the short range forces than arise from the multiple Coulomb scattering. In a further development of the theory, Wilson[4] has shown that a fairly sharp separation in angular range is to be expected between these two types of scattering, and has pointed out that the predicted absence of a single-scattering "tail" to the Gaussian curve for the multiple Coulomb scattering is particularly favorable to the detection of scattering caused by close collisions with nuclear particles.

The following experimental data are of interest

[1] C. D. Anderson, Phys. Rev. **43**, 381 (1933).
[2] P. M. S. Blackett and J. G. Wilson, Proc. Roy. Soc. **A165**, 209 (1938).
[3] E. J. Williams, Proc. Roy. Soc. **A169**, 531 (1939).
[4] J. G. Wilson, Proc. Roy. Soc. **A174**, 73 (1940).

in this connection. Vargus,[5] in 1939, using some of Anderson and Neddermeyer's photographs, investigated the angular distribution of cosmic-ray particles scattered in one centimeter of platinum. With 55 tracks of energies less than 5×10^8 ev, he obtained an approximate Gaussian distribution for the values of the product $\bar{E}\theta$, in which the energy in 10^9 ev is multiplied by the scattering angle in degrees. In Vargus' calculations β was assumed to be unity for cosmic-ray particles.

Wilson[4] summarized his previous results on particles traversing lead, copper and gold, along with new data on 2 cm of gold. From 185 carefully selected pictures of cosmic-ray tracks, he confirmed Williams' conclusion that the angular distribution caused by multiple scattering in the Coulomb field is Gaussian. He took an upper limit of energy at 2×10^9 ev, in order that the region for which earlier measurements indicated a possible anomaly might be excluded. For tracks passing through 2 cm of gold he showed that the exclusion of electrons is complete. For results with lead and copper plates he discarded tracks with energies less than 2×10^8 ev. Hence he concluded that the number of electrons remaining is negligible. Protons, however, are not excluded; but he says that the effect of a proton component of this magnitude (probably about 5 percent or less) is shown to be negligible for the number of tracks observed.

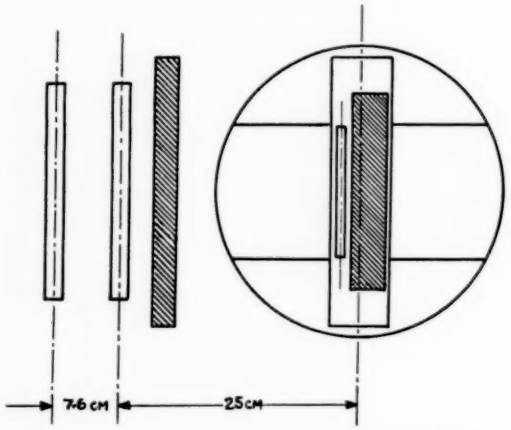

FIG. 1. Arrangement of counter-controlled cloud chamber showing the two large G-M counters and 1-inch lead bar above the chamber, and the small G-M counter and scattering block of 1½-inch tungsten mounted in the horizontal box across the center of the chamber.

[5] J. A. Vargus, Jr., Phys. Rev. **56**, 480 (1939).

Regarding anomalous scattering, Wilson found only one particle out of the 185 measured tracks falling appreciably outside the Gaussian distribution for multiple scattering. This particle had an electron energy of 1.5×10^9 ev and a scattering angle of 4°. He considers this track to be a case of large-angle scattering.

Experimental Arrangement

In the present experiment the scattering block was 3.8 cm of tungsten. Because of its high density (19.06) and large thickness (equivalent in mass to 6.3 cm of lead) this block gives much larger scattering angles than the maximum (approximately 5°) previously recorded. Also the arrangement with the lowest Geiger-Mueller counter mounted directly above the tungsten in the center of the magnetic field removes any bias against recording emergent rays of low energy or with large scattering angle. Wilson pointed out[4] that the geometry of the counters and scattering block determines the efficiency with which large deflections are observed. The above conditions are favorable for detecting cases of anomalous large-angle scattering.

The apparatus used for this experiment consists mainly of the large electromagnet with oil-cooled windings and other accessory equipment as described by Jones and Hughes.[6] The magnet is similar in design to that used by Blackett.[7] The cloud chamber, which was 30 cm in diameter, was mounted with its back plate fixed to one polepiece of the magnet.

A new front plate was made of nonmagnetic stainless steel and to this was attached a brass box extending horizontally across the center of the chamber as shown in Fig. 1. This box was 6.35 cm high and 4.45 cm deep, and was open at the front so that the tungsten scattering block and small Geiger-Mueller counter could be inserted without dismantling the chamber. The six tungsten bars, each $8\times1.25\times0.25$ inches, were placed one above the other in the bottom of the box. Windows of ½-inch plate glass were inserted in the front plate above and below the box, and through these the cosmic-ray tracks

[6] Haydn Jones and Donald Hughes, Rev. Sci. Inst. **11**, 79 (1940).

[7] P. M. S. Blackett, Proc. Roy. Soc. **A154**, 564 (1936).

were photographed. To favor the production of showers, a 1-inch bar of lead was mounted just above the chamber.

The Geiger-Mueller counters were filled with petroleum ether. Two large counters, each electrically shielded in a copper box, were mounted vertically above the chamber. The third counter was shorter and of smaller diameter and was clipped in place inside the box directly over the center of the tungsten. The magnetic field strength was 12,900 oersteds, requiring a magnetizing current of 800 amp. at about 80 v. The small counter operated in the center of this magnetic field.

The curvature measurements were taken over a track length of 8 cm in nearly all cases. The same micrometer device was used for measuring the curvatures as described by Jones and Hughes.[6] The scattering angles were measured to 0.1°. Particular care was taken in the measurements for the cases where the scattering angle was unusually large.

The tracks were photographed on 35-mm ultra-speed panchromatic film with an f:2.8 lens of 5 cm focal length. The illumination was supplied by a water-cooled high pressure capillary mercury arc which ran continuously. A shutter admitted light to the chamber only at the time of expansion. The chamber was filled with argon and ethyl alcohol vapor to a pressure of 88 cm Hg.

Experimental Results

The results obtained from the scattering angle and curvature on 359 tracks are plotted in Fig. 2. In addition to these, there were 92 high energy tracks which had a curvature too small to be measurable with our apparatus. There were also many pictures in which the ray went out at the side, giving too short a track in the bottom to be measurable.

For each track the measurements of scattering angle and of curvature were recorded and averaged. The angle measured was the projection of the true scattering angle on the plane of the chamber. While the radius of curvature really measures momentum rather than energy, still it is convenient to express the momentum in terms of the energy an electron would have if its track curvature were the same as that of the particle.[8] This electron energy $E_e = 300\, H\rho$ was calculated for each track. The geometric mean value $\bar{E}$ of the energies measured in top and bottom of the chamber was then obtained, and the product $\bar{E}\theta$ calculated. Williams[3] shows that the product $\beta E_e\theta$ is a measure of the multiple scattering. In calculating the results β was assumed to be very nearly unity for cosmic-ray particles at these energies.

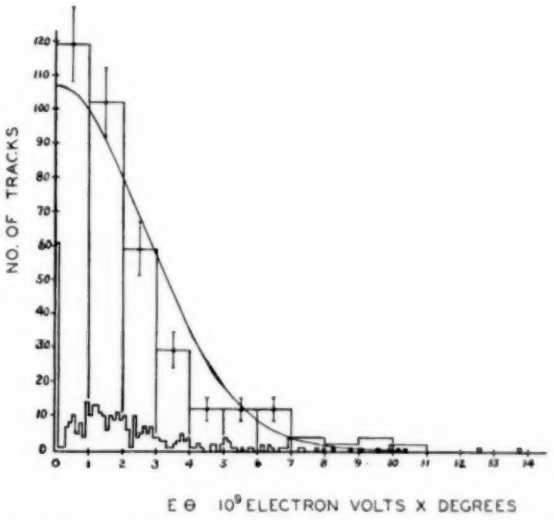

Fig. 2. The distribution of scattering for mesotrons showing expected theoretical Gaussian distribution for multiple scattering. The block diagram was drawn at intervals of 10^8 ev degrees with the number of tracks as ordinate for each group. Then the total number in each 10^9 interval was plotted vertically. The standard statistical errors are indicated.

The values of $\bar{E}\theta$ obtained from the data on these 359 tracks varied from zero to 13.7×10^9 ev degrees. Figure 2 shows a block diagram of the distribution of these values. They were plotted as abscissae at intervals of 10^8 ev degrees, with the number of tracks as the ordinate for each group.

The theoretical mean value of $\bar{E}\theta$ was calculated from the equation given by Wilson:[4]

$$\bar{\theta}_{\text{th}} = (19.5 - 3.1 \log_{10} Z)^{\frac{1}{2}} 600 Ze(Nt)^{\frac{1}{2}}/\beta E,$$

where Z is the atomic number of the scattering material; t the thickness; and N is the number of atoms per cm³.

For 1 cm of lead Wilson obtains the numerical value of $(\theta_{\text{th}} E_e\beta)_{Av}$ as 0.90×10^9 ev degrees. In this experiment with 1.5 inches of tungsten, this

[8] Cf. the system of units recently proposed by B. Rossi, Phys. Rev. 57, 660 (1940).

equation gives 2.2×10^9 as the mean value of the multiple electrical scattering. From the average of the values of $\bar{E}\theta$ obtained from the 359 measurable tracks, the experimental mean value of $\bar{E}\theta$ came out as 2.14×10^9. The very satisfactory agreement of this value with that predicted by Wilson's calculation supports the assumption that the main force responsible for the scattering is that arising from the electric charges of the mesotron and of the nucleus.

A theoretical Gaussian distribution having the same area as the statistical diagram was plotted for this mean value of $\bar{E}\theta$. The experimental values of $\bar{E}\theta$ less than 7×10^9 group themselves satisfactorily about this curve. The presence of a "tail" in the experimental curve, greater than the scattering calculated for large angles from the Gaussian curve, is caused by cases of anomalous large-angle scattering. The experimental results show 10 tracks having a value of $\bar{E}\theta$ greater than 8×10^9, whereas from the Gaussian law only 1.5 were to be expected.

The scattering angles were distributed over a range from zero to maximum of 18.7°. In Table I is given a list of tracks selected to include those with the largest scattering angles. The six tracks with the greatest scattering angles have relatively low energies, but five tracks with angles of 10° or over have energies too high to be measurable with our equipment. The track giving the largest value of $\bar{E}\theta$ (13.73×10^9) had an initial energy of 1.41×10^9 ev, and an emergent energy of 1.03×10^9 ev. The direction of its curvature indicated that this track was caused by a positively charged particle.

TABLE I. *A list of tracks selected to include those with large scattering angles.*

Scattering Angle (degrees)	Charge on Particle	Mean $\bar{E}$ Energy ($\times10^9$ ev)	Product $\bar{E}\theta$ ($\times10^9$ ev degrees)
18.7	+	0.364	6.80
15.8	−	0.439	6.94
15.7	+	0.606	9.53
15.0	+	0.313	4.70
14.8	−	0.392	5.80
14.2	+	0.475	6.75
13.9	(curvature not measurable)		
13.1	−	0.755	9.90
12.9	+	0.972	12.55
12.8	−	0.565	7.23
12.1	+	1.21	13.73
12.1	+	0.836	10.11
11.5	−	0.55	6.34
11.35	+	0.774	8.79
11.2	(curvature not measurable)		
11.1	(curvature not measurable)		
11.0	−	0.472	5.20
10.8	+	0.48	5.16
10.8	−	0.377	4.07
10.7	+	0.394	4.22
10.4	−	0.33	3.42
10.4	(curvature not measurable)		
10.0	(curvature not measurable)		
9.6	+	0.83	7.97
9.2	+	1.12	10.30

Electrons can be taken as practically excluded from these measurements. They would have to penetrate the 1.5 inches of tungsten used as a scattering block without any evident shower production, and, in addition, the 1 inch bar of lead above the chamber, giving a total equivalent thickness of 9.5 cm of lead. Protons are not excluded, and Wilson suggests a probable proton component of about 5 percent or less. He points out that in this energy range protons would give rise to a component of scattering of appreciably larger mean angle than that of mesotrons. That protons do not form a large part of the particles here studied is, however, shown by the normal ratio of the number of negative to those of positive particles. Our results may be, therefore, taken as representing the scattering by mesotrons.

Conclusion

The results of these scattering measurements further confirm the prediction of Williams that the multiple scattering in the Coulomb field of the nucleus should have a Gaussian distribution. Thus these data confirm both the results obtained by Vargus, and also the more detailed analysis by Wilson.

Furthermore, these data present a sufficient number of additional cases of anomalous large-angle scattering to establish a departure from the Gaussian distribution. This further confirms the theory developed by Williams with reference to large-angle single scattering, for which Wilson's results supply only a single example.

I wish to acknowledge with sincere appreciation the advice and inspiring guidance of Professor Arthur H. Compton, and the valuable suggestions of Dr. Bruno Rossi. In addition, may I express gratitude to Dr. Donald J. Hughes for counsel and assistance with the design and operation of the new chamber, and to Mr. Leo Seren for help in its operation.

Correlation Between Cosmic-Ray Intensity at Cheltenham and the Air Temperatures and Pressures for 1939

NIEL F. BEARDSLEY
University of Chicago, Chicago, Illinois
(Received October 10, 1940)

A calculation has been made of correlations between the cosmic-ray data from Cheltenham and radiosonde data from the Anacostia Naval Air Station. The variance of the cosmic-ray intensity is found to depend 15 percent on total air pressure, 40 percent on the distribution of the air mass as correlated with the surface temperature, 10 percent on world-wide changes with 30 percent still unaccounted for. Increased air mass in the upper air reduces the surface cosmic-ray intensity more than a corresponding increase in air mass at lower levels. The calculations use 220 days in 1939.

THERE have recently been published several papers having to do with the effect of the temperature distribution and air mass distribution of the atmosphere above a cosmic-ray meter on the readings of that meter.[1-3]

We have made a number of correlation computations between the 1939 data from a cosmic-ray meter at Cheltenham and radiosonde balloon data from the nearby Naval Air Station at Anacostia. There were 220 days in 1939 on which the balloons reached a height of 12 km and at the same time data were being taken by the cosmic-ray meters at both Cheltenham and also at Huancayo, Peru. We have used the two-hour mean from a type C ionization meter shielded with 12 cm of lead located at Cheltenham, taken at the hour of the radiosonde flight and, as described later, the daily mean of data from a similar meter at Huancayo, Peru. Most of the flights were made at 5 to 6 o'clock in the morning E.S.T.

For these computations, the mass of the air was divided into four layers. The annual mean pressures were

$\bar{P}_{\text{surface}} = 1015.7$ millibars $\quad \bar{P}_{8000} = 362.2$
$\bar{P}_{4000\text{ meters}} = 620.1 \quad \bar{P}_{12,000} = 198.7.$

The variations from the year's means of each layer are indicated by the notation:

P_2 = variation from the year's mean of $P_{\text{surface}} - P_{4000\text{ meters}}$
P_3 = variation from the year's mean of $P_{4000} - P_{8000\text{ meters}}$
P_4 = variation from the year's mean of $P_{8000} - P_{12,000\text{ meters}}$
P_5 = variation from the year's mean of $P_{12,000\text{ meters}}$
P_0 = variation from the year's mean of total barometric pressure
T = variation from the year's mean of surface temperature.

Pressures are measured in millibars and temperatures in degrees centigrade. To avoid double subscripts, 0, 2, 3, 4, 5 as subscripts refer to P_0, P_2, P_3, P_4 and P_5, respectively.

The first computations were purely meteorological in nature and are represented in Fig. 1. Correlation coefficients (r_{ij}) and "path coefficients" (β)[4] were computed between the total pressure and the pressure differences in the different layers. Also similar calculations were made using the surface temperature *vs.* these pressure differences. The regression coefficients were expressed as "b's" computed from equations of the form

$$T = +b_{T2}P_2 + b_{T3}P_3 + b_{T4}P_4 + b_{T5}P_5,$$

giving

$$T = -0.5696P_2 - 0.1121P_3 - 0.2681P_4 + 0.3069P_5.$$

The similar equation for P_0 would, of course, have all b's equal to unity. The regression coefficients were also expressed by the standard partial regression coefficients, the nondimensional "β's" computed from equations of the form

$$P_0/\sigma_0 = \beta_{02}P_2/\sigma_2 + \beta_{03}P_3/\sigma_3 + \beta_{04}P_4/\sigma_4 + \beta_{05}P_5/\sigma_5.$$

There is then between b and β the relation that

[1] N. Beardsley, Phys. Rev. **57**, 336 (1940).
[2] Y. Nishina, Y. Sekido, H. Simamura and H. Arakawa, Phys. Rev. **57**, 663 and 1050 (1940).
[3] D. Loughridge and P. Gast, Phys. Rev. **57**, 938 (1940).
[4] Sewall Wright, Ann. Math. Statistics **5**, 161 (1934).

$b_{ij}=\beta_{ij}\sigma_i/\sigma_j$ where σ_i is the standard deviation, $(P_i^2/N)^{\frac{1}{2}}$. This use of standard units $[(x-\bar{x})/\sigma]$ reduces the variance (square of the standard deviation) of each to unity. Then the square of the total correlation between P_0 or T with P_2, P_3, P_4, P_5 is the total contribution of P_2, P_3, P_4 and P_5 to the variance of P_0 or T expressed as a fraction. This total correlation (R) is given by[5, 6]

$$\sum_{i=2}^{i=5} r_{0i}\beta_{0i}=R^2_{0.2345} \quad \text{and} \quad \sum_{i=2}^{i=5} r_{Ti}\beta_{Ti}=R^2_{T.2345}$$

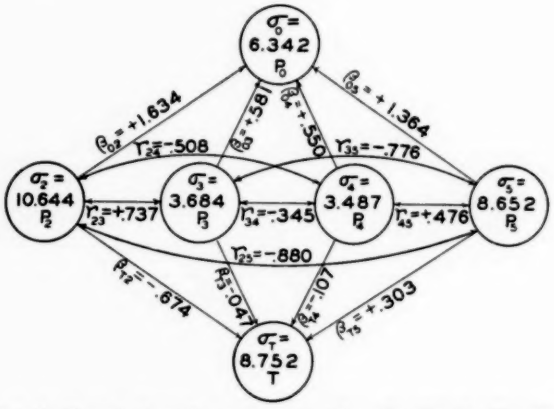

FIG. 1. Correlation diagram connecting P_2, P_3, P_4, P_5 with P_0 and also with T.

in which $r_{0i}\beta_{0i}$ is the contribution of P_i to the variance of P_0. The variance of one quantity because of a second quantity is a better measure of the influence of that second quantity on the first than is either the regression coefficient or the correlation coefficient alone since it depends on both. Correlation coefficients alone measure the closeness of fit of the changes of the two quantities but do not indicate the magnitude and hence the importance of those changes. Regression coefficients give the relative magnitude of the changes of the two quantities but do not indicate the closeness with which these changes follow each other.

Since $P_2+P_3+P_4+P_5=P_0$, $R^2_{0.2345}=1$ and no other factors are involved. However, $R^2_{T.2345}=0.8824$. Since the variance (in standard units) of T is unity, this shows that $1-0.8824=0.1176$ or about 12 percent of the variance of T is not associated with a change of the pressures used. The influence of this unknown agent "U," which is assumed to be independent of the P_i's may be written as

$$r_{TU}\beta_{TU}=1-R^2_{T.2345}.$$

This grouping of unknown effects into a single number causes that number to include (1) all experimental errors, (2) any changes in mass distribution within one (or more) of the chosen layers and (3) any lack of validity in our assumed linearity of regression.

Correlation of Cosmic-Ray Intensity with Air Pressure and Temperature

The bi-hourly means of the departures from balance of the meter at Cheltenham, with bursts deducted but not corrected for barometer or temperature, expressed as tenths percent of the total mean intensity (82 ions cm^{-3} $sec.^{-8}$) were taken at the hour of the radiosonde flight.

I = Variation of these means from their average value.

I was correlated with the pressure intervals and separately with P_0 and T. For dimensional equations we obtained

$$I=-0.8567P_2-0.9120P_3-1.4070P_3-1.9937P_5$$

and

$$I=-1.5517P_0-1.4507T.$$

In all of these computations we have minimized only the variations of the independent variables of the regression lines. This is equivalent to assuming that the errors of the cosmic-ray data, P_0 and T are negligible compared with the errors of P_2, P_3, P_4, P_5. This was done both because of the simplification of such computations and because it seemed reasonable that data taken at the surface would be much more accurate than balloon data. Figure 2 shows the results in terms of correlation coefficients and path coefficients.

$r_{I2}=+0.4298$	$r_{I2}\beta_{I2}=-0.2598$
$r_{I3}=+0.3520$	$r_{I3}\beta_{I3}=-0.0805$
$r_{I4}=-0.5074$	$r_{I4}\beta_{I4}=+0.1695$
$r_{I5}=-0.6243$	$r_{I5}\beta_{I5}=+0.7331$

$$R^2_{I.2345}=+0.5623\sim 56\%$$

$$r_{IU}\beta_{IU}=1-0.5623=0.4377\sim 44 \text{ percent.}$$

[5] H. L. Rietz, *Handbook of Mathematical Statistics*, page 141.
[6] Henry Schultz, *Statistical Laws of Demand and Supply*, page 174.

It appears that about 56 percent of the variance of I is the result of changes of the four pressure intervals leaving about 44 percent unaccounted for. This 44 percent includes all the experimental error, both of radiosonde instruments and of the cosmic-ray meters. Because of the method of computation used, any other quantities not taken into the computations specifically but which are correlated with the pressure intervals and which directly affect the cosmic-ray intensity would be included in the pressure effect. Any other factors which are not correlated with the pressures would appear in this 44 percent. For the P_0T correlation,

$$r_{I0}=-0.2238 \qquad r_{I0}\beta_{I0}=+0.1500\sim 15\%$$
$$r_{IT}=-0.5186 \qquad r_{IT}\beta_{IT}=+0.4483\sim 45\%$$
$$R^2_{I.0T}=+0.5983\sim 60\%.$$

Then $r_{IU}\beta_{IU}=1-0.5983=0.4017\sim 40$ percent, indicating that 15 percent of the variance of I is caused by total pressure and 45 percent is caused by changes of distribution of air mass as measured by the surface temperature leaving only 40 percent unaccounted for. The difference between 40 percent and 44 percent implies that P_0 and T are better sources of correlation than P_2, P_3, P_4, P_5 though the difference is too small to be significant.

It may be that there are other effects (e.g. magnetic) which by being correlated with the surface temperature cause the temperature to be more important than its effect on mass distribution would indicate. As a test of this point, the Cheltenham data were changed by subtracting 1.11 times the variation of the daily means of intensity at Huancayo from the 1939 annual mean. This 1.11 factor is taken from Forbush[7] and is probably not the best factor for 1939 but at least its use reduces the effect of world-wide magnetic changes. Figure 3 shows the results of this new computation. Here the correction for T and P_0 leaves 42 percent of the variance of $I'=I-1.11H$ unaccounted for while P_2, P_3, P_4, P_5 corrections show only 37 percent unaccounted for.

[7] S. E. Forbush, Phys. Rev. **54**, 983 (1938).

$$r_{I'2}=+0.4108 \qquad r_{I'2}\beta_{I'2}=-0.2892$$
$$r_{I'3}=+0.3190 \qquad r_{I'3}\beta_{I'3}=-0.1007$$
$$r_{I'4}=-0.5074 \qquad r_{I'4}\beta_{I'4}=+0.1711$$
$$r_{I'5}=-0.6334 \qquad r_{I'5}\beta_{I'5}=+0.8470$$
$$R^2_{I'.2345}=+0.6281\sim 63\%.$$
$$r_{I'0}=-0.2865 \qquad r_{I'0}\beta_{I'0}=+0.2034$$
$$r_{I'T}=-0.4541 \qquad r_{I'T}\beta_{I'T}=+0.3727$$
$$R^2_{I'.0T}=+0.5761\sim 58\%.$$

The increase in variance caused by P_2, P_3, P_4, P_5 from 56 to 63 percent and the decrease in variance caused by P_0, T from 60 to 58 percent which occur when the cosmic-ray data are corrected for world-wide changes indicate that these changes are correlated with surface temperature. (Such correlation in no way implies that one is the cause of the other.)

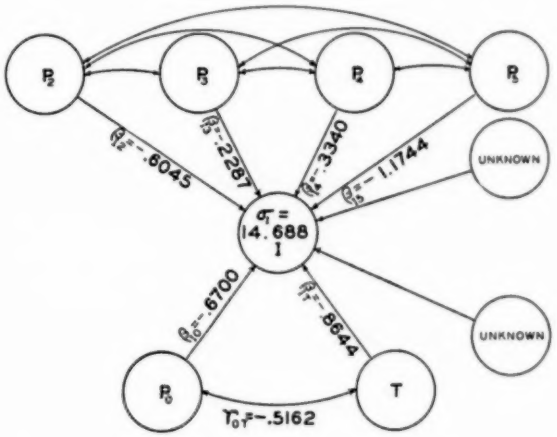

FIG. 2. Correlation diagram connecting the uncorrected cosmic-ray intensity at Cheltenham with P_2, P_3, P_4, P_5 and also with P_0, T.

This temperature-magnetic effect may be tested directly as in Fig. 4 where I is correlated with P_0 and T on the one hand and with P_0, T and H (Huancayo) on the other.

$$r_{I0}\beta_{I0}=+0.1552 \qquad r_{IH}=+0.3260$$
$$r_{IH}\beta_{IH}=+0.1050 \qquad r_{I0}=-0.2238$$
$$r_{IT}\beta_{IT}=+0.4407 \qquad r_{IT}=-0.5186$$
$$R^2_{I.0HT}=+0.7009.$$

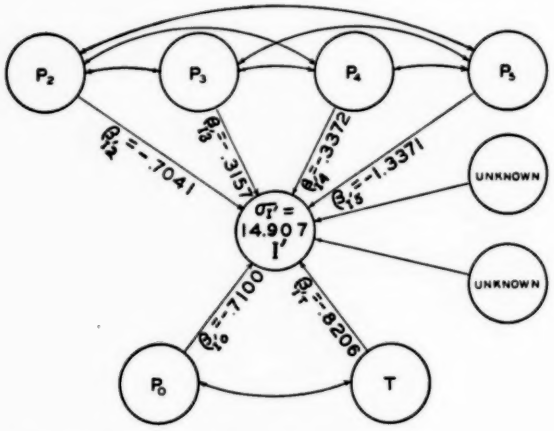

FIG. 3. Correlation diagram connecting the cosmic-ray intensity at Cheltenham which has been corrected for the intensity at Huancayo with P_2, P_3, P_4, P_5 and also with P_0, T.

$r_{TH}=-0.0830$ and $r_{0H}=+0.0962$ are below the level of significance.[8]

Figure 4 attributes about 15 percent of the variance of I to the surface pressure, 45 percent to the effect of temperature and 10 percent to changes in world-wide magnetism as such changes are measured by variations in the intensity at Huancayo where there is little seasonal or even daily change in air conditions.

In a further calculation an equation of the form

$$C_0=b_{C2}P_2+b_{C3}P_3+b_{C4}P_4+b_{C5}P_5$$

was used where C_0 represents the Cheltenham data which have been corrected for both barometer and Huancayo. This equation is not quite a proper assumption since one P can change with the others held constant only if the total pressure changes, yet the data had been corrected for variations in total pressure! Only the relations between these regression coefficients and not their absolute value can have a meaning. Evaluation of this equation gives

$$C_0=+0.2113P_2-0.1128P_3 -0.1962P_4-1.0923P_5. \quad (A)$$

The smaller of these coefficients are of doubtful significance. A similar equation with data not corrected for barometer but corrected for Huancayo gave

$$C=-1.0126P_2-1.2776P_3 -1.4423P_4-2.3038P_5. \quad (B)$$

The almost constant differences between these regression coefficients; 1.2239, 1.1648, 1.2452, 1.2114 are nearly the same as the single regression coefficient of

$$C_0=C+1.2187P_0. \quad (C)$$

It is not possible to separate rigorously the total mass effects from the effects produced by changing the distribution of the air mass since the total mass of air is correlated with the distribution. However, the increasing negative magnitude of the coefficients of Eqs. (A) and (B) with height and the fact that they differ essentially only by the total mass coefficient (with its correlated distribution effect) is significant. Evidently for a constant total amount of air, the concentrating of that air in the upper layers results in a greater reduction in cosmic-ray intensity than concentrating it in the lower layers. This is, of course, in agreement with a negative temperature coefficient as is ordinarily found and is just what is to be expected since mesotrons are supposed to suffer both mass absorption and also a loss in intensity caused by their disintegration.

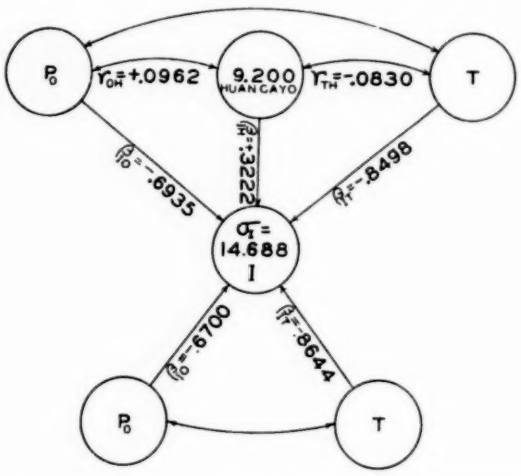

FIG. 4. Correlation diagram connecting the uncorrected cosmic-ray intensity at Cheltenham with P_0, H, T and also with P_0, T.

[8] "Student's" t test tables from R. A. Fisher, *Statistical Methods for Research Workers* (Oliver and Boyd, 1932).

Conclusion

The division of the variance of the cosmic-ray intensity into 15 percent caused by barometric pressure, 45 percent caused by distribution of air mass as correlated with surface temperature and 10 percent caused by world-wide changes leaving 30 percent unaccounted for is, we believe, new, and if it can be corroborated by the 1940 data when they are available, certainly important.

We wish to thank Professor A. H. Compton for discussing this with us, Dr. John A. Fleming of the Department of Terrestrial Magnetism for making available the Cheltenham and Huancayo data and Mr. D. M. Little of the Aerological Division of the U. S. Weather Bureau for supplying us with the necessary air data.

FEBRUARY 1, 1941 PHYSICAL REVIEW VOLUME 59

A Precise Determination of the Energy of the Neutrons from the Deuteron-Deuterium Reaction*

T. W. Bonner†
Rice Institute, Houston, Texas
(Received November 15, 1940)

A precise determination of the energy of the neutrons from the deuteron-deuterium reaction has been made. The energy of the neutrons emitted in the forward direction to the 0.52-Mev deuterons which produced the disintegrations was found to be 3.58 ± 0.03 Mev. The disintegration Q value of the reaction is 3.31 ± 0.03 Mev. The mass of He^3 calculated from this Q value is 3.01698 ± 0.00006 mass units.

THE neutrons produced when deuterium is bombarded by deuterons are known to come from the reaction

$$H^2+H^2\rightarrow He^3+n^1+Q_1 \qquad (1)$$

and those neutrons are now known to be monoenergetic.[1] Such a source of monoenergetic neutrons is most important for neutron scattering experiments as well as for disintegration experiments by neutrons. Furthermore an accurate knowledge of the energy of the neutrons involved in such experiments is essential. For this reason it is important to find their energy accurately at one bombarding energy and angle of observation so that their energies under different bombarding conditions may be accurately calculated.

An accurate knowledge of the energy of the neutrons from reaction (1) also gives one of the best methods of determining the mass of He^3. The value of Q_1 together with the energy liberated in the other deuteron-deuterium reaction

$$H^2+H^2\rightarrow H^3+H^1+Q_2 \qquad (2)$$

gives a direct comparison of the binding energy of He^3 and H^3 as well as a means of finding the stability of He^3 and H^3. Several determinations[2] have already been made on the value of Q_1 and it was the purpose of the present experiment to improve on the accuracy of these determinations.

The method of determining neutron energies in this experiment is the same as that previously used.[3] The energy of the neutrons is obtained from the range of recoil-protons in a methane-filled cloud chamber. Because of the near equality of the mass of proton and neutron, a proton recoiling in the forward direction gets

* A preliminary report of these results was given in Nature **143**, 681 (1939).

† The experimental work was carried out at the Cavendish Laboratory, Cambridge, England, while the writer held a Guggenheim Fellowship.

[1] E. Hudspeth and H. Dunlap, Phys. Rev. **57**, 971 (1940); R. D. Park and J. C. Mouzon, *ibid.* **58**, 43 (1940); H. T. Richards and E. Hudspeth, *ibid.* **58**, 382 (1940); H. H. Barschall and M. H. Kanner, *ibid.* **58**, 590 (1940). All the neutrons produced do not have exactly the same energy. They are monoenergetic only when they are produced in a thin target by deuterons of one energy and are projected at the same angle to the deuteron beam.

[2] P. I. Dee, Proc. Roy. Soc. **148**, 623 (1935); T. W. Bonner and W. M. Brubaker, Phys. Rev. **49**, 19 (1936); E. Baldinger, P. Huber and H. Staub, Helv. Phys. Acta **11**, 245 (1938); T. W. Bonner, Phys. Rev. **53**, 711 (1938).

[3] T. W. Bonner and W. M. Brubaker, Phys. Rev. **47**, 910 (1935); **48**, 742 (1935); **49**, 19 (1936); **50**, 308 (1936).

FIG. 1. A cloud-chamber photograph showing numerous recoil-protons. The neutron source was 55 cm to the right of the chamber. The two longest tracks which are nearly horizontal were the only measurable tracks on this picture. The bright object in the lower left-hand side of the chamber is the holder for the Th source.

very nearly the entire energy of the neutron.[4] The problem of measuring the energies of neutrons then becomes one of measuring proton energies in the ordinary way with the well-established range-energy relations.

Greater accuracy was expected in these measurements than in any previous ones because the neutrons were observed in the forward direction (0°) instead of at 90° to the direction of the bombarding deuterons. Observation of the neutrons in the same direction as the incident deuterons virtually eliminated corrections for angular straggling which are very important at 90°. The effect of deuteron and neutron scattering in the target or target holder was also eliminated. This is because neutrons emitted at 0° have the maximum energy of any produced in the target, and so a few neutrons which have a lower energy because of scattering will not influence the extrapolated range of the recoil-protons. This situation is just the reverse of that at 90° where scattered neutrons or neutrons produced by scattered deuterons could have considerably more energy than those emitted at 90° to the bombarding beam, and hence would increase the value of the extrapolated range.

[4] Because of the slight difference in the mass of the proton and neutron, a neutron with an energy of 4 Mev which makes a head-on collision with a proton retains approximately 1000 volts energy.

EXPERIMENTAL ARRANGEMENT AND RESULTS

The cloud chamber which was used in these experiments was 20 cm in diameter and was placed 55 cm from the deuterium target so that neutrons which traversed the chamber were emitted at an angle of $0°\pm6°$ to the deuteron direction. The path of the resolved deuterons was horizontal so the cloud chamber could be mounted in the usual horizontal position. The chamber was filled with CH_4 and alcohol vapor at a pressure of approximately 2.3 atmos. The deuterium target was a thick one made from "heavy paraffin." A thick target was used instead of a moderately thin one because of the difficulty in obtaining the exact thickness of moderately thin targets. The deuterons were accelerated by the Cavendish high voltage apparatus which was operated at 500 kv. This voltage was measured by a resistance voltmeter which was accurate to $\frac{1}{2}$ percent. The set gave a constant potential except for voltage fluctuations of about 10 kv as observed by the voltmeter. The ripple voltage of the rectifying system was negligibly small. A voltage of 20,000 volts was applied to the ion source so the maximum energy a deuteron could have was 20,000 volts greater than the voltmeter reading. However, the pressure in the discharge was quite high so that usually a positive ion would not get this total voltage drop. A maximum deuteron energy of 520 kev was used in the calculation of the Q value and this is believed to be accurate to within 10 kev.

A shutter was used in the ion path and adjusted so that neutrons entered the cloud chamber only after the chamber was completely expanded. Stereoscopic pictures were taken and reprojected in the usual way through the same camera and lens system.

Five hundred pairs of pictures were taken and on each picture numerous recoil tracks were observed. Figure 1 gives a representative cloud-chamber picture. Only those tracks were measured which were included in the angular cone 0–10° to the neutron direction. A total of 480 tracks were measured which were in the forward

direction. The lengths of these tracks, which all began and ended in the chamber, were measured to an accuracy of 0.5 mm.

Figure 2 gives the integral track-length *vs.* number curve for the recoil-protons. The extrapolated track length is 9.23 ± 0.10 cm. The stopping power of the gas mixture was obtained by the use of a weak source of Th C+C′ which was placed inside the chamber before it was filled with methane. The mean range of the 8.53-cm alpha-particles from Th C′ was determined a few hours before determining the neutron energies. The mean track length was found to be 4.08 ± 0.05 cm. This gives a stopping power of 2.09 ± 0.03 for 8.53-cm alpha-particles. The correction for change of stopping power of CH_4 with range was calculated from the curves of Livingston and Bethe.[5] For 19-cm protons the calculated stopping power was 2.04 ± 0.03. From this stopping power the extrapolated range of the recoil protons was calculated to be 18.83 ± 0.34 cm. Such an extrapolated range can probably be as accurately determined for recoil protons as for the protons produced in reaction (2). The length of a recoil track can probably be determined more accurately because the track begins and ends in the chamber while disintegration protons usually enter the apparatus through windows. An accurate measurement of the stopping power of a window is unnecessary when measuring neutron recoils. The limit of accuracy of the neutron energy in the present experiment is principally set by the determination of the stopping power of the gas and not by the error in the extrapolated range of the recoil protons. The same error would have been encountered in measuring the ranges of disintegration protons instead of recoil protons.

The disintegration Q value of the reaction was found by the method of Livingston and Bethe.[5] In their symbols, the pure range straggling s for particles of this range is 2.03 percent. Since the neutrons were observed at 0°, the angular straggling is vanishingly small. The change in neutron energy between 0° and 6° is somewhat less than 6 kev and the angular straggling can, therefore, be neglected. The total straggling s'' was 2.04 percent. The thick target correction β was calculated to be 0.996 and hence $X_{\text{extr}}=0.52$. Consequently the difference between extrapolated and mean range is $0.52\times0.0204\times18.8=0.20$ cm. It follows that the mean range is 18.63 ± 0.34 cm. This corresponds to a proton energy of 3.53 Mev. The correction in the case of recoils which made angles of 0–10° to the direction of the neutron is $\frac{1}{2}E_2\chi_0^2=0.05$ Mev. Therefore the energy of the neutrons coming from the top layer of the target in the direction of the deuteron is 3.58 ± 0.03 Mev. The disintegration energy is then calculated from the relation $Q_1=(4/3)E_n-(1/3)E_H-(2/3)(2E_nE_H)^{\frac{1}{2}}$. The value of Q_1 is 3.31 ± 0.03 Mev.

This Q value is very close to the value 3.29 ± 0.08 which was previously reported by the writer.[6] However the probable error has been considerably reduced in these new measurements.

Mass of He^3 and the Instability of H^3

The difference between the mass of H^3 and He^3 can be found from reactions (1) and (2). By subtracting (1) from (2) we get

$$H^3-He^3=(n-H)+Q_1-Q_2.$$

Since all three of the terms are accurately known, the mass difference between H^3-He^3 can be accurately determined. The value $(n-H)$ is 0.00080 mass unit or 0.74 Mev[7] with a probable

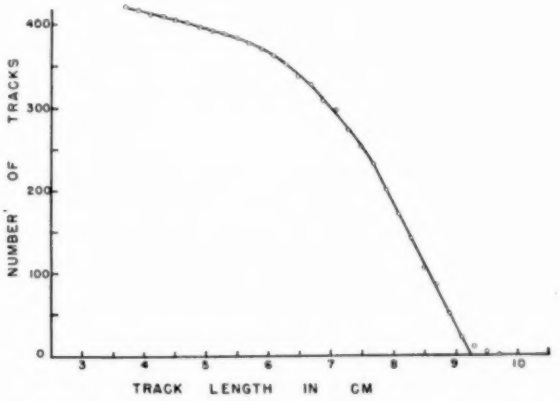

FIG. 2. The integral track-length *vs.* number curve for the recoil protons. The extrapolated track-length is 9.23 ± 0.10 cm. The corresponding extrapolated range is 18.83 ± 0.34 cm.

[5] M. S. Livingston and H. A. Bethe, Rev. Mod. Phys. **9**, 276 (1937).

[6] T. W. Bonner, Phys. Rev. **53**, 711 (1938).

[7] H. A. Bethe, Phys. Rev. **53**, 313 (1938); J. Chadwick, N. Feather and E. Bretscher, Proc. Roy. Soc. **163**, 366 (1937); F. T. Rogers and M. M. Rogers, Phys. Rev. **55**, 263 (1939).

error of 0.04 Mev. Q_2 is 3.98 ± 0.02 Mev.[8] The mass difference H^3-He^3 so computed is 0.07 ± 0.05 Mev. This indicates that H^3 should be unstable. The instability of H^3 was predicted by the writer[6] by this argument using the older value of $Q_1=3.29$ Mev.

Rumbaugh, Roberts and Hafstad[9] have pointed out the discrepancy between the value of Q_1-Q_2 and the value of Q_4-Q_3 as found in the following reactions

$$Li^6+n\rightarrow He^4+H^3+Q_3$$
$$Li^6+H\rightarrow He^4+He^3+Q_4.$$

An analogous relation between H^3 and He^3 is found from these reactions:

$$H^3-He^3=(n-H)+Q_4-Q_3.$$

Obviously Q_4-Q_3 should be equal to Q_1-Q_2. Rumbaugh, Roberts and Hafstad measured Q_3 as 4.97 Mev. From this value of Q_3 and Neuert's value[10] of $Q_4=3.72\pm0.08$ Mev they got a value of $Q_4-Q_3=-1.25$ Mev. This differs by 0.58 Mev from the value $Q_1-Q_2=-0.67$ Mev. Recently Perlow[11] has accurately redetermined Q_4. His value of Q_4 is 3.95 ± 0.06 Mev. This new measurement taken with the value of Q_3 of Rumbaugh, Roberts and Hafstad gives $Q_4-Q_3=-1.02$ Mev. This agrees better with the value Q_1-Q_2 than the previous value of Neuert. Still better agreement is obtained if we use the value of $Q_3=4.86$ Mev which was obtained by Livingston and Hoffman.[12] If we again use Perlow's value of Q_4 we find that $Q_4-Q_3=-0.91$ Mev and $H^3-He^3=-0.17$ Mev. This predicts a stable H^3. However, a radioactive H^3 and a stable He^3 have been discovered by Alvarez and Cornog.[13] Consequently it appears that there is still considerable error in the determination of Q_3 or Q_4.[14]

From the value of Q_1 and Q_2, H^3 is calculated to be unstable by 0.07 ± 0.05 Mev. The experimental value of the maximum energy of the β-rays from H^3 is 0.015 Mev.[13] This value of the instability of H^3 could hardly be in error by more than 10 kev and so this indicates a combined error in Q_1, Q_2, and $(n-H)$ of at least 0.04 Mev. This is not a serious discrepancy in view of the estimated probable errors of 0.02 in Q_2, 0.03 in Q_1 and 0.04 in $(n-H)$.

The mass of He^3 can be determined from a combination of the mass-spectroscopic mass of H^2, Q_1 and the mass difference $(n-H)$. This calculated mass of He^3 is 3.01698 ± 0.00006 mass units. An alternate and slightly more accurate method[15] to get the mass of He^3 is from the combination of Q_2, the mass-spectroscopic masses of H^2 and H^1 and the maximum energy of the β-rays from H^3. This gives the mass of He^3 $=3.01703\pm0.00004$ mass units.

[8] M. L. Oliphant, A. R. Kempton and Lord Rutherford, Proc. Roy. Soc. **149**, 406 (1935).

[9] L. H. Rumbaugh, R. B. Roberts and L. R. Hafstad, Phys. Rev. **54**, 675 (1938).

[10] H. Neuert, Physik. Zeits. **36**, 629 (1935).

[11] G. J. Perlow, Phys. Rev. **58**, 218 (1940).

[12] M. S. Livingston and J. G. Hoffman, Phys. Rev. **53**, 227 (1938). A preliminary account of these experiments, Livingston and Hoffman, Phys. Rev. **50**, 401A (1936), gave a value of $Q_3=4.67$ Mev. Perlow has pointed out that if this value of Q_3 is used the discrepancy disappears.

[13] L. W. Alvarez and R. Cornog, Phys. Rev. **56**, 613 (1939); R. D. O'Neal and M. Goldhaber, *ibid.* **58**, 574 (1940).

[14] Another chain of reactions involving reaction (2) and the reactions $L^6+H^2\rightarrow 2He+22.20$ Mev and $H^2\rightarrow n+H-2.17$ Mev together with the mass-spectrographic mass difference $(2H^2-He^4)$ gives a value of $Q_3=4.51$ Mev, if Bainbridge's masses are used. This indicates that it is probably Q_3 that is in error and not Q_4.

[15] In the calculation of the mass of He^3 from the energy of the β-rays from H^3, we have assumed that the rest mass of the neutrino is zero. If the rest mass of the neutrino is not exactly zero, the mass of He^3 so calculated will be in error by the amount of this rest mass.

Application of a Pressure Electrostatic Generator to the Transmutation of Light Elements by Protons

TOM LAURITSEN, C. C. LAURITSEN AND W. A. FOWLER
W. K. Kellogg Radiation Laboratory, California Institute of Technology, Pasadena, California
(Received November 1, 1940)

The design and performance of a pressure electrostatic generator capable of operating at 1.7 Mv in a cylindrical tank of over-all length 13′ 6″ and diameter 8′ at a pressure of 80 lb. per square inch is discussed. Studies of the gamma-radiation produced in the transmutation of F^{19}, N^{15} and C^{13} by protons are also reported.

INTRODUCTION

THE discovery of resonance processes in the transmutations of the light nuclei has necessitated the use in transmutation experiments of ion beams homogeneous in energy to a few kilovolts with total energies of several million volts. Herb[1] and his collaborators at the University of Wisconsin have demonstrated that the pressure electrostatic generator is capable of delivering over a microampere of analyzed ions with energies up to 2.6 Mev and homogeneous to one-half of one percent in energy, and have recently demonstrated that ions with energies up to 4.5 Mev, or even higher, can be secured without increasing the dimensions of the generator. The fact that these beams can be focused to a diameter of several millimeters even at relatively large distances from the generator has been shown to be a great advantage in regard to the accessibility of auxiliary apparatus, the freedom from extraneous radiation, and the possibility of high precision in employing point sources. During the past several years we have constructed and operated a pressure electrostatic generator similar in principle to the Wisconsin generator but differing in several details which merit some discussion at this time. Numerous electrostatic generators have been constructed and operated during this period. A short historical review of the development of the pressure electrostatic generator is included in a recent publication describing the generator of the Westinghouse Research Laboratories.[2]

[1] Herb, Parkinson and Kerst, Rev. Sci. Inst. **6**, 261 (1935); Phys. Rev. **51**, 75 (1937); Parkinson, Herb, Bernet and McKibben, *ibid.* **53**, 642 (1938); Herb, Turner, Hudson and Warren, *ibid.* **58**, 580 (1940).
[2] Wells, Haxby, Stephens and Shoupp, Phys. Rev. **58**, 162 (1940).

GENERAL DESIGN OF THE GENERATOR. THE HIGH POTENTIAL ELECTRODE AND PRESSURE VESSEL

The generator constructed in this laboratory differs from the Wisconsin generator in being vertical rather than horizontal. This choice of arrangement was dictated by two considerations; first, the high vacuum ion tube can be built completely self-supporting and free from vibrations of the moving generator apparatus, and second, a convenient laboratory arrangement has been found to be one in which the generator equipment is located on a floor above an observation room into which the target tube of the generator projects.

An essential difference in the design of the present generator is the use of a re-entrant system in which the charging belts are contained on either side of the accelerating tube in a four-cornered porcelain structure which supports the corona hoops and the hemispherical high potential electrode. The entire structure is enclosed within a cylindrical air pressure tank with standard belled ends as shown in Fig. 1.

The equipotentials in this type of generator should be somewhat pear-shaped with the top roughly hemispherical about the high potential terminal, the extension at the bottom being governed by a voltage distribution system to be described later. From the best estimates available, it was decided that a tube length, belt length and support member length of about 8 feet should be sufficient for 2 Mv at 5 or 6 atmospheres pressure. From a consideration of the electrostatic problem of a sphere within a sphere, simple computation shows that the minimum field at the surface of the inner sphere

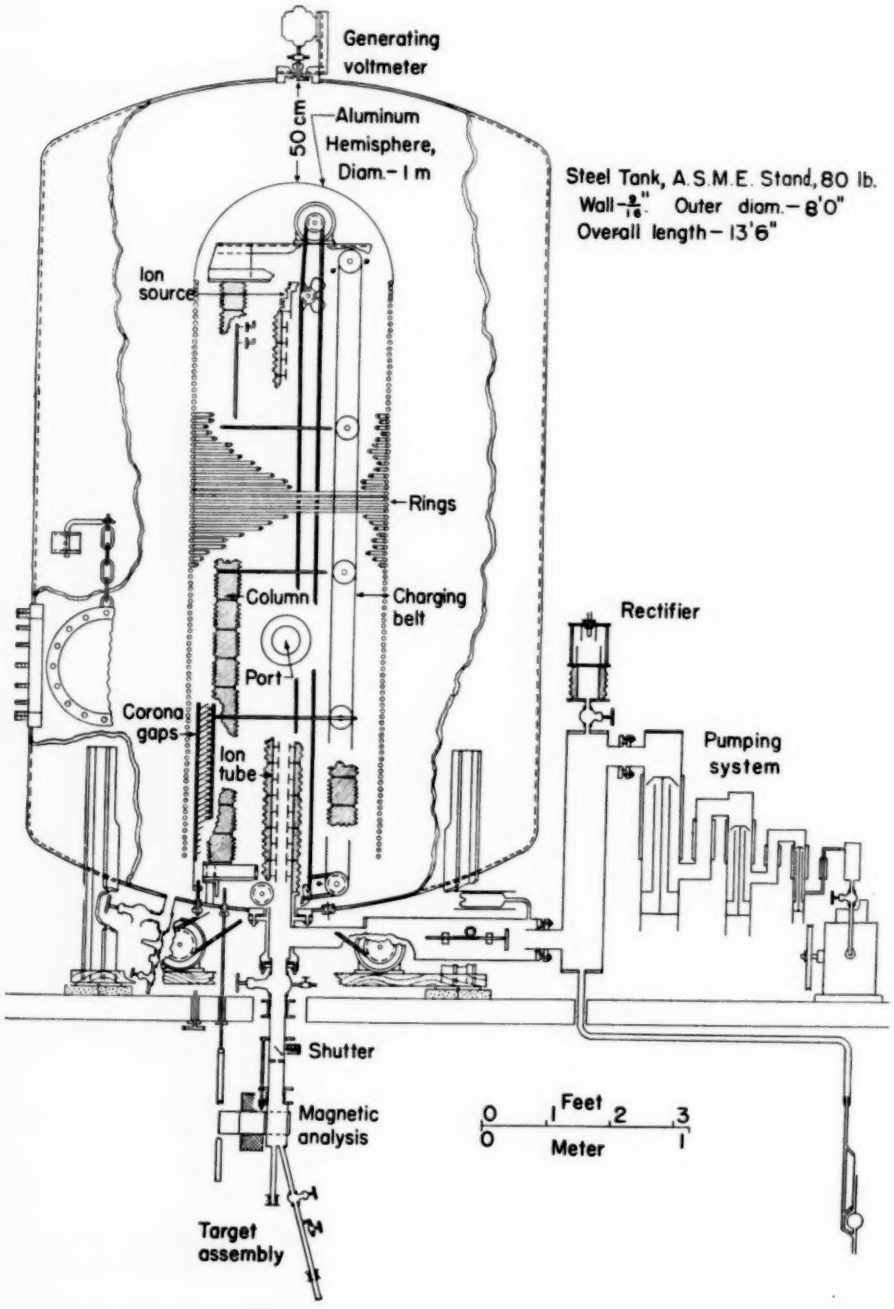

FIG. 1. The pressure electrostatic generator in elevation.

is obtained when the ratio of the radii is 1 : 2, and that at this value the field is twice that for a single, free sphere. Since the breakdown field is 30,000 volts per cm of radius for a free sphere at atmospheric pressure, and since one would expect a nearly linear increase for the first few atmospheres, a radius of 26.6 cm should be sufficient for 2 Mv at a pressure of 5 atmospheres. However, in view of the fact that one rarely gets within 50 percent of the theoretical breakdown expectations, because of the high fields at minor irregularities, an inner hemisphere of 50 cm radius was finally adopted. Because of the fact that the field does not depend critically on the

ratio of the radii near the minimum point, a distance of 60 cm from the terminal to the top of the tank, dictated by convenience, was specified. Subsequent alterations have reduced this distance to approximately 50 cm. From experiments with grounded walls arranged around a smaller generator constructed in open air, the conclusion was reached that the critical point would probably be at the junction to the cylindrical section, so the distance at this point was made 70 cm. For a 1 : 2 ratio of inner to outer diameters concentric cylinders have a field strength at the inner cylinder equal to 72 percent of the field strength at the inner sphere of concentric spheres of the same radii. However, it must be noted that hoops spaced by roughly their diameters make up the "cylindrical" surface in the actual generator, and that the field is thus higher. A high potential terminal somewhat more than hemispherical, supported on a cylindrical column of smaller radius is to be recommended. The hemispherical terminal was spun from aluminum sheet and was turned over a steel hoop of $\frac{5}{8}$-inch section diameter at the periphery. Such a terminal can be lifted easily out of place by one operator when work on the upper end of the generator is necessary. Electrostatic forces can also raise it so it must be held firmly to the generator structure. For convenience in construction, the tank[3] was made cylindrical, rather than pear-shaped, with standard dimensions of 8 feet diameter, 10 feet shell length and 13 feet, 6 inches over-all length, with an 18-inch manhole in the side near the bottom. The hemisphere was put in before the head was welded on; all other parts were put in through the manhole.

Supporting and Insulating Columns. Corona Hoops and Gaps

In the original construction all parts of the apparatus were supported on a square tower constructed of 2-inch$\times\frac{1}{2}$-inch strips of Bakelite. A laminated Bakelite with a paper base and resinoid binder was employed. At voltages near 1.0 to 1.2 Mv considerable sparking was observed along these Bakelite members and subsequent examination showed that sparking and burning had occurred inside the material between the laminations. The Bakelite columns have been replaced with columns consisting of 20 porcelain stand-off insulators connected end to end with $\frac{5}{8}$-inch steel studs. Horizontal steel supports at the quarter heights have been found to give sufficient mechanical stability.

Corona rings made of $\frac{5}{8}$-inch aluminum tubing rest in the corrugations of the porcelain insulators. Light springs in the bottom of the corrugations make contact between the porcelain surface and the rings. The rings can be snapped from corrugation to corrugation with some ease for making accessible the interior of the apparatus.

To improve the stability a set of negative point-to-plane corona gaps, adjustable from outside the tank, which serve to distribute the potential along the ring system, have been installed. The tube and the supporting columns are subdivided by conductors in the grooves of the porcelain elements. Each conductor is connected to a corresponding ring and between adjacent rings are connected the corona gaps. The necessity of electrical connections between all conductors and the gap system cannot be overemphasized.

The corona current constitutes the principal drain of the charge on the dome, and the large steady current flowing in the gaps minimizes the effect of small erratic discharges, and in this way helps to maintain a constant tube potential. The characteristics of the gap system are illustrated by the following data: When the tube is operating at 1 Mv, it is most convenient to use a tank pressure of 60 lb. per sq. in. and a gap separation of $\frac{3}{8}$ inch: under these conditions the current through the corona gap system is about 40 microamperes. To obtain a large corona current, the gap separation is kept as low as possible; of course, as the voltage is raised, the separation must be increased to prevent sparking. The corona current from a grounded needle, extending inward from a position on the wall of the tank just opposite the dome provides an additional current drain on the high potential end of the generator to improve still further the voltage stability. The length of the needle extending inside the tank wall may be varied during operation; it is normally about 1 inch. The

[3] The tank was fabricated by the Pacific Iron and Steel Company of Los Angeles. The wall thickness is $\frac{5}{16}$ inch and the working pressure is 80 lb. per sq. in.

corona current from the needle is of the order of 40 microamperes.

As a result of modifications which it has undergone, the ring system is at present in poor condition; the rings are not uniform in size nor true in shape, and the surfaces of some have been marred. It is believed that the replacement of the rings, especially those near the high potential end of the generator will increase the maximum operating potential. The size and shape of the porcelain elements of the supporting columns are such that an equal spacing of the rings is inconvenient. Moreover, with the present spacing, and with the focusing electrodes connected to the ring system, it is impossible to load equally the several sections of the tube. It is believed that when these conditions are rectified, an appreciable increase in maximum operating potential will be realized.

Charging System

From the best estimates available, it seemed that currents of the order of 200 to 300 microamperes would be necessary to give sufficient stability in the generator to permit a drain of several microamperes in the tube. Also, since there seemed reason to believe that such an outfit had possibilities for conversion into an x-ray installation for yielding therapeutically useful quantities of radiation, an effort was made to give all the current capacity possible, consistent with reasonable clearances in the system. A convenient arrangement was with two 24-inch belts symmetrically arranged about the center. A linear speed of about 4000 feet per minute was specified. Assuming, again, a breakdown field of 30,000 volts per cm at the surface of the belt, a saturation value of 2.7×10^{-9} coulomb per sq. cm is found, giving a theoretical expectation of about 600 microamperes per belt at atmospheric pressure, if the belt carries charge both up and down. Again, up to a few atmospheres, this value should increase almost linearly with pressure.

The belts were charged by means of a set of spray combs, consisting of a row of pins, spaced at $\frac{1}{4}$-inch intervals across the width of the belt, facing the metal roller on which the belt runs, and $\frac{1}{4}$ inch away. The combs were excited with 5000 to 20,000 volts d.c. which was brought in through an insulated lead-in bushing from a source outside the tank. In the original design, the rollers were covered with $\frac{1}{16}$-inch Bakelite sleeves on the theory that the high resistance of the Bakelite would act to stabilize the pin current, giving a more uniform spraying. These sleeves were later discarded. A doubling system[4] was used at the upper roller to pick up the charge from the belt and spray the downgoing side with charge of the opposite sign.

The mechanical problem of running such a wide belt required some care. The eventual solution was a crowning of about $\frac{1}{2}$ degree for 2 inches at each end of the roller and doubling over the edge of the belt for one inch at each edge. Provision was made for adjusting the tension and alignment on both top and bottom rollers. The rollers were made of 4-inch brass tubing with steel end plugs which carried ball bearings running on a fixed shaft mounted on adjustable hangers. Careful balancing was necessary to prevent excessive vibration. Power is transmitted to the bottom rollers by means of serrated vee belts from jack shafts which run through packing glands and are driven by two one-horsepower motors outside the tank. The belt tension was usually about 500 pounds.

Considerable attention was given to the matter of belt material. Canvas, electrical insulation paper, hospital rubber sheeting, and balloon fabric all gave roughly the same current, but mechanically the last two seemed best. The canvas having a rough surface and relatively large stretching, was difficult to drive at high pressure because of air friction; while the paper, having almost no flexibility, was unstable on the rollers. Hospital rubber sheeting with vulcanized joints at forty-five degrees was used for some time, but balloon fabric, because of its lighter weight and greater tensile strength, was finally adopted.

(*Note added in proof.*—A Tilton woven endless belt has recently been installed and found to be very satisfactory especially in regard to smoothness in running.)

The maximum charging current obtained, measured with the terminal grounded, was 360 microamperes per belt, at atmospheric pressure, representing about 60 percent of the theoretical expectation. This current was obtained with 24-

[4] Tuve, Hafstad, and Dahl, Phys Rev. **48**, 315 (1935).

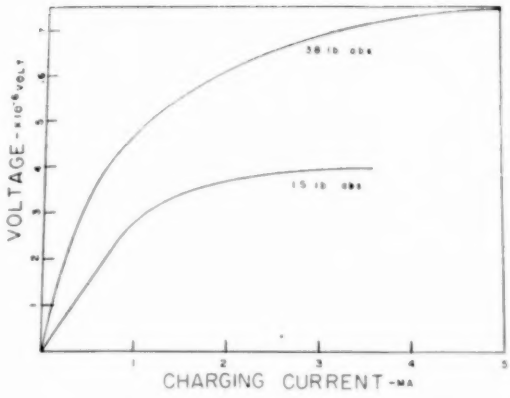

FIG. 2. Terminal voltage *vs.* charging current.

inch hospital sheeting belts, on Bakelite rollers. At fourteen pounds gauge pressure in the tank, a value of 600 microamperes was obtained. No attempt was made to go to higher currents as the attraction between the upgoing and downgoing sides of the belts caused severe rubbing, and the 1.2-milliampere total was considered ample. The voltage used on the spray combs was about 10,000 volts at atmospheric pressure, and increased roughly linearly with increasing pressure.

The charging current delivered by a belt varies to some extent with the dryness of the air. At humidities higher than 50 percent, the current is low and sometimes unsteady. It seems, however, that the surface recovers rapidly on drying: Unless the exposure to humid air has been more than a few hours, an hour or so suffices for drying. Tests on surface leakage, made with a condenser-electrometer arrangement, indicated that the recovery of surface resistivity is not so rapid, taking in some cases a matter of days. Also, it has been found that belts of relatively high leakage along their lengths may still carry as much as half the maximum current; on one occasion a belt which had gotten some calcium chloride solution on it by accident was found to deliver over 100 microamperes, in spite of the fact that it could not maintain more than a few thousand volts along its length. The leakage was clearly seen in a series of streamers, extending from top to bottom and illuminating the whole belt. These facts force one to the conclusion that the charging current does not depend greatly on the surface resistivity of the belt. The fact that a canvas belt, having a very rough surface, gave nearly as much as a smooth rubber belt seems to indicate that the character of the surface is also not very important in this respect.

Considerable trouble was encountered with the Bakelite sleeving on the rollers. It was found that at extremely low humidity, less than 20 percent, the belts completely ceased to charge, and would not draw current on the spray combs, regardless of the spray voltage applied. Letting in moist air did not help unless it was allowed to remain for a day or more. Wiping the Bakelite with damp hands produced immediate, but not complete, cure. The conclusion was reached that the Bakelite became dried out to such an extent that it remained charged in such a way as to prevent charges from leaving the spray comb and charging the belt, effectively neutralizing the spray voltage. A similar difficulty had never been observed in operating the smaller generator in air. It was found that a wire stretched over the top of the roller in such a way as to collect this surface charge as the roller rotated made it again possible to charge the belts. Removing the Bakelite completely cured the trouble, and it has never recurred, regardless of the humidity in the tank. With bare metal rollers, it was necessary to raise the spray comb slightly above the point of tangency to prevent the charge from leaking through the belt. With this arrangement on both top and bottom, the maximum current obtained was 280 microamperes per belt. The spray voltage required was, of course, very much lower, about 5000 volts.

A large amount of the original difficulty in obtaining consistent charging was found to be due to electrical leakage in the doubling system. Because of the rather high voltage—5000 to 10,000 volts—necessary, corona from sharp points on the doubler assembly or the frame connected to the terminal was a definite limitation until the points were filed off. It was also found that the Bakelite insulation was not good enough and hard rubber was substituted. Tests with a "megger" delivering about a thousand volts, showed the resistance to be as low as 20 megohms, while, to maintain 10,000 volts with a current of 100 microamperes, a resistance of 100 megohms is necessary. In order to pick up the requisite current, it proved necessary to move the pick-up combs several inches below the point of

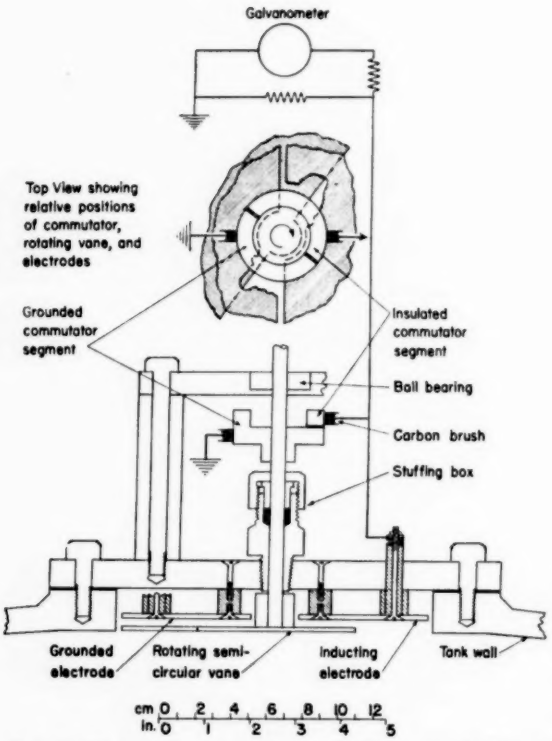

FIG. 3. The generating voltmeter. The grounded sector is driven by a $\frac{1}{3}$-hp induction motor not shown in the figure.

tangency on the roller. With these modifications, the doubler operated quite consistently without outside control, as long as the current was over 100 microamperes.

Something about the stability of the generator and the possible current drain can be learned from the plot of terminal voltage against charging current shown in Fig. 2. It is to be observed that the first linear rise is typical of an ohmic resistance load, while the abrupt flattening is indicative of the onset of corona. The plateau from about 200 microamperes to the maximum value of 600 represents the current which can be drawn —for example, down the tube—without seriously affecting the voltage, and in this region, variations in the current affect the voltage only slightly, giving a high degree of stability to the system.

When the Bakelite supporting column was replaced by porcelain it was found necessary to reduce the belt width to 16 inches. One belt was removed entirely. Sparking down the remaining belt occurred for voltages near 1 Mv for charging currents exceeding 100 microamperes. The situation was greatly improved by the installation of three sets of guides, equally spaced along the belt. Each set consisted of four $\frac{3}{4}$-inch rods in a horizontal plane, two, separated by $\frac{1}{2}$ inch, serving to guide each side of the belt. They were connected to the nearest member of the ring system, and by their subdividing action tended to equalize the potential gradient along the belt and thus to eliminate high local fields. This arrangement was suggested to us by Dr. E. U. Condon of the Westinghouse Research Laboratories who had successfully employed this method. However, the charging belt was the seat of still another trouble: Its flapping produced voltage fluctuations. The guides could not be effective in preventing this without pressing firmly against the belt, and this was objectionable because of the excessive friction and injury to the belt which it entailed. Therefore each set of guides has been replaced by a single 4-inch roller, similar to the two upon which the belt runs, mounted between the two sides of the belt. They play the same role as the guides in distributing the potential along the belt, and in addition greatly improve the mechanical smoothness of the belt operation.[5]

Air for the tank is secured from the compressed air line of the Radiation Laboratory and is dried by passing over flaked calcium chloride. The air is also circulated over a pan containing potassium hydroxide on the floor of the tank.

VOLTAGE CONTROL AND MEASUREMENT

Voltage control is effected by varying the voltage applied to the spray combs, and hence the charging current. The voltage may also be controlled by adjustment of the corona gaps on the tube or of the corona needle in the side of the tank. For larger changes in voltage it is preferable to change the tank pressure. At high tank pressures the molecular beam can be used in the lower voltage region.

In view of the great importance of accurate and reproducible voltage measurement in some of the experiments for which the generator was intended, some care was taken in designing the voltmeter. Of the several possibilities, the generating

[5] When the belt is damp, charge cannot be delivered past the first roller. However, this condition never prevails for a time longer than that necessary to pump up the tank to operating pressures and is thus not a serious inconvenience.

electrostatic voltmeter seemed the best because of its zero current drain and its proven reliability.[1] The design finally adopted is shown in Fig. 3: A grounded semicircular sector, driven by an induction motor, alternately covers and uncovers an insulated semicircular plate in the top of the tank facing the terminal hemisphere. The use of a synchronous motor was found to result in the rectification of stray alternating-current fields. The current from the stationary plate is rectified by means of a commutator and carbon brush and is measured by a galvanometer with high resistance in series to minimize currents from contact potentials and shunted to give a convenient sensitivity. To insure recharging of the stationary plate a second brush connects it to the tank on the off half-cycle.

The voltmeter has been calibrated from time to time usually by bombarding thick targets of CaF_2 with protons in the region of the 862-kv and 927-kv resonances. Even over extended periods of time the voltmeter calibration has been reproducible within 1 percent accuracy. A calibration run in which a thick lithium target was bombarded with the molecular beam and a thick calcium fluoride target with the atomic beam indicated that the values 880, 862 and 927 kv for the well-known resonances in these cases are internally consistent to better than 0.5 percent. Additional observations on the resonances on $F^{19}+H^1$ at 334 kv and 1363 kv, and in Li^7+H^1 at 440 kv checked the linearity of the voltmeter scale to 1 percent. The laboratory intercomparison standards first set up by Tuve[6] and collaborators and extended by Herb[7] have been of inestimable value in the work with this generator.

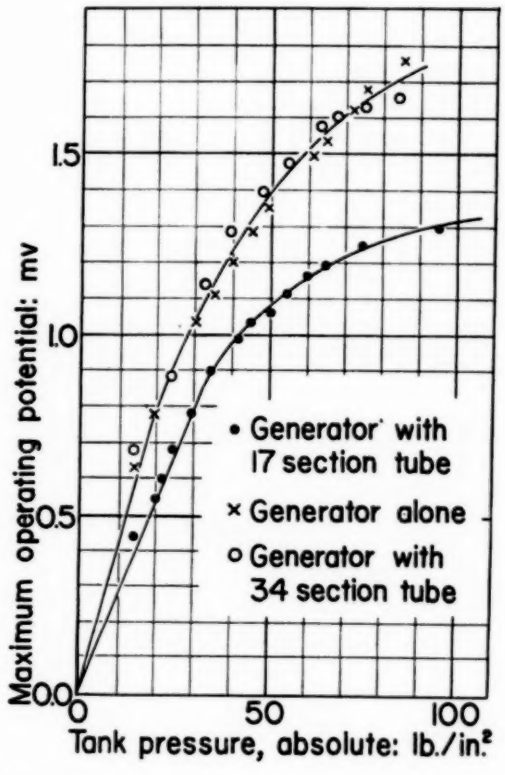

FIG. 4. Maximum operating voltage *vs.* tank pressure.

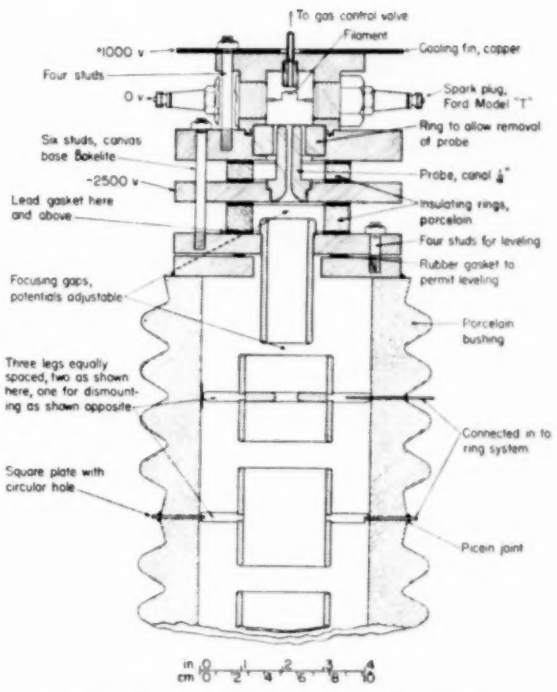

FIG. 5. The ion source and first tube sections.

ACCELERATING TUBE

In the selection of the type of tube to be used, an appeal was again made to previous experience. The use of the short ion path tube in this laboratory has shown its advantages of less critical focusing and comparatively large ion currents because relatively few of the ions suffer collisions in the residual gas in the tube, even when the vacuum is not perfect. The difficulty in the electrostatic generator of distributing the potential in the tube would tend to offset these

[6] Hafstad, Heydenburg and Tuve, Phys. Rev. **50**, 504 (1936).

[7] Bernet, Herb and Parkinson, Phys. Rev. **54**, 398 (1938).

advantages however: An excessively large tube diameter would be required to provide for the necessary telescoping full length shields. The long ion path tube, on the other hand, having a large number of small steps in voltage, is readily adaptable to this construction where the steps are available and space is at a premium; and the experience of Herb and Tuve has shown that focusing is not such a problem as was formerly thought.

The determination of the best number of accelerations for such a tube is rather arbitrary: For minimum aberration in the lenses the requirement is that they be long in comparison with their diameters, and it did not seem likely that the beam would be held smaller than a few cm in diameter if one used the full angular spread of the beam emerging from the ion source. Accordingly, the focusing sleeves were made 2 inches in diameter, $5\frac{5}{8}$ inches long, and spaced $\frac{3}{8}$ inch apart in 6-inch tube sections. To secure maximum possible pumping speed consistent with clearance from the outside of the tube to the belts, an inside diameter of 4 inches was specified for the tube. The sections were made of porcelain, with annular corrugations on the outside, smooth on the inside, and glazed all over. Joints were made with Picein wax, without gaskets. With the $5\frac{5}{8}$-inch focusing electrodes the tube consisted of seventeen accelerating sections. The maximum operating voltage was found to be 1.3 Mv and after numerous attempts in redistributing the voltage had failed to raise this maximum it was decided that the potential was limited by breakdown inside the tube. Examination of the focusing electrodes showed their surfaces at the ends to be pitted, thus confirming this view. To remedy this situation the cylindrical focusing electrodes have been replaced by another set in which the size of the gaps was increased from $\frac{3}{8}$ inch to $\frac{5}{8}$ inch, and their number doubled. The maximum operating voltage has been increased from 1.3 to at least 1.7 Mv; the results of the tests of the operating voltage are shown in Fig. 4. The dimensions of the new electrodes differ from the old only in that the length is 2 inches. This alteration introduced no difficulties in focusing. From our experience the maximum operating voltage is 75 kv per section with 50 kv per section a safe limit.

The ion source (Fig. 5) used was copied from the type formerly used at this laboratory on other tubes.[8] In it the electrons emitted from the hot filament are drawn by a potential of 1000 volts through a region at a pressure of the order of 10^{-3} mm of Hg of the gas to be ionized, and the ions so formed drawn out by a probe at a negative potential of 2500 volts. A canal in the probe allows some of the ions to get out into the tube where they are accelerated by the main field. For focusing, two small accelerations are provided, controllable from outside the tank by means of adjustable needle gaps. To bridge between the $\frac{1}{16}$-inch diameter of the canal and the 2-inch diameter of the sleeves in the tube, the first focusing sleeve was made 1 inch in diameter and is connected to the first ring below the terminal. The second accelerating shield is connected to the second ring. The remainder of the gaps are connected to corresponding corona gap sections.

Power for the ion source is supplied by two transformer-rectifier sets excited by a 500-cycle, 500-watt airplane generator which is driven by a long serrated vee belt. The ion source is cooled by a small fan. The filament, a seven-turn helix of 0.013-inch tungsten, is heated by means of a low voltage transformer, and its temperature, controlled from outside by means of a rheostat, determines the current at any given gas pressure. Gas is supplied from a small tank at high pressure and controlled from outside by a rubber disk valve. All controls are brought down by $\frac{3}{4}$-inch hard rubber rods with steel extensions passing through packing glands in the tank. Rod was chosen in preference to tubing because of the possibility of sparking down the inside of the tubing.

The tube is exhausted by three oil diffusion pumps in series, with a Cenco Hypervac as forepump. The oil pumps have successive diameters of 3, 5 and 8 inches. Valves placed at strategic places in the pumping line and target assembly make it easy to isolate and find leaks in the vacuum system. Brass, wedge-disk, gate valves with nonrising stems have been found to be convenient for this purpose.

The Production of X-Radiation

As has been indicated, some time was spent in investigating the possibilities of the installation

[8] Crane, Lauritsen and Soltan, Phys. Rev. **45**, 507 (1934).

as a source of x-rays. For this purpose, the ion source was connected in such a way as to emit and focus electrons, rather than positive ions. Since, according to the theory of ion optics, focusing depends only on the relative voltages on the lenses, and not at all on the mass of the ions, except for relativistic effects, the main lens system of the tube is suitable either for electrons or positive ions.

It was found that the voltages on the first and second gaps (17-section tube) should be reversed for best operation and that, unless these voltages were fixed by a power supply, electron bombardment could change them and the focal spot would pulsate. Good focusing was obtained by accelerating the electrons to 200-volt energy with the probe, then to 600 volts with the first gap, and then decelerating them back to 200 volts with the second gap. The second gap voltage was found to be quite critical for focusing.

The remainder of the gaps were at the voltage naturally taken up by the corresponding tube sections and did not greatly affect the focusing. With electrons, once the voltages were set, the focusing was quite automatic: No controls were necessary and the spot remained very nearly the same in size and in position from day to day. As the spot was only observed by means of a fluorescent screen on the under side of the target, no precise measurement of its size could be made, but it was certainly less than 5 mm in diameter.

Because of the fact that electrons have a relatively long mean free path, it was possible to obtain high currents and good focusing without much trouble with tube vacuum. Satisfactory operation was obtained at pressures of several times 10^{-5} mm of Hg. Considering that the electrons must travel nearly twelve feet, it would not be surprising if some fraction of the beam was lost. Actually, on some occasions, as much as 300 microamperes of electrons hit the 2-inch target, mostly within a 5-mm spot, with a belt charging current of 600 microamperes at something over 500 kv. The most consistent performance, however, was with about 100 microamperes of electrons at a maximum voltage estimated to be about 1.3 Mv.

The x-ray output, using a gold target, was measured by means of a thimble chamber calibrated against an open air chamber. The maximum output, at 1.3 Mv and 100 microamperes, was 17 roentgens per minute at 60 cm with 1 mm Cu and 0.5 mm Au filtration. Points taken at other voltages indicated that the output per unit current follows roughly a square law as would be expected for unfiltered radiation. Experiments with filters revealed that a filter of 1 mm Pb would make a monochromatic equivalent value in the neighborhood of 800 kv, or only slightly lower than that given for filtered radium radiation (1 Mev). With a filtration of 1 mm Pb and 6 mm Fe, the output was 4.0 r per minute, or about eight times the efficiency obtained with the x-ray tube in the Kellogg Laboratory running at 1 Mv peak alternating current. If one assumes a cubic law for the efficiency of production of filtered radiation, this value is quite reasonable.

Since an output of 15 roentgens per minute is quite adequate for therapeutic purposes, the conclusion is that, once the machine is made to run consistently, with a minimum of maintenance, it is quite feasible as an x-ray source operating between 1 and 2 Mv. Subsequent to the development of this machine, Trump and Van de Graaff[9] have published a description of a more compact unit operating at 1.25 Mv and 1 ma with an output of 250 roentgens per minute per milliampere of target current at 50 cm with 2 mm of Pb and 5 mm of Cu filtration.

The Production of Ions

The ion source has been previously described in this discussion. The ions made in the gas by the electron current are drawn out by the probe at -2500 volts and are focused by variation of the voltage on the first shield, which is connected to the first ring below the terminal. This voltage, about $-10{,}000$ volts, can be varied by means of a needle corona gap and is the principal adjustment. The potential on the next accelerator is also variable, from about $-10{,}000$ to $-30{,}000$ volts. The remainder of the accelerators are controlled together by the main corona gap system, and have little effect on the focusing. In normal operation, the electron current in the ion source is between 50 and 200 milliamperes and the ion current to the probe of the order of 1 milliampere. The currents to the shields are low in comparison to the general flow down the corona gaps.

[9] J. G. Trump and R. J. Van de Graaff, Phys. Rev. **55**, 677 (1939).

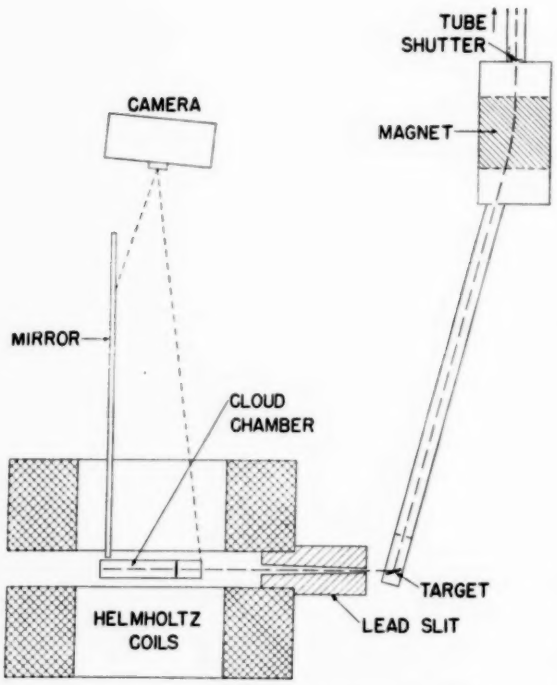

FIG. 6. Cloud chamber and target assembly.

A great deal of difficulty was caused by the distortion of the beam by asymmetry in the tube. It was thought that this effect might be corrected by lining up the tube more accurately, but it was soon evident that mechanical lining up was not sufficiently good. Tests were then made with various tube sections shorted out and the motion of the beam noted. The worst offending section was then corrected and, by this empirical process, the beam brought to the center of the target. For some reason, possibly because of stray charges on the interior of the porcelain, the position of the beam still is rather uncertain, changing a few millimeters in position from day to day, or with changes in voltage. In order to use the beam, it was necessary to put a sylphon in the target tube and move the entrance slit of the magnetic analyzer to suit the spot. A second sylphon made it possible to adjust the relative positions of entrance and exit slits. The beam was deflected through 15° in the magnetic analyzer. The mass 2, 3, and 4 beams of $\frac{1}{4}$-inch diameter are just separable with the analyzer in which the effective diameter of the analyzing field is 4 inches and the exit slit is 3 inches below the lower edge of the field. Holes of $\frac{1}{4}$-inch diameter drilled in 1-inch disks of $\frac{1}{16}$-inch thick fused quartz are used as slits. Lucite windows in the target tube make it possible to view the fluorescence of the quartz under bombardment and thus to locate the position of the beam.

The requirements on tube vacuum for a good ion beam are rather stringent. It is impossible to work with a residual pressure of more than 10^{-5} mm of Hg and for best operation a "sticky vacuum," better than 10^{-6} mm is necessary. These readings are, of course, taken near the pumping system and do not necessarily indicate the exact conditions in the tube; particularly near the top end, where the gas is let in, the pressure may be as high as 10^{-4} or 10^{-3} mm of Hg.

We have secured total unanalyzed currents up to 10 microamperes, mass one beams of hydrogen up to 1.5 microamperes, and mass two beams up to 2.5 microamperes. As the hydrogen pressure in the ion source is increased, the ratio of mass one to mass two beams increases.

Disintegration of F^{19} by protons

A complete discussion of the disintegration of F^{19} by protons is included in the next article of this issue of *The Physical Review*. We propose to discuss here only the measurements of the energy of the radiation produced in the reaction

$$F^{19}+H^1\rightarrow{}^{\gamma}Ne^{20}\rightarrow{}^{\gamma}O^{16}+He^4$$
$$^{\gamma}O^{16}\rightarrow O^{16}+h\nu, \qquad (1)$$

where the superscript, γ, refers to those states of Ne^{20} or O^{16} involved in the production of the 6.2-Mev gamma-radiation. The gamma-radiation has been shown to exhibit resonance at proton bombarding energies of 0.334, 0.479, 0.589, 0.660, 0.862, 0.927, 1.335 and 1.363 Mev.[7] The emission of short range alpha-particles has been definitely established at the first five resonances[10] and unpublished work in this laboratory indicates that it also occurs at the remaining three. The energy release[10] in the reaction has been determined to be 1.74 Mev and since the energy release of the reaction involving long range alpha-emission is 7.95 Mev[11] the predicted gamma-ray energy is 6.21 Mev with an uncertainty of approximately 0.2 Mev. A necessary consequence of the process envisaged in reaction (1) is that the

[10] McLean, Becker, Fowler and Lauritsen, Phys. Rev. **55**, 796 (1939); W. E. Burcham and C. L. Smith, Nature **143**, 795 (1939); W. E. Burcham and S. Devons, Proc. Roy. Soc. **173**, 555 (1939).

[11] Burcham and Smith, Proc. Roy. Soc. **168**, 176 (1938).

alpha-particle energy but not the gamma-ray energy should vary with the resonance energy of the protons. That the alpha-particle energy does vary in the predicted manner has been demonstrated at Cambridge at certain of the lower resonances and confirmed and extended to higher resonances in this laboratory. This section is a discussion of cloud-chamber measurements of the gamma-ray energy at various resonances and is a more detailed discussion of results previously reported.[12] Results similar to those reported here have also been secured at Cambridge[13] with coincidence and spectrograph methods.

The cloud-chamber method of determining gamma-ray energies from the energy of secondary pairs has been discussed in detail in previous reports from this laboratory. The exact experimental arrangement used in these experiments is shown in Fig. 6. The gamma-ray beam was collimated with lead slits and a thin aluminum window was set in the wall of the cloud chamber nearest to the target. A 10-mil Pb lamina was used as secondary emitter. The loss of energy of a fast electron in traversing such a lamina is approximately 0.3 Mev. In order to reduce as far as possible the error caused by fluctuations in the magnetic field, the coil current was read during nearly every expansion by means of a null potentiometer and held constant to $\frac{1}{2}$ percent. The absolute value of the field was checked against an accurate standard solenoid by means of a search coil and a Grassot fluxmeter several times during the course of the experiment and is considered to be accurate to better than 1 percent. The remaining error due to spread in measurement of the tracks was brought to the same order of magnitude as the magnetic field uncertainty by counting enough pairs.

TABLE I. *Results of gamma-ray energy measurements.*

PROTON ENERGY (KEV)	TARGET	RESONANCES INVOLVED (KEV)	NO. OF PAIRS	MEAN ENERGY (MEV)
425	Thick	334	33	6.17±0.10
950	Thick	All≤927	93	6.30±0.06
950	Semi-thick	862,927	29	6.13±0.09
1400	Semi-thick	1335, 1363	49	6.03±0.09
All pairs			204	6.19±0.04

[12] Lauritsen, Fowler and Lauritsen, Phys. Rev. **56**, 858 (1939).
[13] Dee, Curran and Strothers, Nature **143**, 759 (1939).

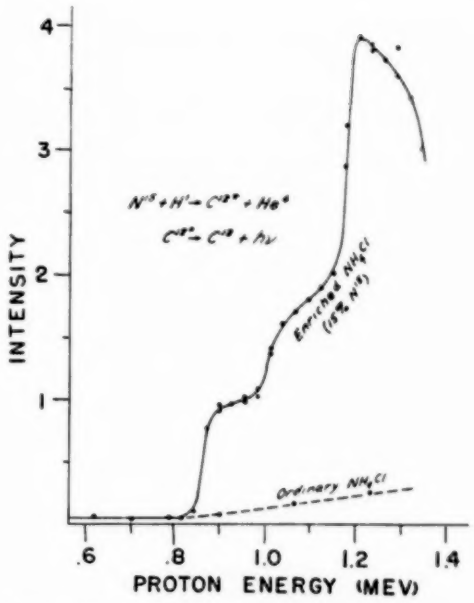

FIG. 7. Excitation curve for gamma-radiation from $N^{15}+H^1$.

The results for various bombarding energies and various targets are shown in Table I. The resonances involved in each experiment are indicated in the third column, the number of pairs measured in the fourth column, and their mean total energy in the fifth. The estimated uncertainty is the mean deviation from the mean divided by the square root of the number of pairs measured. These results indicate that within the statistical uncertainty of approximately 0.1 Mev there is no dependence of gamma-ray energy on the resonance energy of the protons. It is to be pointed out however that these results contain no information on the nature of the radiation produced by protons in the region of bombarding energies from 1.1 to 1.3 Mev. The mean of all the measurements is 6.19±0.04 Mev which, upon including a possible systematic error of 1 percent and rounding off, can be taken as 6.2±0.1 Mev. The deviation from the mean was approximately 0.6 Mev so that no structure in the gamma-ray line involving smaller separations than this would be revealed by these experiments. Recent experiments in this laboratory on the short range alpha-particles reveal no structure in the radiating state of O^{16} to even smaller limits.

At the higher bombarding energies (950 and 1400 kv) there is some evidence for a line at 10.5 Mev but it is certainly less than 5 percent of the

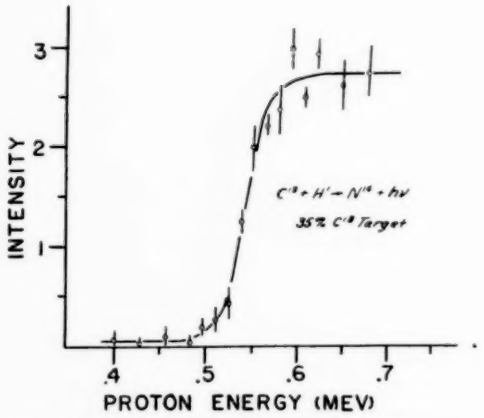

FIG. 8. Excitation curve for gamma-radiation from $C^{13}+H^1$.

main line and could conceivably be due to calcium or to boron contamination. However, it is possible that one or more of the higher resonances allows a weak radiative transition to a 3-Mev state in Ne^{20} with the emission of a 10.5-Mev line and then a further drop to the ground state. In such a case one would not expect to find many low energy pairs because of the low cross section for pair formation at that energy. The few low energy pairs observed can be attributed to radiation degraded by scattering in material surrounding the cloud chamber.

Disintegration of N^{15} by protons[14]

The production of gamma-radiation by the bombardment of N^{15} by protons up to 1.4 Mev in energy has been studied using targets of ammonium chloride containing 14.8 percent N^{15} supplied to us by Professor H. C. Urey and Dr. Harry Thode of Columbia University. The excitation curve for a thick target is shown in Fig. 7 and indicates resonance (half-width ≤ 20 Kev) in the gamma-ray production at proton energies of 0.88, 1.03 and 1.20 Mev. The yields above resonance were found to be 0.4, 0.3 and 1.2×10^{-7} quanta per proton, respectively. The yield from ordinary ammonium chloride targets was small compared to the yield from the enriched targets. Cloud-chamber investigations of the electron and pair secondaries produced in thin lead and carbon laminae by the gamma-radiation indicate that it consists mainly of a line at 4.4 ± 0.2 Mev. This line is to be attributed to the reaction $N^{15}(p, \alpha)C^{12*}$, an excited state in C^{12} at this energy being well known.

Disintegration of C^{13} by protons[15]

The gamma-radiation showing resonance at 560 kv in the bombardment of carbon by protons has been attributed[16] to the reaction $C^{13}(p, \gamma)N^{14}$ for which $Q=8.2$ Mev because the observed energy of the radiation (7.4 Mev) was greater than the available energy in the reaction $C^{12}(p, \gamma)N^{13}$ for which $Q=2.6$ Mev. We have confirmed this conclusion by bombarding a carbon target containing approximately 35 percent C^{13} prepared for us by Dr. C. H. Townes and Professor W. R. Smythe of the California Institute. The excitation curve is shown in Fig. 8. Under the conditions of the experiment the radiation from $C^{12}(p, \gamma)N^{13}$ at 420 kv was not detectable. With an ordinary carbon target the same would have been true of the $C^{13}(p, \gamma)N^{14}$ radiation.[6] Cloud-chamber investigations of the secondary electrons and pairs produced in thin lead and carbon laminae by the gamma-radiation indicate that it consists of three lines at 2.8 ± 0.4, 5.4 ± 0.3 and 8.1 ± 0.2 Mev of approximately equal intensity. These results substantiate the analysis made by Rose[17] of the absorption curves measured by Dee and his collaborators. It is to be concluded that the excited state of N^{14} at 8.1 Mev radiates to the ground state directly or through an intermediate state at 2.8 or 5.4 Mev with equal probability.

(*Note added in proof.*—The recent results of Bonner, Becker, Streib and Rubin as communicated at the Pasadena Meeting of the American Physical Society in December, 1940, indicate that the intermediate state in N^{14} is at 5.4 Mev.)

In conclusion we wish to thank Mr. J. F. Streib who collaborated in recent improvements on the generator and who kindly prepared many of the figures accompanying the text.

[14] W. A. Fowler and C. C. Lauritsen, Phys. Rev. **58**, 192 (1940).

[15] C. C. Lauritsen and W. A. Fowler, Phys. Rev. **58**, 193 (1940).

[16] Dee, Curran and Petržílka, Nature **141**, 642 (1938).

[17] M. E. Rose, Phys. Rev. **53**, 844 (1938).

The Transmutation of Fluorine by Protons

J. F. STREIB, W. A. FOWLER AND C. C. LAURITSEN
W. K. Kellogg Radiation Laboratory, California Institute of Technology, Pasadena, California

(Received November 1, 1940)

The excitation functions for the production of long range alpha-particles, gamma-rays, and electron pairs by the bombardment of F^{19} by protons have been observed simultaneously up to a bombarding energy of 1.5 Mev. The long range alpha and pair curves exhibit resonance peaks superimposed on a background of increasing intensity with increasing bombarding energy. Approximate coincidence in two instances of pair and alpha-resonances suggests that full range alphas and the short range alphas preceding pair emission can be products of competing modes of decay of the same intermediate states of Ne^{20}. This in turn suggests that the state of O^{16} which decays by pair emission has the same parity (even) as the ground states of O^{16} and thus that the pair emission can be due to ordinary electromagnetic forces. The absolute yields of the various processes have been measured and a discussion of the measurement of high energy gamma-ray and pair yields by means of electroscopes is given. The large ratio of gamma-ray yields to long range alpha and pair yields previously observed has been confirmed.

INTRODUCTION

THE transmutation of fluorine by protons has been of considerable experimental and theoretical interest from the very beginnings of nuclear research employing particles accelerated to high velocities by modern electrical methods. The abundant yield of the reactions resulting from the bombardment of fluorine by protons and the fact that naturally occurring fluorine consists of only one isotope (at least to within 1 percent) have been of great advantage to the experimental nuclear physicist. Excited states of Ne^{20} are the intermediate products of the bombardment, while states of O^{16} along with the ground state of He^4 are the final products in the most important cases. Knowledge of the states of these "completed shell" or "alpha-model" nuclei with their particular properties of symmetry in neutrons and protons will be of great importance in the development of an adequate theory of nuclear structure.

The long range alpha-particles

In their report of their early work on disintegration by artificially accelerated particles Cockcroft and Walton[1] announced the production of alpha-particles in the bombardment of fluorine with protons. Similar observations were made by Oliphant and Rutherford.[2] The range of the alpha-particles was less than that observed by later investigators and it is possible that they were spurious, being due to some contaminant.[3] The first observation of alpha-particles which has been consistently verified was by Henderson, Livingston and Lawrence.[3] These observers reported a single alpha-particle group of range 6.7 cm; this was obtained with protons of 1.2 Mev energy. Burcham and Smith[4] have since made a more careful determination of the range; with a proton energy of 0.85 Mev, the alpha-particle range in a direction perpendicular to the beam was 5.90 cm, which corresponds to an energy release of 7.95 Mev; again only a single group was found.

It is now certain that the origin of these alpha-particles is the following reaction:

$$F^{19}+H^1\rightarrow{}^{\alpha}Ne^{20}\rightarrow O^{16}+He^4. \qquad (1)$$

In this equation, the superscript α designates a particular kind of excited state in the intermediate Ne^{20} nucleus which may decay with long range alpha-emission corresponding to the full energy available in the reaction.

In their experiment, Henderson *et al.* found a rapid increase in the yield as the proton energy was increased from 0.7 to 1.5 Mev. Burcham and Devons[5] made a more precise investigation of the excitation curve for proton energies from 0.53 to 0.93 Mev; in addition to a continuous increase

[1] J. D. Cockcroft and E. T. S. Walton, Proc. Roy. Soc. **A137**, 229 (1932).
[2] M. L. E. Oliphant and Lord Rutherford, Proc. Roy. Soc. **A141**, 259 (1933).
[3] Henderson, Livingston and Lawrence, Phys. Rev. **46**, 38 (1934).
[4] W. E. Burcham and C. L. Smith, Proc. Roy. Soc. **A166**, 176 (1938).
[5] W. E. Burcham and S. Devons, Proc. Roy. Soc. **A173**, 555 (1939).

in yield with increasing bombarding energy, they found two resonances at 0.72 and 0.83 Mev.

Gamma-radiation and the short range alpha-particles

McMillan[6] first observed gamma-radiation produced in the bombardment of fluorine with protons. The earliest estimates of the energy of this radiation were based on measurements of its absorption in lead. They were made by McMillan[7] and by Crane, Delsasso, Fowler and Lauritsen,[8] who employed ionization chambers and electroscopes to measure the intensity. The value of the absorption coefficient in lead, 0.49 cm^{-1} gave, according to the Klein-Nishina theory of the Compton effect, a quantum energy of 2 Mev. However, the origin of such a gamma-ray could not be accounted for. Oppenheimer suggested that the inferred value of the energy was too low, and that the absorption was due not only to the Compton effect, but also to pair production. Measurements of the absorption in other elements, tin, copper and aluminum, showed that this suggestion was correct; the results obtained were all consistent with, and uniquely determined the value of approximately 5.4 Mev for the quantum energy.

The technique of these measurements is open to serious criticism.[9] The radiation removed from the beam by the absorber is partly replaced by a secondary radiation whose presence makes the interpretation of the measurements difficult. This objection is eliminated in a method introduced and employed by Delsasso, Fowler and Lauritsen.[10] The gamma-radiation ejects pairs from a thin lead radiator in a cloud chamber; on alternate expansions the beam is passed through the absorbing body; the energy of each pair can be determined from the curvature in a magnetic field of the paths of the two members with sufficient accuracy to decide whether or not it was produced by the primary gamma-ray. The transmission of the absorber is the ratio of the number of full energy pairs produced with the absorber in the beam to the number produced with the absorber removed. In this way the value 0.4 ± 0.1 cm^{-1} was obtained for the absorption coefficient in lead. Using this same method Halpern and Crane[11] found the absorption coefficient in aluminum to be 0.062 ± 0.009 cm^{-1}. These values are consistent with theoretical calculations of the absorption coefficients made from direct determinations of the energy of the gamma-ray.

The energy was determined directly by Crane, Delsasso, Fowler and Lauritsen[8] from the spectrum of positive and negative electrons ejected by the gamma-radiation from a thick lead sheet in a cloud chamber; the electron energies were deduced from the path curvature due to a known magnetic field. The value obtained for the quantum energy was 5.4 Mev.

This method was later modified,[10] and a thin lead radiator was used. This made it possible to associate the two members of a pair and to determine their energies without having the uncertainty of an appreciable energy loss in the material. The value obtained for the quantum energy was 6.0 ± 0.2 Mev. As described in the preceding paper of this issue of *The Physical Review*, Lauritsen, Lauritsen and Fowler have found, by a more careful application of this method, the value 6.2 ± 0.1 Mev.

By measuring with coincidence counters the absorption in aluminum of the secondary electrons ejected by the gamma-ray, Curran, Dee and Petržílka[12] arrived at values of 6.3 and 5.5 Mev for the quantum energy, according as they based their conclusions on the maximum range in the absorber or the half-value thickness. The source of the discrepancy between the two values is difficult to understand as the radiation has not been found to be inhomogeneous as supposed by Curran *et al.* It must be pointed out however that the secondary absorption method must be calibrated by direct determinations of the quantum energy. The work of Dee, Curran and Strothers[13] with a magnetic spectrograph gave 6.5 Mev.

[6] E. McMillan, Phys. Rev. **46**, 325 (1934).
[7] E. McMillan, Phys. Rev. **46**, 868 (1934).
[8] Crane, Delsasso, Fowler and Lauritsen, Phys. Rev. **46**, 531 (1934).
[9] Delsasso, Fowler and Lauritsen, Phys. Rev. **51**, 391 (1937).
[10] Delsasso, Fowler and Lauritsen, Phys. Rev. **51**, 527 (1937).
[11] J. Halpern and H. R. Crane, Phys. Rev. **55**, 258, 260 (1939); E. R. Gaerttner and H. R. Crane, *ibid.* **52**, 582 (1937).
[12] Curran, Dee and Petržílka, Proc. Roy. Soc. **A169**, 269 (1938).
[13] Dee, Curran and Strothers, Nature **143**, 759 (1939).

Long before the origin of the gamma-radiation was understood, its pronounced resonance character had been demonstrated by various investigators.[12,14–16] The most extensive work was by Bernet, Herb, and Parkinson.[17] Their results showed that most of the resonance levels are very narrow: in fact, the observed widths of most of the peaks were thought to be experimental. The low energy part of the curve was investigated more closely by Burcham and Devons.[5] They were able to reduce the observed widths of the peaks at 0.33 and 0.67 Mev to 6 kev, and presumably this is still chiefly experimental. However, the level at 0.59 Mev was found to have a width of 35 kev.

The simplest reaction which has been proposed for the origin of the gamma-radiation is:

$$F^{19}+H^1\rightarrow{}^*Ne^{20}\rightarrow Ne^{20}+\gamma. \qquad (2)$$

From the known masses the quantum energy is expected to be 13.1 ± 0.3 Mev for an 0.33-Mev proton. The discrepancy between this and the observed value definitely rules out this simple process.

The fact that the calculated value is roughly twice the observed energy of the radiation suggested a cascade process in which two quanta of approximately equal energies are emitted:

$$\begin{aligned} F^{19}+H^1&\rightarrow{}^{**}Ne^{20}\rightarrow{}^*Ne^{20}+\gamma_1 \qquad (3)\\ {}^*Ne^{21}&\rightarrow Ne^{20}+\gamma_2. \end{aligned}$$

To detect the simultaneous emission of two quanta which this proposal implies, Dee, Curran and Strothers[13] connected two gamma-ray counters in a coincidence circuit; coincidences occurred with a frequency less than 1 percent of that to which the proposed process would lead.

This hypothesis was subjected to additional tests. According to reaction (3) a change in proton energy should be accompanied by a modification of the gamma-ray spectrum; presumably the energy of the first quantum, γ_1, should increase by 19/20 of the increase in proton energy. However, when the bombarding voltage was raised from 0.330 to 0.86 Mv, the gamma-ray spectrum, as indicated by the maximum range of its secondary electrons in aluminum,[13] measured with coincidence counters, was constant to within 0.05 Mev. The same conclusion was reached when the gamma-ray secondaries were measured with a magnetic spectrograph; no change greater than ±0.1 Mev was observed. A similar result was found by Lauritsen, Lauritsen and Fowler whose results are given in Table I of the preceding paper.

Another possibility which has been considered is the following:

$$\begin{aligned} F^{19}+H^1&\rightarrow{}^{**}Ne^{20}\rightarrow{}^*Ne^{20}+\gamma \qquad (4)\\ {}^*Ne^{20}&\rightarrow O^{16}+He^4. \end{aligned}$$

But the objections given in the preceding paragraph will also apply here and this proposal is not tenable.

The now accepted explanation of the origin of the gamma-rays is the following:

$$\begin{aligned} F^{19}+H^1&\rightarrow{}^{\gamma}Ne^{20}\rightarrow{}^{\gamma}O^{16}+He^4 \qquad (5)\\ {}^{\gamma}O^{16}&\rightarrow O^{16}+\gamma, \end{aligned}$$

where the superscript γ refers to states of Ne^{20} or O^{16} involved in the production of the 6.2-Mev gamma-radiation. According to the masses and the gamma-ray energy these alpha-particles should have somewhat less than 1 cm range. No such group of alpha-particles had been observed in the earlier work on alpha-particle production. Owing to the presence of scattered protons this would have been impossible except at low bombarding energies. An unsuccessful search for this short range group had been made by Burcham and Smith.[4] However, at the time of their work the energy of the gamma-radiation was thought to be 5.7 Mev, and using this figure they calculated for the range of the alpha-particles a value which is now known to be too large. Under the conditions of their experiment—0.85 Mev bombarding voltage—the range of the alpha-particles is still less than that of the scattered protons.

When the higher values for the gamma-ray energy were obtained, the search for the short range alpha-particles was renewed. Calculations based on the new data indicated that only at proton energies less than 0.5 Mev would the range of the alpha-particles exceed that of the

[14] Hafstad, Heydenburg and Tuve, Phys. Rev. **49**, 866 (1936).
[15] Hafstad, Heydenburg, and Tuve, Phys. Rev. **50**, 504 (1936).
[16] Herb, Kerst and McKibben, Phys. Rev. **51**, 691 (1937).
[17] Bernet, Herb and Parkinson, Phys. Rev. **54**, 398 (1938).

protons. These short range alpha-particles were first observed by McLean, Becker, Fowler and Lauritsen[18] who used a proton energy of 0.35 Mev. These observers also showed that this production of alpha-particles displayed a resonance between 0.30 and 0.35 Mev. Such a resonance was already known to exist in the production of gamma-radiation, and the association of the alpha- and gamma-rays seems quite certain. Similar results were obtained almost simultaneously by Burcham and Smith.[19] Burcham and Devons[5] extended this work by showing that the excitation function for the short range alpha-particles is identical with that of the gamma-radiation in the proton energy range from 0.30 to 0.95 Mev. This excitation function has a very striking structure which makes the comparison quite definite. In this work it was necessary to deflect the scattered proton beam by means of a strong magnetic field. Their resolution, particularly in the alpha-particle measurements, was not good, but there is an obvious correspondence between the prominences of their curve and the six known gamma-ray resonances which lie in this energy range. From the range of the alpha-particles, 0.86 ± 0.05 cm, and the masses involved, McLean *et al.* calculate the Q of reaction (5) to be 1.74 ± 0.10 Mev. This leads to the value 6.2 ± 0.2 Mev for the gamma-ray energy. This is in agreement with the best direct determinations. This indirect measurement should give the most reliable value. Within the experimental error, the same value was obtained by Burcham and Devons. These investigators also showed that at the 0.33, 0.66, and 0.87 Mev resonances the differences of the alpha-particle energies is $\frac{3}{4}$ of the corresponding differences in bombarding energy.* This is the result predicted on the basis of reaction (5). On the other hand, if we assume, as implied in reaction (4), that the alpha-particles always originate in the same transition, whatever the bombarding voltage, we would expect the energy of those alpha-particles emitted perpendicularly to the beam to decrease by 1 percent of the increase of proton energy.

These results, together with the previously mentioned observations on the gamma-ray spectrum, provide very conclusive evidence that reaction (5) describes the production of the gamma-radiation at the 0.334, 0.479, 0.589, 0.660, 0.862, 0.927, 1.335 and 1.363 Mev resonances. These resonances contribute approximately 75 percent of the gamma-radiation produced below 1.5 Mev bombarding energy.

Of course, there also is the possibility of a reaction similar to reaction (5) in which the alpha-particle is formed in an excited state, and subsequently emits a photon:

$$F^{19}+H^{1}\rightarrow{}^{*}Ne^{20}\rightarrow O^{16}+{}^{*}He^{4} \qquad (6)$$
$${}^{*}He^{4}\rightarrow He^{4}+\gamma.$$

However, no state of the helium nucleus so near to the ground state as is here required by the quantum energy has been suggested by the many reactions in which alpha-particles are produced.

The production of electron pairs

In the investigations described up to this point no soft gamma-radiation had been discovered; in fact, in all of the experiments, a small amount of filtering was employed to exclude the soft characteristic x-radiation emitted by all targets under proton bombardment.[20] Using a thin wall target tube and a thin wall electroscope, Fowler and Lauritsen[21] found a soft radiation in addition to the characteristic x-radiation. To establish its energy, absorption measurements in lead and aluminum were made at 0.82 and 1.13 Mev bombarding energy. These indicated that the radiation consists of electrons, not gamma-rays as first supposed. This conclusion was checked by cloud-chamber observations made with 0.82 Mev bombarding energy which showed the radiation to consist of electron pairs with total energy estimated as 5.9 ± 0.5 Mev.

By using two electroscopes, one shielded with $\frac{1}{8}$ inch of lead to detect only gamma-radiation, and the second unshielded except for target tube

[18] McLean, Becker, Fowler and Lauritsen, Phys. Rev. **55**, 797 (1939).

[19] W. E. Burcham and C. L. Smith, Nature **143**, 796 (1939).

* The incorrect value $\frac{1}{3}$ for this ratio was published. The experimental values agree more closely with the correct value $\frac{3}{4}$.

[20] Livingston, Genevese, and Konopinski, Phys. Rev. **51**, 835 (1940).

[21] W. A. Fowler and C. C. Lauritsen, Phys. Rev. **56**, 840 (1939).

and electroscope walls to record both gamma-rays and pairs, it was possible to observe simultaneously the excitation functions of these two types of radiation. Their results show that the pair formation as well as the gamma-radiation displays sharp resonances, but the two sets of resonances do not coincide. These are apparently the same pairs observed by Gaerttner and Crane[11] who, working with an alternating voltage supply, had made no attempt to determine the excitation functions of the pairs and the gamma-rays.

The difference between the excitation functions of these two kinds of radiation indicates that the pairs do not originate in the process of ordinary pair internal conversion. For example at 1.22-Mev proton energy, there is a peak in the pair excitation but not in the gamma-excitation and at this point the intensity of the pairs is 30 percent of the gamma-ray intensity. Theoretically the pair internal conversion coefficient for any multipole order radiation is less than one-half of one percent.[22] An apparently satisfactory explanation of this unusual process is that the lowest excited state of O^{16} has angular momentum $J=0$; then decay to the ground state O^{16} which is known to have angular momentum $J=0$ cannot take place with the emission of a single quantum. Calculations of Oppenheimer and Schwinger[22] show that pair formation under these conditions is more probable than the emission of two quanta. The questions involved in this calculation are mentioned below.

One must also consider the possibility that the pairs are formed by transition in the Ne^{20} nucleus. But the existence of many low lying levels in this nucleus[23] makes it unreasonable to expect that gamma-transitions from any state 5.9 Mev above the ground state are rigorously forbidden.

Recently in this laboratory Becker, Fowler, and Lauritsen (unpublished) have observed a group of short range alpha-particles associated with the prominent pair resonance at 1.22 Mev. The alpha-particles were magnetically separated from the scattered protons. The pairs may thus with some certainty be attributed to the reactions:

$$F^{19}+H^1\rightarrow {}^{\pi}Ne^{20}\rightarrow {}^{\pi}O^{16}+He^4 \qquad (7)$$
$${}^{\pi}O^{16}\rightarrow O^{16}+\pi.$$

In accounting for the pair formation it was necessary to assume the state ${}^{\pi}O^{16}$ had angular momentum zero, but the parity was not specified. It would be interesting to know the parity of this state. For if the parity is odd, pair formation can take place only as a result of a non-electromagnetic coupling between the nuclear particles and the pair field such as is postulated in the Gamow-Teller theory of nuclear forces. On the other hand, if the parity is even, pair emission can occur as a result of ordinary electromagnetic forces. If it could be shown that transitions to the states ${}^{\pi}O^{16}$ and O^{16} from the same level in Ne^{20} occur, this would establish the parity of ${}^{\pi}O^{16}$ as even, since normal O^{16} certainly has even parity: a negative result would be an argument for odd parity.[22] The experiment to be described was undertaken to see if such information could be obtained from the excitation curves in the region of higher voltages. Estimates of the yields of the various reactions were also made.

Experimental Procedures

The source of high velocity protons was the pressure electrostatic generator and accelerating tube built and used by Lauritsen, Lauritsen and Fowler and described in the preceding paper. The tube voltage was measured with a generating voltmeter and was checked during every run at some pronounced resonance in the gamma-ray excitation curve. The experimental fluctuation in the energy of the ion beam was not as small as has been secured by Herb *et al.*,[16 17] but was small enough to permit good resolution of the known gamma-ray resonances.

Some unsteadiness in the ion current made necessary an integrating device to measure the total charge carried by the bombarding protons during a run. The target, at the bottom of a Faraday cage, was bombarded by the beam defined by an aperture slightly above the entrance of the cage, and the charge accumulated by the cage was let into a condenser having good insulation, whose potential could be read continuously on an electroscope connected across it.

[22] J. R. Oppenheimer and J. S. Schwinger, Phys. Rev. **56**, 1066 (1939).
[23] T. W. Bonner, Proc. Roy. Soc. **A174**, 339 (1940).

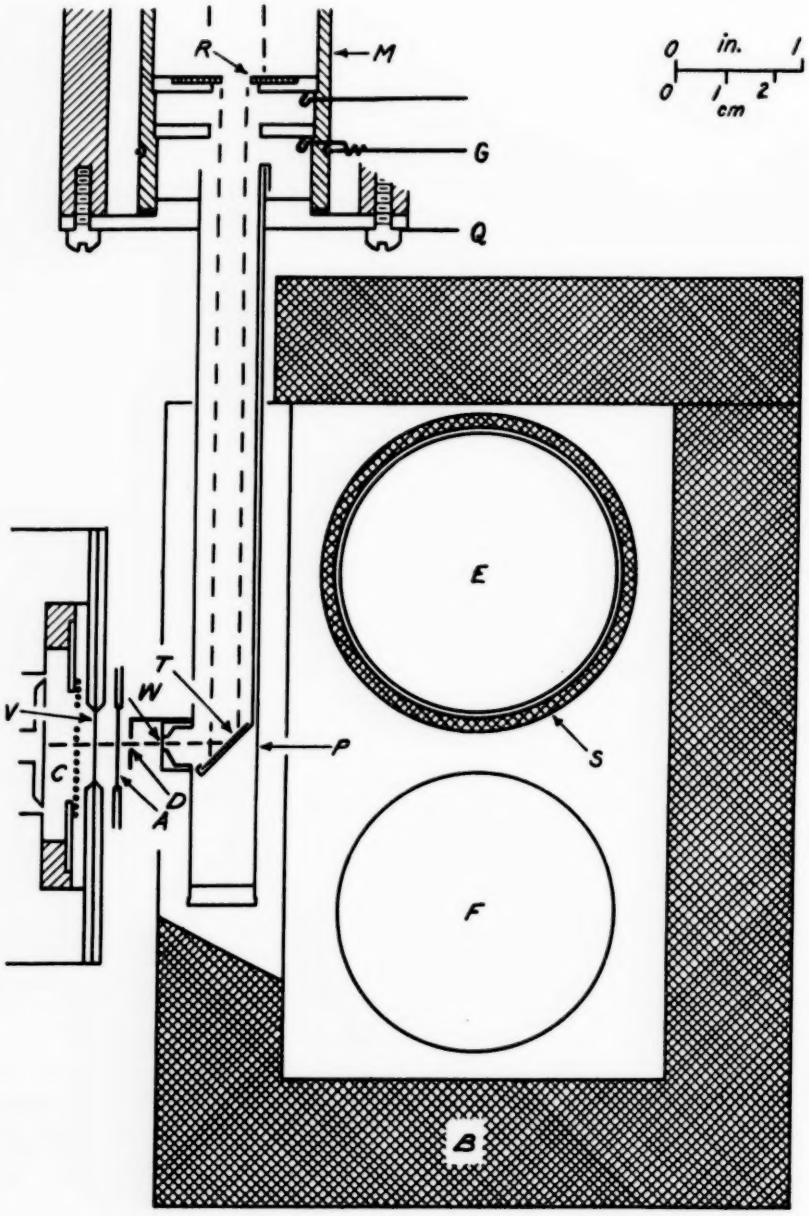

FIG. 1. Arrangement of target tube, electroscope and ionization chamber. The vertical proton beam, shown by dotted lines, is defined by the 0.25-inch hole in the quartz ring *R*. In aligning the target tube, the position of the beam is observed through the transparent Plexiglas tubing *M* by the fluorescence produced in the quartz ring. The connection *Q* is to the current integrator. A negative potential on *G* prevents erroneous current measurements resulting from a gain or loss of secondary electrons. The lead box *B* completely encloses the electroscopes *E* and *F* except for holes admitting the microscope tubes, holes for illumination, and the beveled slot just large enough to accommodate the target tube *P*. *S* is the 0.125-inch lead shield which absorbs electrons originating in the target. Electroscope *E* records only gamma-radiation. Electroscope *F* records both electrons and gamma-radiation. The material between the target and this electroscope is: the target backing, *T*=0.0010 inch of tantalum, the target holder=0.008 inch of phosphor bronze, the target tube=0.004 inch of German silver, and the electroscope wall=0.030 inch of aluminum. The path of an alpha-particle emitted perpendicularly to the proton beam is shown by a dotted line. The particle leaves the tube through the 0.00025-inch aluminum window *W*, and enters the ionization chamber *C* through the similar window *V*. The alpha-particle beam is limited by the aperture *D*. Because of the large window *V*, the position of the ionization chamber is not critical. The aluminum absorber *A* stops scattered protons.

This apparatus was calibrated by observing the electroscope deflection produced by a measured current flowing into the condenser for a measured time. Measurements of the ion current were always made with the condenser negatively charged so that the secondary electrons formed at the defining aperture were repelled from the cage.

It was found that a thin target of TaF_5 formed by the action of hydrofluoric acid on tantalum as described by Bernet *et al.*,[17] and then polished, gave more dependable results than the targets formerly used in this laboratory made by depositing a thin layer of CaF_2 on a copper backing. Two thin target curves were made. Before the second set of data was taken, the target was well polished; being thinner, it then gave a smaller yield, but permitted greater resolution. The thick target was a heavy deposit of CaF_2 on a copper backing.

A formula has been derived[17] for estimating the thickness of thin targets from a comparison

of the thin target and thick target yield curves. The thickness in energy units is given by the ratio of the area under the thin target resonance peak to the corresponding step in the thick target yield curve. For measurements of this kind it is convenient to use the two resonances at 0.862 and 0.927 Mev for these close peaks are very much more intense than the background upon which they are superimposed. In this way the thickness of the thin target was found to be 8 kev for 1-Mev protons during the first observations and 1.4 kev after polishing.

The measurement of the radiations

The possibility of uncertainties in the voltage made it necessary to observe all of the radiations simultaneously. Otherwise resonances in two different radiations occurring close together could not definitely establish the radiations as competing modes of decay of a single level of the compound nucleus. The arrangement of the measuring apparatus is shown in Fig. 1.

The gamma-rays were recorded in a Lauritsen electroscope shielded by $\frac{1}{8}$ inch of lead. The combined effect of the pairs and gamma-rays was recorded in a similar unshielded electroscope. This is the arrangement previously employed by Fowler and Lauritsen.[21] The two electroscopes were placed as close as possible to the target. Within convenience the material between the target and the unshielded electroscope was reduced to a minimum to avoid absorption of the pairs. To decrease the background due to undesired radiation, principally x-rays and gamma-rays originating from ion bombardment of parts of the tube, the electroscopes were almost completely enclosed in a lead box with one-inch walls.

The target was inclined 45° with respect to the beam, and long range alpha-particles ejected at right angles to the beam passed through a thin aluminum window, whose stopping power, measured with the alpha-particles from polonium, was equivalent to 1.8 cm of air. They passed through 1 cm of air, entered the ionization chamber through a similar window, and were counted by means of a four-stage linear amplifier and thyratron recording circuit; the performance of this apparatus was frequently checked with a polonium alpha-particle source. A diaphragm to limit the alpha-particle beam was located between the two windows. This usually was a $\frac{1}{8}$-inch circular hole $\frac{3}{4}$ inch from the center of the target, but was sometimes changed to accommodate the large variations in intensity over the voltage range investigated. The ionization chamber was placed in a position convenient for counting the alpha-particles produced by the low energy protons; then when the voltage was raised above 1.1 Mv scattered protons were able to enter the chamber. It would have been possible to move the ionization chamber farther from the tube so as to count only the alpha-particles, whose range is also increased, but to avoid disturbing the geometrical arrangement it was thought better to insert in front of the chamber aluminum foils to absorb the protons when using potentials over 1 Mv; the number of absorbers was varied with the voltage. The correct stopping power of the absorber was not at all critical; it was varied in steps of 0.18 cm equivalent stopping power of air (0.13 Mev for protons).

Observations were made at voltages differing by 12 kv from 0.3 to 1.6 Mv. A single measurement required on the average about two minutes. The target was usually bombarded with 66 microcoulombs, corresponding to 10 divisions of the current integrator. The length of the run was varied, depending on the intensities under observation. Below 0.6 Mv the molecular ion beam was used.

At resonances, the deflections of the radiation recording electroscopes were of the order of 20 divisions. Background corrections, of the order of 0.5 division, depending on the length of the run, were applied to the electroscope readings. This correction was for the natural leakage, and did not include the effect of stray radiation excited in the tube. Between resonances the observed deflections were sometimes equal to the background correction. Judging from the reproducibility of the observations, the reliability of the electroscope data is about what one would expect from the fact that they can be read to about 0.1 division. The counting rate of the alpha-particles was sufficiently high that no background correction was needed, but not high enough to introduce errors through inability of the counter to resolve successive counts.

The relative sensitivities of the electroscopes to gamma-radiation

The pair excitation was determined by subtracting from the total reading of the unshielded electroscope the effect of the gamma-rays as determined from the shielded electroscope. Thus it was necessary to know their relative sensitivities to gamma-rays in the positions in which the measurements were made. The principal part of the ionization associated with the gamma-radiation is produced by the scattered electrons and the electron pairs ejected from the surrounding matter. However, an important part is produced indirectly through the effects of scattered radiation and the radiation accompanying the annihilation of the electron pair positions. The magnitude of these secondary effects is greatly dependent upon the composition and geometrical arrangement of the material near the electroscope, especially when the material has a high atomic number, as in the present experiment. In view of the complicated nature of these effects and the difficulty of the calculations involved, it seemed best to make the comparison of the electroscopes without any change in the apparatus and using the gamma-radiation in question. This was possible, for rough absorption measurements showed that with a bombarding voltage of 0.335 Mev the intensity of pairs was very small. The presence of a few pairs would not modify the results appreciably. The sensitivity to gamma-radiation of the unshielded electroscope at the position used was found to be 2.0 times that of the shielded electroscope in its position. The pair yield was thus secured by subtracting twice the reading of the shielded electroscope from the reading of the unshielded electroscope.

The absolute sensitivity of the electroscopes

To determine the absolute yield of gamma-rays or pairs a calibration of the absolute sensitivity of the electroscope employed must be made by noting its rate of deflection while exposed to radiation of known intensity. To facilitate calculations in such a measurement it is desirable to surround the electroscope with a medium so dense that within a distance equal to the range of the secondary electrons, the intensity and composition of the radiation is uniform. One must be able to calculate the number of electrons ejected from this medium into the electroscope in terms of the radiation in question. Owing to the complications mentioned above and discussed in more detail below, this is not practicable if the instrument is surrounded by lead. However, if a material of low atomic number is used, these complicating effects become inappreciable and may be disregarded. It should be pointed out that lead is not objectionable as a surrounding medium in the determination of an excitation curve, where only varying intensities of a fixed kind of radiation are involved, but is objectionable when a measurement is to be made of the absolute intensities of one or more gamma-rays of different energy.

Let S be the number of ion pairs per cc produced per second at a distance of one cm from a radium source of one milligram under the conditions of the experiment. Then if D is the number of divisions per second recorded at a distance R from a source of M milligrams we have the reciprocal sensitivity of the electroscope given by:

$$c = SM/R^2D \text{ ion pairs per cc per div.}$$

In these experiments the electroscope was placed in the center of a paraffin sphere 6 inches in diameter and the deflection observed while it was exposed to the radiation from a 1.915-milligram radium standard in equilibrium with its decay products surrounded by 0.5 mm of brass and 1.0 mm of lead placed 100 cm from the electroscope.

The quantity S is given by sAB where s is the strength of a unit radium source with the filtration necessary to remove the very soft radium gamma-rays, A is a factor arising from absorption of the radiation in the walls of the electroscope, and B is the effectiveness, relative to air, of the medium surrounding the electroscope in applying secondary electrons to the electroscope.

Laurence[24] gives an empirical expression for the strength of a unit radium source filtered by platinum of thickness t in millimeters as follows:

$$s = 8.98(1 - 0.13t) \text{ roentgens/mg hr. per cm}^2.$$

[24] G. C. Laurence, Can. J. Research **A15**, 67 (1937).

This relation holds for $t \geq 0.3$ mm. In our units

$$s = 5.19(1 - 0.13t) \times 10^6 \text{ ion pairs per cc/mg sec. per cm}^2.$$

The platinum equivalent of the brass and lead filtration employed in these experiments was $t = 0.66$ mm so that

$$s = 4.74 \times 10^6 \text{ ion pairs per cc/mg sec. per cm}^2.$$

With the softer components of the radiation removed, photoelectric absorption in the paraffin is unimportant. In view of the low atomic numbers of the constituents of paraffin, pair formation absorption may also be neglected. Data given by Lauritsen[25] show that the true absorption of energy by the Compton effect is roughly the same for all components of the radium radiation. The value ${}_e\sigma_a = 0.9 \times 10^{-25}$ cm^2 for the electronic cross section[25] is a reasonable average value. The electron density in paraffin is $n = 3.1 \times 10^{23}$ per cc so that the absorption coefficient and attenuation factor are, respectively, $n_e\sigma_a = 0.028$ per cm and $A = \exp(-n_e\sigma_a x) = 0.87$ for $x = 5.0$ cm, the thickness of the paraffin effective in absorbing the radiation.

The effectiveness, relative to air, of the surrounding medium in supplying secondary electrons to the electroscope must also be known. Laurence[24] designates this quantity by B and has computed it for those cases in which the Compton effect is the only important mechanism in the absorption of the radiation by the medium and the secondaries lose energy only through ionization by collision. For gamma-ray energies between 1 and 2 Mev the values of B for paraffin and for aluminum are constant to within 1 percent and are, respectively, 0.93 and 1.06. The walls of the electroscope are of aluminum and have a thickness 0.038 cm which is about 20 percent of the range of the fastest electrons scattered by the radium radiation. Some average between the values for aluminum and paraffin must be taken. Since a large fraction of the gamma-rays have energies much less than the most energetic, and since the scattered electrons do not in general receive the maximum possible energy, it would seem reasonable to weight the two values equally, yielding the ratio $B = 1.00$. This combination of paraffin and aluminum is thus roughly equivalent to the ideal air equivalent walls.

We observed $D = 0.062$ div. per sec. for the electroscope used in the gamma-ray measurements so that for this electroscope $c = 1.27 \times 10^4$ ion pairs per cc per div. Its volume was 145 cc so that $cV = 1.84 \times 10^6$ ion pairs per div. The corresponding quantities for the pair electroscope were found to be $D = 0.076$ div. per sec., $c = 1.04 \times 10^4$ ion pairs per cc per div., $V = 160$ cc and $cV = 1.66 \times 10^6$ ion pairs per div.

The absolute yield of the gamma-radiation

The gamma-ray electroscope, again with the lead shield removed, was placed inside the paraffin sphere and exposed to the radiation from a thick CaF_2 target, located just outside the sphere and bombarded with 1.04-Mev protons. This voltage was chosen because this point lies on a flat portion of the thick target excitation curve. The gamma-ray yield is given by $Y_\gamma = (4\pi r^2 cd/IA) \times 1.6 \times 10^{-13}$ quanta per proton, where d is the number of divisions observed per microcoulomb of protons bombarding the target at a distance r from the electroscope, I is the ionization per cc produced by a flux of 6.2-Mev radiation of one quantum per cm^2, and A is the absorption factor for this radiation in the electroscope walls. This equation assumes an isotropic distribution of the radiation, an assumption which is justified when the origin of the radiation is considered. A properly weighted value for r must of course be employed.

The essential point is now the calculation of I, which is in detail complicated in the high energy region where pair production, annihilation, and bremsstrahlen all contribute. We shall give here a treatment adequate for the cases where these effects are not too large, i.e., where the gamma-ray energy is under 25 Mev and the atomic number of the material surrounding the electroscope is low. Since no nuclear radiation above 18 Mev has been observed, atomic screening which sets in at much higher energies will not be important.

For the region below 2 Mev several investigations[24–26] of I exist. The derivation depends

[25] C. C. Lauritsen, Am. J. Roent. and Rad. Therapy **30**, 380, 529 (1933).

[26] L. H. Gray, Proc. Roy. Soc. **A156**, 578 (1936).

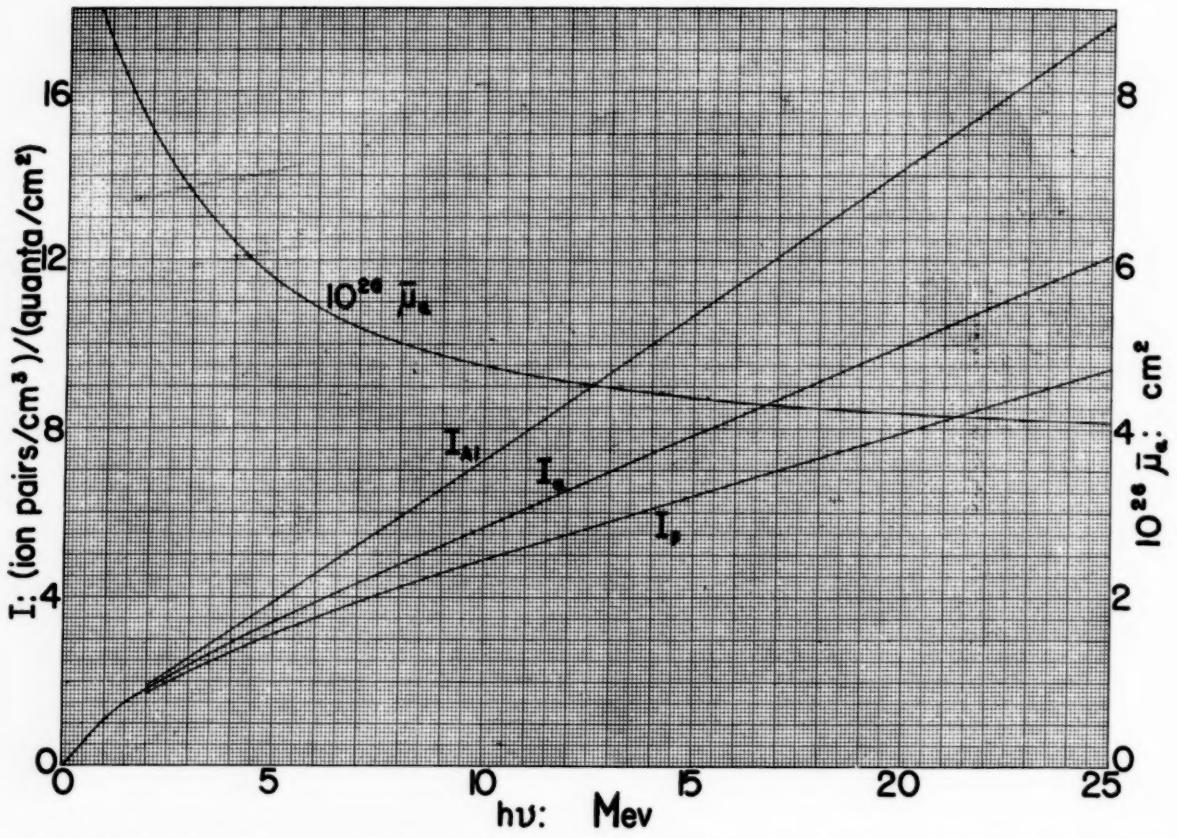

FIG. 2. The variation with energy of the quantities μ_a and I. The quantity μ_a is the true energy absorption cross section per electron for quanta of energy E in air. The quantity I is the number of ion pairs per unit volume produced by a flux of one quantum of energy E per square centimeter in an electroscope filled with air under standard conditions and having walls of aluminum (Al), air equivalent material (a), and paraffin (p).

fundamentally on a theorem due to Gray[26] that the energy equivalent of the ionization measured per cc in a cavity in a solid medium is equal to the energy converted per cc in the medium (W_m) divided by the relative stopping power (dE/dx) of the medium and the gas filling the cavity for the secondaries produced by the radiation. Thus

$$\omega_g I = W_m \frac{(dE/dx)_g}{(dE/dx)_m},$$

where ω_g is the energy lost per ion pair formed in the gas. This theorem assumes a cavity small compared to the range of the secondary electrons in the cavity, a uniform intensity and composition of radiation near the cavity, and that the relative stopping power is independent of the velocity of the secondaries. The first two conditions are satisfied in the energy range under discussion for electroscopes of a convenient size (100 to 200 cc volume) when surrounded by a solid layer thicker than the maximum range of the secondaries as long as the source of radiation is not too close to the electroscope. In our experiments the source was probably too close to fulfill the second condition but we neglect this geometrical factor.

Laurence[24] has derived an analytical expression for Gray's theorem in such a way as to show that elastic scattering of the secondaries does not invalidate the theorem. Laurence also shows that if the relative stopping power is a function of the velocity of the secondaries it is only necessary to average it over the secondary energy. This is equivalent to averaging the stopping power in the gas over the path of the secondary in the medium as can be seen as follows:

$$\int_0^{E_0} \frac{(dE/dx)_g}{(dE/dx)_m} dE = \int_0^{R_0} \left(\frac{dE}{dx}\right)_g dx_m,$$

where E_0 and R_0 are the initial energy and full range of the secondary. In an extension to the energy range where radiation plays a part it is clear from the last expression that only the energy converted into ionization in the chamber must be used in computing $(dE/dx)_g$ but that the full energy loss by radiation as well as ionization must be used in computing the range and hence $(dE/dx)_m$ in the medium. Finally, averaging over the energy distribution of the secondaries, we can write Laurence's expression in the modified form:

$$I=\frac{1}{\omega_g}\int_0^{h\nu}\phi_m(h\nu, E_0)\int_0^{E_0}\frac{(dE/dx)_g'}{(dE/dx)_m}dEdE_0$$

or more conveniently,

$$I=\frac{N_gZ_g}{\omega_g}\int_0^{h\nu}\mu_m(h\nu, E_0)\int_0^{E_0}\frac{\lambda_g'}{\lambda_m}dEdE_0 \times\frac{\text{ion pairs per cc}}{\text{quanta per cm}^2},$$

where I is the ionization per unit volume in the cavity per unit flux of radiation (quanta per cm²) in the medium, N_gZ_g is the number of electrons per cc of gas, $\phi_m(h\nu, E_0)dE_0$ is the number of secondary electrons with energy between E_0 and E_0+dE_0 produced per cm of path in the medium by a quantum of energy $h\nu$, $\mu_m(h\nu, E_0)dE_0$ is the corresponding electronic cross section for secondary production, $(dE/dx)_g'$ is the stopping power by ionization of the gas, $(dE/dx)_m$ is the total stopping power of the medium and λ_g' and λ_m are the corresponding electronic stopping cross sections. If the electroscope is filled with air we have $N_aZ_a/\omega_a=1.20\times10^{19}$ $(\text{ev}\cdot\text{cc})^{-1}$ using $\omega_a=32.5$ electron volts.

It will be seen that the complications involved in applying Gray's theorem are two in number.

1. The energy converted per cc in the medium is a complex function of the gamma-ray energy.

2. The relative stopping power of solid medium and gas is a complex function of their atomic number and of the energy of the secondaries. Of these two effects, the second can be almost completely eliminated by suitable choice of the surrounding medium (air equivalent) and can be made very large indeed by the use of Pb or other heavy elements. In our work with paraffin and aluminum walls this second effect is quite small. For high energy quanta the complications in (1) cannot be eliminated, but can be reduced by using a medium of low Z.

We will first discuss (2). Using Bloch's formula for the stopping from ionization by collision and approximating to the stopping by radiation for the domain 2–25 Mev, by

$$\lambda_{\text{rad}}/\lambda=(\lambda-\lambda')/\lambda\approx EZ/2000\ mc^2,$$

where E is the electron energy, we get

$$\frac{\lambda_a'}{\lambda_m}\approx1-\frac{EZ_m}{2000mc^2}+\frac{2\ln(Z_m/Z_a)}{3\ln(E/A)}$$

where

$$A=(m^{\frac{1}{2}}chRZ_m)^{\frac{1}{2}}.$$

This expression must be averaged, for each secondary, over all its energy and then over the initial energy distribution of the secondaries produced in the solid medium. The first average is

$$\left\langle\frac{\lambda_a'}{\lambda_m}\right\rangle_{h\nu}\approx1-\frac{E_0Z_m}{4000\text{mc}^2}+\frac{2}{23}\ln\frac{Z_m}{Z_a},$$

where the factor 2/23 is a good average value in the domain under discussion.

To return to (1), we need to know $\mu_m(h\nu, E_0)dE_0$, the cross section for producing a secondary of energy E_0 in the medium. If we set $f=E_0/h\nu$ and $\kappa=h\nu/mc^2$ the Klein-Nishina formula and the cross section for pair formation give at high energies:

$$\mu_m(\kappa, f)df=\pi r_0^2df\left[\frac{1}{\kappa}\left(1-f+\frac{1}{1-f}\right)+1.65\frac{Z_m}{137}\frac{\kappa}{\kappa-2}\ln\frac{\kappa}{4.3}\right],$$

where $r_0=e^2/mc^2$ and where the second term which is for pair production is an empirical fit to Heitler's curve[27] in the region from 2 to 25 Mev.

The remaining procedure is to integrate $E_0\langle\lambda_a'/\lambda_m\rangle_{h\nu}$ over the differential cross section. The results are plotted in Fig. 2 for paraffin $(Z_m\approx4.7)$, air $(Z_m=Z_a=7.2)$ and aluminum $(Z_m=13)$ and are given in good numerical

[27] W. Heitler, *The Quantum Theory of Radiation* (Oxford University Press, 1935), p. 201.

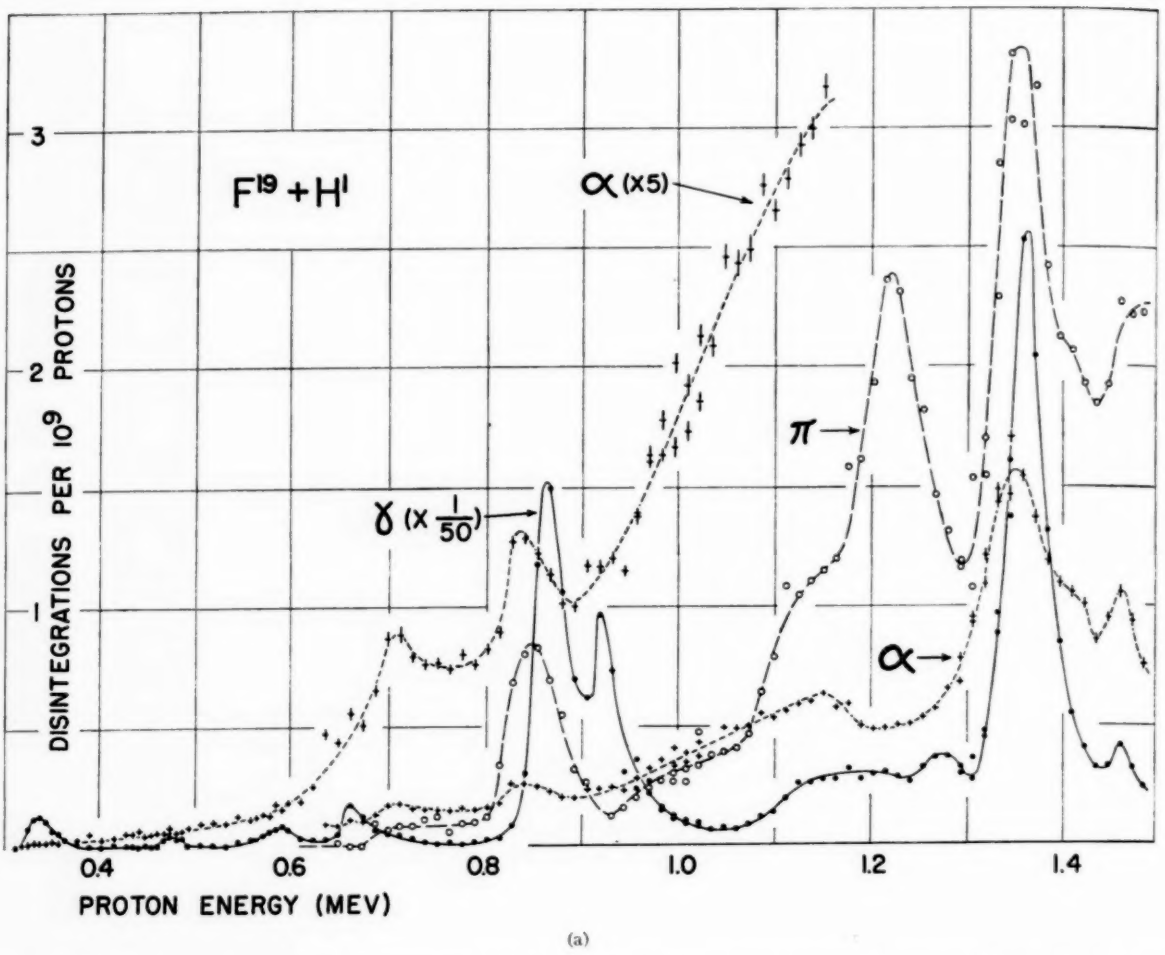

(a)

FIG. 3. The excitation functions. The curves marked γ, α and π refer to the gamma-rays, long range alpha-particles and electron pairs, respectively. In some regions Fig. 3(a) represents a combination of four independent sets of data; Fig. 3(b) (see opposite page) is based on a single set of data. The equivalent target thickness for 1-Mev protons was 8 kev for the upper curve, 1.4 kev for the lower curve. In Fig. 3(b) the upper end of the pair curve has been omitted; while its shape is not known accurately, it is certain that its sharp rise continues until at 1.62 Mev the intensity is about 50 percent greater than at 1.5 Mev.

approximation for $Z_m<20$ and $h\nu<25$ Mev by

$$I=(N_aZ_a/\omega_a)h\nu\bar{\mu}_m$$

ion pairs per cc/quanta per cm^2,

where $\bar{\mu}_m$ is the true energy absorption coefficient per electron for the medium as measured in an air cavity and is given by

$$\bar{\mu}_m=\pi r_0^2\frac{mc^2}{h\nu}\left(1-\frac{h\nu Z_m}{5000mc^2}+\frac{2}{23}\ln\frac{Z_m}{Z_a}\right)\times\left(\ln\frac{h\nu}{1.1mc^2}+\frac{(h\nu-2mc^2)Z_m}{165mc^2}\ln\frac{h\nu}{4.3mc^2}\right).$$

The absorption coefficient for air equivalent walls ($\bar{\mu}_a$) is also given in Fig. 2. The terms $\pi r_0^2mc^2N_aZ_a/\omega_a=1.51$ in our units.

For $Z_m=20$ and $h\nu=25$ Mev the expression for I is correct to about 5 percent. To extend this treatment to higher Z_m and $h\nu$ would require giving up Gray's theorem, since then it is no longer possible to treat the range of the electrons as small, that of the gamma-rays as large, compared to the dimensions of the surrounding medium.

Experimentally it has been shown that for lead $\bar{\mu}$ is only slightly greater than the minimum in the total cross section curve for radiation of both 6.2 Mev and 17.5 Mev.[9] Thus I for a lead lined chamber is proportional to the quantum

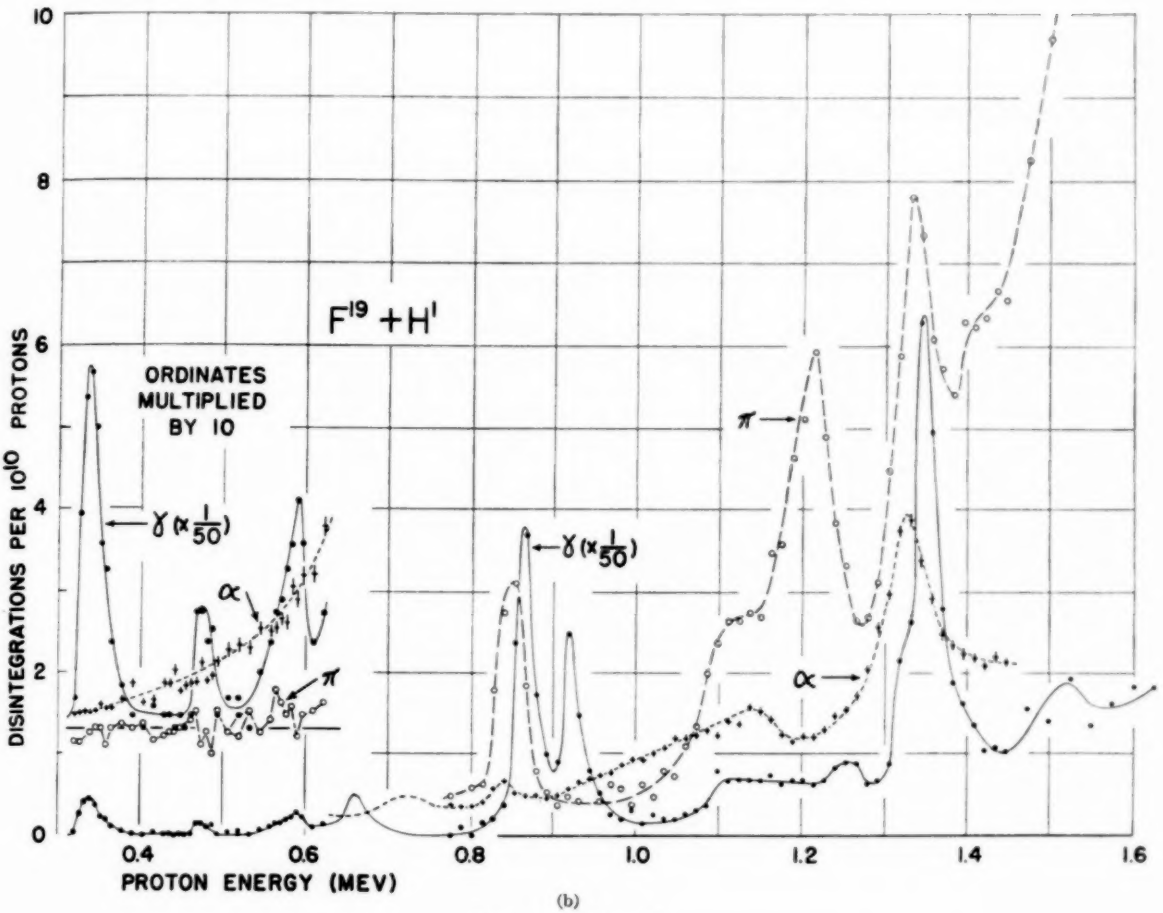

(b)

FIG. 3. (Continued).

energy being given very approximately by

$$I(\text{Pb}) = 0.9h\nu/mc^2$$

ion pairs per cc/quanta per cm².

The derivation for I given above permits of a calculation of the ions produced per unit volume of the electroscope only when the energy and composition of the radiation in the wall is strictly known. In actual practice we wish to know the ionization produced by a monochromatic gamma-ray falling on the external electroscope walls and some question may arise as to the complications arising from the building up of secondary radiation from the Compton effect, radiation of the secondary electrons, and annihilation of positron members of pairs. The answer to this question depends on the geometry of the experiment and only in case the secondary quanta produced in the electroscope walls and escaping therefrom are completely compensated for by scattering in surrounding material can a definite answer be given. Fortunately, almost complete compensation is attained by surrounding the electroscope on all sides by walls thicker than the range of the secondary electrons in the wall material. A further simplification arises from the fact that $\bar{\mu}$ is roughly independent of energy. If $\phi(E)dE$ is the distribution in energy of quanta in the walls near the sensitive volume of the electroscope produced by monochromatic quanta falling on the external electroscope walls, then the energy conversion per unit volume is $n\int \bar{\mu} E\phi(E)dE$ where n is the electron density in the walls. For $\bar{\mu}$ = constant this becomes $n\bar{\mu}W$ where W is the energy remaining in the form of radiation after the quanta have penetrated to a point where their secondaries can reach the electroscope. Since secondaries are produced at all points in the wall surrounding the cavity we can write $W = W_0 \exp[-n\bar{\mu}t]$ where t is the wall thickness. Actually $\bar{\mu}$ is not strictly constant but we use the expression inserting the appropriate

value of $\bar{\mu}$ for the incident radiation in question. For the 5-cm paraffin walls used in these experiments we find $A=\exp[-n\bar{\mu}t]=0.87$ for the filtered radium radiation and 0.92 for the $F^{19}+H^1$ radiation.

The thick target yield was measured at one point (1.04 Mev) and the yield for each resonance was determined from the relative area under the thin target curve for that particular resonance. The results are discussed below.

The absolute yield of the pair emission

The pair measurements were made with a minimum of material between the target and the electroscope. This material consisted of (1) the target backing = 0.010 inch of tantalum, (2) the target holder = 0.008 inch of phosphor bronze, (3) the target tube = 0.004 inch of German silver, and (4) the electroscope wall = 0.030 inch of aluminum. Both the target and the electroscope were surrounded by lead (Fig. 1). Under these conditions the yield of pairs can be computed from the expression

$$Y_\pi=\frac{4\pi r^2 c\omega_\theta d\times 1.6\times 10^{-13}}{n_\theta\int\psi(E)\lambda_\theta' dE+n_\theta\int\phi(E)\bar{\mu}_m E dE}\ \text{pairs per proton,}$$

where r, c, ω_θ, d, λ_θ', n_θ and $\bar{\mu}_m$ are analogous to quantities already defined for gamma-radiation, $\psi(E)dE$ is the energy distribution per pair produced of pair members entering the electroscope and $\phi(E)dE$ is the energy distribution per pair of annihilation quanta and bremmstrahlen quanta in the material surrounding the electroscope.

There is some uncertainty in the distribution in energy of the pair members although the cloud-chamber work of Fowler and Lauritsen[21] gave an energy distribution roughly constant up to the maximum kinetic energy $E_M=4.9$ Mev. If all the electrons lose the same amount of energy E_L or are stopped, if their initial energy is less than that amount, in passing through the material between the target and the ionization chamber, the distribution in energy of the electrons in the chamber will be approximately constant up to a maximum energy, $E_M'=E_M-E_L$. Then

$$n_\theta\int\psi(E)\lambda_\theta' dE=n_\theta\bar{\lambda}_\theta'\int_0^{E_M'}(2/E_M)dE$$
$$=2E_M'^2/E_M R_M',$$

where E_M'/R_M' is taken as a good average value for $n_\theta\lambda_\theta'$, R_M' being the range of an electron of energy E_M', neglecting radiation.

The energy radiated by the pair members over their ranges in the lead box surrounding the electroscope and target can be computed by averaging $EZ_m/2000mc^2$ over their energy distribution. We find

$$\bar{E}_{\text{rad}}=\frac{1}{3}\frac{E_M Z_m}{2000mc^2}E_M.$$

In these experiments $Z_m=82$, $E_M=4.9$ Mev, $E_{\text{rad}}=0.66$ Mev which is equivalent to 1.3 annihilation quanta. This number must be added to

TABLE I. *Yields of the* $F^{19}+H^1$ *reactions in disintegrations per proton from a thick* CaF_2 *target.* In successive columns are recorded the proton energies for particular resonances or voltage regions, the radiation observed, the yield per 10^7 protons, the estimated true widths of the resonance peaks in kev, the stopping cross section in 10^{-15} ev·cm² of CaF_2 per fluorine atom, the proton wave-lengths in 10^{-12} cm, and values for $\omega\gamma=\omega\Gamma_P\Gamma_x/\Gamma$ in ev. The proton energies for the γ-ray resonances are those given by Bernet, Herb and Parkinson. The value zero for a resonance width indicates a width which is probably very small and certainly less than 10 kev. The great width of several peaks may be due to the superposition of two or more resonances. The nonresonant yields for pairs and alphas are the integrated yields to 1.5 Mev below smooth curves drawn through the minima in the excitation functions for pairs and alphas.

E_P (Mev)	R	$Y\times10^7$	Γ (kev)	$\epsilon\times10^{15}$ (ev·cm²)	$\lambda\times10^{12}$ (cm)	$\omega\gamma$ (ev)
0.334	γ	0.18_5	0	24.1	5.20	33
0.479	γ	0.05_2	0	18.4	4.34	10
0.589	γ	0.24_2	25	15.5	3.92	49
0.660	γ	0.46_2	0	14.2	3.70	96
0.6–0.8	π	0.013_2	—	—	—	—
0.72	α	0.007_5	15	13.6	3.54	·1.6
0.84	α	0.006_1	15	12.3	3.30	1.4
0.85	π	0.10_5	15	12.1	3.26	24
0.862	γ	3.34	0	12.0	3.24	760
0.927	γ	2.21	0	11.5	3.12	520
0.9–1.2	α	0.06_4	—	—	—	—
1.14	π	0.07_8	30	10.0	2.81	20
1.22	π	0.20_5	30	9.5	2.72	53
1.1–1.3	γ	3.03	—	—	—	—
1.35	α	0.13_6	25	8.8	2.59	36
1.35	π	0.19_5	25	8.8	2.59	51
1.335	γ	1.25	0	8.9	2.60	330
1.363	γ	7.71	10	8.7	2.57	2020
Nonresonant	π	1.18	—	—	—	—
	α	0.69	—	—	—	—
Total						
to 1.0	γ	6.50	—	—	—	—
to 1.5	γ	22.0	—	—	—	—
"	π	1.78	—	—	—	—
"	α	0.90	—	—	—	—

the two quanta resulting from the annihilation of the positron member of the pair.

The effective secondaries from these quanta were produced in the aluminum walls of the electroscope and inserting the proper value for $\bar{\mu}_m$ we find that the radiation term contributes 2 percent of the denominator of the expression for Y_γ. The quantity E_L was found to be 1.3 Mev and the range of an electron of energy $E_M'=3.6$ Mev was taken to be 14 meters in air. Hence $2E_M'^2/E_M R_M'=3770$ ev per cm.

The yield of the long range alpha-particles

In the case of the alpha-particles the assumption of isotropic distribution is not justified. Their angular distribution has been measured by Ellett, McLean, Young and Plain[28] at voltages from 0.27 to 0.44 Mev. The distribution is practically independent of the proton energy in this range and is described by

$$I(\theta)=1+0.77\cos\theta+0.17\cos^2\theta$$

in the center of mass coordinates. Lacking knowledge of the distribution at higher energies all of the calculations of yield from the alpha-particle intensity perpendicular to the proton beam were made on the basis of an isotropic distribution in laboratory coordinates. If instead, the calculations were based on the above formula, the results would be increased by from 6 percent, at the lower voltage, to 10 percent at the higher voltages. The calculation is made from obvious geometrical considerations.

Experimental Results

The excitation functions and absolute yields

In Fig. 3 are shown the excitation curves obtained on two occasions. The ordinates are given in terms of the number of transmutations per incident proton. For thin targets with a stopping power less than the fluctuations in the tube voltage the ordinates will be proportional to the target thickness. For the second curve a thinner target was used. This accounts for the lower intensity and better resolution. It should be emphasized that the radiation designated as pairs is just that soft component absorbed by $\frac{1}{8}$ inch of lead; in this experiment no further attempt was made to establish the identity of the radiation. As remarked above, the nature of this radiation has been established definitely only at 0.82- and 1.13-Mev bombarding energy.

As stated above, no correction has been applied for undesired radiation from the tube itself, but some control runs were made with a clean tantalum target. The measurements are not very reproducible, but they show that the stray radiation gives a significant background only in the neighborhood of 1.05 Mev where the true gamma-ray intensity is much smaller than shown, and in the region from 1.1 to 1.3 Mev where the gamma-ray intensity is about 25 percent less than that plotted.

It will be observed that the gamma-ray curves are in good agreement with the work of Bernet *et al.*, and the other investigators although the resolution is not quite as good as has been obtained before.

In Table I are given the absolute yields for all resonances below 1.5 Mev. As may be seen by a comparison with Fig. 3, some of the peaks tabulated are superimposed on a continuous background which makes an estimate of the yield to be attributed to the resonance somewhat difficult. In constructing the table, data on gamma-rays given by Bernet *et al.* have been used to fix the energy scale. The full widths at half-maxima for the various resonances were found by subtracting from the observed widths the width due to fluctuations in the tube voltage (25 kev). When zero is given as the width it must be interpreted as an indeterminate width certainly less than 10 kev and probably much smaller.

The yield of a nuclear reaction initiated by proton bombardment is given by

$$Y_X=\frac{\lambda^2}{2\epsilon}\omega\gamma=\frac{\lambda^2}{2\epsilon}\omega\frac{\Gamma_P\Gamma_X}{\Gamma},$$

where the Γ's are the appropriate decay constants in energy units, λ is the wave-length of the incident protons, ω is a statistical weight factor which probably ranges in value from $\frac{1}{4}$ to $\frac{7}{4}$ and ϵ is the energy loss cross section of the incident particle in the target material. The yield is thus a measure of the quantity $\omega\gamma$, which is listed in

[28] Ellett, McLean, Young and Plain, Phys. Rev. **57**, 1083(A) (1940).

Table I for each resonance. We also include λ and ϵ for each resonance. The stopping power of CaF_2 relative to air was taken as 2.0 independent of the proton velocity and the variation of ϵ_{air} was taken from a curve given by Bethe.[29]

From data given by Tuve and Hafstad,[30, 15] Bethe[31] has estimated the yield of gamma-rays from the 0.334-Mev resonance with a CaF_2 target. The result is about 200 times smaller than that obtained in the present experiment. The calculation depends on the cross section at the 0.440-Mev resonance in the production of gamma-rays by proton bombardment of lithium. For this quantity Tuve and Hafstad estimate 10^{-27} cm^2. They do not give the details of the calculation but indicate that it is not very reliable. Their observations were also made with a Lauritsen electroscope. Although the electroscope readings taken by Tuve and Hafstad near the 334 resonance appear to be only somewhat smaller than we would calculate from ours when account is taken of the Pb electroscope walls used in their work, the cross section which they give and thus Bethe's estimated yield is smaller than ours by a factor of 200 and seems to be seriously in error. Recent measurements in the same laboratory by Van Allen and Smith[30] on the yield of the short range alphas from the 334 resonance give a value of $8.9\pm0.5\times10^4$ alphas per microcoulomb or $1.43\pm0.8\times10^{-8}$ alpha per proton in excellent agreement with our yield of 1.8×10^{-8} gamma-ray per proton.

Competitive resonances

The importance of establishing definitely any coincidence in the energy of resonances in different modes of disintegration of the intermediate nucleus has been previously discussed. Such a coincidence indicates that the disintegrations can be considered as competitive modes of decay of the same state of the compound nucleus.

In searching for coincidences in the energy of resonances in different processes it must not be overlooked that there is some possibility for an apparent coincidence between two different kinds of resonances which do not involve the same state of the intermediate nucleus. For example, if N_α alpha-particle resonances, N_γ gamma-ray resonances and N_π pair resonances are distributed at random over an energy range W, the number of pairs of different kinds of resonances separated in energy by less than ω, is on the average:

$$n_{\alpha\gamma}=2(\omega/W)N_\alpha N_\gamma$$

and so forth. In the present case $N_\alpha=4$, $N_\gamma=8$, $N_\pi=4$ so that if we take $\omega=10$ kev we obtain $n_{\alpha\gamma}=0.43$, $n_{\alpha\pi}=0.21$ and $n_{\gamma\pi}=0.43$.

We actually find two coincidences within 10 kev; namely, those between pairs and long range alphas at 0,85 Mev, and 1.35 Mev. On the basis of the above calculations it seems difficult to attribute both of these to accidental coincidences. On the other hand, a close comparison of the curves suggests that in both cases the peaks are slightly separated. A statistical study to determine the reality of the separation was made as follows: On a plot of the observations of each kind of radiation a reasonable curve was drawn to represent the background upon which the resonance is superimposed; this background intensity function was then subtracted from the observed intensity, and the centroid of the remaining intensity function was taken as the resonance energy. The separation at 0.85 Mev was found to be 9 ± 5 kev; the uncertainty is the probable error. This must be compared with the true widths of the peaks which we have estimated as 15 kev. The very prominent pair and long range alpha-particle peaks near 1.35 Mev appear to be coincident. A statistical investigation gives for the separation 6.5 ± 1.5 kev while the widths were both estimated to be 25 kev.

In estimating the probable error in the separation no account was taken of the fact that the observations were made at 12-kev intervals. We think it likely, however, that these separations are real. In both cases the long range alpha lies below the pair resonance in the direction to be expected but by an amount very much larger than that to be expected from the differential variation of the probabilities for alpha-emission over the line breadth. It has been suggested by Professor J. R. Oppenheimer that the observed dissimilarity in long range alpha and pair backgrounds must bring with it differences in the

[29] H. A. Bethe, Rev. Mod. Phys. **9**, 270 (1937).
[30] L. R. Hafstad and M. A. Tuve, Phys. Rev. **48**, 306 (1935); Van Allen and Smith, Phys. Rev. **59**, 108(A) (1940).
[31] H. A. Bethe, Rev. Mod. Phys. **9**, 69 (1937).

interference effects between resonance and background, at least in certain angular ranges, sufficient to give the apparent displacement of the peaks. Since the pair background is relatively the smaller, the displacement from resonance will be mainly in the long range alpha-curve and the resonance energies in Ne^{20} are best taken from the pair curve.

There are several gamma-ray resonances which are within 20 kev of pair resonances but both displacements and line breadth differences are here much too great to be accounted for by interference with the small backgrounds for pairs and gamma-rays.

Discussion

The character of the states

An energy level diagram is shown in Fig. 4. The relative positions of the ground states are determined from the masses. The levels $^{\gamma}O^{16}$ and $^{\pi}O^{16}$ are plotted from a knowledge of the gamma-ray and pair energies. The first six excited states in neon are those found by Bonner. The higher levels are those found in the present and similar experiments.

If we accept the evidence discussed above as indicating competitive resonances in the production of pairs and long range alpha-particles, it is simplest to interpret this as a branching process in the decay of certain states of Ne^{20}. According to Oppenheimer and Schwinger[22] this is reasonable; at energies above 1 Mev the effect of the Coulomb barrier is unimportant for both the long and short range alpha-particles. Following this interpretation the excited states of Ne^{20} produced by proton bombardment of fluorine were classified in four groups, according to the manner of their decay, as indicated in the diagram. As mentioned before, this conclusion implies that the parity of the state $^{\pi}O^{16}$ is even, and that it is possible to account for the pair emission through electromagnetic forces.

To explain the appearance of short range alpha-particles leading to gamma-emission rather than the long range alpha-particles we assume that the states $^{\gamma}Ne^{20}$ and $^{\gamma}O^{16}$ have odd parity and even angular momentum, or vice versa. Then the emission of both the short range alpha-particle leading to pairs and the long range alpha-particle

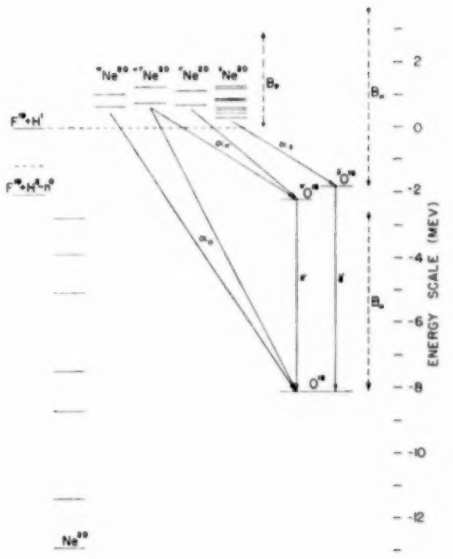

FIG. 4. Energy level diagram. The levels of Ne^{20} above the level $F^{19}+H^1$ are those observed in this and similar experiments. The levels of Ne^{20} plotted in the column above the ground state of Ne^{20} are those found by Bonner. The short dotted line in the left-hand column indicates his bombarding energy; the region between here and the level $F^{19}+H^1$ is unexplored. The transitions marked α_0 are described in reaction (1), those marked α_γ and γ in reaction (5), and those marked α_π and π in reaction (7). The arrows marked B_P and B_α show the barrier heights for protons and alpha-particles, respectively.

are forbidden. The simplest assumption is that some of the states of $^{\gamma}Ne^{20}$ are of the type (1, +) (angular momentum 1, and even parity) and that some of the states $^{\pi}Ne$ and $^{\alpha\pi}Ne$ are of the type (0, +). These two different kinds of states of the neon nucleus might be formed by the two ways of adding the angular momenta of the fluorine nucleus and an s proton. The $^{\alpha}Ne$ states can be assumed to have even parity but probably have even angular momenta greater than zero.

Remaining difficulties

However the picture is far from complete. No explanation has been advanced for the irregular variation in intensity of the various gamma-ray levels. More puzzling still is the very high probability of gamma-ray production compared with the other two processes. All three processes depend on the emission of an alpha-particle from the neon nucleus, and the effect of the barrier favors the long range alpha-particles. This is however compensated for in part by the higher probability of an alpha-particle having an energy

near the average rather than the total excitation energy in the compound nucleus. The three types of states $^{\alpha}Ne^{20}$, $^{\gamma}Ne^{20}$ and $^{\alpha\gamma}Ne^{20}$ are differentiated on the basis of the relative intensities of the long and short range alpha-particles which result from their decay, but a complete explanation for this difference in behavior has not been proposed. Of course the irregular variation of the ratios of the yields of long range alphas to pair-alphas may be understood in part in terms of the fact that large changes in angular momentum would decrease the yield of the shorter range pair-alphas. But the consistently large ratios of gamma-alphas to pair-alphas can apparently not be understood on this basis, especially since $^{\gamma}Ne^{20}$ and $^{\gamma}Ne^{20}$ can both be formed by s collisions and both $^{\gamma}O^{16}$ and $^{\gamma}O^{16}$ by the ejection of an s alpha-particle. It is possible that a new selection rule is involved.[32]

The yield measurements must be supplemented by precise measurements of the total decay width Γ of each resonance and of the distribution in angle of the alpha-particles before a complete description of the properties of the levels of the intermediate nucleus can be given.

In conclusion we wish to express our appreciation to Professor J. R. Oppenheimer for numerous contributions to the theoretical aspects of this discussion.

[32] Streib, Fowler and Lauritsen, Phys. Rev. **58**, 187(A) (1940).

FEBRUARY 1, 1941 PHYSICAL REVIEW VOLUME 59

Velocity-Range Relation for Fission Fragments

N. BOHR
Institute of Theoretical Physics, University of Copenhagen, Copenhagen, Denmark
(Received November 28, 1940)

Considerations indicated in an earlier note as regards the rate of velocity loss of fission fragments along the range are developed in greater detail and a comparison is given between the calculations and more recent experiments. Especially is a more precise estimate given for the charge effective in electronic encounters which are determining for the stopping effect over the first part of range, and for the screening distance in nuclear collisions which are responsible for the ultimate stopping. In the estimate of the effect of electronic interactions, use is made of a comparison with the stopping of α-particles of the same velocities. In this connection, however, a certain correction is necessary due to an intrinsic difference in the stopping formulae to be applied in the two cases. Moreover, fission fragment tracks show, in contrast to α-rays, a considerable range straggling originating in the end part of the range. It is shown that in this respect also the calculation agrees closely with the experimental data.

IN an earlier note[1] the peculiar velocity-range relation for fission fragments revealed by cloud-chamber studies of fragment tracks[2] has been briefly discussed. In particular, it was pointed out that in the different parts of the range we have to do with two essentially different stopping mechanisms. At the beginning of the range, where the total charge of the fragment is still large, the stopping is due practically only to energy transfer to the individual electrons in the atoms of the gas penetrated. With decreasing velocity, however, the fragment charge effective in electronic interactions will rapidly decrease and direct transfer of momentum from the fragment to the gas atoms through close nuclear collisions will gradually become of greater importance. In the last part of the range, such collisions will, in fact, be almost entirely responsible for the stopping effect. In the note it was shown that it is possible, from very simple considerations regarding the way in which the charge of the fragment varies with velocity, to account at least qualitatively for the characteristic features of the experimental velocity-range relation. The continuation of the work,

[1] N. Bohr, Phys. Rev. **58**, 654 (1940).
[2] K. J. Brostrøm, J. K. Bøggild and T. Lauritsen, Phys. Rev. **58**, 651 (1940).

however, has led to essential improvements of the various estimates entering into the calculations and it may, therefore, be of interest to give here a somewhat closer discussion of the question.

The problem of primary importance in the discussion is the estimate of the number of electrons carried with the fragment nucleus on its way through the gas. This number is determined by the balance between the continual capture and loss of electrons by the fragment in encounters with the gas atoms. Here we meet at once with a behavior essentially different from that of high speed particles with small nuclear charge, such as protons and α-rays. In fact, in the latter cases any captured electron will have an "orbital velocity" small compared with the velocity of the particle itself and the probability of electron capture will, therefore, be much smaller than the probability of subsequent electron loss, with the result that the particles will be practically stripped of electrons over nearly the whole range. In the case of fission fragments, however, a considerable number of the electrons in the neutral atom will have orbital velocities larger than the initial velocity of the fragment, and, as stressed in the earlier note, the capture and loss of such electrons will take place under conditions very different from those for electrons more loosely bound.

We shall, for brevity, refer in the following to the ensemble of the electrons in the neutral fragment with orbital velocities greater than the instantaneous fragment velocity V as the "electron core" of the fragment. In the first place, the probability of capture of electrons into states normally occupied by this core will be much larger than that for capture into states of looser binding. Indeed, in collisions with gas atoms sufficiently heavy to possess themselves a corresponding electron core, the probability of capture of the former kind will be quite considerable even in a single collision, if the cores penetrate each other. Moreover, while the electrons outside the core will be easily removed during encounters with the electrons and nuclei of the gas atoms, electrons belonging to the core can obviously not be removed during such encounters, at any rate if the charge of the gas nuclei is smaller than the nuclear charge of the fragment. With a high degree of approximation we may, therefore, assume that the fragment at any instant along its path carries with it a number of electrons just constituting the core.

In this connection it is interesting to note that even in the original fission process we may expect that both fragments escape with their electron cores practically intact. In spite of the violence of the rupture of the original heavy nucleus the initial fragment velocities will, in fact, be considerably smaller than the orbital velocities of the major part of the electrons in the original atom. As a consequence of the almost adiabatic influence on such electrons of the translatory motion of the nuclear fragments, a balance like that described will, therefore, be established, at any rate partially, before the fragments are separated by distances comparable with atomic dimensions.[3]

The calculation in the previous note of the rate of velocity loss of the fragment per unit path was based on the following formula (not stated explicitly there):

$$\frac{1}{N}\frac{dV}{dx}=\frac{4\pi e^4}{M_1 m V^3}(Z_1^{\text{eff}})^2 \sum_s \ln\frac{m V^3}{2\pi\nu_s e^2 Z_1^{\text{eff}}} + \frac{4\pi e^4 Z_1^2 Z_2^2}{M_1 M_2 V^3}\ln\left(\frac{M_1 M_2}{M_1+M_2}\frac{V^2 a_{12}^{\text{scr}}}{Z_1 Z_2 e^2}\right), \quad (1)$$

where N is the number of gas atoms per unit volume, e and m are the electronic charge and mass, $Z_1 e$, $Z_2 e$ and M_1, M_2 the charge and mass of the nuclei of the fragment and gas atoms,

[3] In an earlier attempt to estimate the influence of electron capture on the range-velocity relation of fission fragments, G. Beck and P. Havas [Comptes rendus **208**, 1643 (1939)] assumed that, immediately after the fission process, the fragment nucleus is almost stripped of electrons and that during its passage through the gas it gradually captures electrons at such a rate that the fragment charge decreases with time according to an exponential law. Assuming, further, that the rate of capture is so great that the fragment is practically neutralized before its velocity has fallen to half of its original value and neglecting the stopping and ionizing effects of direct nuclear collisions, they conclude that all ionizing effects of the fragment will disappear long before it is stopped. In particular, they see herein a possible explanation of the apparent discrepancy between range measurements based on the ionizing power of the fragment on the one hand and the transfer of its radioactivity on the other hand. From the excessive deflections of the paths of fragments near the end of the tracks in cloud-chamber pictures it is clear, however, that such discrepancies must rather be ascribed to ordinary thermal diffusion of the fragments in the gas within the period of radioactive decay which is extremely long compared with the time interval in which the fragment has lost all of its initial velocity.

respectively. Z_1^{eff} is the effective charge of the fragment nucleus in electronic encounters and a_{12}^{scr} is the distance between the nuclei where the electronic screening sets an effective limit to the action of their charges in close collisions. The summation in the first term is to be extended over the various electrons in the gas atoms or, rather, over the various virtual atomic oscillators of frequency ν_s, taken with their respective weights.

The first term, which accounts for the contribution to the velocity loss due to energy transfer to the individual atomic electrons, corresponds to the original formula[4] for the stopping of high speed particles, based on simple considerations of classical mechanics. It differs from the quantum-mechanical formula deduced by Bethe[5] by means of the Born approximation method by a factor in the logarithmic argument:

$$\kappa = hV/4\pi E_1 E_2, \qquad (2)$$

where h is Planck's constant, and E_1 and E_2 are the charges of the particles considered; thus, here $E_1 = Z_1^{eff}e$ and $E_2 = e$. The reason that the classical formula and not the Bethe formula is to be applied in our case is that κ, as we shall see below, is small compared with unity over the whole part of the range where electronic interaction constitutes the essential stopping effect. In fact, only for $\kappa \gg 1$ can a simple wave-mechanical diffraction procedure be applied rigorously to a collision between two charged particles, while for $\kappa \ll 1$ classical orbital pictures can, at least with high approximation, be applied to such a collision.[6]

The second term in (1) accounts for the contribution to the velocity loss by direct transfer of momentum from the fragment to the gas atoms through close nuclear collisions. While a few of these collisions give rise to side branches to the fragment track, the main contribution to the stopping effect at the end part of the range is due to numerous collisions which individually are not violent enough to cause visible branching and only add to the ionization of the track. In this case, κ is very small (of the order 10^{-3}) and we have, consequently, to do with a problem in which classical pictures can be applied with an extremely high degree of approximation. In contrast to the case of electronic encounters, where the limit to the energy transfer is set by the dynamic properties of the atomic oscillators indicated by the dependence of the logarithmic argument on ν_s, the limit indicated by the parameter a_{12}^{scr} is here set by the screening of the nuclear charge of the colliding atoms by the static charge distribution of the bound electrons.

The formula for the rate of velocity loss of the fragment given in the previous note was obtained by introducing in (1) the rough estimates

$$Z_1^{eff} = V/V_0 \quad \text{and} \quad a_{12}^{scr} = a_0(1/Z_1 + 1/Z_2), \qquad (3)$$

where the conventional notations

$$V_0 = 2\pi e^2/h \quad \text{and} \quad a_0 = h^2/4\pi^2 me^2 \qquad (4)$$

refer to the velocity and radius of orbit of the electron in the hydrogen atom. A closer examination of the electron distribution in heavy atoms, however, based on the results obtained by the statistical method of Thomas and Fermi leads to the more accurate estimates

$$Z_1^{eff} = Z_1^{\frac{1}{3}} V/V_0 \quad \text{and} \quad a_{12}^{scr} = a_0(Z_1^{\frac{1}{3}} + Z_2^{\frac{1}{3}})^{-\frac{1}{2}}. \qquad (5)$$

The first of the expressions (5) represents the resultant charge of the fragment nucleus and the electron core for velocities not too close to V_0; the second expression represents the screening distance effective in nuclear collisions, which is practically independent of the fragment velocity in the whole interval considered.

Introducing the value (5) for Z_1^{eff} into (2) we get

$$\kappa = 1/2Z_1^{\frac{1}{3}}, \qquad (6)$$

which gives a value for κ quite small compared with unity, since for fission fragments $Z_1^{\frac{1}{3}}$ lies between 3 and 4; thus, the use of classical mechanics in deducing formula (1) is here amply justified. For the comparison with the stopping power of α-rays mentioned below, it is interesting to note that this value for κ is even considerably smaller than the values for κ^{-1} for protons and α-rays in the same velocity interval. As regards the justification of the application of the first term of formula (1) to the electronic stopping of fission fragments it may further be noted that the linear dimensions of the fragment core, for the

[4] N. Bohr, Phil. Mag. **25**, 10 (1913) and **30**, 581 (1915).
[5] H. A. Bethe, Ann. d. Physik **5**, 325 (1930).
[6] Compare F. Bloch, Ann. d. Physik **16**, 285 (1933); and E. J. Williams, Sci. Progress, **121** (1936). For a closer discussion, see reference 11.

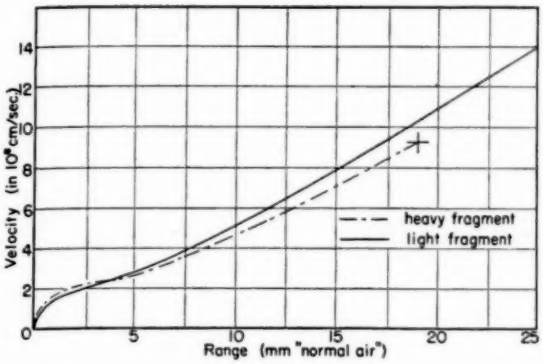

FIG. 1. Empirical velocity-range curves in argon.

radius of which we have approximately

$$r_c = a_0 Z_1^{\frac{1}{2}} V_0 / V, \tag{7}$$

are, of course, just of the same order of magnitude as the minimum distance of approach to a particle of charge Z_1^{eff} by an electron with velocity V, according to classical mechanics.

As pointed out in the previous note, formula (1) gives a value for the rate of velocity loss nearly independent of the velocity in the initial part of the range, corresponding to the almost constant slope of the experimental velocity-range curve in this region. This result follows from the linear dependence of Z_1^{eff} on V as well as from the fact that the sum of the logarithms in the first term of (1) is nearly proportional to V in the velocity interval considered. In estimating the absolute value of this sum by a comparison with the experimental data for stopping of α-rays with the same velocity, it must be taken into account that, owing to the occurrence in the logarithmic argument in (1) of the factor κ which does not appear in Bethe's formula to be applied to such light particles, a not inconsiderable correction has to be introduced. An estimate based on the statistical distribution of the oscillator frequencies ν_s in heavy atoms gives, in fact, that the value of the logarithmic sum will, as for α-rays, be nearly proportional to $Z_2^{\frac{1}{2}}$ but will have a numerical value only about $\frac{3}{5}$ of the value for α-rays with the same velocity.

Since the logarithmic sum is very insensitive to small changes in Z_1, the rate of velocity loss for fission fragments of different charge and mass should be proportional to $Z_1^{\frac{1}{2}}/M_1$ at the beginning of the range. In accordance with the empirical velocity-range curves in argon given in Fig. 1,[7,8] we shall, therefore, expect only a slightly greater slope for the lighter than for the heavier of the two main groups of fission fragments with mass and charge ratios of about 2 : 3. Moreover, as seen from the figure, we obtain a close estimate of the actual total range by extrapolating the initial linear slope of the curves to zero velocity. Using this fact in calculating the total range and applying for α-rays the well-known Geiger range formula we find by means of the first term in (1) for the ratio between the range R_F of a fission fragment and the range R_α of an α-particle with the same initial velocity V_i:

$$R_F/R_\alpha = 5(M_1/Z_1^{\frac{1}{2}})(V_0/V_i)^2, \tag{8}$$

where in determining the numerical factor regard is taken of the difference mentioned above in the values of the logarithmic sum in the two cases considered. The relation (8) is actually found to be in close agreement with the experimental data.

This general agreement may be considered as a sensitive test for the estimate of the effective charge of the high speed fragment in electronic encounters. In this connection it must, however, be noted that it is not justified to assume on the basis of such arguments only that Z_1^{eff} is identical with the total fragment charge for the velocities considered. In fact, a closer consideration shows that, if the fragment carried a number of bound electrons in addition to the core, the reduction in the stopping and ionizing effect would be essentially less than would correspond to the reduction of the total charge. It is, therefore, very interesting that a direct measurement of the fragment charge by Perfilov[9] by means of the deflection in magnetic field of fission fragments expelled in vacuum from thin layers of U_3O_8 has yielded a value of about $20e$. This value agrees, in fact, closely with the expression (5) for Z_1^{eff} at the beginning of the range where V is about 5 V_0.

When we pass to the portion of the range where the velocity is nearing V_0 and where the empirical velocity-range curve exhibits an almost flat

[7] N. Bohr, K. J. Brostrøm, J. K. Bøggild and T. Lauritsen, Phys. Rev. **58**, 839 (1940).
[8] J. K. Bøggild, K. J. Brostrøm and T. Lauritsen, Kgl. Danske Vid. Sels. Math.-fys. Medd. (Math.-phys. Comm., Acad. Sci. Copenhagen) **18**, 4 (1940).
[9] N. A. Perfilov, Comptes rendus Acad. Sci. U.R.S.S. **28**, 5 (1940).

plateau, several circumstances have to be taken into account in applying formula (1). In the first place, the estimate (5) for the fragment charge is, as already mentioned, only valid for a value of V considerably larger than V_0. For smaller velocities the charge will, in fact, decrease more rapidly and approach unity for velocities near V_0, since the very loosest bound electrons in heavy atoms are held almost as firmly as the electron in the hydrogen atom. Next, the basic assumptions in the calculation by which formula (1) is deduced, that the velocity of the moving particle is essentially higher than the orbital velocities of the atomic electrons and that the size of the particle is small compared with the orbital dimensions, are no longer fulfilled when V approaches V_0. Because of these circumstances, the rate of velocity loss will here be considerably smaller than the almost constant value for larger velocities, in agreement with the gradual diminishing of the slope of the velocity-range curve.

Just in the part of the range where the velocity is of the same order as V_0, the stopping effect of nuclear collisions which in the initial part of the range is very small compared with the effect of electronic interaction will, as explained in the previous note, gradually become preponderant, finally causing a steep descent of the velocity-range curve at the very end of the range. This character of the curve corresponds, in fact, to the very rapid increase with decreasing velocity of the factor before the logarithm in the second term of formula (1). Since the argument of the logarithm in this term is for $V=V_0$ still large compared with unity (about 15), the expression for the stopping effect of nuclear collisions will be valid for much smaller velocities than the first term in (1) and hold approximately down to velocities which are only a small fraction of V_0. While the logarithm is very insensitive to small changes in $a_{12}{}^{\text{scr}}$ and has almost the same value for the heavier and lighter fragment group, the factor before the logarithm is essentially larger for the heavier fragment group, giving rise to a still steeper final descent of the velocity-range curve for this group in accordance with the experimental data.

Also in quantitative respects, the course of the velocity-range curves near the end of the range is in close agreement with the second term in formula (1). In fact, if we compare the range R_0 for fission fragments of velocity V_0, deduced from (1) by neglecting entirely the first term, with the total range R_F of the fragments with initial velocity V_i estimated from this term in the manner described above, we find

$$R_0/R_F=k(M_2/m)Z_1^{-4/3}Z_2^{-3/2}(V_0/V_i), \quad (9)$$

where k is a constant which depends on the logarithm in the two terms in (1) and the value of which is about 0.07. Putting $V_i=5V_0$, we get from (9) for argon $R_0=R_F/10$ which fits in very well with the run of the curves on Fig. 1.

As mentioned above, the total range of fission fragments compared with that of α-rays should be practically the same for light and heavy gases. However, we see from (9) that we shall expect that the ratio of the end part of the range (where the stopping depends only on nuclear collisions), to the whole range should (apart from the case of hydrogen, where the value of M_2/Z_2 is abnormally low), be inversely proportional to $Z_2^{\frac{1}{3}}$. This conclusion is also supported by recent measurements on the range of fission fragments in helium[10] which have given a range, relative to that of α-rays, about 20 percent longer than the corresponding range in argon. Such a difference would, in fact, just be explained if the ratio between R_0 and R_F is three times as large in helium as in argon, corresponding to the ratio of the inverse square roots of their nuclear charges.

Range measurements on fission fragments show a very considerable straggling which, as pointed out in the previous note, must be ascribed to the end part of the range. In fact, for the initial part of the range, where the stopping is due to electronic encounters, we shall, just as for α-rays, expect a very small degree of straggling, but at the end part, where the stopping is due to encounters with much heavier particles, the straggling effect will be far greater. Using the same calculations as originally applied for the estimate of α-ray straggling[4] we shall, for the straggling due to nuclear collisions, expect that the range will be statistically distributed according to the formula

$$W(R)=\frac{1}{(2\pi)^{\frac{1}{2}}\rho R_0}\exp\left[-\frac{(R-R_0)^2}{2\rho^2R_0^2}\right], \quad (10)$$

[10] J. K. Bøggild, K. J. Broström and T. Lauritsen, Phys. Rev. **59**, 275 (1941) (following paper).

where $W(R)dR$ is the probability that the range has a value between R and $R+dR$; and R_0 is the mean value of the range, while ρ is a numerical constant approximately given by

$$\rho^2 = 3M_1M_2/4(M_1+M_2)^2. \qquad (11)$$

For helium and argon (11) gives values of ρ equal to 0.16 and 0.37, respectively. Although the relative straggling is thus more than twice as large in argon as in helium, the absolute straggling of the range should be nearly the same, since the value for R_0 for the sensitive end part of the range should be about three times as large in helium as in argon. According to the above estimate of the fraction of the range where nuclear collisions constitute the preponderant stopping effect, we should expect $R_0\rho$ for both gases to be about 5 percent of the total range, in good agreement with the experiments which give for argon, as well as for helium, a straggling of this order of magnitude.[8,10]

The various considerations here indicated are treated in greater detail in a paper shortly to appear in the Communications of the Copenhagen Academy of Science.[11] Especially is a closer discussion given there of the applicability of simple mechanical arguments for the treatment of the stopping and scattering of heavy highly charged atomic particles as well as of the ionization and electron capture by such particles.

Note added in proof.—After the present paper was sent from Copenhagen, we received here the issue of *The Physical Review* of October 15, 1940, which contains an article by W. E. Lamb on the passage of uranium fission fragments through matter. In main features the considerations of this article correspond to the arguments developed here and similar results are obtained. The treatment differs, however, at various points which will be commented upon in the fuller paper referred to above[11] where, also, the results of various experimental investigations not known in Copenhagen when the recent publications from this Institute were completed will be discussed.

[11] N. Bohr, Kgl. Danske Vid. Sels. Math.-fys. Medd. (Math.-phys. Comm., Acad. Sci. Copenhagen), **18**, 8 (1940).

FEBRUARY 1, 1941 PHYSICAL REVIEW VOLUME 59

Range and Straggling of Fission Fragments

J. K. Boggild, K. J. Brostrom and T. Lauritsen
Institute of Theoretical Physics, University of Copenhagen, Copenhagen, Denmark

(Received November 28, 1940)

As reported in an earlier note to *The Physical Review*,[1] a study of the tracks of uranium fission fragments in a cloud chamber filled with argon gas has yielded evidence for two groups of tracks corresponding to the two types of fragments known from direct measurements of their kinetic energies and for chemical analysis of the radioactive products. Direct measurements of the ranges of fragments expelled in both directions simultaneously from thin uranium targets on thin foils in the cloud chamber gave some indication of two groups. Also, a statistical analysis of the number of side branches along the ranges of a large number of tracks from thick targets showed clearly the presence of two different kinds of tracks, of which the one had two to three times as many branches at the other over most of the range, while near the end, the numbers of branches were more nearly equal. On the basis of general considerations regarding the course of the range-velocity curves and the relative charges of the fragments, it was concluded that the heavier particle had the more branches and the shorter range, corresponding to its higher charge and lower initial velocity. Further experiments, both in argon gas[2] and in

[1] N. Bohr, J. K. Boggild, K. J. Brostrom and T. Lauritsen, Phys. Rev. **58**, 839 (1940).

[2] The work on argon is more fully reported in the Kgl. Danske Vid. Sels. Math.-fys. Medd. (Math.-phys. Comm., Acad. Sci. Copenhagen) **18**, 4 (1940).

helium, have yielded more information concerning the grouping, confirmed the assignment of the larger number of branches to the short track, and permitted a comparison of the stopping powers of argon and helium for fission fragments.

Thin evaporated layers (about 0.2 mg/cm²) of uranium on mica foils mounted in the center of a 25-cm cloud chamber were bombarded with slow neutrons and the tracks of both fragments from a given fission process photographed stereoscopically. The stopping power of the gas was determined by measuring the ranges of polonium α-rays, admitted through a window in the side of the chamber. The results of range measurement on 8 pairs and 20 "half-pairs" (in which one member did not end in the illuminated region of the chamber) in argon and 10 pairs and 10 "half-pairs" in helium are given in the accompanying histograms (Fig. 1). The two groups with opposite cross-hatching represent simply the shorter and longer member of each pair while the double cross-hatched groups on the right represent the sums of the ranges of the pairs. While the histograms for the individual members show only little separation into two groups, the grouping is clear from the relatively small spread of the sums. The breadth of this spread is, in fact, a measure of the straggling which is practically independent of the possible variations in grouping as regards the masses and initial velocities of the fragments. Thus, if the fragments from a given fission process had the same average range, the straggling of the individual members should be roughly $\sqrt{\frac{1}{2}}$ of the spread in the sum, while the actual variation of the measured values is nearly three times this amount. On the other hand, the data are quite well fitted by the assumption of two groups, each with a straggling of about $\sqrt{\frac{1}{2}}$ that of the sum group. There is, in fact, no indication that the spread of the groups is essentially larger than this value, in conformity with other evidence which shows that the excited uranium nucleus always divides in approximately the same way. It is interesting to note that the straggling is approximately the same in helium and in argon, estimated as well from the range-sums as from the ranges of individual groups of fragments. The straggling in the latter groups is perhaps a little greater than corresponds to that of the range sums, because of the finite thickness of the uranium layer which, of course, has no influence on the range sums.

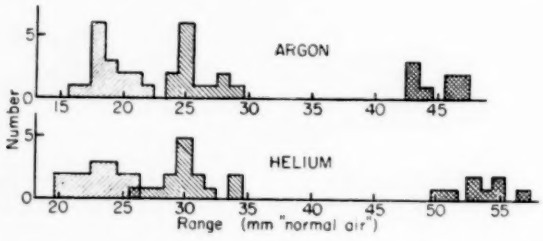

FIG. 1. Ranges and sums of ranges of paired fragment tracks, relative to ranges of α-rays of similar velocities.

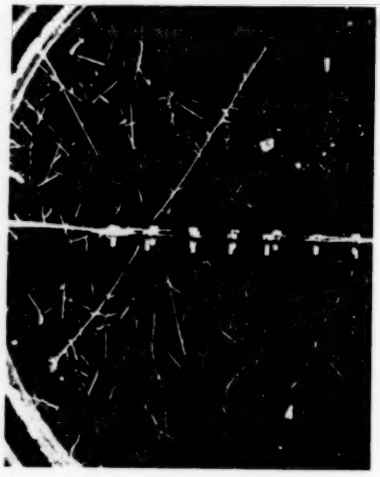

FIG. 2. Typical pair of fragment tracks in helium at 1.3 atmos. pressure. Tracks originate in upper side of 1.2 mg/cm² mica foil. Total length about 13 cm.

In argon, the mean ranges of the two groups, referred to normal air as defined by the stopping of α-particles, are 19 and 25 mm,[3] while the corresponding values in helium are 23 and 30 mm. The difference of about 20 percent between the values for argon and helium is an indication that the stopping power of helium relative to argon is lower for fission particles than for α-particles, presumably because of a smaller rate of velocity loss towards the end of the range, where the stopping is determined by nuclear collisions. As explained in the preceding article by Professor N. Bohr,[4] the stopping power for

[3] The values reported in the previous note have been reduced by corrections to the stopping power of the gas in the cloud chamber.

[4] N. Bohr, Phys. Rev. **59**, 270 (1941) (preceding paper).

fission fragments relative to that for α-rays should, in fact, be nearly the same over the whole part of the range where the stopping is mainly caused by electronic encounters. There it is also pointed out that the straggling must be ascribed practically entirely to the end part of the range, where the effect of nuclear collisions is predominant. It is just because of the relatively greater length of this part of the range in light gases that the resultant straggling in the total range is approximately the same in helium and argon.

Corresponding to the statistical analysis of the branch distribution on the argon tracks, an examination of the branch distribution was also made in helium. We have here not much material from cloud-chamber pictures at low pressure but, fortunately, since in helium the branches are relatively longer in comparison with the length of the whole track, it was possible to perform the analysis at the relatively high pressures used in the range determination of the tracks from thin uranium targets. This circumstance gives the advantage that the separation into groups need not be made by indirect statistical methods but can be based directly on the difference in range. The photograph (Fig. 2) shows a typical example of the paired fragment tracks in helium, with several branches on each member.

The results of the counts indicated a preponderance in branches of the shorter track, with a factor of about 1.5 near the end of the range, and about 1.8 over the remainder of the range. While the number of branches—about 120 in all—is too small to justify definite conclusions, the agreement with the previously estimated values is satisfactory and may be considered to support the general character of the range-velocity curves of the two groups of fragments. A comparison of the absolute numbers of branches within definite energy limits near the end of the range in argon and in helium also gave good agreement with the theoretical expectations.

The authors' sincerest thanks are due Professor Niels Bohr, under whose direction this work has been carried out and whose constant encouragement and active help has made it possible.

FEBRUARY 1, 1941 PHYSICAL REVIEW VOLUME 59

Protons from the Deuteron Bombardment of the Separated Isotopes of Chlorine

E. F. SHRADER* AND ERNEST POLLARD
Sloane Physics Laboratory, Yale University, New Haven, Connecticut

(Received December 13, 1940)

The bombardment of chlorine by 3.2-Mev deuterons is found to give rise to several groups of protons and possibly to one group of alpha-particles. By bombarding targets in which the proportion of heavy chlorine was more than doubled an assignment of some of the groups has been possible. The assignment of Q values is as follows. $Cl^{35}(dp)Cl^{36}$: 6.31; 5.35; and 1.50 Mev. $Cl^{37}(dp)Cl^{38}$: 4.02; 3.02; 2.10. These figures lead to masses of 35.9808 and 37.9806 for the isotopic masses of Cl^{36} and Cl^{38}, respectively. A group which appears at 12 cm range we assign to the light isotope according to the reaction $Cl^{35}(d\alpha)S^{33}$. The Q value is 9.1 Mev which gives a mass of 32.9828 for S^{33} in reasonable agreement with the mass derived from the $S^{32}(dp)S^{33}$ reaction.

INTRODUCTION

THE fact that the bombardment of chlorine by deuterons would give rise to protons has been known, since both the isotopes Cl^{36} and Cl^{38} have been prepared by this reaction.[1] The direct detection of the protons and the measurement of the ranges of the resulting groups is of interest since it permits information

* Now at the Case School of Applied Science, Cleveland, Ohio.

[1] D. C. Grahame and H. J. Walke, see Livingood and Seaborg, Rev. Mod. Phys. **12**, 35 (1940); F. N. D. Kurie, J. R. Richardson and H. C. Paxton, Phys. Rev. **49**, 368 (1936).

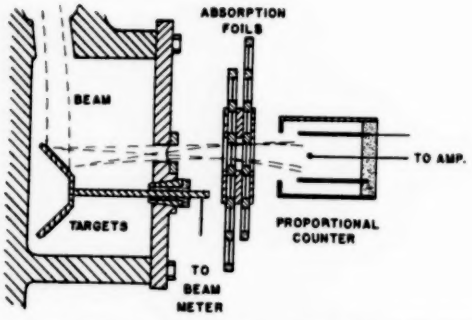

FIG. 1. Bombardment chamber, and detecting arrangements. The beam strikes the target as indicated, causing protons to be emitted in all directions. Those emitted at right angles to the beam emerge through an aluminum foil, pass through various absorbing foils and are detected in a proportional counter.

regarding masses of several nuclear species to be obtained. This information cannot, however, be obtained unless the assignment of the appropriate groups to the isotope responsible can be made, an assignment which is impossible unless the proportion of the two isotopes in targets can be altered. By means of a thermal diffusion isotope separation apparatus it has been possible to obtain targets with definitely different proportions of the two isotopes and an assignment made of all the groups definitely resolved.

EXPERIMENTAL ARRANGEMENTS

The apparatus for the separation of the isotopes has been described elsewhere.[2] The ratio of the heavy to the light isotope was determined by bombarding samples of HCl gas containing the normal proportions and separated proportions by the cyclotron beam for the same time and same beam current. The relative amounts of the 37-minute Cl^{38} were then used to measure the amounts of Cl^{37} present in the two samples. This is a simple method of making such a determination and is particularly to be recommended in this case as HCl is rather unpleasant to introduce into a mass spectrometer.

The chlorine was bombarded as silver chloride, previous experiments having shown that the silver gave a negligible yield in comparison with the yield of protons from the chlorine. The general technique has been described in a previous paper[3] and needs no remark except as concerns the preparation of the targets. We found that a target prepared by precipitation of AgCl with silver nitrate gave uncertain results at long ranges, and decided that some nitrogen had been entrained with the precipitate of silver chloride. Moreover, the layer of AgCl was nonuniform and unsuitable for the detection of proton groups. We therefore prepared targets by electrolysis as follows. The chlorine to be bombarded was obtained first in the form of approximately 0.02*N* HCl. A thoroughly clean piece of silver about 3 cm^2 in area forming the anode, a thin and very uniform layer of AgCl was electroplated from the solution on to the silver. A current of 0.075 ampere flowing for about two minutes is sufficient to coat the surface of the silver with one to two milligrams of chlorine per square centimeter. After allowing to dry in darkness the target was fastened on to an all-silver mounting by means of small silver bolts. In this way contamination may be kept to a minimum. We tested for the prevalent contamination by carbon from the pump oil by bombarding a target for about ten minutes and then looking for N^{13} due to $C^{12}(dn)N^{13}$. We found no activity except the 37-minute activity of Cl^{38}, which means that no proton groups could be caused by carbon contamination. We used thicker targets to study the longer range, low yield groups and targets of about one centimeter air equivalent (about 0.3 Mev) for the more prolific shorter range groups.

EXPERIMENTAL RESULTS

Figure 1 shows the arrangements for bombarding. Absorption curves from targets of

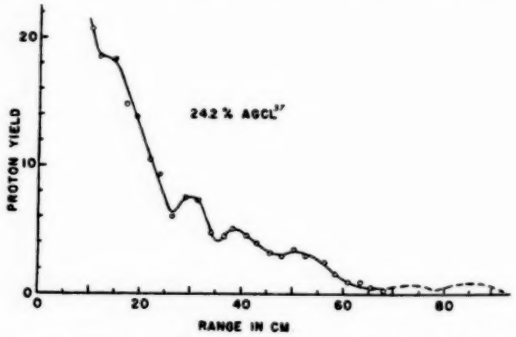

FIG. 2. Absorption curve for protons from a normal target of silver chloride. Six groups appear, with a seventh at very small absorption which is ascribed to alpha-particles.

[2] E. F. Shrader, in course of publication.

[3] E. Pollard, W. L. Davidson, Jr. and H. L. Schultz, Phys. Rev. **57**, 1117 (1940); E. Pollard and W. W. Watson, *ibid.* **58**, 12 (1940).

normal and heavy chlorine (24.2 percent and 53 percent Cl^{37} bombarded by deuterons) were plotted and are shown in Figs. 2, 3 and 4. It is seen from these curves that there are at least six definite proton groups having ranges of 27, 33, 44, 54, 77, and 93 cm (uncorrected for variation of range in Al with velocity) with a possible error of ± 2 cm. If we call the group of 27 cm range group A, that of 33 cm range group B, and so on, it can be seen that the relative yield of the three groups B, C, and D to each other has remained very nearly the same in going from normal chlorine to heavy chlorine. This fact is evidence that all three of these groups arise from the same isotope of chlorine. At the same time the yield of group A has decreased relative to groups B, C, and D in Fig. 3 as compared to Fig. 2. Further the apparent range of the group has decreased as would be expected if the yield of group B had been built up relative to A thus changing the shape of the composite curve. This establishes that group A is due to Cl^{35}, while groups B, C, and D must be assigned to Cl^{37}. The identification of the long range groups E and F was made by comparing them with the yield of group D. Using the yield at 50 cm as a standard it was found that the yield of both the groups, while remaining the same relative to each other, changed by a factor of approximately three in going from one target to the other, the normal sample giving the larger yield. This is the ratio one would expect using the isotope concentrations given. This fact again points to the identification of group D as due to Cl^{37} while at the same time it establishes the fact that the two long range groups E and F are caused by Cl^{35}. The yield of these two long range groups was so small that the background caused by neutron recoils rendered us a little unhappy about our measurement of their ranges although we made something like ten runs on this part of the curve alone. It was therefore decided to use the method of coincidence counting to study this part of the curve[4] with the results shown in Fig. 4 where the upper curve is the average of runs taken by direct counting and the lower is the curve found by coincidence counting. In the second case the yield of coincidences when a thick "infinity" absorber was interposed was about two per minute (these are probably all caused by spurious pulses originating in electrical disturbances) while the yield of coincidences from the chlorine target at 82 cm range was thirty per minute. It can be seen that the coincidence method confirms the previous findings.

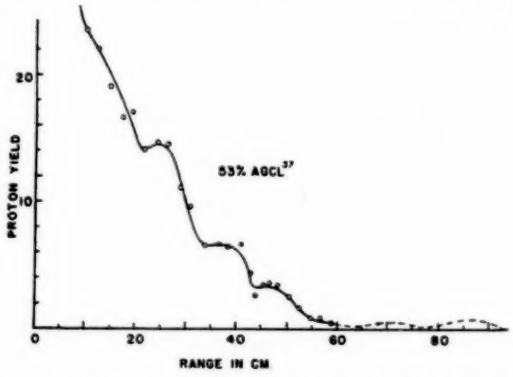

FIG. 3. Absorption curve for protons from a target of silver chloride enriched in the heavy isotope. The six groups are present, but the abundance of the three groups ending at 33, 44 and 54 cm is increased relative to the groups at 27, 77, and 93 cm. These three groups are therefore caused by the bombardment of Cl^{37}.

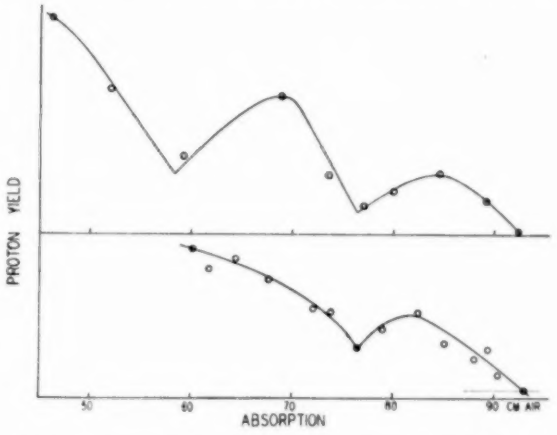

FIG. 4. Absorption curve showing the detail of the long range groups. The upper curve was taken with single counting while the lower was taken by counting double coincidences, which reduces the random background caused by neutron recoils. Three groups are seen, of which the two of longest range are caused by Cl^{35}.

There is evidence that the group at 12 cm range is an alpha-particle group caused by the reaction $Cl^{35}(d\alpha)S^{33}$. Its observation is greatly complicated by the very large yield of protons and the fact that the scattered beam has a range only a little less. The fact that it appears

[4] E. Pollard and R. F. Humphreys, Bull. Am. Phys. Soc. **15**, 7 (1940), Abstract No. 4.

most prominently on the light target is evidence in favor of this assignment.

The groups found here by no means exhaust the number which may actually be present, but rather represent the most favorable transitions in the nuclei of Cl^{36} and Cl^{38}.

Discussion

In Table I are given the energy change values for the reactions $Cl^{35}(dp)Cl^{36}$, $Cl^{37}(dp)Cl^{38}$, and $Cl^{35}(d\alpha)S^{33}$.

The limiting energy change value for the three reactions can be used to derive masses if the masses of the target elements are known. These are not very satisfactory. If a chain of nuclear reactions is employed the best values obtainable for the two stable chlorine isotopes are 34.98107 and 36.97829,[5] while mass-spectroscopic values are 34.97903 and 36.97786.[6] The transmutation values are derived from a series of good determinations of energy change values which agree with the mass-spectroscopic value for P^{31},[7] but not with the value for S^{32}.[7] The mass-spectroscopic value for Cl^{35} given above does not agree with the Q value for the $S^{32}(\alpha p)Cl^{35}$ reaction. There is need for much further work in this region of the elements both by transmutation and the mass spectrometer. If we take the transmutation values, the derived masses for Cl^{36} and Cl^{38} are 35.9808 and 37.9806, with errors as far as the energy changes in this work are concerned of 0.0003.

A check on the consistency of the energy measurements can be made by using the fact that the energy of the beta-ray emitted by Cl^{38} is 4.8 Mev.[8] This gives us the mass of A^{38}, which is linked with that of Cl^{35} by the reaction $Cl^{35}(\alpha p)A^{38}$.[9] The mass of A^{38} which we derive from the work here described is 37.9754, while if the data of Pollard and Brasefield are corrected for the air equivalent of aluminum foils according to Livingston and Bethe[10] the value derived from the alpha-particle bombardment of chlorine is also 37.9754. With the two mass-spectroscopic values given above the values for A^{38} by the two approaches are 37.9734 and 37.9740. Both figures agree within the experimental errors given, but the agreement is more satisfactory for the masses derived from transmutation.

The fact that Cl^{36} has a maximum beta-ray energy of 0.7 Mev[11] enables the mass of A^{36} to be calculated, giving 35.9800. Since Cl^{36} can also emit a positron the mass of S^{36} must also be very close to this value.

The group at 12 cm range, if correctly assigned, leads to the value 32.9828 for the mass of S^{33}, which is in fairly good agreement with the value 32.9826 derived from the $S^{32}(dp)S^{33}$ reaction.[5]

The energy levels obtained for the product nucleus Cl^{38} are consecutive and so can be discussed. It will be noticed that their spacing is roughly one Mev. This can be compared with the spacing of 2 Mev found in the stable nucleus of A^{38} in the reaction $Cl^{35}(\alpha p)A^{38}$. There may be some significance in the fact that Cl^{38} is unstable while A^{38} is stable, but we prefer to think that the manner of production of the final nucleus is responsible for exciting different energy levels and that the spacing observed depends more on selection rules than on the nature of the nucleus itself.

In conclusion we wish to thank Professor W. W. Watson for discussion and help with the isotope separation, and Mr. Harry Schultz for assistance in running the cyclotron. We are also grateful for a grant from the George Sheffield Fund which made possible the construction of the cyclotron.

Table I. *Energy change values.*

Proton Energy (Mev)	Q value (Mev)
Reaction $Cl^{35}(dp)Cl^{36}$	
9.10	6.31
8.15	5.35
4.40	1.50
Reaction $Cl^{37}(dp)Cl^{38}$	
6.85	4.02
5.90	3.02
5.00	2.10
Reaction $Cl^{35}(d\alpha)S^{33}$	9.1

[5] E. Pollard, Phys. Rev. **57**, 1186 (1940).
[6] T. Okuda, K. Ogata, K. Aoki and Y. Sugawara, Phys. Rev. **58**, 578 (1940).
[7] F. W. Aston, Nature **138**, 1094 (1936).
[8] F. N. D. Kurie, J. R. Richardson and H. C. Paxton, reference 1.
[9] E. Pollard and C. J. Brasefield, Phys. Rev. **50**, 890 (1936).
[10] M. S. Livingston and H. A. Bethe, Rev. Mod. Phys. **9**, 272 (1937).
[11] D. C. Grahame and H. J. Walke, reference 1.

The Scattering of Fast Electrons by Heavy Elements. II

J. H. BARTLETT, JR. AND T. A. WELTON
Department of Physics, University of Illinois, Urbana, Illinois

(Received June 13, 1940)

If fast electrons impinge on a mercury atom, the external electrons will modify the nuclear scattering, at least for small angles. We have determined the amount of scattering to be expected, as a function of angle, for 100-kv electrons and for 230-kv electrons. For the former, shielding is effective below 60°, and for the latter, below 15°. For the determination of phase shifts, the electron may be pictured as moving in an effective (Dirac) field, which involves zero, first, and second derivatives of the ordinary (Hartree) field. Three methods were used: (1) integration with the differential analyzer, (2) the WKB procedure, and (3) the first-order Born approximation. Methods (1) and (2) lead to results in good agreement with each other for all angular momenta, and method (3) gives good results for large angular momenta, despite the fact that the first-order correction to the wave function is large. The summation of the series for the scattering amplitudes was accomplished by noting that the phase shifts decreased in an exponential manner for large values of the angular momentum.

IF fast electrons undergo single elastic scattering from an atom, then we expect the angular distribution at sufficiently large angles to be determined by the effect of the nucleus alone, since large deflections accompany close distances of approach. For small angle scattering, however, the outside electrons will exert the controlling influence. In a previous research,[1] the single scattering of fast electrons by mercury nuclei was calculated. In this paper, we present results which include the contributions made by the extranuclear electrons. Since an easy technique for calculation of scattering for electrons of arbitrary energy has not yet been evolved, we have limited ourselves to energies of 100 kv and 230 kv.

For the mercury atom, a Hartree model is used. The spin-orbit interaction and other relativistic characteristics of the incident electron may be included (as will be shown) in an effective central field which acts on this electron. The phase shift caused by this field can then be found, as a function of angular momentum and of incident energy, and the series for the scattering amplitudes summed.

To determine the phase shifts, it is necessary to integrate numerically. The differential equation has a singular point at the origin, but the actual field is approximately Coulomb in the neighborhood, so that the Gordon[2] solutions of Dirac's equation may be used. From $r=0.002$ (atomic unit) to $r=0.26$ (in some cases $r=0.65$) the solution was carried outward on the Massachusetts Institute of Technology differential analyzer. For greater values of the radius, the WKB method has sufficient validity, and was therefore employed.

HARTREE FIELD

The potential energy of an electron at radius r, denoted by Z_p/r, has been tabulated by Hartree.[3] We have fitted these values by means of exponential functions (in order to facilitate differentiation) and find that the effective atomic number Z_p can be represented adequately by the equation $2Z_p=33.7e^{-17.376r}+95.9e^{-3.892r}+30.3e^{-1.253r}$. Near the origin (in the range $r\leq 0.02$) a single exponential suffices, i.e., $Z_p=80e^{-6.3256r}$.

DIRAC FIELD

Darwin[4] writes the Dirac equations for an electron in a central field $V(r)$ as

$$(1/\hbar c)(W+eV+m_0c^2)F + (dG/dr)-(l/r)G=0, \quad (1)$$

$$-(1/\hbar c)(W+eV-m_0c^2)G + (dF/dr)+[(l+2)/r]F=0.$$

If l is a positive integer, then Eqs. (1) have

[1] J. H. Bartlett and R. E. Watson, Phys. Rev. **56**, 612 (1939); Proc. Am. Acad. **74**, 53 (1940).
[2] W. Gordon, Zeits f. Physik **48**, 11 (1928).
[3] D. R. Hartree, Phys. Rev. **46**, 743 (1934), Table III.
[4] C. G. Darwin, Proc. Roy. Soc. London **A118**, 654 (1928). We have used l instead of k for the Legendre polynomial subscript.

solutions regular at the origin. The Dirac angular momentum quantum number j' is equal to $-l-1$ for $j=l+\frac{1}{2}$, and to l for $j=l-\frac{1}{2}$. The solutions of (1) which refer to the state $j=l+\frac{1}{2}$ (or $j'=-l-1$) are denoted by Darwin as F_l, G_l, while those for $j=l-\frac{1}{2}$ (or $j'=l$) are F_{-l-1}, G_{-l-1}. Let us now substitute as follows: $\psi_1=rF$, $\psi_2=-rG$, $\Pi=(1/\hbar c)\times(W+eV+m_0c^2)$, and $\Phi=(1/\hbar c)(W+eV-m_0c^2)$. Then

$$\Pi\psi_1-(d\psi_2/dr)-(j'/r)\psi_2=0, \qquad (2)$$
$$\Phi\psi_2+(d\psi_1/dr)-(j'/r)\psi_1=0.$$

For a Coulomb field, $(eV/\hbar c)=\alpha/r$, where $\alpha=(Ze^2/\hbar c)$. In this case, the equations are

$$(d\psi_1/dr)-(j'/r)\psi_1 =[-(1/\hbar c)(W-mc^2)-(\alpha/r)]\psi_2,$$
$$(d\psi_2/dr)+(j'/r)\psi_2=[(1/\hbar c)(W+mc^2)+(\alpha/r)]\psi_1.$$

These are the same as those of Gordon (reference 2, Eq. (1)). Let us now drop the primes from the j'*s*. The function ψ_1 may be eliminated from (2). We have

$$\left(\frac{d}{dr}-\frac{j}{r}\right)\Pi^{-1}\left(\frac{d\psi_2}{dr}+\frac{j}{r}\psi_2\right)=-\Phi\psi_2.$$

This results in a second-order equation for ψ_2, namely,

$$\frac{d^2\psi_2}{dr^2}+\Pi\left[\frac{d}{dr}\left(\frac{1}{\Pi}\right)\right]\frac{d\psi_2}{dr}+\Pi\left[\frac{d}{dr}\left(\frac{j}{\Pi r}\right)\right]\psi_2 -\frac{j^2}{r^2}\psi_2+\Pi\Phi\psi_2=0. \qquad (3)$$

Equation (3) is of the form

$$\psi_2''+p(r)\psi_2'+q(r)\psi_2=0,$$

where $p(r)=-(d/dr)\log\Pi$, and

$$q(r)=\Pi\Phi-[j(j+1)/r^2]-(j\Pi'/r\Pi).$$

By means of the substitution

$$\psi_2=y\Pi^{\frac{1}{2}}, \qquad (4)$$

one can obtain[5] an equation with no first-order term. It is

$$y''+Q^2(r)y=0, \qquad (5)$$

where

$$Q^2(r)=q-\tfrac{1}{2}p'-\tfrac{1}{4}p^2 =\Pi\Phi-\frac{j(j+1)}{r^2}-\frac{j}{r}\frac{d}{dr}\log\Pi +\frac{1}{2}\frac{d^2}{dr^2}\log\Pi-\frac{1}{4}\left[\frac{d}{dr}\log\Pi\right]^2. \qquad (6)$$

In atomic units, $\hbar=1$, $m_0=1$, $e=1$, and $c=137$. Also, by definition, $p=k\hbar=k$. Accordingly,[6]

$$\Pi\Phi=(1/c^2)[(E-V)^2-c^4] =k^2-(2EV/c^2)+(V^2/c^2),$$

since $E=c[p^2+c^2]^{\frac{1}{2}}$, and hence

$$1-E^2/c^4=-k^2/c^2. \qquad (7)$$

Equation (6) might be written as

$$Q^2(r)=k^2-V_{\text{eff}},$$

where V_{eff} is an effective field in which the electron moves. This field, which we may call the Dirac field, includes all the relativistic effects, and is dependent on the energy. Our expression for $Q^2(r)$ does not agree with that deduced by Rose and Bethe,[7] but it does give the right behavior of the solution near the origin, and must hence be correct.

Near $r=0$, $V=-(Z/r)$, $\Pi=(Z/cr)$, $(dV/dr)=(Z/r^2)$, $(d^2V/dr^2)=-(2Z/r^3)$ and therefore

$$Q^2(r)=k^2+(2EZ/c^2r)+[(\tfrac{1}{4}-\rho^2)/r^2],$$

where $\rho=(j^2-\alpha^2)^{\frac{1}{2}}$. Equation (5) is then solved by the confluent hypergeometric function, which behaves near the origin as $r^{\rho+\frac{1}{2}}$. The function $\psi_2=y\Pi^{\frac{1}{2}}$ then behaves as r^ρ, which result was obtained in another manner by Gordon.[2]

Coulomb Solutions

At $r=0.00195$, the effective atomic number Z_p is[3] 78.95, so that the field is nearly Coulomb out to this point. We have assumed $Z_p=80$ out to $r=0.002$, and have calculated $(y'/y)_{r=0.002}$ from the Gordon solutions.

[5] E. T. Whittaker and G. N. Watson, *Modern Analysis* (Cambridge University Press, 1935), p. 194.

[6] Note the slight change of notation, $W\rightarrow E$, $eV\rightarrow -V$.

[7] M. E. Rose and H. A. Bethe, Phys. Rev. **55**, 277 (1939). The substitution (4) must be used if the first-order term is to be eliminated, so that the disagreement must be caused by some error in the work of Rose and Bethe.

TABLE I. *Initial conditions:* $(z'/z)_{r=0.002}$ *and* $(y'/y)_{r=0.26\ (\text{or } 0.65)}$.

j	(z'/z)	(y'/y)	j	(z'/z)	(y'/y)	j	(z'/z)	(y'/y)
	$E=100$ kv			$E=100$ kv			$E=100$ kv	
1	−335.4	666.4	9	−206.5	−319.8	−1	−96.2	−91.22
2	−243.5	67.16	11	−214.0	150.7	−2	27.15	−265
3	−212.6	−68.71	15	−232.7	−129.2	−3	60.57	82.6
4	−205.6	149.2	19	−254.5	2.0*	−4	76.63	−57.7
5	−198.8	−53.01	24	−282.9	−20.2*	−5	86.14	162.3
7	−201.2	−89.23	29	−312.1	−105.5*	−6	92.5	−51.06
8	−203.2	54.20				−8	100.29	
	$E=230$ kv			$E=230$ kv			$E=230$ kv	
1	−349.3	−28.00	8	−196.0		−2	4.12	
2	−250.0	−278.9	11	−204.4	23.06	−3	42.77	
3	−216.9	145.1	15	−221.2		−4	61.44	
4	−203.7	−113.3	19	−240.1		−5	72.51	
5	−194.6	198.2	−1	−139.7	221.7	−6	79.9	
						−12	98.2	30.51

* (y'/y) for $r=0.65$ rather than 0.26.

In Eq. (3), the solution ψ_2 is determined except for an arbitrary multiplying factor, which might be complex. Since the phase of this factor has no physical significance, we shall take ψ_2 to be real. Inspection of Eqs. (2) then shows that ψ_1 will be real, and the equations are consistent in this respect. The ratio $\psi_1:\psi_2$ is therefore also real.

From (4), we have $y=\psi_2\Pi^{-\frac{1}{2}}$, and

$$y'=(d\psi_2/dr)\Pi^{-\frac{1}{2}}-\tfrac{1}{2}\psi_2\Pi'\Pi^{-\frac{1}{2}}$$
$$=[-(j\psi_2/r)+\Pi\psi_1-\tfrac{1}{2}\psi_2\Pi'\Pi^{-1}]\Pi^{-\frac{1}{2}}.$$

It follows that

$$(y'/y)=-(j/r)+\Pi(\psi_1/\psi_2)-\tfrac{1}{2}(\Pi'/\Pi). \quad (8)$$

This ratio is likewise real.

As in our previous paper,[1] $q=(\alpha/\beta)$ and $q'=q(1-\beta^2)^{\frac{1}{2}}$, where $\beta=(v/c)$. Now $E=mc^2=c^2(1-\beta^2)^{-\frac{1}{2}}$, from which we may conclude that $\beta^2=(m^2-1)/m^2$, so that $q=\alpha m(m^2-1)^{-\frac{1}{2}}$, or $-iq=\alpha m(1-m^2)^{-\frac{1}{2}}$. Then $-iq'=\alpha(1-m^2)^{-\frac{1}{2}}$. Gordon's Eq. (7), which defines n', now becomes $-n'=\rho+iq$.

The substitutions of Gordon are: $\psi_1=(1-m)^{\frac{1}{2}}\times(\sigma_1-\sigma_2)$ and $\psi_2=(1+m)^{\frac{1}{2}}(\sigma_1+\sigma_2)$. If ψ_2 is real, the following results are true: $\sigma_1+\sigma_2=a$ is real, ψ_1 is real, $\sigma_1-\sigma_2=ib$ is imaginary,

$$2\sigma_1=a+ib, \quad 2\sigma_2=a-ib, \quad \sigma_2=\sigma_1^*, \quad (9)$$

and, using (7),

$$\frac{\psi_1}{\psi_2}=\left(\frac{1-m}{1+m}\right)^{\frac{1}{2}}\frac{ib}{a}=-\frac{k}{c(1+m)}\frac{b}{a}. \quad (10)$$

Let

$$F(\alpha,\beta,z)=1+\frac{\alpha z}{1!\beta}+\frac{\alpha(\alpha+1)z^2}{2!\beta(\beta+1)}+\cdots.$$

Gordon's solutions are

$$\sigma_1=c_0^{(1)}r^\rho e^{-ikr}F(\rho+iq+1,\ 2\rho+1,\ 2ikr),$$
$$\sigma_2=c_0^{(2)}r^\rho e^{-ikr}F(\rho+iq,\ 2\rho+1,\ 2ikr), \quad (11)$$

$$\frac{c_0^{(1)}}{c_0^{(2)}}=-\frac{j-iq'}{\rho-iq}=e^{2i\theta+i\pi}, \quad (12)$$

$$2\theta=\tan^{-1}(q/\rho)-\tan^{-1}(q'/j)$$
$$=\tan^{-1}(j'q-\rho q')/(j\rho+qq'). \quad (13)$$

(We have used the equation $j^2+q'^2=\rho^2+q^2$, which is true because $q'^2=q^2-\alpha^2$.)

Determination of (y'/y)

Let us use the symbol Ph for the phase. Also, let

$$v_{\kappa,\rho}(z)=e^{-\frac{1}{2}z}F(\tfrac{1}{2}+\rho-\kappa,\ 2\rho+1;\ z)$$
$$=z^{-\frac{1}{2}-\rho}M_{\kappa,\rho}(z), \quad (14)$$

where M is the confluent hypergeometric function.

From (9),

$$(b/a)=\tan Ph\sigma_1=\tan(Phc_0^{(1)}+Phv). \quad (15)$$

An application of Kummer's formula[8] leads to the result that $(\sigma_1/c_0^{(1)})=(\sigma_2^*/c_0^{(2)*})$. Therefore, from Eq. (9), $c_0^{(1)}=c_0^{(2)*}$, and

$$Phc_0^{(1)}=\theta+\tfrac{1}{2}\pi. \quad (16)$$

The function $v_{\kappa,\rho}(z)$ satisfies the equation

$$v''+[(2\rho+1)/z]v'+[-\tfrac{1}{4}+(\kappa/z)]v=0.$$

A series solution in ascending powers of $z(=2ikr)$ may be found, and is

$$v=1-\frac{\kappa}{\eta}(2ikr)+\frac{\frac{1}{4}\eta+\kappa^2}{2\eta(\eta+1)}(2ikr)^2$$
$$-\frac{\kappa(\frac{3}{4}\eta+\frac{1}{2})+\kappa^3}{6\eta(\eta+1)(\eta+2)}(2ikr)^3+\cdots,$$

where $\eta=2\rho+1$.

This series was summed numerically for $q=0.8$ and $q=1.0564$, and for all values of ρ which were used. From this and Eqs. (8), (10), (15), and (16), the values of $(y'/y)_{r=0.002}$ were computed. These were used as initial conditions for the differential analyzer solutions. They are given in Table I.

[8] Reference 5, p. 338.

WKB Solutions

The WKB method for solving equations such as (5) has been discussed very thoroughly by Langer.[9,10] The usual procedure is to set $y=e^{\int f dr}$, and to expand f in an ascending power series in $\hbar$. As an alternative, we can expand in a descending power series in k, or in Q, which is still better. The equation in f is

$$f'+f^2+Q^2=0. \text{ If } Q^2>0, \text{ put } f=iQ+g,$$

where g satisfies the equation

$$iQ'+g'=-2iQg-g^2. \tag{17}$$

Expand $g=g_1/Q+g_2/Q^2+\cdots$ and compare like powers of Q, obtaining $g_1=-\frac{1}{2}Q'$, and

$$g_l'-(l-1)g_{l-1}=-2ig_{l+1}-\sum_k g_k g_{l-k}$$

in general. From this recursion formula we may determine the successive coefficients in the power series. This series will converge rapidly when Q is large. When we are not in the neighborhood of the turning point $r_1(Q^2=0)$, it usually suffices to take

$$f=iQ-\tfrac{1}{2}(Q'/Q), \tag{18}$$

and the second term here contributes little.

Let

$$\xi=\int_{r_1}^{r} Q dr, \quad S(r)=Q^{-\frac{1}{2}}(r)\xi^{\frac{1}{2}},$$

and $\theta=S''/S$. Then

$$U(r;\alpha,\beta)=S\{\alpha\xi^{\frac{1}{2}}J_{-\frac{1}{3}}(\xi)+\beta\xi^{\frac{1}{2}}J_{\frac{1}{3}}(\xi)\} \tag{19}$$

satisfies the differential equation

$$U''+(Q^2-\theta)U=0.$$

This equation resembles (5) when $\theta\ll Q^2$. Langer[10] finds the asymptotic form of U and is thus able to establish the connection formula

$$|Q(r)|^{-\frac{1}{4}}\exp\left[-\int_r^{r_1}|Q|dr\right] \rightarrow 2Q^{-\frac{1}{4}}(r)\cos\left\{\int_{r_1}^{r}Qdr-\frac{\pi}{4}\right\}, \tag{20}$$

which gives the phase shift for a given Q. He shows that, in evaluating this phase shift, one must replace $l(l+1)$ by $(l+\frac{1}{2})^2$. However, if we use the WKB method for a region completely outside the turning point, the proper quantity to use is still $l(l+1)$, for the connection formula plays no part. Langer notes that when l is small or when E is large, the turning point is near to $r=0$, and the use of the connection formula is then questionable. We shall see that the WKB method is, with these exceptions, quite reliable.

Mott and Massey[11] state that "the condition for classical scattering at a given angle θ is that l_0 should be large, where l_0 is the value of l for which $(\partial\eta_l/\partial l)=\frac{1}{2}\theta$, *and that* η_l *should also be large for this value.*" From this, one infers that the WKB method should yield good results only when the phase shifts are large. Our work does not indicate this.

Phase Shifts

We have used the WKB method (1) to continue the differential analyzer solutions outward and (2) to determine the phase shifts in an independent way.

(1) Continuation of analyzer solutions

Let us denote initial values with the subscript i. As above, set

$$\xi=\int_{r_i}^{r} Q dr,$$

and

$$y=(Q_i/Q)^{\frac{1}{2}}(a\cos\xi+b\sin\xi). \tag{21}$$

Then $y_i=a$, and $y_i'=-\frac{1}{2}a(Q'/Q)_i+bQ_i$. If $a=1$,

$$bQ_i=(y'/y)_i+\tfrac{1}{2}(Q'/Q)_i\cong(y'/y)_i. \tag{22}$$

(The term Q'/Q is approximately $j(j+1)/2r^3Q^2$, and is usually negligible.)

If we put $\xi=kr-\delta(r)$, then $\delta(\infty)$ will be simply related to the phase shift η_k, which is defined[12] so that it vanishes for a free particle, i.e.,

$$y_k\cong rG_k\sim\cos[kr-\tfrac{1}{2}(l+1)\pi+\eta_k]. \tag{23}$$

From (21),

$$y\sim A\sin(kr-\delta)+B\cos(kr-\delta) =(A\cos\delta+B\sin\delta)\sin kr +(B\cos\delta-A\sin\delta)\cos kr.$$

[9] R. E. Langer, Bull. Am. Math. Soc. **40**, 574 (1934).
[10] R. E. Langer, Phys. Rev. **51**, 669 (1937).
[11] N. F. Mott and H. S. W. Massey, *Atomic Collisions* (Oxford University Press, 1933), pp. 92–94.
[12] M. E. Rose and H. A. Bethe, Phys. Rev. **55**, 280 (1939), Eq. (21).

TABLE II. *Phase shifts.*

a. $E=100$ kv

Differential Analyzer				WKB			Curve		Born
l	η_l	$\eta_{l-1}-\eta_l$	Δ_l	η_l	$\eta_{l-1}-\eta_l$	Δ_l	l	η_l	η_l
0		237.9							
1	199.2°	174.2°	25.0°	195.0°	176.0°	18.9°	Same as		
2	149.6	143.9	5.7	150.9	143.4	7.2	D.A.		
3	125.5	121.0	4.5	126.5	122.5	3.7	Up to		
4	110.3	108.1	2.2	109.3	106.9	2.4	$l=8$		
5	97.7	96.7	1.0	98.5	97.0	0.7	6	87.9°	
7	80.7			75.9	75.5		8	74.0	
9	68.5						9	68.2	
							10	63.3	
11	59.3			58.5			11	59.0	
							12	54.9	
							13	51.1	
15	44.4			45.0			14	48.0	
							15	45.0	
							16	42.4	
							17	40.0	
							18	38.0	
19	32.4						19	36.0	34.9°
							20	34.2	
22				31.2			22	31.0	
24	27.8						24	28.3	29.2
							26	26.0	
							28	23.8	
29	21.5			22.2			29		24.6
							30	21.9	
							32	20.2	
							34	18.6	
35				17.9			35		20.1
							36	17.2	
							38	16.0	
							40	14.9	17.2
							45	12.4	14.6
50				10.3			50	10.3	12.6

b. $E=230$ kv

D.A.		WKB			Curve			Born
j	η_j	l	η_l	$\eta_{l-1}-\eta_l$	Δ_l	l	η_l	Δ_l	η_l
−1	207.3°								
1	183.2	1	176.7°	155.1°	21.6°	1	183.2°	21.6°	
2	141.5	2	138.8	130.3	8.5	2	141.5	9.0	
3	120.2	3	118.6	113.2	5.3	3	120.2	5.2	
4	106.2	4	105.1	101.6	3.5	4	106.2	3.5	
5	97.7	5	94.8	92.1	2.7	5	97.7	2.7	
						6	87.3	2.2	
						7	80.5	1.9	
		8			1.7	8	75.0	1.63	
						9	70.0	1.41	
						10	65.7	1.22	
11	64.4	11	62.7			11	62.1	1.05	
						12	59.0	0.92	
						13	56.0	0.80	
						14	53.2	0.68	
		15	49.7		0.6	15	50.8	0.60	
						16	48.4		
						17	46.2		
						18	44.2		
						19	42.3		
		20	41.9			20	40.5		35.2°
						21	38.9		
						22	37.3		
						24	34.4		
						26	31.9		
						28	29.7		
		30	28.1			30	27.7		26.4
						35	23.4		
		40	19.3			40	20.2		20.3
						45	17.7		
		50	15.1			50	15.7		15.9
						55	14.1		
						60	12.7		
		65	11.5			65			11.4
						70	10.5		
		80	9.2			80	8.6		8.4
		100	5.9			100			5.8

$\Delta_l=5.250e^{-0.1441l}$

Combining with (23), and putting

$$(A/B)=\tan\epsilon=b/a, \tag{24}$$

we obtain

$$-\tan\left[\eta_\kappa-\tfrac{1}{2}(l+1)\pi\right]=\left[(A\cos\delta+B\sin\delta)/(B\cos\delta-A\sin\delta)\right]_\infty=\tan(\epsilon+\delta_\infty). \tag{25}$$

Furthermore, if $Q_0^2=k^2-[j(j+1)/r^2]$,

$$-\delta=\xi-kr=\int_{r_i}^{r}(Q-Q_0)dr+\int_{r_i}^{r}Q_0dr-kr$$

$$=\int_{r_i}^{r}(Q-Q_0)dr+rQ_0\Big|_{r_i}^{r}-[j(j+1)]^{\frac{1}{2}}\cos^{-1}\{[j(j+1)]^{\frac{1}{2}}/kr\}\Big|_{r_i}^{r}-kr. \tag{26}$$

The limiting value is

$$-\delta_\infty=\int_{r_i}^{\infty}(Q-Q_0)dr-r_iQ_0^{(i)}-[j(j+1)]^{\frac{1}{2}}\left[\tfrac{1}{2}\pi-\cos^{-1}\left([j(j+1)]^{\frac{1}{2}}/kr_i\right)\right]. \tag{27}$$

ξ was expanded in powers of $s=j(j+1)$ and numerical integrations were performed from $r_i=0.26$ to infinity. The resulting expressions for δ_∞ are

$$\delta_\infty=23.317+0.0211s+5.16\times10^{-6}s^2+\cdots \qquad (E=100\text{ kv})$$
$$\delta_\infty=37.806+0.01312s+0.7565\times10^{-6}s^2+\cdots \qquad (E\geqq230\text{ kv, or }q=0.8).$$

The phase shift η_κ was determined from (22), (24), (25) and (27).

TABLE III. *Coefficients in numerical summation of (33).*

l	a_l	b_l	l	a_l	b_l
		$E=100$ kv			
0	−9.394	0.589	10	−5.985	−5.298
1	−26.216	−0.822	11	−4.039	−4.064
2	−32.942	−7.707	12	−2.750	−2.930
3	−31.721	−11.507	13	−1.949	−2.012
4	−28.265	−12.983	14	−1.154	−1.369
5	−23.620	−12.585	15	−0.778	−0.877
6	−19.089	−11.307	16	−0.455	−0.512
7	−14.906	−10.070	17	−0.315	−0.350
8	−11.337	−8.367	18	−0.037	−0.111
9	−8.404	−6.724	19	0	−0.051

l	a_l	b_l	l	a_l	b_l
		$E=230$ kv			
0	2846.37	850.11	16	269.98	149.42
1	5986.47	1864.48	17	192.99	110.21
2	6994.46	2269.13	18	136.50	80.28
3	6860.86	2320.11	19	95.38	57.66
4	6174.71	2176.12	20	65.70	40.75
5	5277.43	1937.48	21	44.61	28.28
6	4356.53	1666.86	22	29.66	19.13
7	3506.36	1396.93	23	19.25	12.54
8	2767.73	1147.08	24	12.07	7.94
9	2150.64	926.89	25	7.45	4.82
10	1649.03	738.69	26	4.22	2.63
11	1249.97	581.42	27	2.30	1.25
12	937.77	452.45	28	1.09	0.43
13	696.66	348.42	29	0.28	
14	512.65	265.56	30	0.09	
15	373.90	200.26			

(2) Phase shifts from the connection formula

From (20) and (23), we find that

$$\xi-\tfrac{1}{4}\pi=kr-\tfrac{1}{2}(l+1)\pi+\eta_\kappa,$$

and hence,[13]

$$\eta_\kappa=\tfrac{1}{2}(l+\tfrac{1}{2})-\delta_\infty(r_i=r_1),$$

$$=\lim_{r\to\infty}\left(\int_{r_1}^{r}Qdr-\int_{r_0}^{r}Q_0dr\right). \tag{28}$$

This is consistent with (27) if $l+\frac{1}{2}$ be substituted for $[j(j+1)]^{\frac{1}{2}}$.

In Table II are listed the phase shifts as determined (1) with differential analyzer and WKB extension, (2) from the connection formula, (3) from a smooth curve through points found by methods (1) and (2), and (4) by the first-order Born approximation.

Method (4) consisted in applying a formula of Mott and Massey.[14] Since this involves the square of the wave function, the region near the origin contributes little, and the potential may be taken as just $2EV/c^2$.

Results from methods (1) and (2) are in excellent agreement with each other, so that the connection formula method is accurate as well as rapid. The Born phase shifts are surprisingly good, even though the expansion parameter q is not small ($q=0.8$ and 1.056).

INTENSITY OF SCATTERING

With the notation changed as in footnote 4, we have, following Mott[15] and Darwin,[4] as the solutions of (1): F_l, G_l, which refer to the state $j'=-l-1$. The asymptotic form of G_l is $r^{-1}\cos(kr+\delta_l)$. The connection with the previous notation[16] is obtained by setting

$$\eta_{-l-1}-\tfrac{1}{2}(l+1)\pi=\delta_l,\quad \eta_l-\tfrac{1}{2}(l+1)\pi=\delta_{-l-1}.$$

[13] M. E. Rose and H. A. Bethe, Phys. Rev. **55**, 286 (1939), Eq. (103).
[14] Reference 11, p. 28, Eq. (27). See Appendices B and C.
[15] N. F. Mott, Proc. Roy. Soc. **135**, 436 (1932).
[16] See Eq. (23). The quantum number κ of Rose and Bethe (reference 7) is equal to $-j'-1$.

TABLE IV. *Amplitudes, intensity, and polarization.*

a. $E=100$ kv

θ	f R	f I	g R	g I	r	r_c	δ
2°	−460.0	391.0			0.12		
5°	8.5	150.9			0.30		
10°	41.7	25.3			0.49		
15°	23.68	5.19	0.024	−0.187	0.61	1.02	
30°	−0.66	7.123	−0.089	−0.270	0.82	1.06	
45°	−3.06	2.182	−0.272	−0.208	0.94	1.18	
60°	−2.464	0.174	−0.378	−0.054	1.40	1.36	
75°	−1.55	−0.788	−0.378	0.096	1.56		0.009
90°	−0.762	−1.051	−0.327	0.188	1.64	1.68	0.048
105°	−0.280	−1.065	−0.255	0.222	1.89		0.099
120°	0.008	−0.997	−0.179	0.213	2.16	1.78	0.113
135°	0.280	−0.847	−0.115	0.173	2.19		0.120
150°	0.523	−0.639	−0.065	0.117	2.18	1.83	0.086
165°	0.579	−0.482	−0.027	0.058	(1.98)		0.026
180°	0.492	−0.585	0	0	2.10	1.83	

b. $E=230$ kv $(q=0.8)$

θ	f R	f I	g R	g I	r	r_c	δ
2°	380.1	497.6			0.23		
5°	25.1	150.1			0.52		
10°	−42.5	7.2			0.67		
15°	23.3	11.2			1.22	1.04	
30°	0.94	6.25	−0.03	−0.63	1.13	1.17	
45°	−2.03	2.81			1.65	1.37	
60°	−1.60	1.43	0.40	−0.23	1.88	1.58	
75°	−1.21	0.13			1.43		
90°	−0.91	−0.30	0.39	0.03	1.67	1.82	0.025
105°	−0.87	−0.41			2.58		
120°	−0.73	−0.96	0.26	0.09	(5.46)	1.68	
135°	−0.04	0.59			1.59		
150°	−0.09	0.28	0.13	0.05	0.57	1.43	

Then

$$f(\theta)=\tfrac{1}{2}i\sum_{l=0}^{\infty}\{(l+1)(\exp[i(2\eta_{-l-1}-\pi)]+1)+l(\exp[i(2\eta_l-\pi)]+1)\}P_l(\cos\theta)$$

$$=-\tfrac{1}{2}i\sum_{l=0}^{\infty}\{(l+1)(\exp[2i\eta_{-l-1}]-1)+l(\exp[2i\eta_l]-1)\}P_l(\cos\theta), \tag{29}$$

$$g(\theta)=\tfrac{1}{2}i\sum_{l=1}^{\infty}\{\exp[2i\eta_{-l-1}]-\exp[2i\eta_l]\}P_l^1(\cos\theta),$$

$$(2f/i)=\sum_{l=0}^{\infty}(2l+1)(A_l-iB_l)P_l(\cos\theta), \tag{30}$$

where

$$(2l+1)A_l=(l+1)(1-\cos 2\eta_{-l-1})+l(1-\cos 2\eta_l)$$

$$(2l+1)B_l=(l+1)\sin 2\eta_{-l-1}+l\sin 2\eta_l$$

$$(-2g/i)=\sum_{l=1}^{\infty}2\sin\Delta_l\{-\sin\Sigma_l+i\cos\Sigma_l\}P_l^1(\cos\theta), \tag{31}$$

where

$$\Delta_l=\eta_l-\eta_{-l-1},\quad \Sigma_l=\eta_l+\eta_{-l-1}.$$

For large values of l, the phase shifts decrease in an exponential manner, and so we would expect a similar behavior for A_l and B_l, which is in fact found. Exponential functions $A_\infty(l)$ and $B_\infty(l)$ were fitted in this range, as follows:

$$\left.\begin{aligned}A_\infty(l)&=2.490e^{-0.0733l}+8.342e^{-0.250l}\\B_\infty(l)&=2.082e^{-0.0356l}-1.772e^{-0.148l}\end{aligned}\right\}E=100\text{ kv}$$

$$\left.\begin{aligned}A_\infty(l)&=0.9554e^{-0.0382l}+65.1e^{-0.192l}-2912e^{-0.351l}\\B_\infty(l)&=1.310e^{-0.0186l}+49.4e^{-0.188l}-900e^{-0.304l}\end{aligned}\right\}E=230\text{ kv}. \tag{32}$$

Equation (30) may be written

$$(2f/i)=\sum_{l=0}^{\infty}(2l+1)[A_\infty(l)-iB_\infty(l)]P_l(\cos\theta)+\sum_{l=0}^{\infty}(2l+1)[(A_l-A_\infty(l))-i(B_l-B_\infty(l))]P_l(\cos\theta). \tag{33}$$

The first term on the right-hand side may be evaluated by summing analytically, and the second by summing numerically. The analytical summation is based on the formula

$$\sum_{l=0}^{\infty}(2l+1)x^l P_l(\cos\theta)=(1-x^2)/(1-2x\cos\theta+x^2)^{\frac{1}{2}} \tag{34}$$

and on the substitution $x=e^{-a}$, where a is one of the constants in (32).

We give in Table III the coefficients of the second sum,

$$a_l=(2l+1)[A_l-A_\infty(l)] \quad \text{and} \quad b_l=(2l+1)[B_l-B_\infty(l)].$$

This method of summation would be less practical for higher energies, because $P_l(\cos\theta)$ is tabulated[17] only to $l=32$.

At $E=100$ kv, the sum in (31) converges rapidly, and only seven terms were calculated. For $E=230$ kv, however, the convergence is not as good, and one needs about twenty-five terms. One would expect a behavior of this sort, because for higher energies the electrons come closer to the nucleus, and the spin-orbit interaction terms can therefore be of more influence.

After summing the series (30) and (31) for f and g, we have, as in our previous paper, multiplied the values of $|f|^2+|g|^2$ by $(4/q^2)\sin^4\frac{1}{2}\theta$, in order to find the ratio r of our calculated scattering intensity to the "Rutherford" value. Furthermore, the asymmetry 2δ in double scattering, $2\delta=2[(fg^*-gf^*)/(|f|^2+|g|^2)]^2$, has been obtained. The results are given in Table IV, together with r_c, the ratio for a Coulomb field.

Results

The results for 100 kv are what one might expect. At large angles the distribution is practically the same as that obtained for a Coulomb field. (The discrepancies are not large, and are probably caused by small errors in the determination of the phase shifts for small l.) At small angles, in this case angles less than 60°, the effects of shielding become evident, and the intensity of scattering is less than the Coulomb value.

For 230 kv, the calculations are probably not very accurate, since reliance was placed on the WKB method to a great extent. In particular, it would have been desirable to have had data from the differential analyzer for $j=-2$ to $j=-6$, inclusive. (Such runs had been taken, but were later proved to be incorrect.) The values of r in Table IV fluctuate, but it is probably legitimate to conclude that the angular distribution is of the Coulomb character for angles greater than 15°, and that the shielding is only effective for smaller angles.

Summary and Conclusions

For a given value of the Dirac angular momentum quantum number j, one can eliminate one component of the radial wave function, and obtain a single Schroedinger-like equation for the motion of an electron. The electron is influenced by an effective field (we have called it the Dirac field) which is dependent on the energy, and which may be deduced from the Hartree field.

We have calculated the scattering intensity for electrons of 100 kv and 230 kv influenced by mercury atoms. The Hartree field is known, and the Dirac field was found. Phase shifts were determined by three different methods: (1) integration with the aid of the differential analyzer, (2) the WKB method, and (3) with the Born approximation.

The WKB phases are in excellent agreement with the analyzer phases for 100 kv, and in good agreement for 230 kv. This method seems, therefore, to be rather reliable, and our results do not indicate that it should break down for small phase shifts.

The first-order Born approximation results, for large values of l, in phase shifts which agree well with those calculated by the other methods. The first-order wave function is, however, quite different from the unperturbed one, and so the reason for the smallness of higher order corrections to the phase shifts is not known.

[17] H. Tallquist, Soc. Scient. Fennica, Comm. Phys.-Math. **6**, Nos. 3 and 10 (1933).

The angular distribution appears to be Coulombian for large angles, within the limits of error of our calculations. The shielding becomes effective below 60° for 100-kv electrons, and below 15° for 230-kv electrons.

Acknowledgments

We wish to express our appreciation to members of the Departments of Physics and Electrical Engineering, Massachusetts Institute of Technology (Professors Slater, Morse, and Caldwell), for making it possible for us to use the differential analyzer and for advice concerning its operation, and to members of the technical staff (Messrs. Löf, Crawford, Michael, and others) for valuable assistance.

We thank Mr. F. N. Gillette for help with the computations and with the analyzer operation, Mr. W. W. Bartlett for assistance with the analyzer, and Mr. R. W. Potts (N.Y.A.) for his services as computer.

Finally, we gratefully acknowledge the receipt of financial aid from the Graduate School Research Board of the University of Illinois, without which aid this research could not have been brought to completion.

Appendix A

Differential analyzer procedure

Having obtained $(y'/y)_{r=0.002}$, we integrated Eq. (5) outward, setting $Q^2(r)=\mathfrak{F}(r)+j\mathfrak{G}(r)-[j(j+1)/r^2]$, where

$$\mathfrak{F}(r)=k^2-\frac{2EV}{c^2}+\frac{V^2}{c^2}-\frac{1}{2\Pi c}\frac{d^2V}{dr^2}-\frac{3}{4}\frac{1}{\Pi^2c^2}\left(\frac{dV}{dr}\right)^2,$$

and

$$\mathfrak{G}(r)=\frac{1}{r\Pi c}\frac{dV}{dr}.$$

$\mathfrak{F}(r)$ was fed in from one input table, $\mathfrak{G}(r)$ from another, and $1/r^2$ was usually generated by two integrators.

The integration range was divided into three or four sections (0.002−0.016−0.065−0.26−0.65) and dependent variables chosen so as to have the same order of magnitude throughout the section. Near the origin, y behaves as $r^{\rho+\frac{1}{2}}$. We substituted $y=r^{j+1}z$ when $j>0$; $y=r^{|j|}z$ when $j<0$, and used z as the dependent variable. (This made the term in $1/r^2$ vanish.) For large r, y varies sinusoidally, and was used itself. (It might be more accurate to take out the sinusoidal factor, but this was not done for lack of time.) For large values of j, we used the variable $w=yr^{-p}$, where p was some appropriate integer less than j.

Appendix B

Born approximation formulae

The first-order phase shift is to be found from

$$\tan\eta_k=-(\pi/2k)\int_0^\infty(2EV/c^2)[J_{l+\frac{1}{2}}(kr)]^2rdr,$$

where

$$-2rV=2Z_p=33.7e^{-17.376r}+95.9e^{-3.892r}+30.3e^{-1.253r}.$$

The integration and evaluation may be made with the aid of two formulas given by Watson.[18]

$$\int_0^\infty e^{-at}J_\nu(bt)J_\nu(ct)dt=[1/\pi(bc)^{\frac{1}{2}}]Q_{\nu-\frac{1}{2}}\{(a^2+b^2+c^2)/2bc\}.$$

$$Q_l(\cosh\xi)\cong e^{-(l+\frac{1}{2})(\xi-\tanh\xi)}(\operatorname{sech}\xi)^{\frac{1}{2}}K_0[(l+\tfrac{1}{2})\tanh\xi].$$

Appendix C

Note on the Born approximation

Equation (5) may be written in the form

$$y''+\{k^2+[(\tfrac{1}{4}-\rho^2)/r^2]\}y=Uy, \tag{35}$$

where U has a pole of order one at the origin. A fundamental set of solutions of the homogeneous equation ($U=0$) is

$$v_1=(\tfrac{1}{2}\pi kr)^{\frac{1}{2}}J_\rho(kr);\qquad v_2=(\tfrac{1}{2}\pi kr)^{\frac{1}{2}}J_{-\rho}(kr).$$

For simplicity, consider the Coulomb equation

$$u''+\{-\tfrac{1}{4}+[(\tfrac{1}{4}-\rho^2)/r^2]\}u=-(\lambda\alpha/r)u \tag{36}$$

where λ is a constant, and ρ will be taken as independent of α.

I. Let $$u=\sum_{s,t=0}^{\infty}u_{s,t}r^{\omega+s}\alpha^t,$$

and require $u_{0,t}=0$ for $t>0$ (normalization condition). The only acceptable exponent is $\omega=\frac{1}{2}+\rho$, and the recursion formula is

$$[(\rho+s+2)^2-\rho^2]u_{s+2,t}=\tfrac{1}{4}u_{s,t}-u_{s+1,t-1}.$$

(All coefficients with negative subscripts are to vanish.) The nonzero coefficients are found to be those with $s\geqq0$ and $t=s-2p\geqq0$, where

$$p\geqq0.\qquad\text{That is,}\qquad s\geqq t. \tag{37}$$

II. The procedure of I may be modified (*a*) by expanding in powers of α and then (*b*) solving a set of inhomogeneous equations successively. This is convenient for ascertaining the behavior for large r. If $u=\sum_{t=0}^{\infty}u_t\alpha^t$, then

$$u_t''+\{-\tfrac{1}{4}+[(\tfrac{1}{4}-\rho^2)/r^2]\}u_t=-(\lambda u_{t-1}/r),\ t=1,\cdots\infty. \tag{38}$$

Since $u_0=v_1$, the solution of (38) with $t=1$ is[19] $u_1=V_1(r)v_1+V_2(r)v_2$, where $V_1=\lambda\int_a^r(v_1v_2/rW)dr$, $V_2=-\lambda\int_b^r(v_1^2/rW)dr$, and W is the Wronskian of v_1 and v_2. The limits a and b must be such that u is regular at $r=0$. At this point, $u_0=v_1=O(r^{\frac{1}{2}+\rho})$ and $v_2=O(r^{\frac{1}{2}-\rho})$. From (37), $s_{\min}=t$, and so $u_1=O(r^{\frac{1}{2}+\rho})$, V_1 must be $O(r)$ and V_2 must be $O(r^{2\rho+1})$. These conditions will be satisfied if and only if $a=0$ and $b=0$.

[18] Watson, *Bessel Functions* (Cambridge University Press, 1922), pp. 389 and 158.

[19] E. L. Ince, *Ordinary Differential Equations* (Longmans, 1927), p. 122.

Evidently the above conclusions will be true when U still has a pole of order one at $r=0$, but is non-Coulomb. With V_1 and V_2 modified accordingly, the first-order wave function will be

$$u=\{1+\alpha V_1(r)\}v_1+\alpha V_2(r)v_2. \quad (39)$$

At large r, $v_1\sim\sin(kr-\frac{1}{2}\rho\pi)$ and $v_2\sim\cos(kr+\frac{1}{2}\rho\pi)$. Hence $u\sim$const $\{\cos(kr-\frac{1}{2}l\pi)\sin\eta_\kappa+\sin(kr-\frac{1}{2}l\pi)\cos\eta_\kappa\}$ where

$$\tan\eta_\kappa=\frac{\{1+\alpha V_1(\infty)\}\sin\frac{1}{2}(l-\rho)\pi+\alpha V_2(\infty)\cos(l+\rho)\pi}{\{1+\alpha V_1(\infty)\}\cos\frac{1}{2}(l-\rho)\pi-\alpha V_2(\infty)\sin(l+\rho)\pi}$$
$$=\alpha V_2(\infty) \text{ to first order in } \alpha.$$

At $r=\infty$, the first-order wave function contains $\alpha V_1(\infty)$, which is of order unity,[20] and so the function has been greatly modified by the perturbation. Nevertheless, as seen above, this is without effect[21] on the *first-order* phase shift.

[20] We calculated $\alpha V_1(\infty)$ for $l=22$, $E=100$ kv assuming the potential to be $-2EV/c^2$, and integrating numerically with the aid of a Gegenbauer formula (reference 18, p. 390). The result, which should be roughly correct, was near unity.

[21] This became clear during a discussion with Drs. Lamb and Nordsieck of Columbia University, to whom thanks are due for their interest and help.

FEBRUARY 1, 1941 PHYSICAL REVIEW VOLUME 59

A Note on the Analysis of Liquid X-Ray Diffraction Patterns

NEWELL S. GINGRICH
University of Missouri, Columbia, Missouri

(Received November 18, 1940)

The corrected intensity curve given by Eisenstein and Gingrich for the diffraction of x-rays by liquid argon has been subjected to four different fittings, one of them including a weak fourth peak, to determine how sensitive the atomic distribution curve is, to errors in fitting. An analysis has been made for these four cases. The first peak of the atomic distribution curve has about the same shape in each case, the area under this peak varies by less than ten percent, and the position of its maximum remains constant to within about one and one-half percent. The small secondary peak becomes a plateau by the introduction of a weak fourth peak in the intensity curve.

THE method of the Fourier integral analysis of x-ray diffraction patterns[1] is reasonably straightforward in principle, but, in practice, difficulties sometimes arise which make the conclusions from this analysis somewhat uncertain. Thus, for example, it is assumed that at large angle, the scattered x-rays are wholly made up of incoherent and independent coherent radiation, and in this way, the experimental intensity curve is placed on the same scale as the Nf^2 curve. Experimentally, one chooses a point in the diffraction curve beyond which no interference effects can be observed and then makes a fitting of the curves at this point. With weak radiation at large angles, it is difficult to be sure that this point is chosen at large enough angle, and hence uncertainty in the results and conclusions is introduced. Since there is no obvious general approach to the discussion of the effect of different fitting of curves, a few special cases have been worked out to illustrate the effect upon the atomic distribution curve in the case of liquid argon of different fittings in the experimental intensity curve for liquid argon.

In previous work[2] with liquid argon, the experimental curves obtained in several trials consistently showed three maxima, at values of $\sin\theta/\lambda$ of 0.154, 0.280 and 0.415, respectively. One, or possibly two films, showed a faint trace of a fourth maximum, but the films with apparently the best patterns did not show convincing evidence of the existence of the fourth peak, for if it existed on them, it must have had a height no greater than the fluctuations of the microphotometer. With a small camera, of 5.08 cm radius, two overexposed pictures were taken to investigate the region where slight indications of a fourth peak occurred. Superimposed on the dense background, there appeared a weak fourth

[1] B. E. Warren and N. S. Gingrich, Phys. Rev. **46**, 368 (1934).

[2] A. Eisenstein and N. S. Gingrich, Phys. Rev. **58**, 307 (1940).

peak at about $\sin\theta/\lambda=0.56$. This is to be compared with the reported value[3] of 0.59. The fully corrected intensity curve of Eisenstein and Gingrich[2] was refitted in four ways to illustrate the effect of various fittings. These curves and fittings are shown in Fig. 1. Curve 1 of this figure shows the intensity curve fitted at D, $\sin\theta/\lambda=0.5$; curve 2 shows the intensity curve as used for curve 1, but with a weak fourth peak added at about $\sin\theta/\lambda=0.56$, and with fitting at C, $\sin\theta/\lambda=0.63$; curve 3 is identical with curve 2, but without the fourth peak, and the fitting is at B, $\sin\theta/\lambda=0.6$; curve 4 is the intensity curve without the fourth peak, but with fitting at A, $\sin\theta/\lambda=0.7$. In curve 1, the fitting appears low and in curve 4, it appears high.

The $si(s)$ function was calculated and plotted for each of these cases and the curves were analyzed with the use of a Coradi[4] analyzer. The results of this work are plotted in Fig. 2, giving $4\pi R^2\rho(R)$ as a function of R in each case. The numbers on the curves refer to the numbers in Fig. 1. The shapes of the curves are probably reliable up to 6.0A, but beyond that, the points are too far apart to show detail, and hence, the curves will be compared only with respect to the first peak and the small secondary hump. The position of the maximum of the first peak from what appears to be the best interpolation between points 0.14A apart is 3.88A for curve 1, 3.84A for curve 2, 3.88 for curve 3, and 3.85A for curve 4. Thus, this quantity varies by about one and one-half percent when the fitting is varied from $\sin\theta/\lambda=0.5$ to $\sin\theta/\lambda=0.7$ or when a fourth peak is added. The area under the first peak depends upon how the isolated peak is drawn in. Two different ways were used to draw in the peak; first, an isolated symmetrical peak was drawn, and second, a straight vertical line was drawn from the lowest point just beyond the first peak, down to the axis. The areas so obtained were 6.96 and 7.72 for curve 1, 6.50 and 7.42 for curve 2, 6.88 and 7.32 for curve 3, and 6.80 and 7.64 for curve 4. These areas, indicating the number of nearest neighbors,

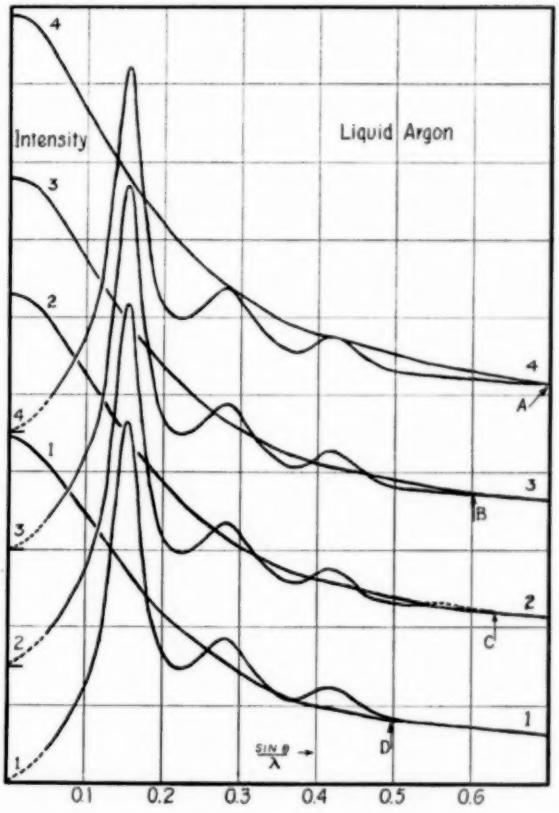

FIG. 1. The fully corrected intensity curve for liquid argon is fitted to the Nf^2 curve in four different ways: in curve 1, the fitting is made at $\sin\theta/\lambda=0.5$, in curve 2 a weak fourth peak is added, and fitting is made at $\sin\theta/\lambda=0.63$, in curve 3, fitting is made at $\sin\theta/\lambda=0.60$, and in curve 4, fitting is made at $\sin\theta/\lambda=0.70$.

vary by about ten percent for a given type of peak reconstruction. The shape of the first peak varies slightly from curve to curve, but not markedly. Perhaps the greatest effect is shown in the secondary hump of curve 2. Here the distinct hump of the other curves becomes almost a plateau. This is undoubtedly caused chiefly by the addition of the very weak fourth peak in the intensity pattern. Features which appear in the intensity pattern at large values of $\sin\theta/\lambda$ are greatly magnified in the $si(s)$ function, due partly to the high values of s and partly to the low values for Nf^2. However, in spite of the large contribution to the $si(s)$ function of the fourth intensity peak, there is relatively little effect upon the shape, position, or area under the first peak of the distribution curve.

One cannot generalize from these results and

[3] K. Lark-Horovitz and E. P. Miller, Nature **146**, 459 (1940).

[4] I am indebted to Professor G. G. Harvey of the Massachusetts Institute of Technology for the use of M. I. T. Coradi analyzer.

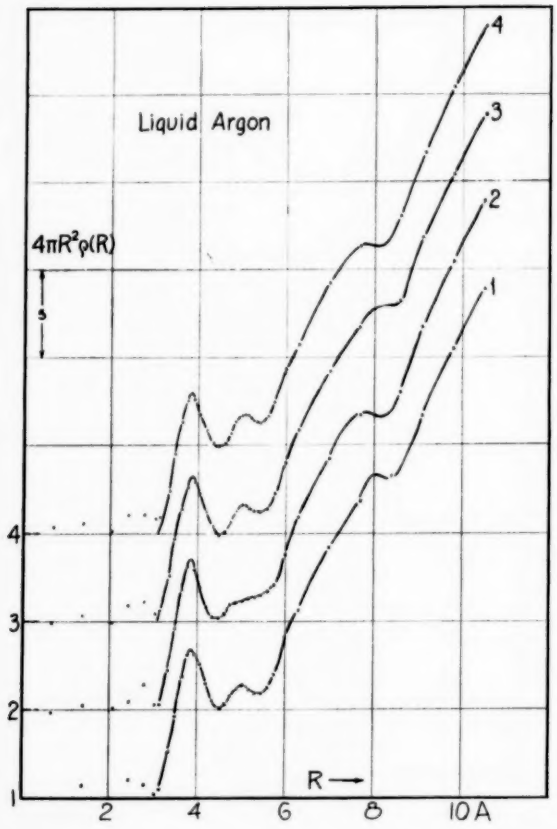

FIG. 2. The distribution curves for the four different fittings are shown, to illustrate the effect of fitting upon characteristics of the distribution curve.

conclude that in all cases, fitting could be made anywhere from sin $\theta/\lambda=0.5$ to sin $\theta/\lambda=0.7$ with the position of the maximum of the first peak in the distribution curve constant to within about one percent. The relative effect of various fittings upon the position of this first peak seems to depend considerably upon the diffraction pattern studied. Thus, in the case of liquid sulphur,[5] fitting at sin $\theta/\lambda=0.5$ gave a position for the maximum of the first peak of the distribution curve different by about 10 percent from that obtained when fitting was made at sin $\theta/\lambda=0.65$. In the present work, the different fittings led to areas under the first peak which differed by about 10 percent. This is as large a difference as has been observed in other cases when different fittings were tried. The introduction or the suppression of detail in the distribution curve is apparently fairly susceptible to the type of fitting. This is illustrated not only in the present work with argon, but also in the cases of sodium[6] and potassium.[7]

It is concluded that in the case of the "corrected" experimental intensity curves of liquid argon as obtained by Eisenstein and Gingrich, variations in fitting, or the addition of a fourth peak in the intensity curve will not alter the position of the first peak of the distribution curve by more than about one and one-half percent nor the area under that peak by more than about 10 percent. The addition of a weak fourth peak in the intensity pattern does, however, tend to make a plateau out of the second small peak in the distribution curve. This latter alteration is in agreement with the recent work of Lark-Horovitz and Miller.[3]

[5] N. S. Gingrich, J. Chem. Phys. **8**, 29 (1940).
[6] F. H. Trimble and N. S. Gingrich, Phys. Rev. **53**, 278 (1938).
[7] C. D. Thomas and N. S. Gingrich, J. Chem. Phys. **6**, 411 (1938).

Notes on Intensities of Radiofrequency Spectra

H. C. TORREY
Department of Physics, The Pennsylvania State College, State College, Pennsylvania
(Received October 21, 1940)

In order to compare theoretical and observed line shapes of radiofrequency spectra, one must take account of the inhomogeneity in velocity of the beam molecules. The theoretical expression for line shape is integrated over the velocity distribution in the beam and the result is expressed in terms of integrals studied by Zahn and Laporte. The important parameters in the theory of line shapes are the matrix elements of the interaction with the radiation field. These are evaluated in the case of atoms with electronic angular momentum $J=\frac{1}{2}h$ and arbitrary nuclear spin.

INTRODUCTION

RECENT studies[1-5] of radiofrequency spectra at the hands of Rabi and others have given valuable information of nuclear magnetic dipole and electric quadripole moments as well as of certain dynamical properties of molecules. Such information has so far been obtained chiefly from measurements of the positions of resonance minima. In certain instances additional or corroboratory information may be obtained through study of the shapes of the spectral lines, since intensities and half-widths of these lines depend on the off-diagonal matrix elements of the interaction with the radiation field. In order to compare observed and theoretical line shapes it is necessary to take account of the velocity distribution in the beam. This effect is studied here in Part I. In Part II the interaction matrix elements are found for all magnetic fields in the case of atoms with electronic angular momentum $J=\frac{1}{2}h$ and arbitrary nuclear spin I. The very simple results found should be of some value in orienting experimental work.

As is well known, radiofrequency spectra are studied through the effects of absorption and stimulated emission of magnetic dipole radiation on atoms or molecules (or on neutrons, as in the experiments of Alvarez and Bloch)[3] in a beam. The general effect is to change orientation with respect to the field. In all important work so far this is brought about by passing the beam through a region in which there is a magnetic field consisting of two components, one steady: $\mathbf{H}_0$, and one oscillatory: $\mathbf{H}_1$. We shall confine our attention to this case. Although the two components in practice are usually perpendicular or nearly so, we shall not need to make this assumption.

Consider the general case of an atom or molecule in such a field. The significant part of the Hamiltonian may be written:

$$\mathcal{H}=\mathcal{H}'+\mathcal{H}''+V. \tag{1}$$

$\mathcal{H}'$ contains all internal interaction dependent on orientation, $\mathcal{H}''$ is the interaction with $\mathbf{H}_0$ and V the interaction with $\mathbf{H}_1$. $\mathcal{H}''$ and V are pre-

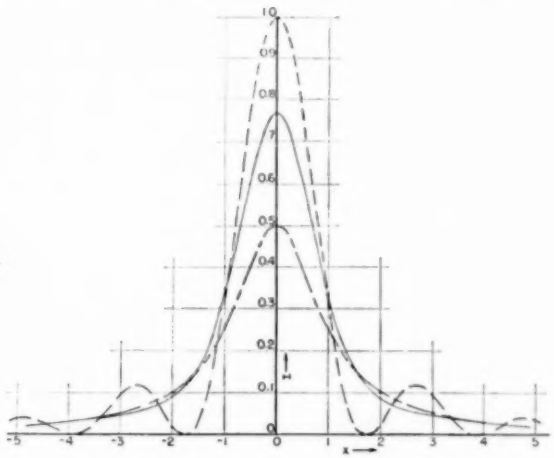

FIG. 1. Theoretical line shapes. Intensity (I) plotted against frequency (x) measured from resonance in units of b_{pq}. - - - - uniform velocity and optimum $H_1(\beta_0=\pi)$. ——— average over velocity distribution with optimum $H_1(\beta_0=1.200\pi)$. — — — — average over velocity distribution with large $H_1(\beta_0\gg\pi)$. $I=\frac{1}{2}(1+x^2)^{-1}$.

[1] I. I. Rabi, S. Millman, P. Kusch and J. R. Zacharias, Phys. Rev. **55**, 526 (1939).
[2] J. M. B. Kellogg, I. I. Rabi, N. F. Ramsey, Jr. and J. R. Zacharias, Phys. Rev. **56**, 728 (1939).
[3] L. W. Alvarez and F. Bloch, Phys. Rev. **57**, 111 (1940).
[4] J. M. B. Kellogg, I. I. Rabi, N. F. Ramsey, Jr. and J. R. Zacharias, Phys. Rev. **57**, 677 (1940).
[5] P. Kusch, S. Millman and I. I. Rabi, Phys. Rev. **57**, 765 (1940).

sumed to be linear in the field components, diamagnetic effects being neglected. Since V is proportional to the oscillatory component of the field it will be a function of the time of the form: $V=V_0\cos(\omega t+\delta)$ where ω is the angular frequency of $\mathbf{H}_1$. The probability amplitudes C_n for the eigenstates of the static part of the Hamiltonian satisfy the Schrödinger equations:

$$i\hbar dC_n/dt=\sum_m(n|\mathfrak{H}|m)C_m. \tag{2}$$

The probability, P_{pq}, for the transition $p\rightleftarrows q$ is given by $|C_q|^2$ where C_q is found by solving (2) under the initial conditions: $|C_p|=1$, $C_m=0$ $(m\neq p)$. P_{pq} will be appreciable only in the neighborhood of resonance, i.e., when $\omega\sim\omega_{pq}\equiv|W_p-W_q|/\hbar$ (W_p and W_q are the energies of the states p and q). If then no other state is in near resonance with either p or q at the same frequency only C_p and C_q will be very different from zero and (2) reduces to the pair of equations:

$$\begin{aligned} i\hbar dC_p/dt&=[W_p+(p|V_0|p)\cos(\omega t+\delta)]C_p+(p|V_0|q)\cos(\omega t+\delta)C_q,\\ i\hbar dC_q/dt&=[W_q+(q|V_0|q)\cos(\omega t+\delta)]C_q+(q|V_0|p)\cos(\omega t+\delta)C_p. \end{aligned} \tag{3}$$

Apart from the diagonal elements of V_0, these equations have the same form as for a simple spin of $\frac{1}{2}h$ interacting with an external field, for which case transition probabilities have been found by Rabi[1,6] and Bloch and Siegert.[7] It is shown in Appendix I that these diagonal elements do not appear in the approximate solution of (3) valid near resonance and provided $V_0\ll\hbar\omega_{pq}$. We have then for P_{pq} the familiar result:

$$P_{pq}=\frac{b_{pq}^2\sin^2\pi t[b_{pq}^2+(\nu-\nu_{pq})^2]^{\frac{1}{2}}}{b_{pq}^2+(\nu-\nu_{pq})^2}, \tag{4}$$

where $b_{pq}=|(p|V_0|q)|/\hbar$ and cyclic frequencies $\nu=\omega/2\pi$ and $\nu_{pq}=\omega_{pq}/2\pi$ have been introduced.

The conditions under which Eqs. (2) reduce to (3) occur frequently. If these conditions are not met, special methods must be used which are beyond the scope of this paper. However, in the important case in which the energy levels of $\mathfrak{H}'+\mathfrak{H}''$ are equally spaced, the transition probability may be expanded in powers of an expression similar in form to the right side of (4) through a general theorem[1] due to Majorana. The resulting polynomial may be averaged over the velocity distribution by an obvious extension of the methods of Part I below.

I. Effect of Velocity Distribution

When transitions take place they are usually manifested by reductions in intensity of the beam, because the part of the beam that has made transitions no longer follows the same subsequent path and misses the detector. Hence if all particles spend the same time in the oscillatory field, formula (4) when properly weighted gives the shape of the spectral line $p\rightleftarrows q$.[8] This however will be true only if the beam is homogeneous in velocity. Since the beam is usually produced by thermal effusion it may be assumed to have a velocity distribution given by:

$$fdv=2e^{-v^2/\alpha^2}v^3dv/\alpha^4, \tag{5}$$

where fdv is the fraction of particles passing any point in given time that have velocities v in the range dv and $\alpha=(2kT/m)^{\frac{1}{2}}$; T is the absolute temperature of the source, m is the mass of a particle and k is Boltzmann's constant. To find a usable expression for the line shape one must integrate (4) over the velocity distribution (5). Introducing the abbreviations:

$$\begin{aligned} y&=v/\alpha, & x&=(\nu-\nu_{pq})/b_{pq},\\ \beta_0&=2\pi lb_{pq}/\alpha, & \beta&=\beta_0(1+x^2)^{\frac{1}{2}}, \end{aligned} \tag{6}$$

[6] I. I. Rabi, Phys. Rev. **51**, 625 (1937).
[7] F. Bloch and A. Siegert, Phys. Rev. **57**, 522 (1940).
[8] Certain apparatus effects may contribute to line width. It is assumed here that these are not important.

TABLE I. $\bar{P}(\beta_{0m},x)$ *as a function of* x.

x	$\bar{P}(\beta_{0m},x)$	x	$\bar{P}(\beta_{0m},x)$	x	$\bar{P}(\beta_{0m},x)$
0.0	0.7658	1.4	0.1828	2.8	0.05093
0.2	0.7360	1.6	0.1373	3.0	0.04708
0.4	0.6559	1.8	0.10601	3.5	0.03819
0.6	0.5473	2.0	0.08520	4.0	0.03064
0.8	0.4334	2.2	0.07146	4.5	0.02435
1.0	0.3304	2.4	0.06227	5.0	0.01952
1.2	0.2464	2.6	0.05583		

where l is the length of path in the oscillatory field, we have:

$$\bar{P}_{pq}(\beta_0,x)=2(\beta_0/\beta)^2\int_0^\infty e^{-y^2}y^3\sin^2(\beta/2y)dy=(\beta_0/\beta)^2(\tfrac{1}{2}-I(\beta)), \tag{7}$$

where

$$I(\beta)=\int_0^\infty e^{-y^2}y^3\cos(\beta/y)dy \tag{8}$$

$$=\text{R.P. } J_3(i\beta)$$

and

$$J_m(z)=\int_0^\infty e^{-u^2-z/u}u^m du.$$

The integrals $J_m(z)$ have been studied by Zahn[9] and Laporte,[10] who have found convergent and asymptotic expansions for them.

In order to determine the line shape from (7) one needs to know β_0. Here we may distinguish three cases.

(a) The oscillatory field, $\mathbf{H}_1$, has been so adjusted that the peak intensity, $\bar{P}_{pq}(\beta_0,0)=\frac{1}{2}-I(\beta_0)$, is a maximum. It is clear from expression (4) that, for a single velocity α, this will be true for $\beta_0=n\pi$ $(n=1,2\cdots)$ and that for $n=1$ we shall have the best resolution. We should accordingly think that the optimum value of β_0 for (7) would be about π. It is shown in Appendix II that it is in fact given by:

$$\beta_{0m}=1.200\pi. \tag{9}$$

From (6) $\beta\geq\beta_0$, hence we should expect that for $\beta_0=\beta_{0m}$ an asymptotic series for $I(\beta)$ would be useful. This is readily found from Laporte's result[10] and is (see Appendix II):

$$I(\beta)\sim\left(\frac{\pi}{3}\right)^{\frac{1}{2}}\frac{\beta}{2}\exp\left[-\frac{3}{2}\left(\frac{\beta}{2}\right)^{\frac{1}{3}}\right]\sum_p K_p\left(\frac{2}{\beta}\right)^{\frac{1}{3}}\sin\left[\frac{3\sqrt{3}}{2}\left(\frac{\beta}{2}\right)^{\frac{1}{3}}+\frac{p\pi}{3}\right]. \tag{10}$$

The values of the first few coefficients of K_p are:

$$K_0=1, \qquad K_3=-0.017879,$$
$$K_1=0.97222, \qquad K_4=\ \ 0.004594,$$
$$K_2=0.14853, \qquad K_5=-0.000762.$$

Further coefficients may be found with a recursion formula given in Appendix II, but it is seldom necessary to go beyond K_5. Equation (10) has been checked by numerical integration for $\beta=1.2\pi$. It is evident that even for values of β as low as 2 this series will give accurate results. By using (10) and setting $\beta_0=\beta_{0m}$, $\bar{P}_{pq}$ has been tabulated as a function of x in Table I and the resulting curve is

[9] C. T. Zahn, Phys. Rev. **52**, 67 (1937).
[10] O. Laporte, Phys. Rev. **52**, 72 (1937).

TABLE II. $\bar{P}(\beta_0,0)$ *as a function of* β_0.

β_0	$\bar{P}(\beta_0,0)$	β_0	$\bar{P}(\beta_0,0)$	β_0	$\bar{P}(\beta_0,0)$
0	0	0.4	0.03771	0.8	0.1341
0.1	0.00248	0.5	0.05747	0.9	0.1647
0.2	0.00985	0.6	0.08051	1.0	0.1966
0.3	0.02167	0.7	0.1064	1.2π	0.7658 (max.)

shown in Fig. 1, where it is compared with the unaveraged distribution (4). Whereas the right side of (4) has a marked oscillatory character, this is mostly washed out by the velocity distribution. The peak intensity is 0.766. The curve descends on either side and oscillates with small and decreasing amplitude about the curve $\frac{1}{2}(1+x^2)^{-1}$. These oscillations are for the most part too small to be seen in the figure. The width at half-maximum of $\bar{P}(x)$ is 1.787. In terms of frequency this is

$$\Delta\nu = 1.787 b_{pq}. \tag{11}$$

The matrix elements b_{pq} may thus be determined from the half-widths or conversely. They may also be found from (9). Combining (9) with (11) we have:

$$\tau\Delta\nu = 1.072, \tag{12}$$

where $\tau = l/\alpha$ and is the time spent in the oscillatory field by a molecule with velocity α. This is a more accurate statement of the familiar result, $\tau\Delta\nu \sim 1$, often used in estimating half-widths. Equation (12) holds of course only for the optimum field H_1, which may be accurately determined beforehand through use of (9) if enough details of the interactions are known to enable calculation of b_{pq}.

(b) The elements b_{pq} are proportional to H_1. If the proportionality factor happens to be so small that it is not feasible to use a large enough value of H_1 to satisfy (9), the line will appear, if at all, as weak in intensity. The asymptotic series (10) may not now be used. Instead one may use a convergent series for $I(\beta)$ which is obtained from Zahn's development[9] of $J_3(z)$ about the origin. The result is:

$$P_{pq}(\beta_0,x) = \tfrac{1}{4}\beta_0^2[1 - 0.2028\beta^2 - 0.01156\beta^4 - 0.000128\beta^6 \cdots + \beta^2 \log \beta^2(0.0833 + 0.00278\beta^2 + 0.000025\beta^4 \cdots)]. \tag{13}$$

In Table II the peak intensity, $\bar{P}(\beta_0,0)$, is given as a function of β_0 in the range $0 \leqslant \beta_0 \leqslant 1$.

(c) If the oscillatory field is large compared to the optimum, i.e., if $\beta_0 \gg \pi$, then $I(\beta) \sim 0$ and

$$\bar{P}_{pq}(\beta_0,x) \sim 1/2(1+x^2). \tag{14}$$

This curve is shown also in Fig. 1. Its half-width is $\Delta\nu = 2b_{pq}$, which is not very different from (11). Hence for oscillatory fields above the optimum, the width is roughly proportional to H_1.

II. ATOMS WITH $J=\frac{1}{2}$, I ARBITRARY[11]

The radiofrequency spectra of atoms with electronic angular momentum $J=\frac{1}{2}$ coupled with nuclear spin have been extensively studied[5,12] and further work is in progress. We assume for the Hamiltonian (1):

$$\mathcal{H}' = (\Delta W/I + \tfrac{1}{2})\mathbf{I}\cdot\mathbf{J}; \quad \mathcal{H}'' = \mu_0(g_i\mathbf{I} + g_j\mathbf{J})\cdot\mathbf{H}_0; \quad V = \mu_0(g_i\mathbf{I} + g_j\mathbf{J})\cdot\mathbf{H}_1. \tag{15}$$

Here ΔW is the separation of the h.f.s. components in the absence of field, $\mathbf{I}$ is the nuclear spin assumed arbitrary, $\mathbf{J}$ the electronic angular momentum ($J=\frac{1}{2}$), μ_0 the Bohr magneton and g_i and

[11] Angular momentum hereinafter is expressed in units of $\hbar = h/2\pi$.
[12] S. Millman and P. Kusch, Phys. Rev. **58**, 438 (1940).

g_j the Landé g factors for the nucleus and electronic configuration, respectively (g_i, g_j have the opposite signs of their respective moments). We may assume without loss of generality that $\mathbf{H}_0 = H_0\mathbf{k}$, and $\mathbf{H}_1 = (H_{1x}\mathbf{i} + H_{1z}\mathbf{k}) \cos(\omega t + \delta)$ where $\mathbf{i}$ and $\mathbf{k}$ are unit vectors parallel to the x and z axes.

We start with a representation A in which $\mathbf{F}^2 (\mathbf{F} = \mathbf{I} + \mathbf{J})$ and $F_z = m$ are diagonal. This is not the desired representation B since $\mathcal{H}''$ is not diagonal in it. However, $\mathcal{H}''$ is diagonal in m and its only off diagonal elements are of the form $(F|\mathcal{H}''|F \pm 1)$. Thus the secular determinant factors into quadratics which are solved to give the energies W_{Fm}. For the sake of brevity these are not quoted here but may be found in reference 5. We now use these energies to find the expansion of eigenstates φ in representation B in terms of the eigenstates ψ of representation A. We shall label each φ in terms of the ψ from which it is derived adiabatically as the field increases from 0. The general expansions of this form are:

$$\varphi_{I\pm\frac{1}{2},m} = A_{I\pm\frac{1}{2},m}\psi_{I+\frac{1}{2},m} + B_{I\pm\frac{1}{2},m}\psi_{I-\frac{1}{2},m}. \tag{16}$$

We find for the coefficients after normalization:

$$\text{for} \quad m \neq \pm(I+\tfrac{1}{2}) \begin{cases} A_{I\pm\frac{1}{2},m} = \dfrac{1}{\sqrt{2}}\left(1 \pm \dfrac{1+2mx/(2I+1)}{R_m}\right)^{\frac{1}{2}} \\ B_{I\pm\frac{1}{2},m} = \mp\dfrac{1}{\sqrt{2}}\left(1 \mp \dfrac{1+2mx/(2I+1)}{R_m}\right)^{\frac{1}{2}} \end{cases} \tag{17}$$

$$\text{for} \quad m = \pm(I+\tfrac{1}{2}) \qquad A_{I+\frac{1}{2}\pm(I+\frac{1}{2})} = 1, \quad B_{I+\frac{1}{2},\pm(I+\frac{1}{2})} = 0,$$

where

$$R_m = \left(1 + \frac{4mx}{2I+1} + x^2\right)^{\frac{1}{2}}, \quad x \equiv (g_j - g_i)\mu_0 H_0/\Delta W.$$

The allowed transitions $p \rightleftarrows q$ are those for which $(p|V_0|q)$ does not vanish. The selection rules are the same as when $H_0 \sim 0$, i.e.,

(a) $|\Delta F| = 1,0 \quad \Delta m = \pm 1 \quad (\pi$ components),

(b) $|\Delta F| = 1 \quad \Delta m = 0 \quad (\sigma$ components).

Calculation of the matrix elements in representation B, $(F,m|V_0|F',m') = \varphi_{Fm}^* V_0 \varphi_{F'm'}$, completes the solution of the problem. These are readily found from (15), (16), (17) and the familiar matrices of angular momentum. They are as follows:

(a) π components. The exact expressions are lengthy and for the sake of brevity are omitted. If, however, it is legitimate to neglect g_i in comparison with g_j, as is almost always the case, these expressions assume a very simple form:

$$(F,m|V_0|F',m\pm1) = \tfrac{1}{2}H_{1z}[(\mu_\infty \pm \mu_{F,m})(\mu_\infty \mp \mu_{F',m\pm1})]^{\frac{1}{2}}, \tag{18}$$

where $\mu_{F,m}$ are the magnetic moments of the states F,m:

$$m \neq \pm I \pm \tfrac{1}{2}, \qquad \mu_{I\pm\frac{1}{2},m} = \mp\frac{x + 2m/(2I+1)}{R_m}\mu_\infty,$$

$$\mu_{I+\frac{1}{2},\pm(I+\frac{1}{2})} = \mp\mu_\infty$$

and $\mu_\infty = g_j\mu_0/2$ is the limiting value of $|\mu_{Fm}|$ as the field becomes large.

(b) σ components.

$$(F,m|V_0|F',m) = -\mu_0(g_j - g_i)\left[1 - \left(\frac{2m}{2I+1}\right)^2\right]\frac{H_{1z}}{2R_m}. \tag{19}$$

If g_i is neglected in comparison with g_j this may be put into a form similar to (18) as follows:

$$(F,m\,|\,V_0\,|\,F',m)=-H_{1z}(\mu_x^2-\mu_{F,m}^2)^{\frac{1}{2}}. \tag{20}$$

Since the magnetic moments have been extensively tabulated these results should be easy to use.

If one takes the limit as $H_0\to 0$ of (18) and (20), one finds the selection rules for the complete Paschen-Back effect as: $\Delta m_J=\pm 1$, $\Delta m_I=0$. The reason the lines $\Delta m_I=\pm 1$, $\Delta m_J=0$ appear to be excluded is the neglect of g_i in (18). This is not important, however, at fields available in the laboratory.

The author is indebted to Professor I. I. Rabi for stimulating discussions.

Appendix

I. If the variables are separated in Eqs. (3) of the text, it is clear that we shall have two linear homogeneous equations of the second order with coefficients periodic in t with period $2\pi/\omega$. Floquet's theorem[13] therefore applies, according to which particular solutions exist of the form

$$C_p=\sum_{n=-\infty}^{+\infty}A_n e^{i(\lambda-n\omega)t},$$
$$C_q=\sum_{n=-\infty}^{+\infty}B_n e^{i(\lambda-n\omega)t}, \tag{21}$$

where λ is a constant to be found by substituting in (3) and eliminating the coefficients A_n, B_n. As a result of this substitution one obtains an infinite set of linear homogeneous equations in A_n and B_n. We are interested, however, only in the approximation that neglects high frequency terms in the Heisenberg representatives $e^{iWpt/\hbar}C_p$ and $e^{iWqt/\hbar}C_q$. We may distinguish particular solutions by their behavior as $V_0\to 0$. We have the possibilities

$$\text{(a)}\quad C_p'\sim A_0e^{-iWpt/\hbar}\quad C_q'\sim 0$$

and

$$\text{(b)}\quad C_p''\sim 0\quad C_q''\sim B_0e^{-iWqt/\hbar}.$$

The corresponding approximate solutions found by substituting (21) in (3) and neglecting high frequency terms are:[14]

$$\text{(a)}\quad C_p'=A_0e^{i\lambda pt}$$
$$C_q'=-\tfrac{1}{2}\frac{(q\,|\,V_0\,|\,p)e^{-i\delta}}{W_q-\hbar(\lambda_p-\omega)}A_0e^{i(\lambda_p-\omega)t} \tag{22}$$

and

$$\text{(b)}\quad C_p''=-\tfrac{1}{2}\frac{(p\,|\,V_0\,|\,q)e^{i\delta}}{W_p-\hbar\lambda_q}B_0e^{i\lambda qt}, \tag{23}$$
$$C_q''=B_0e^{i(\lambda_q-\omega)t},$$

where λ_p and λ_q are the roots of the quadratic

$$(W_p+\hbar\lambda)(W_q+\hbar(\lambda-\omega))=\tfrac{1}{4}|\,(p\,|\,V_0\,|\,q)\,|^2,$$

λ_p being the root that approaches $-W_p/\hbar$ as V_0 tends to zero. Combining (22) and (23) and assuming that initially $|C_p|=1$, $C_q=0$ we have for our required solution

$$C_q=\frac{(q\,|\,V_0\,|\,p)e^{-i(\omega t+\delta)}}{2\hbar(\lambda_p-\lambda_q)}(e^{i\lambda pt}-e^{i\lambda qt}), \tag{24}$$

whence we get Eq. (4) of the text. If a higher approximation is desired it is easily obtained by using further terms of (21), as these series converge rapidly when V_0 is small.

II. Laporte gives the asymptotic expansion of $J_m(z)$ (see (8) above) as:

$$J_m(z)\sim(\pi/3)^{\frac{1}{2}}\cdot(z/2)^{m/3}\cdot\exp\left[-3(z/2)^{\frac{2}{3}}\right]\cdot\sum_{p=0}^{\infty}K_p(m)(2/z)^{2p/3}. \tag{25}$$

The summation is to be taken only so far as the terms decrease. An examination of Laporte's work shows that this formula is valid for $-3\pi/4<\arg z<3\pi/4$. Thus it may be used for $z=\beta e^{i\pi/2}$ (β real). The first two coefficients are given by Laporte as[15]

$$K_0=1,\quad K_1=(m^2+m-\tfrac{1}{3})/12.$$

[13] E. T. Whittaker and G. N. Watson, *Modern Analysis*, fourth edition (Cambridge University Press), p. 412.
[14] It is assumed without loss of generality that $W_q>W_p$.
[15] Laporte also gives K_2 but his expression for it is in error. The coefficient of $n(n=\frac{1}{2}(m-1))$ should be -2 instead of -4.

Although further terms may be obtained following his method, they are much more easily found by use of the recursion formula:

$$36pK_p(m) = [(2m+2p-1)(2m-2p+3)-(m-2p-1)(m-2p-2)]K_{p-1}(m)-\tfrac{1}{6}(2m+2p-1)(m-2p+1)(m-2p+4)K_{p-2}(m),$$

which follows from (25) in conjunction with the formulas[9, 16]

$$dJ_m(z)/dz=-J_{m-1}(z);\quad 2J_m(z)=(m-1)J_{m-2}(z)+zJ_{m-3}(z).$$

In order to find the value of β_0 that makes the peak intensity, $\frac{1}{2}-I(\beta_0)$, a maximum, we have $d(\frac{1}{2}-I(\beta_0))/d\beta_0=0$ or, since $dJ_3(z)/dz=-J_2(z)$,

$$\text{I.P. } J_2(i\beta_0)=0.$$

Using Laporte's expansion we find $\beta_{0m}=1.200\pi$.

[16] Differentiation of the above asymptotic expansion may be shown to be valid.

FEBRUARY 1, 1941 PHYSICAL REVIEW VOLUME 59

Self-Consistent Field Calculations for Zn, Ga, Ga$^+$, Ga^{+++}, As, As$^+$, As^{++}, As^{+++} *

W. HARTREE AND D. R. HARTREE
University of Manchester, Manchester, England
AND
MILLARD F. MANNING
Department of Physics, University of Pittsburgh, Pittsburgh, Pennsylvania

(Received October 21, 1940)

Results of self-consistent field calculations without exchange for Zn, Ga, Ga$^+$, Ga^{+++}, As, As$^+$, As^{++}, As^{+++} are reported. Tables of the wave functions and effective nuclear charges are given. The wave functions for electrons inside of the 3*d* have been assumed the same for different stages of ionization. The calculations have been carried to an estimated consistency of 0.02 in the *Z*'s. A few remarks on the relation to the structure of solids are included.

INTRODUCTION

IF the wave function for a many-electron atom is expressed as a product of one-electron wave functions, each of these functions has the form $\Phi(\phi)\Theta(\theta)P(r)/r$. The solutions for Φ and Θ are well known. The differential equation which P satisfies is

$$\frac{d^2P}{dr^2}+\left[2v-\epsilon-\frac{l(l+1)}{r^2}\right]P=0, \qquad (1)$$

where $2v$ is the potential energy of an electron at r in Rydberg units, ϵ is the negative of the energy expressed in the same units, l is the azimuthal quantum number, and r is the radius expressed in Bohr units. The square of the radial function P is a measure of the charge enclosed between a sphere of radius r and one of radius $r+dr$.

In carrying out a self-consistent field calculation one first assumes a charge distribution, from this computes the potential energy of an electron as a function of r, and then uses these values of the potential energy and the appropriate value of

TABLE I. *Values of P/r^{l+1} near origin for neutral* Zn.

r	1*s*	2*s*	2*p*	3*s*	3*p*	3*d*	4*s*
0.000	100.0	100.0	1000	100.0	1000	1000	100.0
0.005	86.1	85.8	928	85.8	928	951	85.8
0.010	74.1	73.3	861	73.2	861	906	73.2
0.015	63.8	62.2	801	62.0	799	863	62.0
0.020	55.0	52.4	745	52.1	742	823	52.0

TABLE II. *Values of ϵ and $I=\int_0^\infty P^2dr$ for* Zn.

	1*s*	2*s*	2*p*	3*s*	3*p*	3*d*	4*s*
ϵ	706	84.5	75.7	9.32	6.25	0.991	0.539
I	0.0955	1.033	1.707	7.02	12.23	13.81	178.9

* Prepared for publication by Millard F. Manning, University of Pittsburgh, Pittsburgh, Pennsylvania. Shortly after the outbreak of the war in Europe, Mr. W. Hartree sent to this country a set of the results of his recent unpublished self-consistent field calculations with the request that they be made available to interested physicists in this country. Only the wave functions and not the effective nuclear charges were received. The undersigned has calculated these and supplied the textual material. Professor Hartree has commented on the manuscript but has not seen the proof. Correspondence about this paper and requests for reprints should be addressed to the undersigned. M. F. M.

TABLE III. *Values of P for neutral* Zn.

r	1s	2s	2p	3s	3p	3d	4s	r	3s	3p	3d	4s
0.000	0.00	0.00	0.000	0.00	0.000	0.0000	0.00	1.2	1.33	−1.99	2.53	−3.09
.005	.43	.43	.023	.43	.023	.0001	.43	0.3	1.04	−1.63	2.32	−4.01
.010	.74	.73	.086	.73	.086	.0009	.73	0.4	0.81	−1.33	2.13	−4.82
.015	.96	.93	.180	.93	.180	.0029	.93					
.020	1.10	1.05	.298	1.04	.297	.0066	1.04	1.6	.48	−0.87	1.78	−6.13
.025	1.18	1.09	.433	1.08	.431	.0123	1.08	1.8	.28	−0.56	1.49	−7.06
.030	1.22	1.08	.580	1.06	.576	.0202	1.06	2.0	.16	−0.35	1.24	−7.65
.035	1.23	1.02	.735	1.00	.729	.0307	1.00	2.2	.10	−0.22	1.04	−7.98
.040	1.21	0.93	.894	0.90	.884	.0437	0.90	2.4	.06	−0.13	0.86	−8.09
								2.6	.03	−0.08	.72	−8.04
.05	1.13	0.66	1.21	0.62	1.19	.078	0.61	2.8	.02	−0.05	.60	−7.87
.06	1.01	+0.34	1.52	+0.28	1.48	.123	+0.27	3.0	.01	−0.03	.50	−7.61
.07	0.87	−0.01	1.80	−0.09	1.73	.180	−0.09	3.2		−0.02	.42	−7.29
.08	.75	−0.36	2.05	−0.45	1.95	.246	−0.45	3.4		−0.01	.35	−6.92
.09	.62	−0.69	2.27	−0.78	2.12	.322	−0.79	3.6			.29	−6.52
.10	.52	−0.99	2.44	−1.08	2.24	.407	−1.09	3.8			.24	−6.11
								4.0			.20	−5.70
.12	.35	−1.50	2.70	−1.54	2.34	.60	−1.55					
.14	.23	−1.87	2.82	−1.81	2.28	.81	−1.81	4.5			.13	−4.70
.16	.14	−2.09	2.84	−1.90	2.08	1.04	−1.89	5.0			.08	−3.79
.18	.09	−2.20	2.78	−1.83	1.76	1.27	−1.80	5.5			.05	−3.01
.20	.06	−2.22	2.67	−1.64	1.37	1.51	−1.59	6.0			.03	−2.36
.22	.03	−2.17	2.51	−1.34	0.92	1.75	−1.28	6.5			.02	−1.83
.24	.02	−2.08	2.33	−0.98	+0.44	1.98	−0.90	7.0			.01	−1.41
.26	.01	−1.95	2.14	−0.58	−0.06	2.20	−0.48	7.5				−1.08
.28	.01	−1.80	1.94	−0.15	−0.55	2.40	−0.04	8.0				−0.82
.30		−1.64	1.75	+0.28	−1.04	2.59	+0.40					
								9				−0.47
.35		−1.25	1.31	1.31	−2.13	3.00	1.43	10				−0.26
.40		−0.91	0.95	2.16	−3.01	3.30	2.25	11				−0.14
.45		−0.64	.67	2.79	−3.65	3.51	2.80	12				−0.08
.50		−0.44	.46	3.21	−4.07	3.64	3.09	13				−0.04
.55		−0.30	.32	3.44	−4.31	3.70	3.15	14				−0.02
.60		−0.20	.21	3.52	−4.39	3.71	3.01	15				−0.01
.7		−0.09	.10	3.37	−4.24	3.61	2.34					
.8		−0.04	.04	2.98	−3.85	3.43	1.13					
.9		−0.01	.02	2.53	−3.37	3.21	+0.19					
1.0			.01	2.08	−2.87	2.98	−0.96					
0.1				1.67	−2.41	2.75	−2.07					

l in Eq. (1) which is then solved subject to standard boundary conditions. The solution obtained for P usually corresponds to a charge density which is different from that originally assumed. A new charge distribution is then assumed[1] and the process repeated. This is continued until initial and final estimates agree within a certain tolerance.[2]

Actually the comparisons are usually made in terms of the effective nuclear charges, designated by Z_{nl}, of the various different groups. For a particular nl group of electrons, the effective nuclear charge is defined by

$$Z_{nl}=2(2l+1)\int_\infty^r P^2dr \Big/ \int_\infty^0 P^2dr. \qquad (2)$$

For these calculations the maximum discrepancy between estimated and calculated values of Z for any one type is less than 0.03. For the inner groups the discrepancy is seldom greater than 0.01 and for the entire atom the maximum discrepancy is probably not greater than 0.04.

All the various stages in a self-consistent field calculation have to be carried out either numerically or by some type of integrator such as a differential analyzer. All of these calculations were carried out by standard numerical methods.

In earlier work on copper[2] the $3d$ functions proved very troublesome. A small change in the initial field produced a much larger change in the final field. For Zn the added nuclear charge relieves this situation somewhat and for Ga and As the $3d$ functions were much more stable. Indirect evidence for this is afforded by the small change in $2Z_{3d}$ between Ga^{+++} and Ga^{+}.

[1] M. F. Manning and L. Goldberg, Phys. Rev. **53**, 662 (1938).
[2] D. R. Hartree, Proc. Roy. Soc. **A141**, 282 (1933).

TABLE IV. *Values of 2Z for neutral* Zn.

r	$(1s)^2$	$(2s)^2$	$(2p)^6$	$(3s)^2$	$(3p)^6$	$(3d)^{10}$	$(4s)^2$	r	$(3s)^2$	$(3p)^6$	$(3d)^{10}$	$(4s)^2$
0.000	4.00	4.00	12.00	4.00	12.00	20.00	4.00	0.7	1.85	5.94	12.21	3.93
.005	3.99	4.00	12.00	4.00	12.00			.8	1.27	4.33	10.41	3.92
.010	3.91	3.99	12.00	4.00	12.00			.9	0.83	3.05	8.81	3.92
.015	3.76	3.98	12.00	4.00	12.00			1.0	.53	2.09	7.42	3.92
.020	3.53	3.96	12.00	3.99	12.00			1.1	.33	1.41	6.23	3.91
.025	3.25	3.94	11.99	3.99	12.00			1.2	.20	0.94	5.21	3.90
.030	2.95	3.91	11.98	3.99	12.00			1.3	.12	.62	4.50	3.87
.035	2.63	3.89	11.97	3.98	12.00			1.4	.07	.40	3.64	3.83
.040	2.31	3.87	11.94	3.98	11.99	20.00	4.00					
								1.6	.03	.17	2.54	3.69
.05	1.73	3.85	11.87	3.98	11.98	20.00	4.00	1.8	.01	.07	1.76	3.49
.06	1.25	3.83	11.73	3.98	11.96			2.0		.03	1.22	3.25
.07	0.88	3.83	11.54	3.98	11.94			2.2		.01	0.85	2.98
.08	.60	3.83	11.28	3.98	11.91			2.4			.58	2.69
.09	.41	3.82	10.95	3.97	11.86			2.6			.40	2.40
.10	.27	3.80	10.56	3.97	11.82	20.00	4.00	2.8			.27	2.11
								3.0			.19	1.84
.12	.11	3.67	9.62	3.95	11.72	19.98	4.00	3.2			.12	1.59
.14	.05	3.44	8.54	3.92	11.61	19.97	4.00	3.4			.08	1.37
.16	.02	3.14	7.41	3.88	11.52	19.95	3.99	3.6			.06	1.17
.18		2.78	6.30	3.84	11.44	19.91	3.99	3.8			.04	0.99
.20		2.40	5.25	3.80	11.40	19.85	3.99	4.0			.02	.83
.22		2.02	4.30	3.78	11.37	19.78	3.99					
.24		1.67	3.48	3.76	11.36	19.67	3.99	4.5			.01	.53
.26		1.36	2.78	3.75	11.36	19.55	3.99	5.0				.33
.28		1.09	2.19	3.75	11.36	19.39	3.99	5.5				.20
.30		0.86	1.71	3.75	11.34	19.21	3.99	6.0				.12
								6.5				.07
.35		.45	0.89	3.73	11.21	18.64	3.99	7.0				.04
.40		.23	.45	3.64	10.88	17.92	3.98	7.5				.02
.45		.11	.22	3.46	10.33	17.07	3.98	8.0				.01
.50		.05	.10	3.20	9.59	16.14	3.97					
.55		.03	.04	2.88	8.72	15.14	3.96					
.60		.02	.02	2.53	7.79	14.16	3.94					

RESULTS

Zinc

The calculations for zinc were carried out only for the lowest state of the neutral atom. It is interesting to note that the *3d* functions are much more contracted than the corresponding functions for the Cu^+ ion and that the eigenvalue is larger numerically. As a consequence the *3d* electrons are not affected in ordinary chemical processes and Zn is divalent, whereas Cu is sometimes divalent, indicating that *3d* functions are involved. In metallic Zn the distance between nearest neighbors is 2.83 Bohr units. Reference to Table IV shows that only 0.1 of a *3d* electron lies outside of this radius. For Cu the overlap is much greater. The small overlap in Zn indicates that the ion-core repulsion is not important in determining the properties of metallic Zn. This is confirmed by the fact that the crystal structure of Zn does not correspond to a close packing of spheres.

Reference to Table IV indicates that about half the charge density of the *4s* electrons lies outside of $R=2.83$. This is in accord with a general principle formulated by Slater.[3]

TABLE V. *Values of* P/r^{l+1} *near origin for* Ga.

	Ga^+							Ga
r	*1s*	*2s*	*2p*	*3s*	*3p*	*3d*	*4s*	*4p*
0.000	100.0	100.0	1000	100.0	1000	1000	100.0	1000
0.005	85.6	85.4	926	85.4	925	950	85.4	925
0.010	73.4	72.5	858	72.4	857	903	72.4	857
0.015	62.9	61.2	795	61.0	793	859	61.0	793
0.020	53.9	51.2	737	50.9	735	817	50.8	735

TABLE VI. *Values of* ϵ *and* $I=\int_0^\infty P^2 dr$ *for* Ga^+, Ga^{+++}, Ga.

	Ga^+							Ga^{+++}	Ga	
	1s	*2s*	*2p*	*3s*	*3p*	*3d*	*4s*	*3d*	*4s*	*4p*
ϵ	756	92.2	82.8	11.14	7.79	2.20	1.28	3.92	0.787	0.281
I	0.0866	0.929	1.436	6.26	10.06	9.25	101.2	9.12	109.5	617

[3] J. C. Slater, Phys. Rev. **36**, 57 (1930).

TABLE VII. *Values of P for neutral and ionized* Ga.

	Ga+							Ga+++	Ga			Ga+				Ga+++	Ga	
r	1s	2s	2p	3s	3p	3d	4s	3d	4s	4p	r	3s	3p	3d	4s	3d	4s	4p
0.000	0.000	0.000	0.000	0.000	0.000	0.0000	0.000	same	same	0.000	1.0	1.83	−2.46	2.42	−1.52	2.41	−1.52	+0.40
.005	.428	.427	.023	.427	.023	.0001	.427	as	as	.023	1.1	1.45	−2.03	2.19	−2.60	2.18	−2.60	1.54
.010	.734	.725	.086	.724	.086	.0009	.724	for	for	.086	1.2	1.13	−1.65	1.98	−3.57	1.97	−3.57	2.64
.015	.943	.918	.179	.915	.178	.0029	.915	Ga+	Ga+	.178	1.3	0.87	−1.33	1.78	−4.40	1.77	−4.40	3.67
.020	1.078	1.024	.295	1.017	.294	.0065	1.016			.294	1.4	.66	−1.06	1.60	−5.11	1.58	−5.12	4.63
.025	1.156	1.059	.428	1.048	.425	.0122	1.046			.425								
.030	1.190	1.038	.572	1.021	.568	.0200	1.018			.568	1.6	.37	−0.67	1.28	−6.14	1.26	−6.17	6.34
.035	1.191	0.971	.723	0.947	.716	.0303	0.944			.716	1.8	.21	−0.41	1.02	−6.74	0.99	−6.79	7.75
.040	1.168	0.870	.878	0.838	.866	.0432	0.834			.866	2.0	.11	−0.25	0.81	−7.00	.77	−7.08	8.89
											2.2	.06	−0.15	.64	−6.98	.60	−7.09	9.79
.05	1.076	0.595	1.18	0.545	1.16	.077	0.539			1.16	2.4	.03	−0.09	.50	−6.77	.46	−6.92	10.5
.06	0.952	+0.263	1.48	+0.197	1.43	.121	+0.189			1.43	2.6	.02	−0.05	.40	−6.42	.35	−6.61	11.0
.07	.820	−0.088	1.74	−0.168	1.67	.176	−0.178			1.67	2.8	.01	−0.03	.31	−5.99	.26	−6.22	11.4
.08	.692	−0.435	1.98	−0.523	1.87	.240	−0.533			1.86	3.0		−0.01	.24	−5.51	.20	−5.77	11.6
.09	.575	−0.762	2.17	−0.849	2.02	.314	−0.858			2.00	3.2		−0.01	.19	−5.02	.15	−5.31	11.8
.10	.472	−1.06	2.33	−1.135	2.12	.395	−1.143			2.10	3.4			.15	−4.53	.11	−4.84	11.8
											3.6			.11	−4.05	.08	−4.38	11.8
.12	.310	−1.54	2.55	−1.56	2.18	.58	−1.56			2.16	3.8			.09	−3.59	.06	−3.94	11.7
.14	.199	−1.87	2.65	−1.79	2.09	.78	−1.78			2.05	4.0			.07	−3.17	.04	−3.53	11.5
.16	.125	−2.07	2.65	−1.83	1.86	.99	−1.81			1.81								
.18	.077	−2.15	2.57	−1.72	1.52	1.21	−1.68			1.47	4.5			.04	−2.26	.02	−2.63	10.9
.20	.047	−2.14	2.44	−1.48	1.12	1.43	−1.42			1.05	5.0			.02	−1.57	.01	−1.92	10.1
.22	.029	−2.07	2.28	−1.15	0.67	1.64	−1.08			0.59	5.5			.01	−1.07		−1.38	9.2
.24	.017	−1.95	2.10	−0.76	+0.19	1.85	−0.67			+0.10	6.0				−0.71		−0.98	8.3
.26	.010	−1.81	1.91	−0.34	−0.29	2.04	−0.24			−0.39	6.5				−0.47		−0.69	7.4
.28	.006	−1.66	1.72	+0.09	−0.77	2.22	+0.21			−0.87	7.0				−0.30		−0.48	6.5
.30	.004	−1.50	1.53	0.52	−1.22	2.39	0.65			−1.32	7.5				−0.19		−0.33	5.6
											8.0				−0.12		−0.22	4.9
.35	.001	−1.11	1.12	1.52	−2.24	2.73	1.63			−2.31								
.40		−0.79	0.80	2.31	−3.02	2.97	2.37			−3.04	9				−0.04		−0.10	3.5
.45		−0.55	.55	2.87	−3.57	3.13	2.83			−3.50	10				−0.02		−0.04	2.5
.50		−0.37	.38	3.21	−3.90	3.21	3.01			−3.70	11				−0.01		−0.02	1.7
.55		−0.25	.25	3.38	−4.05	3.23	2.97			−3.70	12						−0.01	1.2
.60		−0.16	.17	3.40	−4.07	3.21	2.75			−3.53								
											14							0.6
.7		−0.07	.07	3.16	−3.84	3.07	1.92	3.07	1.92	−2.84	16							.3
.8		−0.03	.03	2.74	−3.42	2.87	+0.82	2.87	+0.82	−1.86	18							.2
.9		−0.01	.01	2.27	−2.94	2.65	−0.36	2.64	−0.36	−0.75	20							.1

TABLE VIII. *Values of 2Z for* Ga.

	Ga+							Ga+++	Ga			Ga+				Ga+++	Ga	
r	$(1s)^2$	$(2s)^2$	$(2p)^6$	$(3s)^2$	$(3p)^6$	$(3d)^{10}$	$(4s)^2$	$(3d)^{10}$	$(4s)^2$	$(4p)$	r	$(3s)^2$	$(3p)^6$	$(3d)^{10}$	$(4s)^2$	$(3d)^{10}$	$(4s)^2$	$(4p)$
0.000	4.00	4.00	12.00	4.00	12.00	20.00	4.00	20.00	4.00	2.00	0.7	1.66	5.39	10.87	3.90	10.76	3.90	1.99
.005	3.98	4.00	12.00	4.00	12.00						0.8	1.10	3.81	8.96	3.89	8.82	3.89	1.98
.010	3.90	3.99	12.00	4.00	12.00						0.9	0.70	2.60	7.30	3.89	7.15	3.89	1.98
.015	3.74	3.98	12.00	4.00	12.00						1.0	.43	1.73	5.91	3.88	5.75	3.89	1.98
.020	3.50	3.96	12.00	3.99	12.00						1.1	.26	1.13	4.76	3.87	4.59	3.87	1.98
.025	3.21	3.93	11.99	3.99	12.00						1.2	.15	0.72	3.82	3.83	3.65	3.83	1.98
.030	2.89	3.91	11.98	3.99	12.00						1.3	.09	.46	3.05	3.76	2.88	3.78	1.98
.035	2.56	3.89	11.96	3.98	11.99						1.4	.05	.29	2.43	3.67	2.27	3.69	1.97
.040	2.24	3.86	11.94	3.98	11.99	20.00	4.00	20.00	4.00	2.00								
											1.6	.01	.11	1.53	3.42	1.38	3.46	1.95
.05	1.65	3.84	11.85	3.98	11.98	20.00	4.00	20.00	4.00	2.00	1.8		.04	0.95	3.09	0.83	3.15	1.92
.06	1.18	3.84	11.70	3.98	11.96						2.0		.01	.59	2.71	.49	2.79	1.88
.07	0.82	3.84	11.48	3.98	11.93						2.2			.36	2.32	.28	2.42	1.82
.08	.55	3.83	11.19	3.98	11.89						2.4			.22	1.94	.16	2.06	1.75
.09	.37	3.82	10.83	3.97	11.85						2.6			.13	1.60	.09	1.73	1.68
.10	.24	3.78	10.40	3.97	11.80	20.00	4.00	20.00	40.0	2.00	2.8			.08	1.29	.05	1.43	1.60
											3.0			.04	1.03	.03	1.16	1.51
.12	.10	3.63	9.39	3.94	11.68	19.98	4.00	19.98	4.00	2.00	3.2			.02	0.81	.01	0.94	1.42
.14	.04	3.37	8.25	3.91	11.57	19.96	4.00	19.96	4.00		3.4			.01	.63		.75	1.33
.16	.02	3.04	7.08	3.86	11.48	19.93	3.99	19.93	3.99		3.6				.49		.60	1.24
.18	.01	2.65	5.93	3.82	11.41	19.88	3.99	19.88	3.99		3.8				.37		.47	1.15
.20		2.26	4.88	3.79	11.37	19.80	3.99	19.80	3.99		4.0				.28		.37	1.07
.22		1.87	3.95	3.77	11.35	19.70	3.99	19.70	3.99									
.24		1.52	3.15	3.76	11.35	19.57	3.99	19.56	3.99		4.5				.13		.19	0.86
.26		1.22	2.48	3.75	11.34	19.40	3.99	19.40	3.99		5.0				.10		.10	.68
.28		0.96	1.93	3.75	11.31	19.21	3.99	19.20	3.99		5.5				.03		.05	.52
.30		.74	1.48	3.75		18.98	3.99	18.96	3.99	2.00	6.0				.01		.02	.40
											6.5						.01	.30
.35		.38	0.75	3.71	11.12	18.26	3.98	18.24	3.99	2.00	7.0							.22
.40		.18	.36	3.59	11.70	17.38	3.97	17.34	3.98	2.00	7.5							.16
.45		.08	.17	3.37	10.05	16.36	3.96	16.32	3.96	2.00	8.0							.11
.50		.04	.08	3.07	9.21	15.27	3.94	15.21	3.95	1.99								
.55		.02	.04	2.72	8.27	14.14	3.93	14.07	3.93	1.99	9							.06
.60		.01	.02	2.35	7.28	13.02	3.91	12.93	3.92	1.99	10							.03
											11							.01
											12							.01

TABLE IX. *Values of P/r^{l+1} near origin for* As^{+++} *and* As.

	As^{+++} AND As							As
r	$1s$	$2s$	$2p$	$3s$	$3p$	$3d$	$4s$	$4p$
0.000	100.0	100.0	1000	100.0	1000	1000	100.0	1000
0.005	84.8	84.5	921	84.5	921	947	84.5	921
0.010	71.9	71.0	849	70.9	848	897	70.9	848
0.015	61.0	59.1	783	58.9	781	850	58.9	781
0.020	51.8	48.7	723	48.3	720	807	48.3	720

TABLE X. *Values of ϵ and $I=\int_0^\infty P^2dr$ for* As^{+++}.

	$1s$	$2s$	$2p$	$3s$	$3p$	$3d$	$4s$
ϵ	866	110.0	99.7	15.76	12.02	5.575	3.29
I	0.07155	0.750	1.0145	4.975	6.825	4.47	47.6

TABLE XI. *Values of ϵ and $I=\int_0^\infty P^2dr$ for* As^{++}, As^{+} *and* As.

	As^{++}		As^{+}		As		
	$(4s)^2$	$(4p)$	$(4s)^2$	$(4p)^2$	$(3d)^{10}$	$(4s)^2$	$(4p)^3$
ϵ	2.481	1.734	1.768	1.0485	3.312	1.180	0.468
I	51.55	99.5	55.6	123.0	4.53	57.8	157.1

Gallium

The calculations were carried out first for Ga^+. For Ga^{+++} it was assumed that the charge densities for all the electrons inside $3d$ are the same as for Ga^+. The validity of this assumption is indicated by the fact that the maximum change in $2Z_{3d}$ between Ga^+ and Ga^{+++} is only 0.17 and inner electrons would be affected much less.

For Ga, $2Z_{3d}$ was assumed the same as for Ga^+. The reason this can be done is that the charge distribution of the added $4p$ is almost completely outside the $3d$ and also because there is a compensatory change in the $4s$ functions when the $4p$ is added. At no point where the charge density of the $3d$ is appreciable is the sum of $2Z_{4s}+2Z_{4p}$ for Ga different by more than 0.04 from $2Z_{4s}+2$ for Ga^+.

Although the charge distributions for inner electrons differ very little for different degrees of ionization, this is not true for the eigenvalues. This is because the addition of a valence electron

TABLE XII. *Values of P for* As^{+++}.

r	$1s$	$2s$	$2p$	$3s$	$3p$	$3d$	$4s$	r	$2s$	$2p$	$3s$	$3p$	$3d$	$4s$
0.000	0.000	0.000	0.000	0.000	0.000	0.0000	0.000	0.7	−0.039	0.041	2.73	−3.10	2.21	+1.03
.005	.424	.423	.023	.422	.023	.0001	.422	.8	−0.014	.016	2.26	−2.65	1.99	−0.21
.010	.719	.710	.085	.709	.085	.0009	.709	.9	−0.005	.006	1.80	−2.18	1.76	−1.43
.015	.915	.887	.176	.883	.176	.0029	.883	1.0	−0.002	.002	1.39	−1.76	1.54	−2.54
.020	1.036	.975	.289	.967	.288	.0064	.967	1.1	−0.001	.001	1.05	−1.39	1.34	−3.49
.025	1.100	.992	.417	.979	.415	.0120	.978	1.2			0.79	−1.09	1.16	−4.26
.030	1.121	.953	.555	.933	.551	.0196	.931	1.3			.58	−0.84	0.99	−4.85
.035	1.111	.870	.698	.843	.691	.0297	.840	1.4			.42	−0.65	.85	−5.27
.040	1.078	.755	.844	.718	.831	.0421	.714							
								1.6			.22	−0.37	.61	−5.68
.05	0.973	.457	1.129	.403	1.102	.074	.397	1.8			.11	−0.21	.43	−5.64
.06	.844	+0.114	1.395	+0.043	1.346	.117	+0.035	2.0			.05	−0.12	.31	−5.30
.07	.712	−0.238	1.630	−0.321	1.549	.168	−0.330	2.2			.03	−0.07	.21	−4.80
.08	.589	−0.577	1.831	−0.663	1.708	.229	−0.673	2.4			.01	−0.03	.15	−4.22
.09	.480	−0.888	1.996	−0.967	1.819	.297	−0.976	2.6				−0.02	.10	−3.62
.10	.387	−1.162	2.124	−1.223	1.882	.372	−1.229	2.8				−0.01	.07	−3.04
								3.0					.05	−2.52
.12	.244	−1.585	2.280	−1.573	1.877	.537	−1.570	3.2					.03	−2.07
.14	.150	−1.850	2.322	−1.712	1.718	.718	−1.696	3.4					.02	−1.68
.16	.091	−1.981	2.277	−1.666	1.441	.905	−1.631	3.6					.01	−1.34
.18	.054	−2.005	2.171	−1.472	1.078	1.093	−1.415	3.8					.01	−1.06
.20	.032	−1.951	2.026	−1.170	0.660	1.278	−1.088	4.0						−0.84
.22	.019	−1.846	1.858	−0.793	+0.212	1.454	−0.689	4.5						−0.45
.24	.011	−1.707	1.680	−0.374	−0.244	1.618	−0.250	5.0						−0.24
.26	.006	−1.552	1.502	+0.062	−0.692	1.770	+0.203	5.5						−0.12
.28	.003	−1.391	1.329	0.497	−1.120	1.907	0.647	6.0						−0.06
.30	.002	−1.232	1.166	0.915	−1.520	2.028	1.066	6.5						−0.03
								7.0						−0.02
.35	.001	−0.874	0.817	1.82	−2.36	2.26	1.94	7.5						−0.01
.40		−0.595	.555	2.49	−2.95	2.41	2.50	8.0						
.45		−0.394	.368	2.91	−3.32	2.48	2.75							
.50		−0.255	.241	3.12	−3.50	2.49	2.73							
.55		−0.162	.156	3.16	−3.52	2.46	2.50							
.60		−0.102	.100	3.09	−3.45	2.39	2.11							

TABLE XIII. *Values of 2Z for* As^{+++}.

r	$(1s)^2$	$(2s)^2$	$(2p)^6$	$(3s)^2$	$(3p)^6$	$(3d)^{10}$	$(4s)^2$
0.000	4.00	4.00	12.00	4.00	12.00	20.00	4.00
.005	3.98	4.00	12.00	4.00	12.00		
.010	3.88	3.99	12.00	4.00	12.00		
.015	3.69	3.97	12.00	4.00	12.00		
.020	3.42	3.95	11.99	3.99	12.00		
.025	3.10	3.92	11.99	3.99	12.00		
.030	2.76	3.90	11.97	3.99	12.00		
.035	2.41	3.88	11.95	3.98	11.99		
.040	2.07	3.86	11.92	3.98	11.99	20.00	4.00
.05	1.48	3.84	11.80	3.98	11.97	20.00	4.00
.06	1.02	3.83	11.61	3.98	11.95	20.00	
.07	0.68	3.83	11.34	3.98	11.90	20.00	
.08	.44	3.83	10.98	3.97	11.85	20.00	
.09	.28	3.80	10.55	3.97	11.80	20.00	
.10	.18	3.74	10.05	3.96	11.74	19.99	4.00
.12	.07	3.53	8.89	3.93	11.61	19.97	4.00
.14	.03	3.21	7.62	3.88	11.50	19.94	3.99
.16	.01	2.82	6.37	3.84	11.41	19.88	3.99
.18		2.39	5.19	3.80	11.35	19.79	3.98
.20		1.97	4.15	3.77	11.33	19.66	3.98
.22		1.58	3.26	3.75	11.32	19.50	3.98
.24		1.25	2.52	3.75	11.32	19.29	3.98
.26		0.97	1.92	3.74	11.31	19.03	3.98
.28		.73	1.44	3.74	11.28	18.72	3.98
.30		.55	1.07	3.74	11.22	18.37	3.98

r	$(1s)^2$	$(2s)^2$	$(2p)^6$	$(3s)^2$	$(3p)^6$	$(3d)^{10}$	$(4s)$
0.35		0.26	0.50	3.66	10.87	17.34	3.97
.40		.11	.22	3.46	10.24	16.10	3.95
.45		.05	.09	3.16	9.37	14.76	3.92
.50		.02	.04	2.79	8.34	13.37	3.88
.55		.01	.02	2.39	7.25	11.99	3.85
.60			.01	2.00	6.17	10.68	3.83
.7				1.31	4.27	8.28	3.81
.8				0.81	2.81	6.31	3.81
.9				.47	1.79	4.72	3.80
1.0				.27	1.10	3.50	3.77
1.1				.15	0.67	2.57	3.69
1.2				.08	.40	1.86	3.56
1.3				.04	.23	1.35	3.38
1.4				.02	.14	0.97	3.17
1.6				.01	.05	.49	2.65
1.8					.02	.24	2.11
2.0					.01	.12	1.60
2.2						.05	1.17
2.4						.03	0.82
2.6						.01	.56
2.8							.38
3.0							.25
3.2							.16
3.4							.10
3.6							.06
3.8							.04
4.0							.02
4.5							.01

TABLE XIV. *Values of P for* As^{++}, As^{+}, As.

	As^{++}		As^{+}		As		
r	$(4s)^2$	$(4p)$	$(4s)^2$	$(4p)^2$	$(3d)^{10}$	$(4s)^2$	$(4p)^2$
0.000	same	same	same	same	same	same	0.000
.005	as	as	as	as	as	as	.023
.010	for	for	for	for	for	for	.085
.015	As^{+++}	As^{+++}	As^{+++}	As^{+++}	As^{+++}	As^{+++}	.176
.020							.288
.025							.415
.030							.550
.035							.690
.040							.830
.05							1.100
.06							1.342
.07							1.543
.08							1.699
.09							1.806
.10							1.865
.12	−1.570	1.848	−1.570	1.848	0.537	−1.570	1.848
.14	−1.696	1.674	−1.696	1.675	0.718	−1.696	1.676
.16	−1.631	1.382	−1.631	1.383	0.905	−1.631	1.384
.18	−1.415	1.003	−1.415	1.005	1.093	−1.415	1.007
.20	−1.088	0.570	−1.088	0.572	1.278	−1.088	0.575
.22	−0.689	+0.111	−0.690	+0.114	1.455	−0.690	+0.117
.24	−0.250	−0.353	−0.251	−0.349	1.620	−0.251	−0.346
.26	+0.202	−0.805	+0.201	−0.801	1.772	+0.200	−0.798
.28	0.645	−1.232	0.644	−1.228	1.909	0.643	−1.224
.30	1.064	−1.624	1.063	−1.619	2.031	1.062	−1.615
.35	1.94	−2.41	1.93	−2.41	2.27	1.93	−2.40
.40	2.50	−2.91	2.50	−2.91	2.41	2.50	−2.91
.45	2.76	−3.13	2.76	−3.13	2.49	2.76	−3.13
.50	2.74	−3.11	2.74	−3.12	2.50	2.75	−3.13
.55	2.51	−2.91	2.51	−2.93	2.47	2.52	−2.94
.60	2.12	−2.57	2.12	−2.59	2.40	2.13	−2.61

r	As^{++} $(4s)^2$	As^{++} $(4p)$	As^{+} $(4s)^2$	As^{+} $(4p)^2$	As $(3d)^{10}$	As $(4s)^2$	As $(4p)^2$
0.7	+1.04	−1.61	+1.05	−1.65	2.22	+1.06	−1.67
.8	−0.19	−0.47	−0.18	−0.51	2.00	−0.17	−0.55
.9	−1.41	+0.71	−1.40	+0.66	1.78	−1.39	+0.62
1.0	−2.52	1.86	−2.51	1.81	1.56	−2.50	1.76
1.1	−3.48	2.92	−3.47	2.86	1.36	−3.46	2.82
1.2	−4.25	3.85	−4.25	3.81	1.17	−4.25	3.77
1.3	−4.86	4.67	−4.86	4.63	1.01	−4.86	4.60
1.4	−5.29	5.35	−5.31	5.34	0.87	−5.32	5.32
1.6	−5.75	6.34	−5.80	6.39	.63	−5.82	6.42
1.8	−5.76	6.90	−5.85	7.02	.45	−5.89	7.12
2.0	−5.47	7.09	−5.62	7.32	.32	−5.68	7.50
2.2	−5.02	7.02	−5.21	7.37	.23	−5.29	7.64
2.4	−4.48	6.75	−4.70	7.22	.16	−4.81	7.60
2.6	−3.91	6.35	−4.17	6.95	.11	−4.29	7.45
2.8	−3.36	5.87	−3.64	6.58	.08	−3.78	7.19
3.0	−2.84	5.35	−3.14	6.16	.05	−3.29	6.88
3.2	−2.38	4.81	−2.68	5.71	.04	−2.84	6.53
3.4	−1.98	4.29	−2.27	5.24	.02	−2.44	6.16
3.6	−1.63	3.78	−1.91	4.78	.01	−2.08	5.78
3.8	−1.33	3.31	−1.60	4.32	.01	−1.77	5.40
4.0	−1.08	2.87	−1.33	3.89		−1.50	5.02
4.5	−0.62	1.97	−0.83	2.94		−0.97	4.13
5.0	−0.35	1.31	−0.50	2.16		−0.62	3.35
5.5	−0.20	0.85	−0.30	1.56		−0.39	2.69
6.0	−0.11	.54	−0.18	1.10		−0.25	2.13
6.5	−0.06	.33	−0.10	0.77		−0.16	1.68
7.0	−0.03	.21	−0.06	.53		−0.10	1.31
7.5	−0.02	.12	−0.03	.37		−0.06	1.02
8.0	−0.01	.07	−0.02	.25		−0.04	0.79
9		.02	−0.01	.11		−0.01	.46
10		.01		.05			.27
11				.02			.16
12				.01			.09
13							.05
14							.03
15							.01
16							.01

TABLE XV. *Values of 2Z for* As^{++}, As^{+}, As.

	As^{++}		As^{+}		As				As^{++}		As^{+}		As		
r	$(4s)^2$	$(4p)$	$(4s)^2$	$(4p)^2$	$(3d)^{10}$	$(4s)^2$	$(4p)^3$	r	$(4s)^2$	$(4p)$	$(4s)^2$	$(4p)^2$	$(3d)^{10}$	$(4s)^2$	$(4p)^3$
0.000	4.00	2.00	4.00	4.00	20.00	4.00	6.00	1.6	2.75	1.67	2.84	3.46	0.53	2.88	5.37
.10	4.00	2.00	4.00	4.00	19.99	4.00	6.00	1.8	2.23	1.49	2.35	3.17	.27	2.40	5.02
.12	4.00	2.00	4.00	3.99	19.97	4.00	5.99	2.0	1.74	1.29	1.87	2.83	.14	1.93	4.61
.14	3.99	1.99	3.99	3.99	19.94	3.99	5.99	2.2	1.31	1.09	1.45	2.48	.07	1.52	4.17
.16	3.99	1.99	3.99	3.99	19.88	3.99	5.99	2.4	0.96	0.90	1.09	2.13	.03	1.16	3.72
.18	3.98	1.99	3.98	3.99	19.79	3.99	5.99	2.6	.69	.72	0.81	1.80	.01	0.88	3.29
.20	3.98	1.99	3.98	3.99	19.67	3.98	5.99	2.8	.48	.57	.59	1.50		.65	2.88
.22	3.98	1.99	3.98	3.99	19.51	3.98	5.99	3.0	.33	.45	.42	1.24		.48	2.50
.24	3.98	1.99	3.98	3.99	19.30	3.98	5.99	3.2	.23	.34	.30	1.01		.35	2.16
.26	3.98	1.99	3.98	3.99	19.04	3.98	5.99	3.4	.15	.26	.21	0.82		.25	1.85
.28	3.98	1.99	3.98	3.99	18.74	3.98	5.99	3.6	.10	.19	.14	.65		.18	1.58
.30	3.98	1.99	3.98	3.99	18.40	3.98	5.98	3.8	.06	.14	.10	.52		.13	1.34
								4.0	.04	.10	.07	.41		.09	1.13
.35	3.97	1.99	3.97	3.98	17.37	3.97	5.98								
.40	3.95	1.98	3.95	3.97	16.15	3.95	5.96	4.5	.01	.05	.03	.22		.04	0.73
.45	3.92	1.97	3.93	3.95	14.81	3.93	5.94	5.0		.02	.01	.11		.02	.46
.50	3.89	1.96	3.90	3.94	13.43	3.90	5.93	5.5		.01		.06		.01	.29
.55	3.87	1.95	3.88	3.92	12.07	3.88	5.91	6.0				.03			.18
.60	3.84	1.94	3.86	3.91	10.75	3.86	5.89	6.5				.01			.11
								7.0				.01			.06
.7	3.82	1.94	3.84	3.90	8.38	3.84	5.88	7.5							.04
.8	3.82	1.93	3.84	3.89	6.41	3.84	5.87	8.0							.02
.9	3.81	1.93	3.83	3.89	4.82	3.84	5.87								
1.0	3.78	1.93	3.80	3.89	3.60	3.81	5.86	9							.01
1.1	3.71	1.92	3.74	3.87	2.66	3.75	5.84								
1.2	3.60	1.89	3.63	3.83	1.94	3.64	5.80								
1.3	3.43	1.86	3.48	3.77	1.42	3.50	5.73								
1.4	3.23	1.81	3.29	3.69	1.03	3.32	5.64								

raises the potential energy of an electron at all points inside.

For solid Ga the distance between closest neighbors is 3.09 Bohr units. Reference to Table VIII shows that there is a negligible overlap of the 3*d* functions but a considerable overlap of the 4*s* and 4*p* functions.

Arsenic

The calculations were carried out first for As^{+++} and then for As^{++}, As^{+}, and As. Since the maximum change in $2Z_{3d}$ between As^{+++} and As is 0.10, it is safe to assume that the Z's for intermediate stages of ionization can be found by linear interpolation. The changes in the inner electrons are of course less than for the 3*d* electrons and hence negligible.

The 4*s* and 4*p* charge distributions are quite different from one stage of ionization to the other and where the charge densities are greatest a linear interpolation between the extremes would not check the intermediate stages of ionization.

The distance between nearest neighbors in metallic arsenic is 3.20 Bohr units. Reference to Table XV shows that there is only a small overlap of the 4*s* electrons but considerable overlap of the 4*p* electrons. The latter will therefore be responsible for most of the properties of the solid.

In Tables I–XV the values of P as tabulated are not normalized but tables of normalizing factors are given.

The authors are indebted to Professor J. C. Slater for cooperation during the preparation of the manuscript.

Self-Consistent Field Calculations for Ge^{++} and Ge*

W. HARTREE AND D. R. HARTREE
University of Manchester, Manchester, England
AND
MILLARD F. MANNING
Department of Physics, University of Pittsburgh, Pittsburgh, Pennsylvania

(Received November 30, 1940)

Results of self-consistent field calculations for Ge^{++} and Ge are reported. Tables of the wave functions and effective nuclear charges are given. The wave functions inside of the $3d$ have been assumed the same for the two stages of ionization. The calculations have been carried to a consistency of 0.02 electronic unit in the Z's.

IN the previous paper results of self-consistent field calculations for Zn, Ga, As and some of their ions have been reported. In this paper results for Ge^{++} and Ge are reported (see Tables I–IV). Before this series of calculations was begun there were no results available for atoms between Cu and Rb. The first atom in this region for which calculations were made was As. For this atom the initial fields were estimated between Cu and Rb by a method described by Hartree.[1] After the results for As were obtained, values for Ga were interpolated between Cu and As. In a similar manner the initial fields for Zn and Ge were estimated from the available results for their neighbors. It should be remarked that at large values of r a linear interpolation between the Z's for As and Ge did not give satisfactory values for the Z's for Ge.

RESULTS

The maximum difference between the values of $2Z_{3d}$ for Ge^{++} and Ge is only 0.04, so that it is safe to assume that the $3p$ and other inner wave functions would show negligible changes. This is partly because most of the $3d$ charge density is inside of the region of appreciable charge density of the valence electrons and partly because the addition of the two $4p$ electrons causes a redistribution of the charge density of the $4s$ electrons which partially compensates for the changes in total charge density caused by introduction of the $4p$ electrons. Since the valence electrons in Ge and neighboring atoms have small l values, the process of obtaining a self-consistent solution of the equations is much more rapid than for elements with a nearly filled d shell or for elements with only one electron outside of a filled d shell.

* Prepared for publication by Millard F. Manning, University of Pittsburgh, Pittsburgh, Pennsylvania. For explanation see previous paper. These results were received from Professor Hartree after the others were ready for publication. The tables are reproduced here in the same form as when received. The textual material has been supplied by the undersigned. Correspondence about this paper and requests for reprints should also be addressed to him.—M. F. M.

[1] D. R. Hartree, Physik. Zeits. **30**, 517 (1929).

TABLE I. *Values of* ϵ *and* $I=\int_0^\infty P^2dr$ *for* Ge^{++} *and* Ge.

	Ge^{++}							Ge		
	$1s$	$2s$	$2p$	$3s$	$3p$	$3d$	$4s$	$3d$	$4s$	$4p$
ϵ	810.8	100.8	91.0	13.26	9.75	3.73	2.21	2.44	0.989	0.386
I	0.314	3.334	1.199	22.34	8.26	6.365	266	6.395	308	268

TABLE II. *Values of* P/r^{l+1} *for* Ge^{++} *and* Ge.

	Ge^{++}							Ge
r	$1s$	$2s$	$2p$	$3s$	$3p$	$3d$	$4s$	$4p$
0.000	200.0	200.0	1000	200.0	1000	1000	200.0	1000
0.005	170.4	169.9	923	169.9	923	948	169.9	923
0.010	145.3	143.5	853	143.3	852	900	143.3	852
0.015	123.9	120.3	789	119.9	787	855	119.8	787
0.020	105.6	99.9	730	99.3	727	812	99.2	727

TABLE III. *Values of P for* Ge^{++} *and* Ge.

	Ge^{++}							Ge		
r	$1s$	$2s$	$2p$	$3s$	$3p$	$3d$	$4s$	$3d$	$4s$	$4p$
0.000	0.00	0.00	0.000	0.00	0.000	0.0000	0.00	Same	Same	0.000
.005	0.85	.85	.023	.85	.023	.0001	.85	as	as	.023
.010	1.45	1.44	.085	1.43	.085	.0009	1.43	for	for	.085
.015	1.86	1.80	.177	1.80	.177	.0029	1.80	Ge^{++}	Ge^{++}	.177
.020	2.11	2.00	.292	1.98	.291	.0065	1.98			.291
.025	2.25	2.05	.422	2.03	.420	.0121	2.02			.420
.030	2.31	1.99	.563	1.95	.559	.0198	1.95			.559
.035	2.30	1.84	.711	1.79	.703	.0300	1.78			.703
.040	2.24	1.62	.860	1.55	.849	.0426	1.55			.848
.050	2.05	1.05	1.155	0.94	1.13	.0755	0.93			1.13
.06	1.79	+0.37	1.435	+0.23	1.39	.119	+0.22			1.385
.07	1.53	−0.34	1.685	−0.50	1.61	.172	−0.51			1.605
.08	1.28	−1.02	1.90	−1.19	1.785	.234	−1.21			1.78
.09	1.05	−1.66	2.08	−1.82	1.915	.305	−1.84			1.905
.10	0.85	−2.23	2.225	−2.37	1.995	.383	−2.38			1.98
.12	.55	−3.14	2.41	−3.15	2.025	.56	−3.14			2.00
.14	.34	−3.73	2.48	−3.51	1.895	.75	−3.48			1.86
.16	.21	−4.06	2.45	−3.51	1.64	.95	−3.45			1.59
.18	.13	−4.16	2.36	−3.20	1.29	1.15	−3.10			1.225
.20	.08	−4.10	2.22	−2.66	0.875	1.35	−2.51		−2.52	0.80
.22	.05	−3.92	2.055	−1.95	+0.42	1.55	−1.76		−1.77	+0.335
.24	.03	−3.67	1.875	−1.14	−0.045	1.73	−0.92		−0.92	−0.14
.26	.02	−3.37	1.69	−0.28	−0.51	1.90	−0.02		−0.03	−0.615
.28	.01	−3.05	1.51	+0.59	−0.965	2.06	+0.87		+0.86	−1.065
.30		−2.73	1.335	1.45	−1.39	2.20	1.73		1.72	−1.49
.35		−1.98	0.955	3.36	−2.815	2.49	3.60		3.60	−2.38
.40		−1.38	.665	4.82	−3.00	2.68	4.91		4.92	−2.99
.45		−0.93	.45	5.80	−3.45	2.79	5.62		5.63	−3.325
.50		−0.62	.30	6.35	−3.695	2.83	5.79		5.82	−3.42
.55		−0.40	.20	6.55	−3.785	2.82	5.51		5.53	−3.32
.60		−0.26	.13	6.49	−3.75	2.78	4.89		4.92	−3.065
.7		−0.11	.055	5.90	−3.455	2.61	2.96	2.61	3.01	−2.24
.8		−0.04	.025	5.01	−3.015	2.40	+0.59	2.40	+0.66	−1.17
.9		−0.02	.01	4.08	−2.535	2.17	−1.84	2.17	−1.76	−0.01
1.0		−0.01	.005	3.23	−2.085	1.94	−4.14	1.95	−4.06	+1.15

	Ge^{++}				Ge		
r	$3s$	$3p$	$3d$	$4s$	$3d$	$4s$	$4p$
1.1	2.50	−1.69	1.73	−6.20	1.73	−6.13	2.27
1.2	1.91	−1.35	1.53	−7.95	1.53	−7.91	3.31
1.3	1.45	−1.08	1.35	−9.40	1.35	−9.38	4.26
1.4	1.08	−0.84	1.18	−10.54	1.19	−10.56	5.11
1.6	0.59	−0.505	0.90	−11.98	0.91	−12.11	6.51
1.8	.32	−0.30	.68	−12.51	.69	−12.78	7.56
2.0	.17	−0.175	.51	−12.36	.52	−12.79	8.29
2.2	.09	−0.10	.38	−11.74	.39	−12.34	8.75
2.4	.05	−0.055	.28	−10.84	.29	−11.60	9.01
2.6	.03	−0.03	.21	−9.78	.22	−10.70	9.09
2.8	.01	−0.015	.15	−8.67	.16	−9.72	9.06
3.0		−0.01	.11	−7.57	.12	−8.72	8.92
3.2			.08	−6.53	.09	−7.76	8.69
3.4			.06	−5.58	.07	−6.84	8.41
3.6			.045	−4.72	.05	−6.02	8.09
3.8			.03	−3.96	.035	−5.25	7.74
4.0			.02	−3.30	.025	−4.57	7.37
4.5			.01	−2.04	.01	−3.16	6.42
5.0			.005	−1.22	.005	−2.15	5.50
5.5				−0.70		−1.45	4.64
6.0				−0.39		−0.96	3.86
6.5				−0.21		−0.62	3.19
7.0				−0.11		−0.42	2.61
7.5				−0.06		−0.27	2.12
8.0				−0.03		−0.18	1.72
9				−0.01		−0.08	1.11
10						−0.04	0.70
11						−0.02	.43
12						−0.01	.27
13							.16
14							.09
15							.05
16							.03
17							.02
18							.01

TABLE IV. *Values of 2Z for* Ge^{++} *and* Ge.

	Ge^{++}							Ge		
r	$(1s)^2$	$(2s)^2$	$(2p)^6$	$(3s)^2$	$(3p)^6$	$(3d)^{10}$	$(4s)^2$	$(3d)^{10}$	$(4s)^2$	$(4p)^2$
0.000	4.00	4.00	12.00	4.00	12.00	20.00	4.00	20.00	4.00	4.00
.005	3.98	4.00	12.00	4.00	12.00					
.010	3.91	3.99	12.00	4.00	12.00					
.015	3.72	3.99	12.00	4.00	12.00					
.020	3.46	3.95	12.00	3.99	12.00					
.025	3.16	3.95	12.00	3.99	12.00					
.030	2.82	3.90	11.98	3.99	12.00					
.035	2.49	3.90	11.98	3.99	12.00					
.040	2.16	3.86	11.93	3.98	11.99	20.00	4.00	20.00	4.00	4.00
.05	1.56	3.84	11.82	3.98	11.97	20.00	4.00	20.00	4.00	4.00
.06	1.09	3.84	11.66	3.98	11.95	20.00	4.00	20.00	4.00	
.07	0.75	3.84	11.41	3.98	11.92	20.00	4.00	20.00	4.00	
.08	.49	3.83	11.08	3.98	11.88	20.00	4.00	20.00	4.00	
.09	.32	3.81	10.69	3.97	11.83	20.00	3.99	20.00	3.99	
.10	.20	3.76	10.22	3.96	11.77	19.99	3.99	19.99	3.99	4.00
.12	.08	3.58	9.14	3.93	11.65	19.98	3.99	19.98	3.99	4.00
.14	.03	3.29	7.94	3.90	11.54	19.95	3.99	19.95	3.99	4.00
.16	.01	2.93	6.71	3.85	11.45	19.90	3.98	19.90	3.98	4.00
.18		2.52	5.55	3.81	11.38	19.84	3.98	19.84	3.98	4.00
.20		2.12	4.50	3.78	11.35	19.74	3.98	19.74	3.98	4.00
.22		1.73	3.58	3.76	11.33	19.60	3.98	19.60	3.98	4.00
.24		1.39	2.81	3.75	11.33	19.43	3.98	19.44	3.98	4.00
.26		1.09	2.17	3.75	11.33	19.22	3.98	19.23	3.98	4.00
.28		0.84	1.66	3.75	11.31	18.98	3.98	18.98	3.98	4.00
.30		.64	1.26	3.74	11.27	18.69	3.98	18.69	3.98	3.99
.35		.31	0.60	3.69	11.01	17.82	3.97	17.82	3.98	3.99
.40		.14	.28	3.53	10.49	16.76	3.96	16.77	3.97	3.98
.45		.06	.12	3.28	9.73	15.58	3.94	15.59	3.95	3.98
.50		.03	.05	2.94	8.80	14.33	3.91	14.35	3.92	3.97
.55		.01	.02	2.57	7.77	13.08	3.89	13.09	3.90	3.96
.60			.01	2.19	6.74	11.84	3.87	11.87	3.89	3.95

	Ge^{++}				Ge		
r	$(3s)^2$	$(3p)^6$	$(3d)^{10}$	$(4s)^2$	$(3d)^{10}$	$(4s)^2$	$(4p)^2$
0.7	1.49	4.82	9.55	3.84	9.59	3.86	3.94
0.8	0.95	3.29	7.57	3.84	7.61	3.86	3.94
0.9	.58	2.16	5.94	3.84	5.97	3.86	3.94
1.0	.34	1.40	4.61	3.82	4.64	3.85	3.94
1.1	.20	0.88	3.55	3.78	3.59	3.81	3.93
1.2	.11	.54	2.71	3.70	2.75	3.75	3.92
1.3	.06	.33	2.06	3.59	2.09	3.65	3.90
1.4	.03	.20	1.56	3.44	1.60	3.52	3.86
1.6	.01	.07	0.88	3.05	0.91	3.18	3.76
1.8		.02	.49	2.60	.52	2.77	3.61
2.0		.01	.27	2.13	.28	2.34	3.42
2.2			.15	1.69	.16	1.93	3.20
2.4			.08	1.30	.09	1.56	2.96
2.6			.04	0.97	.05	1.24	2.72
2.8			.02	.72	.03	0.96	2.47
3.0			.01	.52	.02	.74	2.23
3.2				.37	.01	.56	2.00
3.4				.26		.43	1.78
3.6				.18		.32	1.57
3.8				.12		.24	1.39
4.0				.08		.18	1.22
4.5				.03		.08	0.86
5.0				.01		.04	.60
5.5						.02	.40
6.0						.01	.27
6.5							.18
7.0							.12
7.5							.08
8.0							.05
9							.02
10							.01

Behavior of Young's Modulus of Beta-Brass Single Crystals at Low Temperature

JOHN S. RINEHART*
Department of Physics, State University of Iowa, Iowa City, Iowa
(Received November 29, 1940)

Young's modulus for seven single crystals of beta-brass has been measured at liquid oxygen, and dry ice and acetone temperatures. The reciprocals of the moduli in different directions in the crystal lattice were found to vary linearly with temperature down to −183°C and the anomalous behavior of these quantities, observed at room temperature, persisted.

INTRODUCTION

RECENTLY the author[1] reported measurements made upon the temperature dependence of Young's modulus of beta-brass single crystals above room temperature in a study of the effect of disordering upon this quantity. Incidently, these measurements showed that at temperatures above room temperature (but before disordering is appreciable), Young's modulus behaved differently for different directions in the crystal lattice. The reciprocals of the modulus in the three directions, [111], [110], and [100], varied linearly with temperature, but whether it increased or decreased with rising temperature depended entirely upon the direction in the crystal lattice. Beta-brass is known to be extremely highly anisotropic[1,2] with respect to the value of Young's modulus in different directions of the crystal lattice. The ratio in the two extreme directions, at room temperature, is about 8.2. A plot of this anisotropy against temperature showed it to be increasing fairly rapidly at room temperature. The author felt, perhaps, that at lower temperatures the material might behave in a more normal fashion, i.e., all three $1/E$ *versus* temperature curves might assume a positive (or negative) slope and the material become more isotropic. For these reasons measurements of Young's modulus were made at temperatures below room temperature on the same seven crystals used in the former investigation.[1]

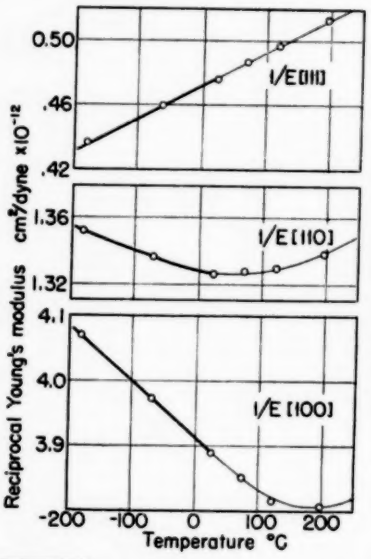

FIG. 1. Reciprocals of Young's modulus in the three principal directions of the crystal lattice *versus* temperature. Heavy part of curves shows region investigated in this study.

MEASUREMENTS AND RESULTS

The only change made in the apparatus and method of measurement from that of the previous investigation was the substitution of a cryostat in place of a furnace for varying the temperature of the crystals. This cryostat consisted of a suitably insulated test tube into which the crystal holder and crystal could be placed and the whole immersed in a bath of the low temperature mixture. Two baths were used, dry ice and acetone, and liquid oxygen. In each case the crystal was left in the low temperature mixture sufficiently long to be reasonably certain that it had reached temperature equilibrium. The temperature of the crystal, when placed in the dry ice and acetone bath, was measured with

TABLE I. *Reciprocal of Young's modulus in principal directions in crystal lattice.*

TEMPERATURE (°C)	−183	−68
$1/E$[111] (cm²/dyne)	0.436×10^{-12}	0.459×10^{-12}
$1/E$[110] (cm²/dyne)	1.352	1.336
$1/E$[100] (cm²/dyne)	4.069	3.968

* Now at Fort Hays Kansas State College, Hays, Kansas.

[1] J. S. Rinehart, Phys. Rev. **58**, 365 (1940).

[2] W. Webb, Phys. Rev. **55**, 297 (1939).

a copper-constantan thermocouple. In the second case, it was assumed that the crystals had acquired the temperature of the liquid oxygen.

The results are given in Table I and are shown graphically in Figs. 1 and 2, in which are plotted the values of $1/E[111]$, $1/E[110]$, $1/E[100]$ $(=s_{11})$, and $E[111]/E[100]$. It is evident from Fig. 1 that the reciprocal of Young's modulus varies linearly with temperature in the three different directions in the crystal lattice down to at least liquid oxygen temperature. There is no evidence whatsoever that the material is becoming more isotropic. On the contrary, $1/E[100]$ continues its anomolous behavior clear up to the end of the region investigated. At -183°C Young's modulus in this direction, i.e., along the cube edge, is about seven percent lower than at room temperature. This means that cooling the material makes it considerably less rigid in this particular direction. In the [111] direction the reciprocal of the modulus acts normally, hence the anisotropic character of the material becomes even more pronounced, as is shown in Fig. 2.

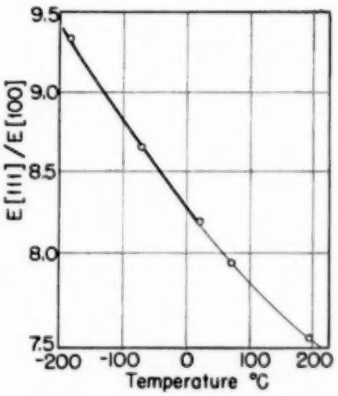

FIG. 2. Anisotropy of Young's modulus in two extreme directions in the crystal lattice *versus* temperature. Heavy part of curve shows region investigated in this study.

In conclusion, the author wishes to thank the Physics Department of the State University of Iowa for the facilities placed at his disposal, and Professor E. P. T. Tyndall for many helpful suggestions.

FEBRUARY 1, 1941 PHYSICAL REVIEW VOLUME 59

On the Theory of Volume Magnetostriction

R. SMOLUCHOWSKI
Palmer Physical Laboratory, Princeton University, Princeton, New Jersey

(Received December 14, 1940)

Volume magnetostriction is considered on the basis of the molecular field theory. Instead of the assumption of a saturation magnetization independent of volume at absolute zero (I_0), made in the original interpretation by Becker and Kornetzki, another procedure is adopted. The dependence of saturation magnetization (I) on temperature for coupled ($j=1$) and uncoupled ($j=\frac{1}{2}$) electrons is assumed to be given by a Brillouin function. With the experimental data on the magnetostriction of iron this method allows us to obtain values for (a) the molecular field "constant" N, (b) its dependence on the relative change of volume, $(1/N)(\partial N/\partial\omega)$, and (c) the dependence on volume of the saturation magnetization at $T=0$, $(1/I_0)(\partial I_0/\partial\omega)$. The value of N and $(1/N)(\partial N/\partial\omega)$ agrees with that obtained from the magneto-caloric measurements. The dependence of I_0 on volume agrees with the value expected from the change of density. Another check on the value of $(1/N)(\partial N/\partial\omega)$ is made by considering the "magnetic" specific heat, a part of which is shown, by thermodynamical considerations, to be proportional to this quantity. All quantitative checks of our theory, including the probable change of the Curie point under pressure are more satisfactory if electrons coupled in pairs ($j=1$) are assumed than if uncoupled ($j=\frac{1}{2}$) electrons are considered.

THERE are two ways to approach the problem of ferromagnetism theoretically. One is based essentially on the classical concepts of elementary magnets and the so-called molecular field. The other uses the methods of the modern theory of solid state and in particular the structure of the electron bands. The latter, however, is largely undeveloped. The molecular field theory even though models not easily connected with the band structure are assumed,

is a useful working hypothesis and as such is widely used.

We shall be concerned here only with volume magnetostriction, i.e., the change of total volume under the influence of the magnetization produced by a magnetic field. Thus the problems related to the reorientation of moments and the influence of internal stresses will be excluded. The discussion of these questions was opened up by the experimental and theoretical investigations of Becker and Kornetzki.[1] These authors based their investigations on the second, and simpler, of the above models and we shall follow them in this respect. They further assumed that the saturation magnetization is volume independent which enabled them to avoid a specification of the exact form of the dependence of magnetization upon temperature $I=I(T)$. In the present note, we shall assume a certain definite Brillouin function for the dependence of the saturation magnetization $I(T)$ on temperature, at constant volume, and study the behavior of other magnitudes such as the field factor and the saturation magnetization at absolute zero. This method seems to yield more satisfactory results and we can check it in various ways by comparing data deduced from specific heat and magnetocaloric measurements. Also other conclusions such as a change of the Curie point are more satisfactory. An interesting result is that a much better agreement with experiment is obtained for "magnetic" electrons coupled in pairs rather than for uncoupled.

I

We assume the elementary magnets to be electrons with a magnetic moment $jg\mu_B$ where μ_B is the Bohr magneton, g is the Landé factor which measures the coupling between orbital and axial moments of the electron in an atom, and j is a quantum number. For electrons coupled in pairs $j=1$, for uncoupled $j=\frac{1}{2}$, and for the classical statistical distribution of magnetic moments in a field $j\to\infty$. Let I and I_0 be the saturation magnetization per unit volume at the temperature T and at absolute zero, respectively. Then the behavior of the system of elementary magnets under consideration is given by the equation:[2]

$$\frac{I}{I_0}=\frac{2j+1}{2j}\coth\frac{2j+1}{2j}a-\frac{1}{2j}\coth\frac{a}{2j}=L_j(a) \quad (1)$$

with "a" equal to

$$\frac{jg\mu_B}{kT}(H_0+NI), \quad (2)$$

where $L_j(x)$ is called a Brillouin (or Langevin, for $j\to\infty$) function and N is a constant independent of temperature and magnetization. Equation (1) expresses the assumption, made by Weiss, that a ferromagnetic substance can be described as if it consisted of elementary magnets influenced by the external field H_0, and the internal field NI, proportional to the magnetization. Since H_0, under the usual experimental conditions, is 10^{-3} to 10^{-4} times smaller than NI it can be omitted. We shall make this assumption frequently. From (1) and (2) it can be deduced that there is no magnetization possible for temperatures higher than

$$\theta=\frac{j+1}{3j}\frac{(jg\mu_B)^2}{k}nN=\frac{j+1}{3j}\frac{I_0N}{k}(jg\mu_B) \quad (3)$$

in which n is the number of elementary magnets per unit volume (thus $I_0=njg\mu_B$). Substituting (3) into (2) and neglecting H_0 we obtain

$$\frac{I}{I_0}=\frac{j+1}{3j}\frac{T}{\theta}a, \quad (4)$$

which, together with (1) gives I/I_0 as a function of T/θ, a relation which is usually compared with experiment. The curve for $j=\frac{1}{2}$, corresponding to uncoupled electrons having magnetic moment either parallel or antiparallel to the field, fits the experimental data on the whole better than any other although for low temperatures the curve for $j=1$ shows a better agreement.[3]

The essential magnitude in this theory is of course the field constant N connected, according to Heisenberg, with the exchange interaction

[1] M. Kornetzki, Zeits. f. Physik **98**, 289 (1936); R. Becker, Zeits. f. Physik **87**, 547 (1934); R. Becker, and W. Döring, *Ferromagnetismus* (J. Springer, Berlin, 1939).

[2] E.g., F. Bitter, *Introduction to Ferromagnetism* (McGraw Hill, 1937); E. C. Stoner, *Magnetism and Matter* (Methuen, 1934).

[3] See, e.g., L. F. Bates, *Modern Magnetism* (Cambridge University Press, 1939).

between the electrons of the atoms in the crystal lattice. It is little known to what extent N is really a constant or even how it depends upon other factors. We want to discuss this problem somewhat more in detail. The exchange forces between the electrons of the atom which we know to be the electrons of the unfilled $3d$ shell depend upon the distance between the atoms. We might thus expect N to be volume dependent, or, since the measurements are done mostly under constant pressure, to be indirectly temperature dependent. In other words we assume the Weiss equation (1) to hold strictly only for $I(T)$ curves corresponding to constant volume. The experimental evidence is difficult to obtain since the relation between I/I_0 and T/θ is independent of N because of the relative character of the coordinates. According to experiments in the case of iron, magnetization decreases with decreasing volume. Therefore if $I_v(T)$ is a curve obtained at constant volume, corresponding to temperature T_0 (for instance, room temperature), and $I_p(T)$ a similar curve obtained at normal pressure we would expect $I_v(T)$ to lie lower than $I_p(T)$ for $T>T_0$ and the opposite for $T<T_0$. Thus we would have, in general, a different saturation magnetization at absolute zero I_0' and a different Curie temperature θ'. The actual measurements[1,4] are not made by keeping the volume constant but rather by measuring the relative change of volume $\delta\omega=\delta V/V$ due to magnetization at constant pressure that is the quantity $\partial\omega/\partial H$, at different temperatures. From this we can calculate the values which one would obtain by performing the measurements at constant volume.

From Eqs. (1) and (2) we have, in general, with H, p and T as independent variables

$$\left(\frac{\partial I}{\partial T}\right)_{pH}=\frac{\partial I_0}{\partial\omega}3\alpha\frac{I}{I_0}+I_0L'\cdot\left[\frac{-\mu}{kT^2}(H_0+NI)+\frac{\mu}{kT}N\left(\frac{\partial I}{\partial T}\right)_p+\frac{\mu 3\alpha}{kT}I\frac{\partial N}{\partial\omega}\right],$$
$$\left(\frac{\partial\omega}{\partial H}\right)_{Tp}=\frac{\partial I_0}{\partial\omega}\kappa\frac{I}{I_0}+I_0L'\cdot\left[\frac{\mu}{kT}N\frac{\partial\omega}{\partial H}+\frac{\kappa\mu}{kT}I\frac{\partial N}{\partial\omega}\right], \tag{5}$$

where $\mu=\mu_B jg$ is the moment of elementary magnet and α and κ are the linear expansion and compressibility coefficients, respectively. L' is the derivative of the function $L(a)$ with respect to a. We have taken into account also the known relation

$$(\partial I/\partial p)_{TH}=-(\partial\omega/\partial H)_{Tp},$$

which can be derived from the thermodynamical considerations.[5] Eliminating now L' and taking into account the relation

$$\left(\frac{\partial I}{\partial T}\right)_v=\left(\frac{\partial I}{\partial T}\right)_p-\frac{3\alpha}{\kappa}\frac{\partial\omega}{\partial H}, \tag{6}$$

we have

$$\frac{1}{N}\frac{\partial N}{\partial\omega}=-\frac{1}{\kappa}\frac{\partial\omega}{\partial H}\frac{1+H/NI}{T(\partial I/\partial T)_v}+\frac{I}{I_0}\frac{\partial I_0}{\partial\omega}\left(\frac{1+H/NI}{T(\partial I/\partial T)_v}-\frac{1}{I}\right) \tag{7}$$

or for $H=0$

$$\frac{1}{N}\frac{\partial N}{\partial\omega}=-\frac{1}{\kappa}\frac{\partial\omega}{\partial H}\frac{1}{T(\partial I/\partial T)_v}-\frac{1}{I_0}\frac{\partial I_0}{\partial\omega}\frac{1}{D(a)} \tag{8}$$

with

$$D(a)=a\frac{L'(a)}{L(a)}=\frac{(\partial I/\partial T)_v}{(\partial I/\partial T)_v-I/T}. \quad \text{(see Eq. (10))}$$

Let us first make the assumption that I_0 is not dependent upon volume, an assumption which we shall show later is not quite justified and let $H=0$. Then (7) reduces to a formula obtained by Kornetzki,[1] which gives the dependence of N upon volume from known experimental values of $\partial\omega/\partial H$ and $(\partial I/\partial T)_p$. The advantage of this procedure is that the function $L(a)$ does not appear in our calculation.

The only measurements suitable for these considerations are those made by Kornetzki on iron. Some other later and perhaps more accurate[4] investigations essentially confirm these results but are less systematic. Unfortunately, too few data useful for our purpose are known in the case of nickel which is otherwise better known and shows fewer irregularities than iron.

[4] J. L. Snoek, Physica **4**, 853 (1937); O. v. Auwers, Physik. Zeits. **34**, 824 (1933); W. Döring, Zeits. f. Physik **103**, 560 (1936)

[5] See, e.g., P. Epstein, *Thermodynamics* (John Wiley and Sons, 1937), p. 350, or R. Becker, reference 1.

TABLE I.

°C	$-\left(\frac{\partial I}{\partial T}\right)_p$	I_p	$\frac{\partial\omega}{\partial H}\times10^{10}$	$3\alpha\times10^5$	$\kappa\times10^{12}$	$-\left(\frac{\partial I}{\partial T}\right)_v$	I/T	$D(a)$
20	0.195	1711.8	6.7	3.21	5.81	0.232	5.842	0.03815
40	0.216	1707.8	7.8	3.31	5.88	0.260	5.456	0.04545
60	0.237	1703.4	8.9	3.41	5.95	0.288	5.115	0.05328
80	0.258	1698.4	10.0	3.50	6.03	0.316	4.811	0.06168
100	0.279	1693.2	11.1	3.60	6.09	0.345	4.539	0.07065

°C	a	$j=\frac{1}{2}$ N	I_0	a	$j=1$ N	I_0
20	2.850	7590	1723.3	4.872	6488	1725.1
40	2.743	7822	1722.0	4.657	6640	1724.4
60	2.646	8049	1720.6	4.462	6786	1723.4
80	2.556	8266	1719.0	4.282	6924	1722.5
100	2.471	8470	1717.5	4.115	7053	1721.8

If we insert the experimental data into Eq. (7) and assume, $(1/I_0)(\partial I_0/\partial\omega)=0$ we obtain for $(1/N)(\partial N/\partial\omega)$ values from 16.9 at 20°C to 14.2 at 100°C (these values are slightly different from those obtained by Kornetzki because of the use of other, more recent, values for α and κ) or for $(1/N)(\partial N/\partial T)$ values from 5.43×10^{-4} at 20°C, to 5.10×10^{-4} at 100°C.

The assumption that I_0 is independent of volume and some of the consequences of these calculations which will be discussed later are not altogether satisfactory. Thus we are led to ask whether the magnitude of N and its dependence upon T, cannot be obtained in another way. Let us go back to Eq. (5). Instead of assuming I_0 constant we shall use the other alternative and make the calculation with a function $L(a)$, that is a certain value of j, and study the change of N and I_0 on volume. In order to do so we rewrite Eq. (5) in the form

$$\left(\frac{\partial I}{\partial T}\right)_p=3\alpha I\left(\frac{1}{I_0}\frac{\partial I_0}{\partial\omega}+I_0L'\frac{\mu}{kT}\frac{\partial N}{\partial\omega}\right)+I_0L'\left[\frac{-\mu}{kT^2}(H+NI)+\frac{\mu}{kT}N\left(\frac{\partial I}{\partial T}\right)_p\right],$$

$$\frac{\partial\omega}{\partial H}=\kappa I\left(\frac{I}{I_0}\frac{\partial I_0}{\partial\omega}+I_0L'\frac{\mu}{kT}\frac{\partial N}{\partial\omega}\right)+I_0L'\left[\frac{\mu}{kT}N\frac{\partial\omega}{\partial H}\right] \quad (9)$$

from which we get after simple transformation

$$\left(\frac{\partial I}{\partial T}\right)_v=I_0L'\frac{\mu}{kT}\left[\left(\frac{\partial I}{\partial T}\right)_v-\frac{H+NI}{T}\right],$$

which for $H=0$ gives

$$D(a)=a\frac{L'(a)}{L(a)}=\frac{(\partial I/\partial T)_v}{(\partial I/\partial T)_v-I/T}. \quad (10)$$

For $j=\frac{1}{2}$ we have $L(a)=\tanh a$ and

$$a\frac{L'(a)}{L(a)}=a\left(\frac{1}{L(a)}-L(a)\right);$$

for $j=1$, $L(a)=(3/2)\coth(3a/2)-\frac{1}{2}\coth\frac{1}{2}a$. In Eq. (10) on the right side we have only known values (see relation (6)) for a certain range of temperatures, on the left side only N is unknown. In this way we can obtain N as a function of temperature, or rather of volume, and also, having assumed a certain j, we can see to what extent I_0, appearing as a constant in Eq. (1), is volume dependent.

Table I gives the results for $j=\frac{1}{2}$ and $j=1$, based on the same experimental data. We see, first of all, that N has a value of about 7000–8000 which is higher than that usually assumed[1,6] on the basis of other measurements in the same range of temperature. It seems to us, however, that, as is explained later, our value probably corresponds to the intrinsic magnetization which is of importance in magnetostriction effects. We see that in both cases N increases with increasing temperature in accord with the experimental fact that the magnetization increases with volume. The magnitude I_0, on the contrary, decreases with increasing volume. Both N and I_0 show smaller changes for $j=1$ than for $j=\frac{1}{2}$. From these values we can obtain the quantities $(1/N)(\partial N/\partial\omega)$ and $(1/N)(\partial N/\partial T)$. Similarly we obtain $(1/I_0)(\partial I_0/\partial\omega)$ and $(1/I_0)(\partial I_0/\partial T)$ either directly[7] from Table II or from the full Eq. (7) where we insert the value of $(1/N)(\partial N/\partial\omega)$

[6] E. C. Stoner, Trans. Roy. Soc. **235**, 165 (1935).

[7] The quantity I_0 has an immediate physical significance only at $T=0$. At higher temperatures it must be derived from measurable quantities by Eq. (1) and it is only in connection with (1) that it is defined. Thus for different forms of (1) different values of I_0 will result. The same holds for the derivatives of I_0.

obtained above. Table II gives the values corresponding to 20°C and 100°C.

These results suggest that the assumption of a constant, volume independent, saturation magnetization at absolute zero is not right. Also without these considerations we can draw a similar conclusion if we write $I_0=(\rho/A)L\tau\mu_B$ where ρ is the density at absolute zero, A is the atomic weight, L is the Loschmidt number, and τ is the average number of electrons responsible for ferromagnetism per atom; for iron this has the value 2.2. A change of volume, of course, changes the density and with the help of the relation $(d\rho/d\omega)=-\rho$ we obtain

$$\frac{1}{I_0}\frac{\partial I_0}{\partial \omega}=-1. \tag{11}$$

We see that both values of Table II are close to the value obtained in (11).

In addition to ρ we may also have τ dependent on volume and influence I_0. The degree to which bands in metals are filled[8] depends upon the relative position of the $4s$ band and the $3d$ band which is responsible for magnetism. Their positions, in turn, depend upon the interatomic distance and one could calculate this dependence if the form of the bands for iron were known. Unfortunately, this is not the case but it can be shown that with reasonable assumptions based on the known electronic structure of copper and nickel a dependence of ρ upon volume is of the right order of magnitude to show up in $(1/I_0)(\partial I_0/\partial\omega)$. This might be the reason that the values in Table II are not closer to -1.

We see also that the relative change of N with volume or temperature in this calculation is more than twice as great as in the case considered by Kornetzki. This relation is of importance for any quantum-mechanical approach to the problem of magnetostriction. It seems, therefore, desirable and interesting to see if the dependence of N upon interatomic distance can be related to other effects and its value checked using other experimental data. One of the important consequences of this dependence appears in the problem of specific heat of ferromagnetic substances, and we shall discuss this subject somewhat in detail.

[8] See, e.g., F. Seitz, *Modern Theory of Solids* (McGraw Hill, 1940); N. F. Mott and H. Jones, *Properties of Metals and Alloys* (Oxford, 1936).

II

Since the application of thermodynamics to the problem of ferromagnetism involves rather delicate steps we shall derive the formula for specific heat and take care to avoid questionable assumptions. Some similar considerations have been carefully discussed by Becker.[1] Let us consider a ferromagnetic metal in a field H_0, first at absolute zero with all elementary magnets parallel, and thus with a maximum magnetization I_0. As compared with a nonferromagnetic material it undergoes a small change of shape because of the attraction between the elementary magnets. The energy $U(T)$ of a gram atom of this metal at higher temperature, say at room temperature, can be expressed as a sum of two terms. The first term $U_1=U_1(T, I_0)$ corresponds to the energy which the metal would have if its magnetization were kept constant, thus with the deformation due to I_0; the second term

$$U_2=\int_{I_0}^{I}\left(\frac{\partial U}{\partial I}\right)_{Tp}dI$$

represents the decrease of energy due to the lower saturation magnetization $I(T)$ at higher temperatures. The outside pressure p is always kept constant. We are allowed to apply this thermodynamical procedure since the range of temperatures, which is of interest to us, is far below the Curie point of iron (1047°K) and our metal is practically one macroscopic domain. Therefore we do not need to trouble about the influence of the individual small domains which, at higher temperatures, are difficult to treat thermodynamically.

TABLE II.[7]

		$\frac{1}{N}\frac{\partial N}{\partial\omega}$	$\frac{1}{N}\left(\frac{\partial N}{\partial T}\right)_p\cdot10^4$	$\frac{1}{I_0}\frac{\partial I_0}{\partial\omega}$	$\frac{1}{I_0}\left(\frac{\partial I_0}{\partial T}\right)_p\cdot10^4$
20°C	$j=\frac{1}{2}$	47.5	15.3	−1.19	−0.38
	$j=1$	36.4	11.7	−0.70	−0.23
100°C	$j=\frac{1}{2}$	33.4	12.0	−1.23	−0.44
	$j=1$	25.6	9.2	0.69	−0.25

The specific heat at constant pressure and constant magnetic field is thus:

$$C_{pH}=\left(\frac{\partial U_1}{\partial T}\right)_{pH}+\left(\frac{\partial U_2}{\partial T}\right)_{pH}+C^{D}_{pH}(T)+\left[\frac{\partial}{\partial T}\int_{I_0}^{I}\left(\frac{\partial U}{\partial I}\right)_{Tp}dI\right]_{pH}. \quad (12)$$

Since the deformation affects the vibration of the atoms in the lattice points very little the first term is practically equal to the Debye specific heat at temperature T. This is based on the following considerations. Let us estimate the force acting on the surface of the magnetized body due to the mutual interaction of the elementary magnets. The surface magnetization is then $4\pi I_0$ and thus the force per unit surface $\sim I_0^2$, which is of the order of 10^6-10^7 dynes per cm^2. For simplicity we can assume now that this is an isotropic pressure since a one-directional force would have an influence of a similar order of magnitude. Thus, using a formula from Grüneisen's theory,[9] we have

$$\left(\frac{\partial C_v}{\partial p}\right)_T=-\left(\frac{\partial C_v}{\partial T}\right)_p\frac{T}{C_p}\left(\frac{\partial V}{\partial T}\right)_p=-\left(\frac{\partial C_v}{\partial T}\right)_p\frac{TV}{C_p}3\alpha_l, \quad (13)$$

where V is atomic volume and α_l the linear expansion coefficient. From this we can see that neither C_v nor (C_p-C_v) changes enough, under the influence of the magnetization I_0, to be taken into account since it is several orders of magnitude too small. In order to evaluate the second term of formula (12) we must derive an expression for $(\partial U/\partial I)_{T,p}$. From the six magnitudes U, H, V, p, T, and I, we choose the last three as independent variables and proceed by generalizing Becker's considerations. The work done by changing the magnetization is

$$\delta A=HV\cdot\delta I-p\cdot\delta V$$

and

$$\delta U=\left(\frac{\partial U}{\partial I}\right)_{Tp}\delta I+\left(\frac{\partial U}{\partial T}\right)_{Ip}\delta T+\left(\frac{\partial U}{\partial p}\right)_{IT}\delta p;$$

thus the potential energy HI is not included in U. The expression

$$\frac{\delta Q}{T}=\frac{1}{T}\left[\left(\frac{\partial U}{\partial I}\right)-HV+p\left(\frac{\partial V}{\partial I}\right)\right]\delta I+\frac{1}{T}\left[\left(\frac{\partial U}{\partial p}\right)+p\left(\frac{\partial V}{\partial p}\right)\right]\delta p+\frac{1}{T}\left[\left(\frac{\partial U}{\partial T}\right)+p\left(\frac{\partial V}{\partial T}\right)\right]\delta T$$

must be a perfect differential and thus we have a series of relations between the derivatives of the expressions in brackets (factors before δI, δp, δT). One of them gives

$$\left(\frac{\partial \bar{U}}{\partial I}\right)_{Tp}=H-T\left(\frac{\partial H}{\partial T}\right)_{Ip}-TH\left(\frac{\partial \omega}{\partial T}\right)_{Ip}-p\left(\frac{\partial \omega}{\partial I}\right)_{Tp}, \quad (14)$$

where $\bar{U}$ is energy per unit volume and $\partial\omega=\partial V/V$ is, correspondingly, the relative change of volume.

The only other relation which we need to take into account is the expression

$$I=f[(H+NI)/T],$$

which is a generalization of Eq. (1) since we do not specify the actual form of the function f. This relation plays the role of an equation of state. From it we have $H+NI=T\varphi(I)$ where, again, φ is a certain function. Keeping in mind the fact that N, as we assumed, is only volume dependent we have

$$\left(\frac{\partial H}{\partial T}\right)_{Ip}=\varphi(I)-I\frac{dN}{d\omega}\left(\frac{\partial \omega}{\partial T}\right)_{Ip}=\frac{H+NI}{T}-I\frac{dN}{d\omega}\left(\frac{\partial \omega}{\partial T}\right)_{Ip}, \quad (15)$$

which we can insert into (14). We obtain thus

TABLE III. *Specific heats,* $\bar{C}_p$.

T	$\frac{1}{I}\left(\frac{\partial I}{\partial T}\right)_p\cdot10^4$	$\bar{C}_p(\frac{1}{2})$	$\bar{C}_p(1)$	$\bar{C}_p'$	$\bar{C}_{p(\text{exp.})}$
20°C	−1.11	0.59	0.46	0.38	0.53
100°C	−1.65	0.89	0.71	0.62	0.74

[9] E. Grüneisen, *Handbuch der Physik*, Vol. X (1926).

the important relation

$$(\partial\bar{U}/\partial I)_{Tp}=-NI+T(\partial p/\partial I)_{VT}(\partial\omega/\partial T)_{Ip} - p(\partial\omega/\partial I)_{Tp}, \quad (16)$$

which we can use to evaluate the second term in Eq. (12). Remembering that the upper limit of the integral is a function of T we have

$$\left(\frac{\partial\bar{U}_2}{\partial T}\right)_{pH}=-\tfrac{1}{2}I^2\frac{dN}{d\omega}\left(\frac{\partial\omega}{\partial T}\right)_{pH}-NI\left(\frac{\partial I}{\partial T}\right)_{pH} +\tfrac{1}{2}I_0^2\frac{dN}{d\omega}\left(\frac{\partial\omega_0}{\partial T}\right)_{pH}+K(I,T,V), \quad (17)$$

where $(\partial\omega_0/\partial T)_{pH}$ denotes the thermal expansion coefficient measured at a constant magnetization I_0. We have made use of the relation

$$(\partial p/\partial I)_{VT}=-H-V(\partial H/\partial V)_{IT}, \quad (18)$$

which can be deduced easily by the same procedure which leads to formula (14) except that, one must treat I, V, T as independent variables.

It can be shown that outside of the first three terms in (17) all others, included in $K(I, T, V)$, are several orders of magnitude too small to play any role in view of the experimental errors. For the same reasons $(\partial\omega/\partial T)_{pH}$ can be put equal to $(\partial\omega_0/\partial T)_{pH}$. We arrive, therefore, at the conclusion that the specific heat (in calories per gram atom) of a ferromagnetic substance at temperature T can be written as a sum

$$C_p=C_{pH}^D(T)+\bar{C}_p, \quad (19)$$

where $C_{pH}^D(T)$ is the corresponding Debye specific heat and

$$\bar{C}_p=-\frac{A}{\rho}\frac{NI^2}{J}\left[\frac{1}{I}\left(\frac{\partial I}{\partial T}\right)_{pH} -\frac{1}{2}\frac{1}{N}\left(\frac{\partial N}{\partial T}\right)_{pH}\left(\frac{I_0^2}{I^2}-1\right)\right], \quad (20)$$

where

$$\left(\frac{\partial N}{\partial T}\right)_{pH}=\frac{dN}{d\omega}\left(\frac{\partial\omega}{\partial T}\right)_{pH}.$$

Here A is the atomic weight, ρ is the density, and $J=4.185\times10^7$ cal./erg is the mechanical heat equivalent. The first term of (20) gives the usual "magnetic" contribution to the specific heat

$$\bar{C}_p'=-\frac{A}{\rho}\frac{NI}{J}\left(\frac{\partial I}{\partial T}\right)_{pH} \quad (21)$$

frequently studied at the Curie point, and the second is the additional term due to the volume dependent N. We want now to compare both formulas (20) and (21) with experiment and see if our method of interpreting magnetostriction data and the resulting dependence of N upon volume is compatible with the specific heat measurements.

On the basis of data given in Tables I and II we can compute $\bar{C}_p$ for 20°C and 100°C in case of $j=\frac{1}{2}$ and $j=1$. Table III gives the results in calories per gram atom, where $\bar{C}_p(\frac{1}{2})$ and $\bar{C}_p(1)$ correspond to the cases $j=\frac{1}{2}$ and $j=1$ and where $\bar{C}_p'$ is obtained from the formula (21).

In order to compute $C_{pH}^D(T)$ in (12) we must know the characteristic temperature θ_D for iron. For a ferromagnetic it can be obtained by extrapolation from neighboring nonferromagnetic elements or from the results of measurements at low temperatures where other contributions are small. In the empirical formula of Lindemann.[10]

$$\theta_D=c(T_M/AV^{\frac{1}{3}})^{\frac{1}{2}},$$

where T_M is the melting point, A is the atomic weight, and V is the atomic volume (per gram atom), c is a constant which varies slowly in the periodic system. For chromium it has the value 142, for copper 131; if we assume for iron $c=136$ then we obtain $\theta_D=400$. On the other hand measurements of Duyckaerts[11] and of Keesom and Kurrelmeyer[12] indicate that θ_D at very low temperatures is equal to about 460, which is close to the value deduced from elastic constants, and equal to 430 at temperatures above 50°K. We put thus $\theta_D=460$. Using Debye's table or curve one obtains for C_v, the specific heat of lattice vibrations at constant volume, 5.30 at 20°C and 5.54 cal./degree×gram atom at 100°C. From the known relation $C_p-C_v=TV(3\alpha_l)^2/\kappa$ we obtain for the corrections for lattice dilatation the quantities 0.09 and 0.14, respectively. The anharmonicity of the vibrations does not play any role at these temperatures. We have, thus,

[10] Cf. reference 8.
[11] G. Duyckaerts, Physica **6**, 401 (1939).
[12] W. H. Keesom and B. Kurrelmeyer, Physica **6**, 633 (1939).

for the total lattice energy contribution 5.39 and 5.68 at 20°C and 100°C, respectively. Unfortunately, no measurements of the specific heat of iron in a field of about 2000 gauss or more are known, so we must compare our data with results obtained at $H=0$.

Experimental data on specific heat of iron were, until recently, very scattered. The new results, however, of Sykes,[13] Baerlecken,[14] and Awbery and Griffith[15] are consistent to a high degree of accuracy. Interpolating their results we obtain for C_p the values 5.92 and 6.42 at 20°C and 100°C, respectively. This gives us for $\bar{C}_p$(exp.) the values 0.53 and 0.74 which are tabulated in the last column in Table III. In comparing these figures with our theoretical values we see that they agree well with $\bar{C}_p(1)$. The scattering of experimental values of C_p makes an error of about ± 0.05 possible. We see that $\bar{C}_p'$ in which the dependence of N on volume was not taken into account is about 30 percent too low to explain the observed specific heat. A correction calculated from magnetostriction data for $j=1$ fits the expected values best; those for $j=\frac{1}{2}$ are too high. A similar calculation with Kornetzki's data is not possible since to his value of $(1/N)(\partial N/\partial T)$ no value of N is uniquely associated. However his $(1/N)(\partial N/\partial T)$, as we saw, is smaller by more than a factor of two and one might expect, correspondingly, the differences $(\bar{C}_p-\bar{C}_p')$ to be smaller by the same factor. There does not seem to be justification for drawing far-reaching conclusions from the fact that $\bar{C}_p$(exp.) agrees rather with $\bar{C}_p(1)$ and not with $\bar{C}_p(\frac{1}{2})$ in Table III. However, we shall see that there are a few other similar instances where a quantitative check of our theoretical results is better for $j=1$ than for $j=\frac{1}{2}$ and we postpone some general remarks until later.

The main result is the fact that the model, the assumptions underlying our study of magnetostriction, and the resulting dependence of N on volume are in accord with a similar approach to the problem of specific heat, and make the agreement with experiment better in both cases.

[13] C. Sykes and H. Evans, J. Iron and Steel Inst. **138**, 1258 (1938).
[14] H. Baerlecken, Dissertation, Aachen (1933).
[15] J. H. Awbery and E. Griffiths, Proc. Roy. Soc. **174**, 1 (1940).

III

We want to mention now a few other interesting points in connection with our calculations. As it is well known an adiabatic change of the magnetic field changes the temperature of a ferromagnetic substance. This magnetocaloric effect can also be used to determine the molecular field constant N for various temperatures. However the effect can well be measured only at temperatures not far from the Curie point and therefore experimental data obtained by Potter[16] cover only the range of temperatures 720° to 840°C in the case of iron. Up to the Curie point θ, N increases gradually; between θ and $\theta+60°$ it more than doubles its value and then remains rather constant. From these data one obtains, for $T<\theta$ for the relative change of N with volume[17] $(1/N)(\partial N/\partial\omega)=19$ for a single crystal and about 30 for electrolytic (polycrystalline?) iron. We see that these values are in a good agreement with our results in Table II, obtained for temperatures more than 600 degrees lower.

On the other hand the absolute values of N are in our case, as mentioned before, larger than those obtained from magnetocaloric or other measurements below θ and correspond rather to those deduced from measurements above θ. Stoner[6] has pointed out that only the latter represent the true intrinsic field since the values obtained from the magnetocaloric effect below θ are too small because of the domain size effect and the difference between the apparent and intrinsic magnetization. It seems thus that values of N deduced from magnetostriction experiments below the Curie point represent the conditions within regions of uniform saturation better than those obtained from other data for the same temperatures.

Further, on the basis of values tabulated in Table I we can see the extent to which the experimental data are represented by a curve defined by Eq. (1). We have assumed that with constant I_0 and N the curve represents the dependence of magnetization on temperature at constant volume only. Let us consider the range

[16] H. H. Potter, Proc. Roy. Soc. **146**, 362 (1934).
[17] See J. B. Austin and R. H. H. Pierce, Jr., Physics **4**, 409 (1933). Linear expansion coefficient at these temperatures is about 1.6×10^{-5}.

of temperatures 293 to 373°K (20° to 100°C) for which the experimental data are known. We calculate the magnetization which iron would have at 373°K if it were kept at the volume corresponding to 293°K. One gets $\Delta I=(\partial\omega/\partial H)(3\alpha/\kappa)\Delta T\leqq 5$ and thus $I_{v_{373}}=I_{v_{293}}-5=1688.2$ which together with the known I_0 corresponding to volume at 293°K for $j=\frac{1}{2}$, ($I_0=1723.3$) gives us $a=2.288$ and $T=360$°K, or $a=3.87$ and $T=365$°K for $j=1$, ($I_0=1725.1$). In case of good agreement with the theory we should get 373°K. We see that the curve for $j=1$ fits the experimental results at constant volume better than the curve for $j=\frac{1}{2}$, and of course much better than it fits the constant pressure measurements. A certain discrepancy, however, still exists.

Another interesting problem is the change of the Curie temperature with the change of volume. So far no direct measurements have been made. Kornetzki, however, extrapolating his measurements, calculated the Curie point at the volume corresponding to room temperature. He obtains $\theta_v'=668$°K (395°C) which compared with the constant pressure Curie point at $\theta_p'=1047$°K (774°C) would give an improbably large shift of about 380 degrees. On the basis of the formula (3) we can calculate the Curie point assuming the validity of this formula and of other assumptions underlying this theory—in particular of the constancy of I_0 and N throughout the whole range of temperatures at constant volume. We obtain, for $j=\frac{1}{2}$, $\theta_v''=903$°K (630°C) or, for $j=1$, $\theta_v''=1030$°K (757°C). Both values are higher than θ_v' and correspond to a shift of 144 and 17 degrees, respectively. It would be very interesting to make an experimental check of these results since they lie so far apart that even at lower temperatures a definite indication might be obtained.

We have made a survey of the consequences of considering magnetostriction of iron on the basis of the molecular field theory. It indicates that certain conclusions which can be drawn from the dependence of N upon volume are plausible and agree with experiments in those cases where a comparison is possible. The very great sensitivity of N upon interatomic distance seems to be pretty well established. With respect to the rather better agreement in general of the numerical values for $j=1$ than for $j=\frac{1}{2}$, which has been mentioned frequently, it should be stressed that this fact can be understood and expected. In a ferromagnetic we have ions with none, one, two, etc., holes in the *3d* shell depending upon the particular structure of the electron levels in a given metal. Not all atoms have the same number of holes, but one might expect most of them to have a number which is close to the number of Bohr magnetons per atom. In the case of iron, as mentioned before, there are 2.2 holes per atom. Thus the value $j=1$, which corresponds to two coupled electrons and which seems to give a better fitting with experiment, indicates that the two holes are coupled and are parallel giving a resultant magnetic moment.

One must not forget, however, that the experimental data are extremely scarce and that iron shows many irregularities and is much more difficult to discuss theoretically than is, for instance, nickel. Unfortunately, all we know about nickel from this point of view is that at room temperature $\partial\omega/\partial H$ is about 1×10^{-10} and thus much smaller than for iron. Applying formula (7) and assuming I_0 constant one obtains $(1/N)(\partial N/\partial\omega)\sim 3$ and one can estimate the correction of the magnetic specific heat due to this term. The result is a change of about 10 percent, which is within the limits of error for this region of temperature, as discussed in detail by Stoner. Thus, until more systematic data for nickel are available, no conclusions can be drawn in this case.

From the present development of the study of electron bands in ferromagnetics we know that the problem of specific heat and of exchange interaction is a complicated one and it is rather surprising that the simple model of elementary magnets and molecular field works as well as it apparently does. A discussion of the more modern methods of approach, however, is beyond the program of this paper.

The author wishes to express his sincerest thanks to Professor E. Wigner for his advice and helpful criticism during the course of this work.

Note on the Radiation Properties of Heavy Nuclei

V. F. WEISSKOPF
University of Rochester, Rochester, New York

(Received December 23, 1940)

THERE is so far no way to calculate radiative transition probabilities between nuclear levels of heavy nuclei. We here propose a way of estimating the order of magnitude of these processes. In spite of its crude and over-simplified assumptions, it represents the experimental facts known so far.

We assume that the absorption probability of a nucleus in its ground state, averaged over an energy interval which contains a great number of excited levels, is proportional to the intensity at the nucleus of the spherical harmonic component of the light wave which is absorbed. This assumption is supposed to be valid for light wave-lengths for which $\lambda\!\!\!^{-}=\lambda(2\pi)$ is large compared to the nuclear radius.[1] It is equivalent to the statement that the absorption probability, if averaged over the level resonances, depends on the light intensity alone and not on the frequency, as long as the wave-length is large enough. (The corresponding assumption for the absorption of neutrons leads to the so-called "$1/v$-law" for slow neutrons.) In case of a 2^l-pole transition the light quantum absorbed is represented by the $(l-1)$st spherical harmonic. We therefore would obtain for the absorption cross section into an energy region of the nucleus, E Mev above the ground state:

$$\sigma^{(l)}=C\cdot E^{2l-1}. \tag{1}$$

The constant C must be determined experimentally and is found to be roughly equal for all elements.* We further assume that most of the occurring nuclear transitions are quadrupole transitions. From the investigation of the γ-spectra of radioactive nuclei it is known that dipole and quadrupole transitions are about equally probable among lowest levels. It then follows from (1) that quadrupole radiation is dominant for higher frequencies.

The average 2^l-pole emission probability $\bar{\Gamma}^{(l)}$ from a state with an excitation energy E can be derived from the cross section $\sigma^{(l)}(E)$ of the reverse process: ($\bar{\Gamma}^{(l)}$ is measured in energy units after multiplication with h)

$$\bar{\Gamma}^{(l)}=\frac{g}{2\pi^2\,\lambda\!\!\!^{-2}\omega(E)}\,\sigma^{(l)}(E). \tag{2}$$

Here g is the statistical weight of the ground state and $\omega(E)$ the level density of the combining levels with an excitation energy E (an n times degenerated level is considered as n levels) and $\lambda\!\!\!^{-}$ the wave-length of the emitted light (times $1/(2\pi)$).

There are three independent groups of experiments which all agree to the formulas derived. Bothe and Gentner[2] have made measurements of absorption cross sections of photo-effects on 9 identified heavy nuclei ($A>60$) with γ-rays from proton bombarded lithium and boron. The former gives a γ-ray of 17 Mev, the latter mainly two rays of 16.6 and 11.8 Mev in the intensity ratio 1 : 7. According to (1) the ratio of the cross sections for the two radiations ought to be $\sigma_{\mathrm{Li}}{}^{(2)}/\sigma_{\mathrm{B}}{}^{(2)}=2.12$. (For dipole radiation this ratio would be 1.18.) The actual ratios lie between 1.5 and 2.7 with one exception (Ga^{70}) which has the ratio 1.1. The average ratio is 2.3. The constant C is of the same order of magnitude for all elements investigated. The average value is $C=0.65\times10^{-29}$ cm^2/(Mev)^3 and all values are found between 0.23 and 1.0×10^{-29}.

The second group are the photo-fission experiments by the Pittsburgh group.[3] Here U and Th were irradiated by a γ-radiation of 6.3 Mev produced by proton bombardment of fluorine. Fission was observed and the cross section for its production was found to be $3.6\pm1.0\times10^{-27}$ cm^2

[1] This assumption has been put forward by Weisskopf and Ewing, Phys. Rev. **57**, 472 (1940). In the present note it is worked out in more detail and applied to more recent experiments.

* Here and in the following considerations electric multipole radiation only is taken into account. Magnetic multipole radiation can be neglected except in special transitions where the electric transition is forbidden by selection rules (e.g., in isomeric transitions).

[2] W. Bothe and W. Gentner, Zeits. f. Physik **112**, 45 (1939).

[3] Haxby, Shoupp, Stephens and Wells, Phys. Rev. **57**, 1088 and **58**, 199 (1940); **59**, 57 (1941).

for U and $1.7\pm0.5\times10^{-27}$ cm² for Th.[4] Since the γ-ray energy is near to the binding energy of the neutron, (Wheeler[5] calculated the latter and found 6.1 Mev for U and 6.2 Mev for Th), the excitation of the nucleus would lead in most cases to fission rather than to neutron expulsion. The fission cross section should therefore be equal or slightly smaller than the absorption cross section. The above value of C would give $\sigma^{(2)}(6.3\text{ Mev})=1.6\times10^{-27}$ cm² which is as close to the observed values as one might expect. If dipole radiation were assumed, we would find a cross section of 1.2×10^{-26} cm² from Bothe and Gentner's result and formula (1).

Finally, actual life times of nuclear levels have been measured in radioactive nuclei as quoted by Bethe[6] and recently also in stable nuclei as for In^{115} and Pb by Waldman and Collins[7] and Guth.[8] They have been found to be all of the order of 10^{-12} sec. which corresponds to a transition probability to lower levels $\Gamma\sim10^{-3}$ ev. The radiation emitted is of the order of 1 Mev in all cases observed. (The values of Γ in five elements investigated lie between 0.6 and 2 millivolts, the excitation energy between 0.61 and 1.8 Mev.) Formula (2) gives an average value of the transition probability from an excited state to the ground state and should be used only for higher excitations with close lying levels. If we still try to apply it for low levels we get $\bar{\Gamma}^{(2)}=0.8\times10^{-3}$ ev by putting $\omega(E)=1(\text{Mev})^{-1}$. The latter value for the level density is of the order of the expected average distance of lowest levels combining with the ground state.

The following consideration indicates that the experimental value of C in (1) is within the theoretical expectations. The average value of the quadrupole moment

$$Q=\sum_i\int r_i^2\psi_0^*\psi_E d\tau$$

of the transition[9] from the ground state ψ_0 to a state with the energy E can be calculated from the cross section $\sigma(E)$ by means of the formula:

$$|Q|^2=\frac{15}{8\pi^3}\frac{C^3\hbar^3}{E^3}\frac{\sigma^{(2)}(E)}{e^2\omega(E)}.$$

Here the ground state is assumed to be non-degenerate. The following relation must hold:

$$\int_0^\infty|Q|^2\omega(E)dE=\rho^4,$$

where ρ^4 is the average value of $(\sum_i r_i^2)^2$ in the ground state. We expect formula (1) to be valid until $\lambda\sim$radius of the nucleus, that is for $E<40$ Mev. If we assume $\sigma(E)$ falling off above that energy, we obtain

$$\rho^4\sim\frac{15}{8\pi^3}\int_0^{40\text{ Mev}}\frac{C^3\hbar^3}{e^2}CdE\sim10^{-48}\text{ cm}^4,$$

which is of the expected order of magnitude.

[4] A rough estimate of the order of magnitude expected by the theory has been given by Bohr and Wheeler (N. Bohr and J. A. Wheeler, Phys. Rev. **56**, 426 (1939)) but without taking into account the frequency dependence of the nuclear photo-effect.

[5] J. A. Wheeler, personal communication.

[6] H. A. Bethe, Rev. Mod. Phys. **9**, 229 (1937).

[7] Waldman and Collins, Phys. Rev., in print.

[8] E. Guth, Phys. Rev., in print.

[9] The summation is taken over all protons.

Letters to the Editor

PROMPT publication of brief reports of important discoveries in physics may be secured by addressing them to this department. Closing dates for this department are, for the first issue of the month, the eighteenth of the preceding month, for the second issue, the third of the month. Because of the late closing dates for the section no proof can be shown to authors. The Board of Editors does not hold itself responsible for the opinions expressed by the correspondents.

Communications should not in general exceed 600 words in length.

Relative Abundances of the Oxygen Isotopes

BYRON F. MURPHEY
Department of Physics, University of Minnesota, Minneapolis, Minnesota
January 18, 1941

ASTON[1] gave the abundance ratios $O^{16}/O^{18}=536$ and $O^{18}/O^{17}=4.2$. Mecke and Childs[2] give for atmospheric oxygen $O^{16}:O^{18}:O^{17}=630\pm20:1:0.2$. Smythe[3] has measured $O^{16}/O^{18}=503\pm10$. A little later Bleakney and Hipple[4] reported values for this ratio clustering around 500 in over a hundred analyzed samples, but gave no estimate of error.

A new determination of the O^{18}/O^{17} ratio has been made, with the 60° mass spectrometer of Nier[5] to separate the singly ionized molecular oxygen ions of masses 32, 33 and 34. Though the present work is to fix more closely the O^{18}/O^{17} ratio which has generally been taken as 5, a check was also made on the value of O^{16}/O^{18}. Commercial oxygen from two different tanks was analyzed several times, ten readings being taken for each analysis. Air samples also were analyzed. As a test for discrimination in the mass spectrometer, runs were made under a wide variety of conditions and at different times. At no time did the O^{16}/O^{18} ratio as computed from the relative heights of the mass 32 and 34 peaks differ by more than 3 percent from 500.

It thus appears that the apparatus does not discriminate appreciably, and that the samples analyzed are representative of the samples analyzed by Smythe and Bleakney and Hipple. In each of ten separate measurements of the O^{18}/O^{17} ratio, a complete mass spectrum of the 33 peak and its adjacent valleys has been taken in order to obtain an accurate determination of the background. From the ratio of the deflections corrected for background, the average value of O^{18}/O^{17} is 4.9 ± 0.2.

From the values $O^{16}/O^{18}=500\pm15$ and $O^{18}/O^{17}=4.9\pm0.2$, one is able to calculate the physical-to-chemical mass scale conversion factor to be 1.000275 ± 0.000009. By far the larger part of this uncertainty is due to the possible error in the ratio O^{16}/O^{18}.

My thanks are due to Dr. A. O. Nier for his suggestion of the problem and for aid in working it out.

[1] F. W. Aston, Nature **130**, 21 (1932).
[2] R. Mecke and W. H. J. Childs, Zeits. f. Physik **68**, 362 (1931).
[3] W. R. Smythe, Phys. Rev. **45**, 299 (1934).
[4] W. Bleakney and J. A. Hipple, Phys. Rev. **47**, 800 (1935).
[5] A. O. Nier, Rev. Sci. Inst. **11**, 212 (1940).

Radioactive Isotopes of Germanium

G. T. SEABORG, J. J. LIVINGOOD AND G. FRIEDLANDER
Department of Chemistry, Radiation Laboratory, Department of Physics, University of California, Berkeley, California
January 13, 1941

WE have studied the radioactive isotopes of germanium produced by deuteron and neutron bombardment of germanium, fast neutron bombardment of arsenic and selenium, and deuteron bombardment of gallium. We were able to make isotopic assignments for four germanium periods and to establish the existence of a pair of isomers in Ge^{71}.

Ge^{71}: 40±2 hours and 11 days.—Sagane[1] has reported a 26-hour and a 6-day period from both slow and fast neutron bombardment of germanium; without chemical separation he assigned the positron active 26-hour activity to Ge^{71} and suggested that the 6-day period may be due to a gallium isotope. In an alpha-particle bombardment of zinc, Mann[2] obtained chemically identified germanium isotopes with half-lives of 37 hours and 195 days and an intermediate period whose half-life, although not given by Mann, turns out, from his curves, to be 11 days. These three periods have to be distributed between Ge^{67}, Ge^{69}, and Ge^{71}.

Bombarding gallium with 8-Mev deuterons we found in the germanium fraction a 40±2-hour positron-emitter and an 11-day activity. These are almost certainly due to Ge^{69} or Ge^{71}, produced by the d, $2n$ reaction from the only stable gallium isotopes, Ga^{69} and Ga^{71} (d, n reactions would lead to stable germanium isotopes). But since the bombardment of germanium with 16-Mev deuterons also produced a 40±2-hour and an 11-day germanium period, both periods must be assigned to Ge^{71}, formed by the d, p reaction from Ge^{70}. Absorption measurements show that the positrons of the 40-hour activity have an energy of 1.2 Mev, which agrees with Sagane's 1.15 Mev for his 26-hour period.[3] The 11-day activity emits particles of about 0.6-Mev energy, and no gamma-rays. The absence of annihilation radiation indicates that very few, if any, positrons are emitted; the particles may be conversion electrons following K-electron capture.

Ge^{75}: 89±2 minutes.—In slow neutron bombardments of germanium Amaldi *et al.*[4] obtained a 30-minute period, while Sugden[5] reported a 2-hour activity. Pool, Cork, and Thornton[6] found a 1.3-hour activity in fast neutron bombardment of germanium. Sagane[1] found a negative beta-emitter of 81 minutes half-life in slow and fast neutron and in deuteron bombardments of germanium and assigned it to Ge^{75}. No chemical analyses were reported in any of the experiments quoted. We found that 16-Mev deuteron bombardment of germanium produced a 90-minute period in the germanium fraction. To fix the assignment we bombarded arsenic with fast neutrons. The germanium fraction decayed with a period of 89±2 minutes over about 10 half-lives. This activity must be formed from the only stable arsenic isotope, As^{75}, by the n, p reaction, and must therefore be due to Ge^{75}. We also found the same period (about 90 minutes) in the germanium fractions of fast neutron bombardments of germanium and selenium, where Ge^{75} can be formed by the reactions $Ge^{76}(n, 2n)Ge^{75}$

and $Se^{78}(n, \alpha)Ge^{75}$, respectively. Absorption measurements show the maximum energy of the beta-particles from the 89-minute activity to be 1.2±0.1 Mev, in agreement with Sagane's value of 1.1 Mev for his 81-minute period.[3] Gamma-rays are present but their intensity relative to the beta-particles is rather low.

Ge^{77}: 12 hours.—Sagane[1] reported a negative beta-emitter of 8 hours' half-life from slow neutron and deuteron bombardments of germanium and assigned it to Ge^{77}, because fast neutrons had produced very little of this activity. Our experiments confirm this assignment but show the half-life to be about 12 hours. This period, chemically identified as due to germanium, was produced by the *d, p* reaction in the bombardment of germanium with 16-Mev deuterons and by the *n, α* reaction in the fast neutron bombardment of selenium. These results, combined with the fact that the 12-hour period did not appear in fast neutron bombardments of either germanium or arsenic, make its assignment to Ge^{77} certain. The growth of As^{77} (90 days)[7] from this activity has not yet been investigated.

Ge^{69}.—In addition to the periods discussed, Sagane[1] reported a positron-emitting 29-minute activity which he obtained from fast neutrons on germanium only and therefore assigned to Ge^{69}. We failed to observe this period from the reactions $Ge^{70}(n, 2n)Ge^{69}$ and $Ga^{69}(d, 2n)Ge^{69}$ and Mann[2] did not find it from the reaction $Zn^{66}(\alpha, n)Ge^{69}$. These facts lead us to reject Sagane's assignment. The 195-day period reported by Mann[2] may be due to Ge^{69}.

It is a pleasure to thank the Rockefeller Foundation and the Research Corporation, whose financial support made this work possible.

[1] R. Sagane, Phys. Rev. **55**, 31 (1939); Phys. Rev. **53**, 212 (1938).
[2] W. B. Mann, Phys. Rev. **54**, 649 (1938); Phys. Rev. **53**, 212 (1938).
[3] Sagane, Kojima and Miyamoto, Proc. Phys.-Math. Soc. Japan **21**, 728 (1939).
[4] Amaldi, D'Agostino, Fermi, Pontecorvo, Rasetti and Segrè, Proc. Roy. Soc. **A149**, 522 (1935).
[5] S. Sugden, Nature **135**, 469 (1935).
[6] Pool, Cork, and Thornton, Phys. Rev. **52**, 239 (1937).
[7] Sagane, Kojima, Miyamoto and Ikawa, Proc. Phys.-Math. Soc. Japan **21**, 660 (1939).

Radioactive Isotope of Protoactinium

G. T. Seaborg, J. W. Gofman and J. W. Kennedy
Department of Chemistry, Radiation Laboratory, Department of Physics, University of California, Berkeley, California
January 15, 1941

HAHN and Strassmann[1] have recently pointed out that the radioactivity of 25 days half-life assigned[2] to $_{91}Pa^{233}$, originally reported by Meitner, Strassmann and Hahn[2] to be the daughter of the 26-minute $_{90}Th^{233}$ produced by neutron capture in thorium, might actually be due to an isotope of zirconium. There is a 26-day zirconium[1] formed in the fission of uranium by neutrons, and hence probably also in the fission of thorium by neutrons. Since Meitner, Strassmann and Hahn[2] used zirconium as the carrier material for their radioactive substance, the question arises as to whether their 25-day radioactivity from thorium plus neutrons might be due to an isotope of zirconium rather than protoactinium.

We have investigated this point and our experiments definitely show that, in agreement with the original conclusions of Meitner, Strassmann and Hahn,[2] slow neutron bombardment of thorium produces a protoactinium of approximately 25 days half-life.[3] About 10 g of thorium nitrate, encased in a large paraffin block, was exposed for an hour to the neutrons produced during the bombardment of phosphorus with 100 microamperes of deuterons in the 60-inch cyclotron. The thorium was dissolved and precipitated from acid solution as the iodate, after the addition of appropriate carriers for the fission products, and then, after redissolving the thorium iodate in concentrated hydrochloric acid, successive precipitations of zirconium phosphate were performed. This showed that a 25-day period was growing from a parent of approximately 26 minutes half-life, presumably $_{90}Th^{233}$. The cross section for the production of the 25-day activity was very much greater than that of any of the fission products (e.g., antimony, tellurium, iodine, etc.). The absence in the zirconium phosphate fractions of the 17-hour zirconium, known[4] to be produced in the fission of uranium by neutrons, suggests that the amount of radioactive zirconium formed from fission in this experiment was negligible.

Final proof that the 25-day activity is an isotope of protoactinium, and not of zirconium, was obtained by separating protoactinium and zirconium by fractional crystallization[5] of zirconium oxychloride from hydrochloric acid solution. A sample of greater intensity was prepared, zirconium carrier was added and the sample was purified carefully and converted to zirconium oxychloride. The fractional crystallizations showed that the specific activities (activity per milligram ZrO_2) of the first fractions were of the order of 5 percent of the specific activity of the over-all sample, showing an accumulation of the activity in the mother liquor as should be the case for protoactinium. A sample of 17-hour zirconium was prepared (from uranium plus neutrons) and subjected to a similar series of fractional crystallizations; in this case the specific activities of all the fractions were the same as that of the over-all sample, as was to be expected.

Absorption measurements show the presence of a gamma-ray, and an upper limit for the beta-rays of about 0.4 Mev.

A search for $_{92}U^{233}$ activity from the decay of $_{91}Pa^{233}$ was made by chemically separating uranium. This uranium fraction was inactive with respect to beta-particle emission. The question of alpha-radioactivity is being investigated. $_{90}Th^{233}$ and $_{91}Pa^{233}$ are members of the $4n+1$ series of radioactive elements (the series which is missing among the natural radioactivities).

It is a pleasure to thank Professor Ernest O. Lawrence for his continued interest. We wish to express our gratitude to the Rockefeller Foundation and the Research Corporation, whose financial support made this work possible.

[1] O. Hahn and F. Strassmann, Naturwiss. **28**, 543 (1940).
[2] L. Meitner, F. Strassmann, and O. Hahn, Zeits. f. Physik **109**, 538 (1938).
[3] The same result has been obtained by A. V. Grosse and co-workers at Columbia University. (Private communication.)
[4] A. V. Grosse and E. T. Booth, Phys. Rev. **57**, 664 (1940).
[5] A. V. Grosse, Ber. d. D. Chem. Ges. **61**, 238 (1928).

The β-Ray Spectrum of $_{91}$Ekatantalum^{233} *

E. HAGGSTROM
Pupin Physics Laboratories, Columbia University, New York, New York
January 11, 1941

THE investigations of A. V. Grosse, E. T. Booth and J. R. Dunning[1] definitely established the existence of a β-emitting isotope of ekatantalum produced by irradiating thorium with slow neutrons. They found the half-life of this product to be 27.4±0.3 days. It was assumed that the $_{91}$Et^{233} decayed with the emission of a β-particle into $_{91}$U^{233} and to test this hypothesis the β-ray spectrum of this substance was examined. It was found to consist mainly of conversion lines, some of the most intense of which were very close to those of $_{91}$Pa^{231}. To dispel any doubts as to the purity of the Et^{233} two separate curves were taken 27 days apart. Similar runs were made on a source of protactinium prepared by A. V. Grosse. The intensity of all the lines in the spectrum of Et^{233} decay at the same rate of approximately 27 days while the protactinium remained the same. Furthermore, closer examination revealed definite differences in the energies and structure of the lines of the spectra of ekatantalum and protactinium.

Because of the complex structure of the β-ray spectrum of $_{91}$Et^{233}, it is difficult to distinguish the nuclear disintegration electrons from the conversion electrons due to gamma-radiation. A very large fraction of the β-activity is due to conversion lines of which at least four can be distinguished at 63, 77, 192 and 293 kev. From Fig. 1 it appears that these lines are superposed on a continuous spectrum of relatively small intensity whose maximum energy end-point is masked by the line at 192 kev. By subtracting this line from the continuous background the end-point appears to lie in the neighborhood of 230 kev. Above 230 kev the spectrum consists most probably of a single conversion line at 293 kev.

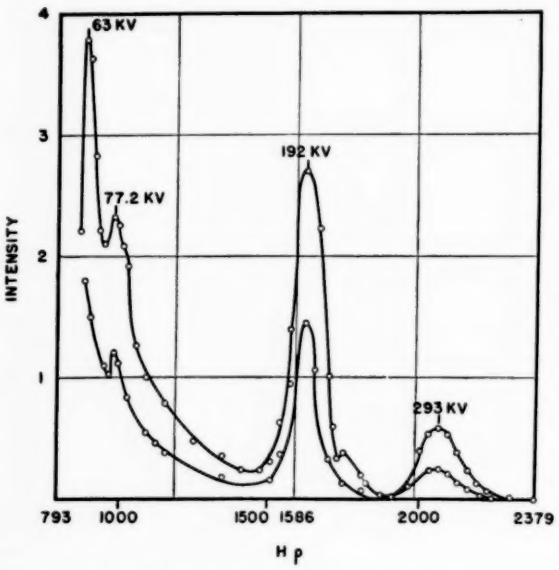

FIG. 1. Beta-ray spectrum of $_{91}$ekatantalum^{233}.

Because of the complexity of the spectrum it is planned to re-examine Et^{233} with greater resolving power (the present resolving power, i.e., half-width of line divided by $H\rho$ at maximum intensity, is 5 percent). The energies involved are in the region where corrections for absorption in the counter window (0.5-mil Çellophane) must be applied. A more detailed study with greater resolving power and thinner window is in progress which should yield more significant values of the end-point of the continuous spectrum and the energies of the gamma-rays.

[1] A. V. Grosse, E. T. Booth and J. R. Dunning, Phys. Rev. **59**, 322 (1941).

* Publication assisted by the Ernest Kempton Adams Fund for Physical Research of Columbia University.

The Fourth (4n+1) Radioactive Series*

A. V. GROSSE, E. T. BOOTH AND J. R. DUNNING
Pupin Physics Laboratories, Columbia University, New York, New York
January 11, 1941

SINCE the discovery by Fermi and his co-workers[1] of $_{90}$Th^{233}, a type 4n+1 radioactive product, numerous attempts[2,3] have been made to determine its successive disintegration products. The discovery of fission by Hahn and Strassmann has generally cast doubt upon the interpretation of previous work in this field, and quite recently Hahn and Strassmann[4] themselves questioned their original interpretation in regard to this series. We began work more than a year ago to renew these investigations.

Measurements were first made on the half-life of the thorium capture product, Th^{233}, and the thickness of aluminum required to reduce the ionization-chamber readings to one-half. These were found, respectively, to be 23.0 minutes and 0.020 cm. Similar experiments with U^{239} yielded 23.5 minutes and 0.018 cm for the equivalent values. To dispel any doubts that these two decaying products might be the same, uranium surrounded by cadmium was irradiated with neutrons in a paraffin geometry near the cyclotron. To this irradiated sample a small amount of thorium was added as a carrier and precipitated as a fluoride. This thorium precipitate contained less than one percent of the uranium activity, thus proving definitely that the two products are not identical.

It has been found that the thorium captures neutrons by a strong resonance process similar to uranium. Three identical samples of thorium (50 mg ThO_2) painted on nickel sheets were exposed to neutrons from the cyclotron in a paraffin geometry. One sample was surrounded by no absorbers, the second by 0.40 g/cm^2 of cadmium, and the third by 1.4 g/cm^2 of boron. The initial activities of the 23-minute periods were in the ratio of 100 : 55 : 11. This is interpreted as evidence that thorium has a strong resonance capture above the cadmium cut off at an energy less than 25 ev.

A search was made for "$_{91}$A^{233}" reported by I. Curie[2] to be the first disintegration product and to have a period of from 2 to 3 minutes. Thorium was irradiated with neutrons in a paraffin geometry, and element 91 separated with zirconium phosphate, the precipitate being placed upon an ion chamber in less than five minutes after the end of the irradiations. No short period was found in any of a number

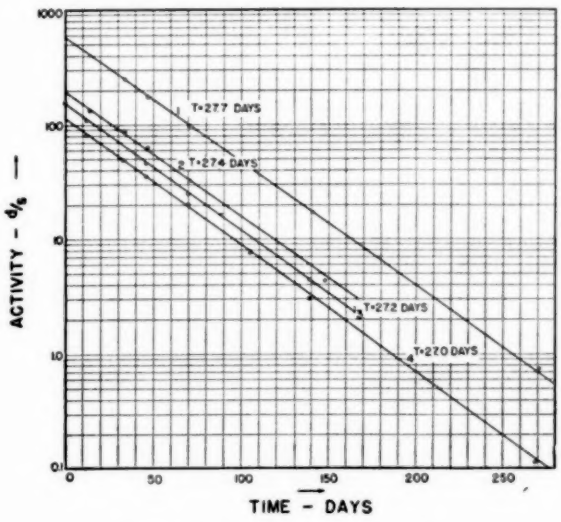

FIG. 1. Decay curves of $_{91}$ekatantalum^{233}.

of experiments. Under the same chemical conditions UX_2 (brevium) was separated from uranium practically quantitatively. A further search revealed a β-emitting isotope of ekatantalum (Et) from thorium irradiated with slow neutrons, with a period of 27.4 days. Since this isotope is excited by slow neutrons and the number of active atoms is quantitatively in approximate agreement with the number of active atoms of Th^{233} formed under the same conditions, it is presumed to be the daughter of Th^{233}.

A strong preparation of $_{91}Et^{233}$ was made by irradiating 7 kg of thorium nitrate in solution (kindly supplied by the Maywood Chemical Company) near the cyclotron for about 50 hours. It was concentrated by a factor of 350,000 by a procedure originally used for the isolation of protactinium.[5] A practically quantitative separation was effected using 20 grams ZrO_2 as a carrier. A final concentrate of 20 mg ZrO_2 was obtained by means of the spiral process[5] and contained initially about 10^{14} atoms of $_{91}Et^{233}$. This separation from Zr disproves the recent suggestion by Hahn and Strassmann[4] that their 25-day activity from thorium precipitated by zirconium phosphate may be an isotope of zirconium, and definitely proves that their "pre-fission" interpretation was correct.[6]

The decay of the sample has been followed for nearly a year, some of the curves being shown in Fig. 1. Curves 1, 3, and 4 were made through a thickness of 2 mils of aluminum between the source and ion chamber, while curve 2 was made through 10 mils. The mean value of the half-life from these and other measurements is 27.4 ± 0.4 days; decay curves through 1.5 and 4.5 g/cm^2 of lead showed the same period. The radiation as shown by cloud-chamber experiments consists of negative electrons[7] and rather strong γ-rays. As has been shown by absorption measurements and more accurately by E. Haggstrom,[8] the maximum energy of the electrons is somewhat less than 300 kev.

Further studies are being made of the decay products.

One of us (A. V. G.) expresses his appreciation to the John Simon Guggenheim Memorial Foundation for the grant of a fellowship. The aid of the Research Corporation is gratefully acknowledged.

[1] E. Fermi, E. Amaldi, O. D'Agostino, B. Pontecorvo, F. Rasetti and E. Segrè, Proc. Roy. Soc. **A149**, 522 (1935).
[2] I. Curie, H. v. Halban and P. Preiswerk, Comptes rendus **200**, 1841 (1935).
[3] O. Hahn and L. Meitner, Naturwiss. **17**, 320 (1935); L. Meitner, F. Strassmann and O. Hahn, Zeits. f. Physik **109**, 538 (1938).
[4] O. Hahn and F. Strassmann, Naturwiss. **28**, 543 (1940).
[5] A. V. Grosse, Ber. d. D. Chem. Ges. **61**, 238 (1928).
[6] A confirmation of this result has been obtained by G. T. Seaborg and J. W. Gofman at the University of California (private communication).
[7] We wish to thank Mr. G. Weil for making the cloud-chamber observations.
[8] E. Haggstrom, Phys. Rev. **59**, 322 (1941).
* Publication assisted by the Ernest Kempton Adams Fund for Physical Research of Columbia University.

Nomenclature of Nuclear Particles

C. MØLLER
Institute of Theoretical Physics, University of Copenhagen, Copenhagen, Denmark
December 10, 1940

FOLLOWING the original proposal of Belinfante,[1] the writer has in a recent note on the meson theory of nuclear forces[2] used the word "nuclon" as a common notation for the heavy nuclear constituents, neutrons and protons. In the meantime, however, it has been pointed out to me that, since the root of the word nucleus is "nucle," the notation "nucleon" would from a philological point of view be more appropriate for this purpose, and I am therefore glad to have the opportunity to call the attention of interested physicists to this point.

[1] F. J. Belinfante, *Theory of Heavy Quanta*, Proefschrift, s'Gravenhage, 1939.
[2] C. Møller, Phys. Rev. **58**, 1118 (1940).

Fission Products of Uranium by Fast Neutrons

Y. NISHINA AND T. YASAKI
Nuclear Research Laboratory, Institute of Physical and Chemical Research, Komagome, Hongo, Tokyo, Japan

AND

K. KIMURA AND M. IKAWA
Chemical Institute, Faculty of Science, Imperial University of Tokyo, Tokyo, Japan
December 23, 1940

IN continuing our work[1] on the fission of uranium produced by fast neutrons, we found in the following way that rhodium and ruthenium isotopes are also produced by fission.

The uranium oxide, U_3O_8, carefully purified and freed from its disintegration products, was exposed for about 12 hours to fast neutrons produced by bombarding lithium with 3 Mev deuterons of some ten microamperes from our cyclotron. From the irradiated sample, rhodium was separated as metal and ruthenium as sulphide. Each fraction which was carefully freed from the known fission products such as molybdenum, palladium, silver, cadmium, antimony, tellurium, iodine, caesium, barium, lanthanum, etc., was examined for its activity.

The rhodium fraction shows a decay curve of a single period 34 hours, while the ruthenium fraction gives two

periods, about 4 hours and 60 hours, respectively. Since the activity of ruthenium is weak, the determination of its periods is not exact and the above values are to be taken as provisional.

The 34-hour rhodium was found to be an electron emitter and the maximum energy of the β-rays, as determined by an absorption method according to Feather, comes out to be 0.5 Mev. Since the 34-hour period is not known for rhodium, its mass number must be larger than 105 and it is expected to transform itself into palladium. We therefore made the search for a radioactive palladium in the rhodium fraction after about 30 hours from its separation. As was expected from the simple decay curve of rhodium, we found no activity in the palladium fraction. We thus conclude that the decay product of the 34-hour rhodium is probably a stable palladium isotope Pd^{106}, Pd^{108} or Pd^{110}, unless it has either a very short or a very long period.

The above investigations were carried out as a part of the work of the Atomic Nucleus Sub-Committee of the Japan Society for the Promotion of Scientific Research. We acknowledge the assistance given by our laboratory colleagues in connection with the irradiation of samples.

[1] Y. Nishina, K. Kimura, T. Yasaki, M. Ikawa and H. Ezoe, Nature **146**, 24 (1940). Y. Nishina, K. Kimura, T. Yasaki and M. Ikawa, Phys. Rev. **58**, 660 (1940).